STRENGTH OF DIFFERENT ANATOLIAN SANDS IN WEDGE SHEAR, TRIAXIAL SHEAR, AND SHEAR BOX TESTS

A THESIS SUBMITTED TO
THE GRADUATE SCHOOL OF NATURAL AND APPLIED SCIENCES
OF
THE MIDDLE EAST TECHNICAL UNIVERSITY

BY

YUSUF ERZİN

IN PARTIAL FULFILLMENT OF THE REQUIREMENTS FOR THE DEGREE OF
DOCTOR OF PHILOSOPHY
IN
THE DEPARTMENT OF CIVIL ENGINEERING

JANUARY 2004

Approval of the Graduate School of Natural and Applied Sciences.

_____

Prof. Dr. Canan Özgen
Director

I certify that this thesis satisfies all the requirements as a thesis for the degree of Doctor of Philosophy.

_____

Prof. Dr. Erdal Çokça
Head of Department

This is to certify that we have read this thesis and that in our opinion it is fully adequate, in scope and quality, as a thesis for the degree of Doctor of Philosophy.

_____	_____
Prof. Dr. Asuman Türkmenoğlu Co-Supervisor	Prof. Dr. Türker Mirata Supervisor

Examining Committee Members

Prof. Dr. Teoman Norman (Chairman) _____

Prof. Dr. Yıldız Wasti _____

Prof. Dr. Asuman Türkmenoğlu _____

Prof. Dr. Reşat Ulusay _____

Prof. Dr. Türker Mirata _____

ABSTRACT

STRENGTH OF DIFFERENT ANATOLIAN SANDS IN WEDGE SHEAR, TRIAXIAL SHEAR, AND SHEAR BOX TESTS

Erzin, Yusuf
Ph. D., Department of Civil Engineering
Supervisor: Prof. Dr. Türker Mirata
Co-supervisor: Prof. Dr. Asuman Türkmenoğlu

2004, 227 pages

Past studies on sands have shown that the shear strength measured in plane strain tests was higher than that measured in triaxial tests. It was observed that this difference changed with the friction angle ϕ_{cv} at constant volume related to the mineralogical composition. In order to investigate the difference in strength measured in the wedge shear test, which approaches the plane strain condition, in the triaxial test, and in the shear box test, Anatolian sands were obtained from different locations in Turkey. Mineralogical analyses, identification tests, wedge shear tests (cylindrical wedge shear tests (cylwests) and prismatic wedge shear tests (priswests)), triaxial tests, and shear box tests were performed on these samples.

In all shear tests, the shear strength measured was found to increase with the inclination δ of the shear plane to the bedding planes. Thus, cylwests ($\delta = 60^o$)

yielded higher values of internal friction ϕ by about 3.6^o than priswests ($\delta = 30^o$) under normal stresses between 17 kPa and 59 kPa. Values of ϕ measured in cylwests were about 1.08 times those measured in triaxial tests ($\delta \approx 65^o$), a figure close to the corresponding ratio of 1.13 found by past researchers between actual plane strain and triaxial test results. There was some indication that the difference between cylwest and triaxial test results increased with the ϕ_{cv} value of the samples. With the smaller δ values (30^o and 40^o), priswests yielded nearly the same ϕ values as those obtained in triaxial tests under normal stresses between 20 kPa and 356 kPa.

Shear box tests ($\delta = 0^o$) yielded lower values of ϕ than cylwests (by about 7.9^o), priswests (by about 4.4^o), and triaxial tests (by about 4.2^o) under normal stresses between 17 kPa and 48 kPa. It was shown that the shear strength measured in shear box tests showed an increase when δ was increased from 30^o to 60^o; this increase (about 4.2^o) was of the order of the difference (about 3.6^o) between priswest ($\delta = 30^o$) and cylwest ($\delta = 60^o$) results mentioned earlier. Shear box specimens with $\delta = 60^o$, prepared from the same batch of any sample as the corresponding cylwests, yielded ϕ values very close to those obtained in cylwests.

Keywords: Angle of internal friction, peak strength, plane strain test, sand, shear box test, shear strength, triaxial compression test, ultimate strength, wedge shear test

ÖZ

DEĞİŞİK ANADOLU KUMLARININ KAMA KESME, ÜÇ EKSENLİ VE KESME KUTUSU DENEYLERİNDEKİ DAYANIMI

Erzin, Yusuf
Doktora, İnşaat Mühendisliği Bölümü
Tez Danışmanı: Prof. Dr. Türker Mirata
Ortak Tez Danışmanı: Prof. Dr. Asuman Türkmenoğlu

2004, 227 sayfa

Kumlar üzerinde yapılan önceki çalışmalar, düzlemsel boy değişimi deneylerinde ölçülen kayma dayanımının üç eksenli deneylerinde ölçülenden daha yüksek olduğunu göstermiştir. Bu farkın mineral bileşimine bağlı olan değişmez hacimdeki kayma dayanımı açısı ϕ_{cv} ile değiştiği gözlenmiştir. Düzlemsel boy değişimi koşullarına yakın olan kama kesme deneyleri ile üç eksenli deneyler ve kesme kutusu deneylerinde ölçülen dayanımlar arasındaki farkı araştırmak amacıyla, Türkiye'deki farklı yörelerden kum örnekleri alınmıştır. Bunlar üzerinde mineral analizler, tanımlama deneyleri, kama kesme deneyleri (silindirsel kama kesme deneyleri (skkd) ve prizmatik kama kesme deneyleri (pkkd)), üç eksenli deneyler ve kesme kutusu deneyleri yapılmıştır.

Tüm kesme deneylerinde, ölçülen kayma dayanımının kayma düzlemi ile sıkıştırma katmanları arasındaki açıyla (δ) arttığı görülmüştür. Bu nedenle, 17 kPa ile 59 kPa arasında değişen dikey gerilmeler altında skkd ($\delta = 60^o$), pkkd

($\delta = 30^o$)'den yaklaşık olarak 3.6^o daha yüksek içsel sürtünme açısı ϕ değerleri vermiştir. Skkd'de ölçülen ϕ değerleri üç eksenli deneylerde ($\delta \approx 65^o$) ölçülenin yaklaşık 1.08 katı olarak bulunmuştur ki bu katsayı, önceki araştırmacılarca gerçek düzlemsel boy değişimi deneyleri ve üç eksenli deneyler arasında bulunan 1.13 değerine yakındır. Üç eksenli ve skkd sonuçları arasındaki bu farkın, örneklerin ϕ_{cv} değerleriyle arttığını gösteren belirtiler gözlenmiştir. Daha küçük δ açılarıyla (30^o ve 40^o) yapılan pkkd, 20 kPa ile 356 kPa arasında değişen dikey gerilmeler altında, üç eksenli deneylerden elde edilen ϕ değerlerine çok yakın sonuçlar vermiştir

Kesme kutusu deneyleri ($\delta = 0^o$), 17 kPa ile 48 kPa arasında değişen dikey gerilmeler altında, skkd'den (yaklaşık olarak 7.9^o), pkkd'den (yaklaşık olarak 4.4^o) ve üç eksenli deneylerden (yaklaşık olarak 4.2^o) daha düşük ϕ değerleri vermiştir. Kesme kutusu deneylerinde, δ açısının 30 dereceden 60 dereceye artırılmasıyla, kayma dayanımında bir artış gözlenmiştir. Bu artış (yaklaşık olarak 4.2^o) daha önce belirtilen skkd ($\delta = 60^o$) ve pkkd ($\delta = 30^o$) sonuçları arasındaki farkla (yaklaşık olarak 3.6^o) aynı düzeydedir. Herhangi bir örneğin, skkd örneklerinin hazırlandığı bölümünden elde edilen kesme kutusu örnekleri ($\delta = 60^o$) skkd'den bulunan ϕ değerlerine çok yakın sonuçlar vermiştir.

Anahtar kelimeler: Düzlemsel boy değişimi deneyi, en yüksek dayanım, içsel sürtünme açısı, kama kesme deneyi, kayma dayanımı, kesme kutusu deneyi, kum, nihai dayanım, üç eksenli basınç deneyi

TO MY PARENTS

ACKNOWLEDGEMENTS

The subject of this thesis was suggested by Prof. Dr. Türker Mirata, and the work has been carried out under his supervision. The author wishes to express his sincere gratitude to Prof. Mirata for his close supervision, guidance and encouragement throughout this study, and for correcting the manuscript; and to his co - supervisor Prof. Dr. Asuman Türkmenoğlu for her valuable guidance during the mineralogical analyses.

Special thanks are also extended to Prof. Dr. Teoman Norman for his valuable help in the selection of the sites for sampling, and during the mineralogical and particle shape analyses; and to both Prof. Norman and Prof. Dr. Yıldız Wasti for their valuable suggestions as members of the Ph.D. progress tracking committee.

The author would also like to thank Mr. Ali Bal of the Soil Mechanics Laboratory for his valuable help during the shear tests, Ms. İnciser Girgin for the mineralogical analyses, Mr. Mehmet Ekinci for some of the drawings, and last but not least, his wife and family for their endless support.

TABLE OF CONTENTS

LIST OF TABLES

TABLES Page

LIST OF FIGURES

FIGURES Page

LIST OF ABBREVIATIONS AND SYMBOLS

ABBREVIATIONS

cylwest	Cylindrical wedge shear test
C	Cylindrical wedge shear test series
EAURF	Extensively altered ultrabasic rock fragments
EIRF	Extrusive igneous rock fragments
Fig.	Figure
Figs.	Figures
HPTCPU	Hydraulic pump type constant pressure unit
iswest	In situ wedge shear test
IIRF	Intrusive igneous rock fragments
LC	Load cell
LP1, LP2	Grooved plates
MRF	Metamorphic rock fragments
priswest	Prismatic wedge shear test
P	Prismatic wedge shear test series
S	Shear box test series
SB	Single ball
SP	Poorly graded sand
SRF	Sedimentary rock fragments
T	Triaxial test series
TF	Tuffaceous rock fragments
TM	Test mould
TM(S)	Stationary half of the test mould
vol.	Volume
VCMD	Volume change measurement device

LATIN SYMBOLS

A	Area of the shear box test specimen
A_c	Corrected area of shear plane
b	Inner width of test mould
B_g	Breakage factor
C_c	Curvature coefficient
C_u	Uniformity Coefficient
d	The length of shearing plane of test mould
d_c	Diameter of the circumscribing circle
d_i	Diameter of the inscribed circle
d_k	Diameter of curvature of the sharpest corner
D	Distance between the grooves on LP1 and the single ball SB
D_i	Inside diameter of the test mould in cylwests
D_r	Initial relative density
D_{10}	Effective size
D_{30}	Largest size of the smallest 30 %
D_{60}	Largest size of the smallest 30 %
dv/du	Rate of dilatancy
e	Void ratio
e_{max}	Maximum void ratio
e_{min}	Minimum void ratio
e_o	Initial void ratio
E	Coefficient of angularity measured by an indirect method based on permeability
G_s	Specific gravity
h_1	Height from the flat part of the serrated plate to the top of the shear box
I_R	Relative dilatancy index
M_B	the sum of moments about single ball SB of all components between the grooves of plate LP1 and SB when $\theta = 0^o$

n	Porosity
n_c	Initial clearance between the two halves of the test mould
n_{max}	Maximum porosity
n_{min}	Minimum porosity
n_r	Initial relative porosity
p'	Mean effective stress
P	Main load
Q	Lateral load
Q_g	A constant as a function of grain type
r	Correlation coefficient
R_F	Roundness of a particle
S_R	Riley sphericity
t_p	Thickness of the loading pad
u	Shear displacement in shear box tests
$\bar{u}$	Average shear displacement in wedge shear tests
v	Normal displacement in shear box tests
v_s	Volume decrease per unit volume
$\bar{v}$	Average normal displacement in wedge shear tests
V_c	Cell pressure valve of the triaxial cell
V_p	Pore pressure valve of the triaxial cell
w	Water content
w_{opt}	Optimum water content
W	The total weight of the soil wedge, the test mould TM and the grooved loading plate LP1
W_{BC}	Weight of ball cage
W_d	Additional dead weight
W_{LP}	Weight of the grooved loading plate LP2
W_{qn}	The component normal to Q of the simply supported reaction due to the self-weight of the lateral loading device
W_t	Total dead weight

X	Component of all forces parallel to P
Y	Component of all forces normal to P

GREEK SYMBOLS

α	True angle between the shear plane and the axis of the test mould
α_i	The angle between A_1B_1 and the initial direction of P
α_n	The angle between the shearing plane of the test mould and initial direction of P
α_r	The angle between A_1B_1 and the rotated direction of P
β	Slight rotation of test mould
Δy_p	Shift in the positive y direction applied to P prior to testing,relative to the initial centroid of shearing plane
δ_x	Displacements measured in the positive X direction
δ_y	Displacements measured in the positive y direction
δX_q	Increase in X due to the lateral load Q
δY_q	Increase in Y due to the lateral load Q
$\delta\theta$	Small angle introduced to avoid division by zero when $\theta = 0$
$\delta\sigma/\sigma$	Percentage difference between the normal stress at the trialing end of soil wedge and average normal stress
ε_v	Volumetric strain
$(\varepsilon_v)_f$	Volumetric strain at failure
ε_1	Axial strain
$(\varepsilon_1)_f$	Axial strain at failure
ε_2	Intermediate principal strain
ε_3	Minor principal strain
θ	The angle between the main load and horizontal
μ	Coefficient of friction
ν	Poisson's ratio
ρ_{bulk}	Bulk density

$(\rho_d)_{min}$	Minimum dry density
ρ_{dry}	Dry density
ρ_{dmax}	Maximum dry density
σ	Normal stress
σ_o	Mean normal stress
σ_1	Major principal stress
σ_1'	Major principal effective stress
σ_2	Intermediate principal stress
σ_3	Minor principal stress (or confining pressure)
σ_3'	Minor principal effective stress
(σ_1/σ_3)	Principal stress ratio
$(\sigma_1/\sigma_3)_f$	Maximum principal stress ratio at failure
$(\sigma_1 - \sigma_3)$	Principal stress difference
τ	Shear stress
τ_f	Shear strength
ϕ	Angle of internal friction
ϕ_c	Peak friction angle obtained from the results of cylindrical wedge shear tests under the lower ranges of normal stress
ϕ_{cu}	Peak friction angle obtained from the result of the cylwest on untested specimen.
ϕ_{cv}	Angle of friction at constant volume (or ultimate friction angle)
$(\phi_{cv})^{ps}$	Ultimate friction angle measured in plane strain tests
$(\phi_{cv})^{t}$	Ultimate friction angle measured in triaxial tests
ϕ_{c2}	Peak friction angle defined by two cylindrical wedge shear tests under about the same normal stress
ϕ_d	Peak friction angle
ϕ_{ds}	Peak friction angle measured in direct simple shear test
ϕ_f	A semi-empirical friction angle
ϕ_{ps}	Peak friction angle measured in plane strain tests
$(\phi_{ps})_{max}$	Maximum peak friction angle measured in plane strain tests

$(\phi_{ps})_{min}$	Minimum peak friction angle measured in plane strain tests
ϕ_{pa}	Peak friction angle obtained from the combined results of all prismatic wedge shear tests
ϕ_{ph}	Peak friction angle obtained from the results of prismatic wedge shear tests under the higher ranges of normal stress
ϕ_{pl}	Peak friction angle obtained from the results of prismatic wedge shear tests under the lower ranges of normal stress
ϕ_{pu}	Peak friction angle obtained from the result of the priswest on untested specimen.
ϕ_{sa}	Peak friction angle obtained from the combined results of all shear box tests on specimens compacted directly in the shear box
ϕ_{sc}	Peak friction angle obtained from the results of shear box tests on specimens taken from the shear plane of previously sheared samples compacted in the cylwest mould under the lower ranges of normal stress
ϕ_{sh}	Peak friction angle obtained from the results of shear box tests on specimens compacted directly in the shear box under the higher ranges of normal stress
ϕ_{sl}	Peak friction angle obtained from the results of shear box tests on specimens compacted directly in the shear box under the lower ranges of normal stress
ϕ_{sp}	Peak friction angle obtained from the results of shear box tests on specimens taken from the shear plane of previously sheared samples compacted in the priswest mould under the lower ranges of normal stress
ϕ_{t}	Peak friction angle measured in triaxial tests
ϕ_{ta}	Peak friction angle obtained from the combined results of all triaxial tests
ϕ_{th}	Peak friction angle obtained from the results of triaxial tests under the higher ranges of normal stress

ϕ_{tl}	Peak friction angle obtained from the results of triaxial tests under the lower ranges of normal stress
ϕ_{tu}	Peak friction angle obtained from the result of the triaxial test on untested specimen.
ϕ_{uc}	Ultimate friction angle obtained from the results of cylindrical wedge shear tests under the lower ranges of normal stress
ϕ_{upa}	Ultimate friction angle obtained from the combined results of all prismatic wedge shear tests
ϕ_{uph}	Ultimate friction angle obtained from the results of prismatic wedge shear tests under the higher ranges of normal stress
ϕ_{upl}	Ultimate friction angle obtained from the results of prismatic wedge shear tests under the lower ranges of normal stress
ϕ_{uta}	Ultimate friction angle obtained from the combined results of all triaxial tests
ϕ_{utl}	Ultimate friction angle obtained from the results of triaxial tests under the lower ranges of normal stress
ϕ_{uth}	Ultimate friction angle obtained from the results of triaxial tests under the higher ranges of normal stress
ϕ_{μ}	The angle of friction between the mineral particles
ψ	The angle between the failure plane and the plane on which the major principal stress acts

CHAPTER 1

INTRODUCTION

Shear strength of sands is influenced by many factors such as void ratio, confining stress, intermediate principal stress, particle composition. Denser sands have higher friction angles compared with loose sands; this is due to the better interlocking in the former; this interlocking decreases as the confining stress increases, because particles become flattened at contact points, sharp corners are crushed, and particles break, reducing the friction angle (Lambe & Whitman, 1979). The amount of crushing in sand increases with confining pressure and depends on the mineral composition, gradation, and shape of particles (Vesic & Clough, 1968). For a sand composed of strong and rigid particles, very little crushing is observed and the particles remain dilatant even at high pressures compared with sand of soft particles (Seed & Lee, 1967). A particle of a given size undergoes less breakage when in a well graded sand, since in a well graded sand there are many interparticle contacts and the load per contact is thus less than in a uniform sand (Lambe & Whitman, 1979). More crushing occurs in larger particles; this is due to the fact that increasing the particle size increases the load per particle, and hence crushing begins at a smaller confining pressures (Lambe & Whitman, 1979).

The effect of intermediate principal stress is seen in the results of triaxial and plane strain tests. Shear strength of sands measured in plane strain tests is greater than that measured in triaxial tests (section 2.1.4). The reason for the increased resistance in the plane strain tests is that the sand particles are given less freedom in the way that they can move around adjacent particles so as to overcome interlocking

(Mitchell, 1976). The greatest difference is observed in dense sands at low confining pressures and the smallest difference occurs in either loose sands at all confining pressures or dense sands at sufficiently high confining pressures to prevent dilation (Lee, 1970).

"The composition of sand can have an important influence on its friction angle, indirectly by influencing initial void ratio, and directly by influencing the amount of interlocking occurring for a given void ratio." (Kezdi, 1974.) Composition effect can be explained in terms of the size, shape, and gradation of the particles, and the type of minerals making up the sand. Particle shape effect can be expressed in terms of the spherictiy and angularity. Sands composed of less spherical and more angular particles have larger friction angles, because these particles interlock more thoroughly than rounded and spherical ones. For sands with grains of low strength, for example decomposed granite, calcareous sand, and shaley alluvial sand, particle crushing can be quite significant even under the low pressures commonly encountered in a soil deposit (Ueng & Chen, 2000).

On the basis of the earlier two paragraphs, the peak friction angle measured in plane strain tests (ϕ_{ps}) is higher than that measured in triaxial tests (ϕ_t), and this difference changes with the degree of particle crushing related to mineralogical composition. In order to investigate the difference in strength measured in the wedge shear test, which approaches the plane strain condition (section 2.4), in the triaxial test, and in the shear box test, Anatolian sands were obtained from different locations in Turkey. These locations, suggested by Norman (2000(a)), were in Şereflikoçhisar (Ankara), Bafra (Samsun), Sinop, Ceyhan (Adana), and Yumurtalık (Adana). In addition to these, one more sample was obtained from Kazan (Ankara).

A minimum of 350 kg of sand was taken from each of the chosen locations, transported to the Soil Mechanics Laboratory of METU, and prepared for mineralogical and granulometric analyses, and shear tests. Mineralogical and particle shape analyses for each sample are presented in Chapter 3. Physical and compaction

properties of each sample are presented in Chapter 4. The shear strength of each sample was measured firstly in the wedge shear tests (cylindrical wedge shear test (cylwest) and prismatic wedge shear test (priswest)) (Chapter 5), secondly in the triaxial test (Chapter 6), and finally in the shear box test (Chapter 7). Discussions of the results of the shear tests are presented in Chapter 8. Conclusions and recommendations are presented in Chapter 9.

As all the stresses used in this thesis are effective stresses, the word "effective" has been omitted in referring to the peak and ultimate angles of friction, and no prime sign ($'$) has been used in the symbol ϕ, or the relevant normal stresses.

CHAPTER 2

REVIEW OF RELEVANT LITERATURE

2.1 Factors Affecting Shear Strength of Sands

Lambe & Whitman (1979) divided the factors that affect the shear strength of sands into two general groups. The first group includes those factors that affect the shear resistance of any given sand: void ratio, confining stress, loading conditions, etc. The second group includes those factors that cause the strength of one sand to differ from the strength of another for the same confining stress and void ratio. These factors are the size, shape, and gradation of the particles, and the type of minerals making up the sand.

The paragraphs in some of the following sub-sections have been numbered for ease of reference.

2.1.1 Effect of Rate of Dilatation

The stress – dilatancy equation was derived for saturated drained sands by Rowe (1962). Unless otherwise stated, the following paragraphs have been summarized from Rowe (1969).

The stress – dilatancy equation is

$$R = D.K \quad \text{……………………………………………………………………}(2.1)$$

where $R = (\sigma_1/\sigma_3)$; σ_1 and σ_3 are the major and minor principal stresses at failure. D and K are defined by

$$D = \left(1 - \frac{dv_s}{d\varepsilon_1}\right) \quad \text{…………………………………………………………..}(2.2)$$

$$K = \tan^2\left(45 + \frac{\phi_f}{2}\right) \quad \text{…………………………..………………………...}(2.3)$$

where

v_s = volume decrease per unit volume;

ε_1 = major principal compressive strain;

ϕ_f = a semi-empirical friction angle which varies between the limits given below, and has been found to fit experimental observations by Barden & Khayatt (1966).

The value of ϕ_f depends on the relative density, pressure range, and the stress path, and varies in triaxial compression tests, between a lower value ϕ_μ when the sand is sheared in the densest state, and an upper value ϕ_{cv} when the sand is sheared in the loosest state, where ϕ_μ is the angle of friction between the mineral particles, and ϕ_{cv} is the angle of friction at constant volume. In plane strain tests, for all states of packing, $\phi_f = \phi_{cv}$. The values of ϕ_μ are correlated with ϕ_{cv} as shown in Fig. 2.1, which has been found to match experimental results. The references on this figure are those quoted by Rowe (1969).

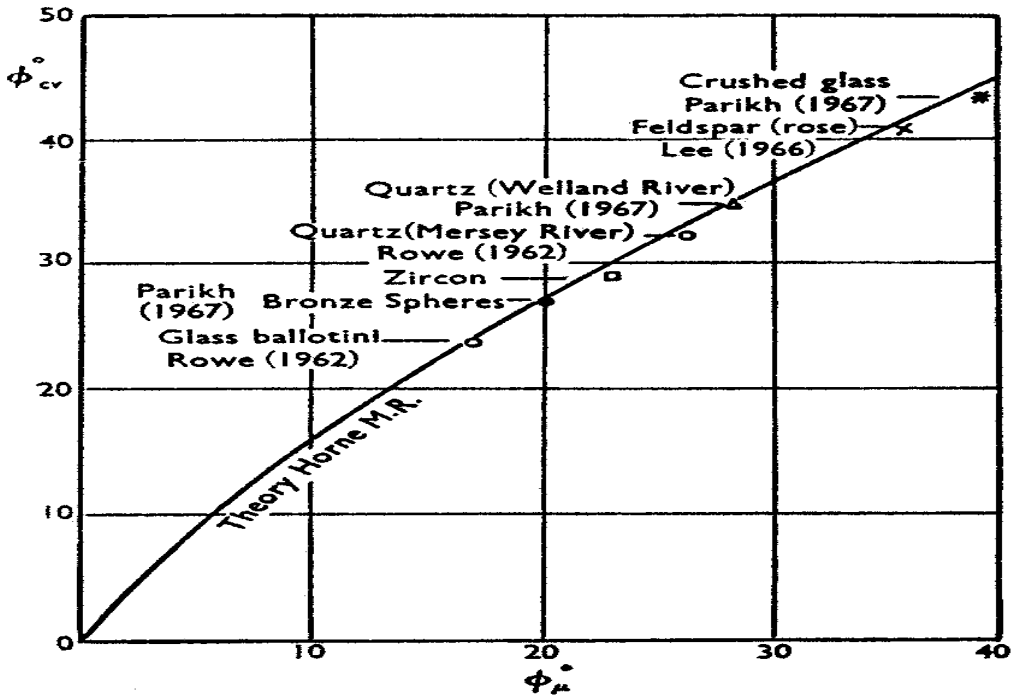

Figure 2.1. Relation between ϕ_μ and ϕ_{cv} (after Rowe, 1969)

Assuming that *D* (equation (2.2)) varies approximately between 1 and 2 for the loosest and densest states both in triaxial compression and plane strain tests, and by substituting these values in equation (2.1) together with the limiting values of $\phi_f = \phi_{cv}$ and $\phi_f = \phi_\mu$ for the loosest and densest states in triaxial compression tests, and $\phi_f = \phi_{cv}$ for both states in plane strain tests, Rowe (1969) has plotted the limiting values of peak friction angle ϕ_d calculated from the corresponding values of $R = (\sigma_1/\sigma_3)$ for different sands (Appendix A), natural and artificial, for triaxial compression (T) and plane strain (P.S.) tests, as shown in Fig. 2.2. These limiting values were connected by continuous straight lines, following the trend shown by the dashed experimental lines for the results of triaxial compression and plane strain tests performed on these sands. The initial relative porosity in Fig. 2.2 is defined (Adel, 2001) as

$$n_r = \frac{n_{max} - n}{n_{max} - n_{min}} \quad \text{.....(2.4)}$$

where n_{max}, n_{min}, and n are the maximum, minimum, and current porosity of the sand. The relation between relative porosity and relative density is given in Appendix B.

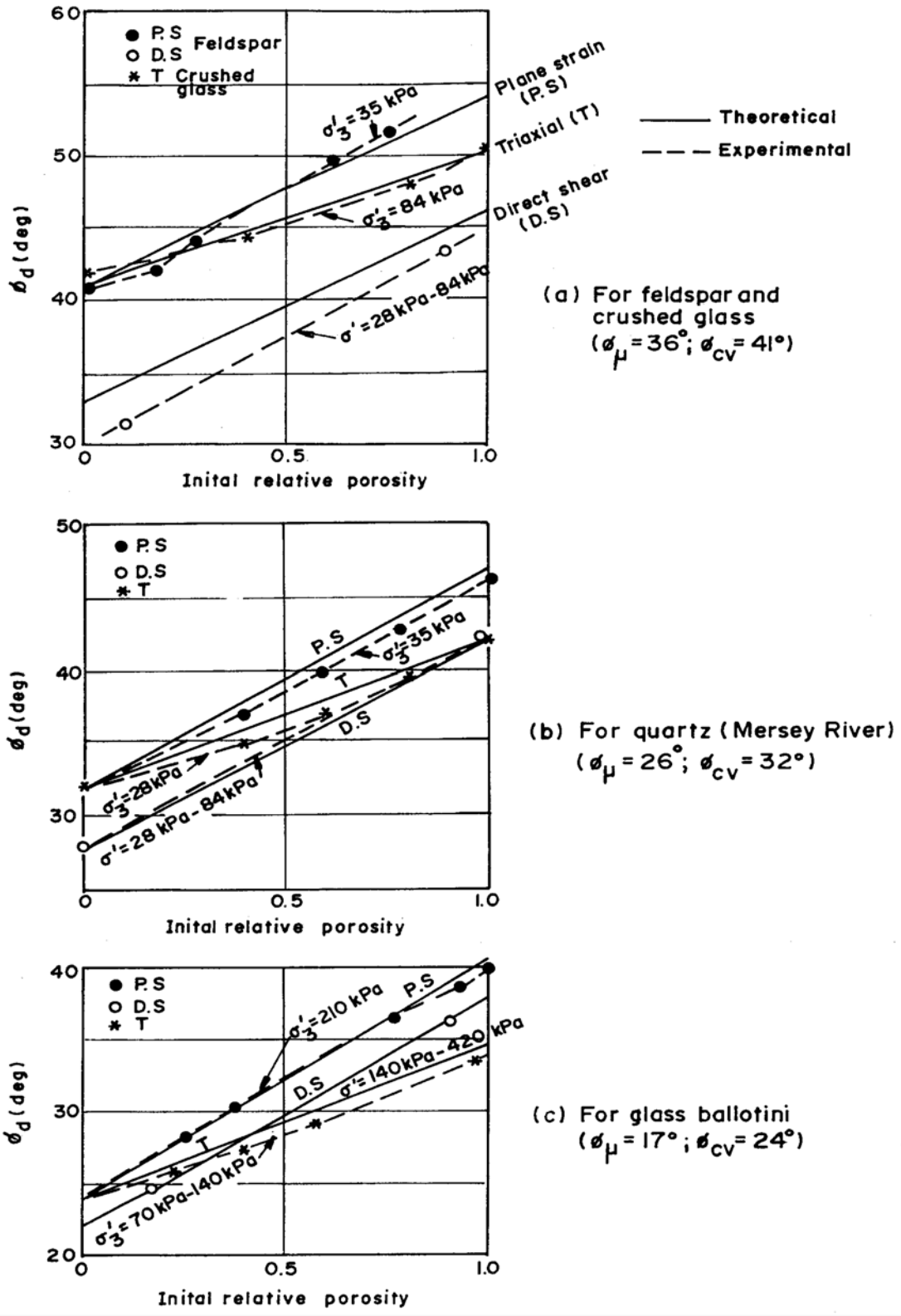

Figure 2.2. Comparisons of ϕ_d values measured in plane strain, triaxial compression, and direct shear tests with theoretical peak strength limits (after Rowe, 1969)

Rowe (1969) also derived the following relation between the peak friction angles measured in direct simple shear ϕ_{ds} and plane strain ϕ_{ps} for all states of packing.

$$\tan\phi_{ds} = \tan\phi_{ps}\cos\phi_{cv} \quad \text{.....(2.5)}$$

Experimental results presented show that the conventional shear box test results are also closely consistent with equation (2.5). Rowe (1969) used equation (2.5) and the results of conventional shear box tests to plot the curves shown in Fig. 2.2 for the direct shear (D.S.) test.

The relations in Fig. 2.2 allow overall comparison of ϕ_d values in the three types of test when the effects of the orientation of the shear plane and of the confining pressure and so the crushing of sand particles on the measured ϕ_d values were disregarded. These effects are discussed in subsequent sub-sections.

2.1.2 Effect of Initial Void Ratio

Void ratio is perhaps the most important single parameter that affects the strength of sands (Mitchell, 1976; Maeda & Miura, 1999(a)). Generally, for drained tests either in triaxial or direct shear tests, the lower the void ratio, the higher the shear strength. The effect of void ratio on the friction angle (ϕ_d) can be explained by the phenomenon of interlocking (Lambe & Whitman, 1979). The denser the sand, the greater the interlocking, and so the greater the value of ϕ_d.

Bardet (1997) gives possible ranges of the peak friction angle ϕ_d and the friction angle ϕ_{cv} at constant volume at different densities for different frictional soils (Table 2.1), which is in conformity with Lambe & Whitman's (1979) views that the lower the void ratio, the higher the shear strength.

Table 2.1. Friction angles at peak strength and at constant volume for cohesionless soils (after Bardet, 1997)

Classification	ϕ_d (degrees)		ϕ_{cv} (degrees)
	Medium dense	Dense	Loose
Silt (non -plastic)	28 - 32	30 - 34	26 - 30
Uniform fine to medium sand	30 - 34	32 - 36	26 - 30
Well – graded sand	34 - 40	38 - 46	30 - 34
Sand and gravel	36 - 42	40 - 48	32 -36

2.1.3 Effect of Confining Stress

1. The strength and stress-strain-dilatancy behaviour of sand varies remarkably with confining stress σ_3 (Bishop, 1966). At very low confining stresses, the sand particles are relatively free to move with respect to each other and dilatancy effect can cause a significant increase in friction angle ϕ_d. As the confining stress increases, dilatancy effects gradually disappear due to particle crushing, causing a notable reduction of ϕ_d (Vesic & Clough, 1968).

2. To clarify the degree of confining stress dependency of stress-strain-dilatancy behaviour of sand, Vesic & Clough (1968) introduced the concept of a *breakdown stress*, which represents the mean normal stress level, defined as

$$\sigma_o = \frac{\sigma_1 + \sigma_2 + \sigma_3}{3} \quad \text{.....(2.6)}$$

at which all dilatancy effects disappear, and beyond which the shear strength of the sand is not affected by its initial void ratio. Vesic & Clough (1968) stated that this stress was affected by the mineral composition, gradation, and shape of particles. The mineral composition should affect this stress through two parameters, namely crushing strength of the mineral at particle contacts and the mineral's angle of physical friction. The lower this crushing strength, the lower should be the breakdown stress. Also, the poorer the gradation and the smaller the particle sphericity, the lower should be the breakdown stress.

3. The stress-strain-dilatancy behaviour of sands under various σ_3 values was investigated by a number of researchers. A summary of each follows.

4. Bishop (1966) quotes stress, strain, and volume change curves of Ham River sand obtained by Skinner 1964-1966 (quoted by Bishop, 1966). The individual grains of Ham River sand are predominantly quartz minerals with rounded shapes (Hardin, 1985). The results of the tests at failure are shown in Fig. 2.3, where ε_v is the volumetric strain, dilatation positive, and the test numbers are denoted on the curves. From Fig. 2.3, Bishop (1966) pointed out the following.

(a) For loose sand the reduction in volume during shear rises rapidly with increase in σ_3 up to about 6830 kPa, and then more gradually as σ_3 is increased to 27 590 kPa.

(b) Dense sand is strongly dilatant at the low confining pressure of 690 kPa and shows almost zero rate of volume change at failure when σ_3 reaches 3450 kPa. At higher values of σ_3, dense sand shows an increasingly marked reduction in volume during shear and at σ_3 = 27 590 kPa, its behaviour approximates to that of loose sand.

5. Bishop (1966) also examined the Mohr envelopes for loose and dense sands. He noted that at low pressures, there is a considerable difference in the friction angles obtained from dense and loose sands; at high pressures, however, this difference becomes increasingly less significant and at 27 590 kPa the strengths of dense and loose sands are essentially the same. These results indicate that the breakdown stress (paragraph (2)) of Ham River sand calculated from equation (2.6), as in equation (2.7) for the triaxial test, is 30 500 kPa

$$\sigma_o = \frac{2\sigma_3 + \sigma_1}{3} \quad \text{.....(2.7)}$$

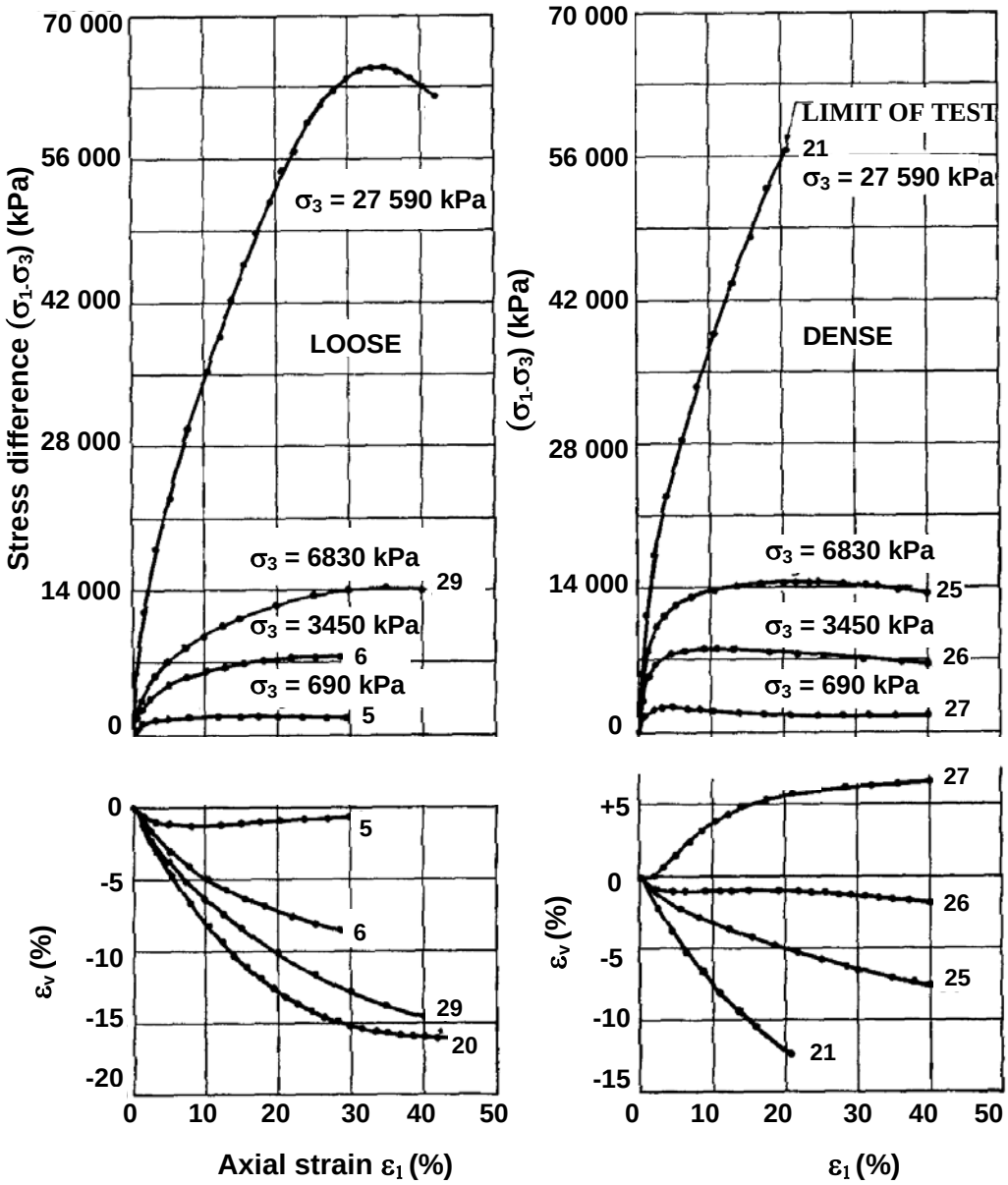

Figure 2.3. Results of drained tests on Ham River sand (after Bishop, 1966)

6. Seed & Lee (1967) investigated the drained strength characteristics of sands over a wide range of confining pressures. The soil used for this investigation was fine uniform sand that had been dredged from the Sacramento River. The individual grains were mostly feldspar and quartz minerals with subangular to subrounded shapes. Seed & Lee (1967) examined the relationships between stress, strain, and volume change in a series of drained triaxial tests on dense sand under increasing confining pressures, and observed that an increase in σ_3 increased the

strain to failure, and decreased the tendency to dilate. Similar results were obtained from a series of drained triaxial tests on loose sand. The pattern is similar to that for dense sand, except that at low pressures the tendency for dilation is not so strong as for dense sand. Seed & Lee (1967) also found that the local slope of the Mohr envelope for dense sand at low confining stresses σ_3, below 800 kPa, was about 41^o, but at the higher values of σ_3, up to 4000 kPa, it reduced to about 24^o. A similar trend was observed for the loose sand, the corresponding reduction being from 34^o to 24^o. These results indicate that the breakdown stress (paragraph (2)) of Sacramento River sand, calculated from equation (2.7) is 7000 kPa.

7. Vesic & Clough (1968) performed triaxial tests on Chattahoochee sand to investigate the effect of σ_3 on the behaviour of cohesionless soils. The individual grains of Chattahoochee sand were predominantly quartz and some mica minerals with subangular shapes (Hardin, 1985). Under the mean normal stresses σ_o (equation (2.6)) below 100 kPa, there was very little crushing, and dilatancy effects were quite significant. At higher σ_o, up to 10 000 kPa, crushing became more pronounced, and dilatancy effects gradually disappeared. At σ_o = 10 000 kPa, dilatancy effects completely disappeared, indicating that the breakdown stress (paragraph (2)) of Chattahoochee sand is 10 000 kPa.

8. Breakdown stresses of Ham River sand, Chattahoochee sand, and Sacramento River sand were found as 30 500 kPa, 10 000 kPa, and 7000 kPa by Skinner (1964-1966) (quoted by Bishop, 1966), Vesic & Clough (1968), and Seed & Lee (1967) respectively (paragraphs (5) to (7)). It is seen that (i) Ham River sand of predominantly quartz minerals with rounded shapes has the highest breakdown stress; (ii) Chattahoochee sand of predominantly quartz and some mica minerals with subangular shapes has the intermediate breakdown stress; (iii) Sacramento River sand of mostly feldspar, the grains of which have lower resistance to crushing compared to quartz grains (Norman, 2000(b)), and quartz minerals with subangular to subrounded shapes has the lowest breakdown stress. This is a confirmation of the views, quoted in paragraph (2), that mineral composition and shape of sand particles

affect breakdown stress, and that for sands with grains of low strength and angular shape, breakdown stress is lower.

9. Maeda & Miura (1999(b)) studied the deformation – failure behaviour of some 80 granular materials in a series of triaxial tests at σ_3 values between 50 kPa and 400 kPa. The peak angle of friction ϕ_d was found to decrease with an increase in σ_3, as observed by Bishop (1966), Seed & Lee (1967), and Vesic & Clough (1968) (paragraphs (5) to (7) respectively). Maeda & Miura (1999(b)) stated that the higher reduction in the values of ϕ_d was observed on granular materials which possess a high value of angularity and *void ratio extent* (difference between maximum void ratio, e_{max}, and minimum void ratio, e_{min}). Void ratio extent is controlled mainly by the gradation, shape, and size of the sand particles (Youd, 1973; Shahu & Yudhbir, 1998; Maeda & Miura, 1999(a)). For specimens consisting of uniformly graded, rounded particles (e.g., Leighton Buzzard sand and glass beads), the value of $(e_{max} - e_{min})$ is roughly one half of the corresponding value for specimens consisting of well graded, angular particles (e.g., Kalpi sand and Biddulph sand) for any given value of average particle size (Yudhbir et al., 1991) (quoted by Shahu & Yudhbir, 1998).

10. From paragraphs (5), (6), (7), and (9), the reduction in ϕ_d of sands, observed with an increase in σ_3, seems to be linked with the gradation, shape, and the mineralogical composition of the sand particles.

2.1.4 Effect of Intermediate Principal Stress

1. The effect of intermediate principal stress σ_2 is seen in the results of triaxial and plane strain tests. The triaxial test simulates an axisymmetric condition (three-dimensional strain), and the plane strain test simulates a two-dimensional loading condition (two-dimensional strain). Denoting the major, intermediate, and minor principal stresses σ_1, σ_2, and σ_3, respectively, and the corresponding principal strains by ε_1, ε_2, and ε_3, the stress - strain conditions are given as follows:

For the plane strain test,

$$\sigma_1 > \sigma_2 > \sigma_3 \qquad \varepsilon_1 \neq 0 \quad \varepsilon_2 = 0 \quad \varepsilon_3 \neq 0$$

For the triaxial compression test,

$$\sigma_1 > \sigma_2 = \sigma_3 \qquad \varepsilon_1 \neq 0 \quad \varepsilon_2 = \varepsilon_3 \neq 0$$

2. Shear strength of sands measured in plane strain tests is greater than that measured in triaxial tests (Leussink & Whitke, 1963; Lee, 1970; Cornforth, 1973; Schanz & Vermeer, 1996). The reason for the increased resistance in the plane strain tests comes about because the sand particles are given less freedom in the way that they can move around adjacent particles so as to overcome interlocking (Mitchell, 1976).

3. A number of researchers investigated the variation of the difference between the peak friction angles measured in plane strain tests (ϕ_{ps}) and triaxial tests (ϕ_t) with density and confining pressure. A summary of each follows.

4. Leussink & Whitke (1963) performed plane strain and triaxial tests on glass balls with a constant diameter of approximately 15 mm at confining pressures σ_3 of between 50 kPa and 300 kPa. They obtained $\phi_{ps} = 51.4^o$ and $\phi_t = 40.7^o$, indicating a difference of about 11^o between the peak friction angles.

5. Lee (1970) performed plane strain and triaxial tests on specimens of Sacramento River sand prepared at two different initial relative densities D_r of 38% and 78% at σ_3 values of 30 kPa to 1000 kPa. The difference ($\phi_{ps} - \phi_t$) was 8^o for dense specimens at σ_3 values lower than 100 kPa, and vanished both for loose specimens at all σ_3 values and for dense specimens at sufficiently high σ_3 values to prevent dilation. These results indicate that ($\phi_{ps} - \phi_t$) is linked with dilatation and so with σ_3 and density.

6. Cornforth (1973) performed plane strain and triaxial tests on specimens of Brasted sand prepared at initial D_r values ranging from 15% to 80% at σ_3 = 280 kPa. The results of these tests indicated the following. The values of ϕ_{ps} were higher than those of ϕ_t. A decrease in D_r caused the difference (ϕ_{ps} - ϕ_t) to decrease. The difference was about 4^o to 5^o for dense specimens and decreased to about 1^o for loose specimens. The ultimate strength of the sand at all densities was approximately constant and nearly the same in both plane strain and triaxial tests. These results indicate that, in contrast to the peak strength, the ultimate strength of sand is independent of strain conditions and void ratio.

7. Similar results were obtained by Hussaini (1973) who performed plane strain and triaxial tests on specimens of Chattahoochee sand prepared at initial D_r between 30 % and 100 %, at σ_3 = 490 kPa. The results of these tests are shown in Fig. 2.4, from which the following can be noted.

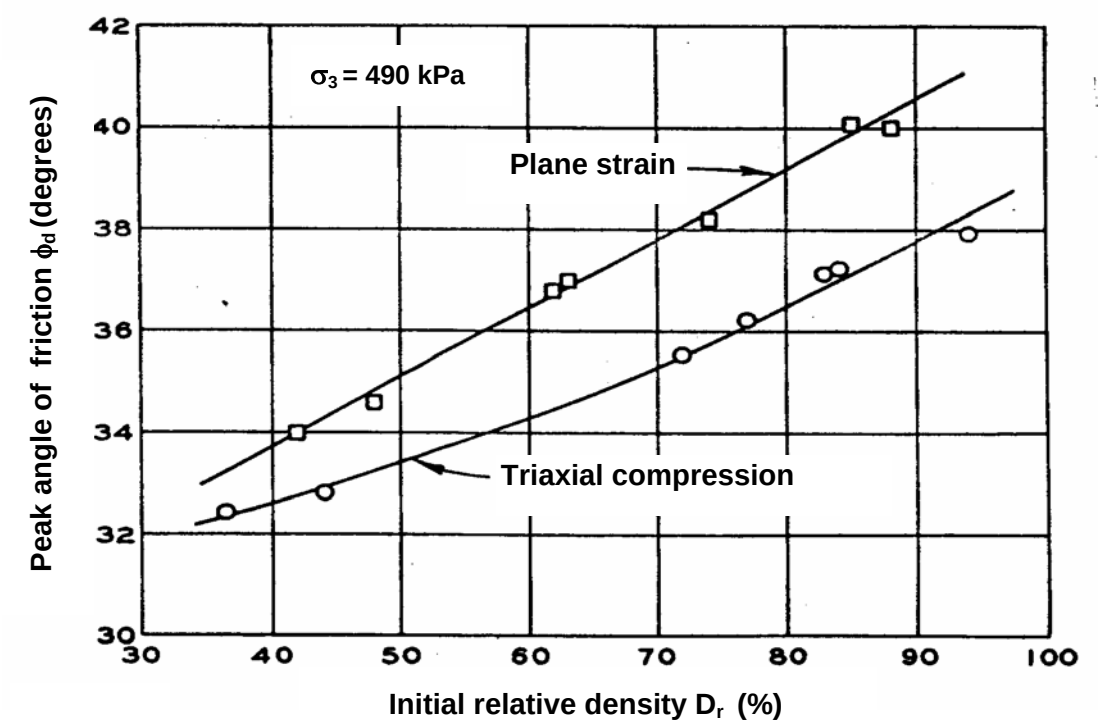

Figure 2.4. Variation of the peak angle of friction with initial relative density for Chattahoochee sand (after Hussaini, 1973)

(a) An increase in D_r resulted in an increase in both ϕ_{ps} and ϕ_t.

(b) The values of ϕ_{ps} were higher than those of ϕ_t. A decrease in D_r caused the difference (ϕ_{ps} - ϕ_t) to decrease, as observed by Lee (1970) and Cornforth (1973) (paragraphs (5) and (6)); the difference was about 3^o for dense sand and about 1^o for loose sand.

8. Marachi et al. (1981) performed plane strain and triaxial tests on specimens of Monterey sand prepared at densities ranging from loose to dense, under $\sigma_3 = 70$ kPa to 3450 kPa. Specimens were prepared to initial void ratios e_o of 0.75, 0.65, and 0.55, corresponding to initial D_r of 27 %, 60 %, and 90 % respectively. Typical stress - strain curves for plane strain and triaxial tests at $\sigma_3 = 70$ kPa are shown in Fig. 2.5, from which the following can be noted.

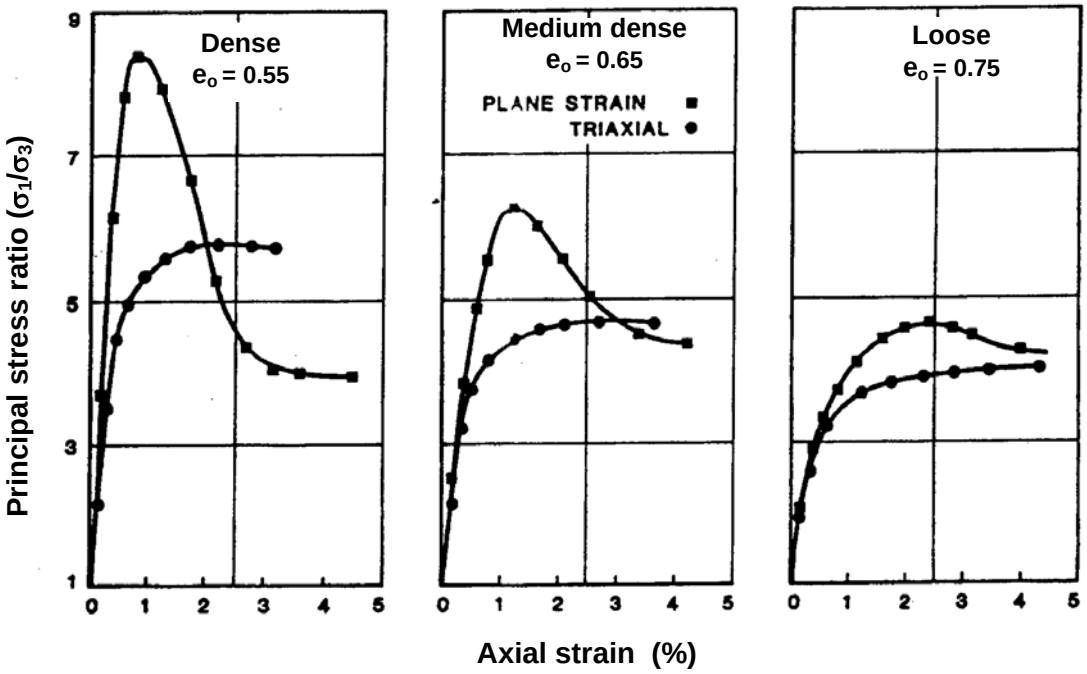

Figure 2.5. Stress - strain relationship for plane strain and triaxial specimen ($\sigma_3 = 70$ kPa) (after Marachi et al., 1981)

(a) The plane strain test yields higher values of maximum principal stress ratio $(\sigma_1/\sigma_3)_f$ than the triaxial test for the same void ratio.

(b) An increase in e_o causes a decrease in $(\sigma_1/\sigma_3)_f$ for both triaxial and plane strain tests.

(c) When e_o increases, the difference between the $(\sigma_1/\sigma_3)_f$ values for plane strain and triaxial tests decreases.

(d) The plane strain specimens fail or reach $(\sigma_1/\sigma_3)_f$ value at smaller values of axial strain $(\varepsilon_1)_f$ than the triaxial specimens.

(e) The values of $(\varepsilon_1)_f$ for plane strain and triaxial tests are larger for loose specimens than for dense specimens.

9. Fig. 2.6 shows the variation of ϕ_d with σ_3 for the triaxial and plane strain tests. This figure indicates the following.

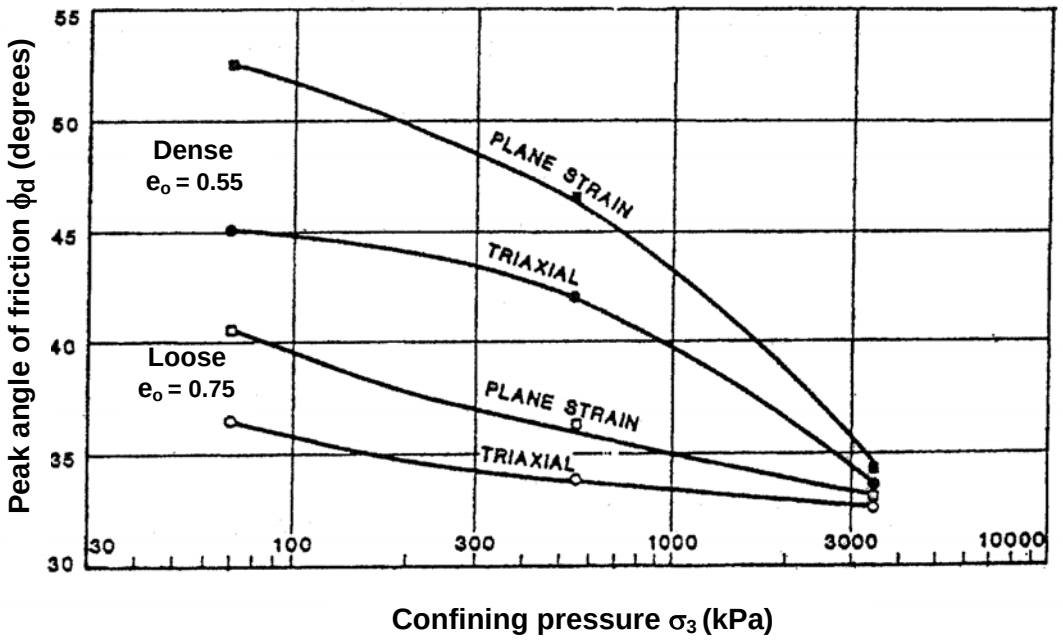

Figure 2.6. Variations of peak angles of friction with confining pressure (after Marachi et al., 1981)

(a) The difference $(\phi_{ps} - \phi_t)$ is greatest for dense specimens at $\sigma_3 = 70$ kPa; $(\phi_{ps} - \phi_t)$ is about 7^o and 4^o for tests for e_o values of 0.55 and 0.75 respectively. When e_o or σ_3 increases, the difference between $(\phi_{ps} - \phi_t)$ decreases. This difference is about

1^o for $\sigma_3 = 3450$ kPa. These results confirm Lee's (1970) findings (paragraph (5)) that the difference between values of ϕ_{ps} and ϕ_t is linked with dilatation.

(b) The ϕ_d values are found to be higher for dense sands than for loose sands, which is due to greater interlocking in the former in conformity with Lambe & Whitman's (1979) views (section 2.1.2). For both dense and loose specimens, an increase in σ_3 causes a decrease in ϕ_d measured in both tests, which is due to particle crushing, as discussed in section 2.1.3.

10. By considering Matsuoka's (1974) (quoted by Wroth, 1984) failure criterion for soils, Wroth (1984) investigated the effect of intermediate principal stress on shear strength. He gives the following approximate relation.

$$8\ (\phi_{ps}) = 9\ (\phi_t) \qquad \text{.....(2.8)}$$

11. This equation does not take into account factors which influence shear strength of sands such as density, confining stress, mineralogical composition, inclination of the shear plane to the bedding planes.

12. Bolton (1986) collated extensive data on the strength and dilatancy of 17 sands available in the literature in plane strain and triaxial tests at different densities and confining pressures to produce empirical relations by which ϕ_d could be predicted. He introduced a relative dilatancy index (I_R), in terms of relative density and applied stress level, of the form

$$I_R = D_r\ [Q_g - \ln(p')] - s \qquad \text{.....(2.9)}$$

where p' (kPa) is the mean effective stress $(\sigma_1' + \sigma_3') / 2$; Q_g is a function of grain type, and s is a constant.

13. In deriving simple correlations amongst I_R, D_r, and p', it was found that $Q_g = 10$ and $s = 1$ gave the best fit for the different sands collated. This yielded

$$I_R = D_r [10 - \ln(p')] - 1 \quad \text{.....(2.10)}$$

14. Bolton (1986) also obtained the following correlations between I_R and $(\phi_d - \phi_{cv})$:

For plane strain tests

$$(\phi_{ps}) - (\phi_{cv})^{ps} \approx 5\, I_R \quad \text{.....(2.11)}$$

For triaxial tests

$$(\phi_t) - (\phi_{cv})^{t} \approx 3\, I_R \quad \text{.....(2.12)}$$

where $(\phi_{cv})^{ps}$ and $(\phi_{cv})^{t}$ are the ultimate friction angles measured in plane strain and triaxial tests respectively.

15. Bolton (1986) stated that the sands presented in his study were mainly of quartz and feldspar ($Q_g = 10$); the presence of substantial proportions of mica, calcite or other materials ($Q_g \approx 5$ to 8) would be bound to affect both ϕ_{cv} and the crushing which reduces I_R at high stresses; this implies that the parameter Q_g in equation (2.9) should be reduced for soils of weaker grains.

16. Schanz & Vermeer (1996) have eliminated I_R between equations (2.11) and (2.12), and obtained the following equation to correlate ϕ_{ps} and ϕ_t for sands.

$$\phi_t = (3\, \phi_{ps} + 2\, \phi_{cv}) / 5 \quad \text{.....(2.13)}$$

where ϕ_{cv} is assumed to be the same in plane strain and triaxial tests. As seen, this equation is independent of Q_g and s but is dependent on ϕ_{cv} which is affected by mineralogy (paragraph (15)).

17. Schanz & Vermeer (1996) checked the validity of equation (2.13) with their own data together with data from additional sources (Cornforth (1964) and Leussink et al. (1966), quoted by Schanz & Vermeer, 1996), as in Fig. 2.7. All the sands, the results of which have been quoted in Fig. 2.7, consist mainly of quartz and feldspar grains, and their ϕ_{cv} have been assumed to be the same. For sands of weaker grains, a lower ϕ_{cv} would be expected (paragraph (15)). Schanz & Vermeer (1996) also report that for loose specimens the difference between ϕ_{ps} and ϕ_t is very small or nil, as observed by previous researchers (Lee, 1970; Cornforth, 1973; Hussaini, 1973; Marachi et al., 1981) (paragraphs (5), (6), (7), and (9) respectively).

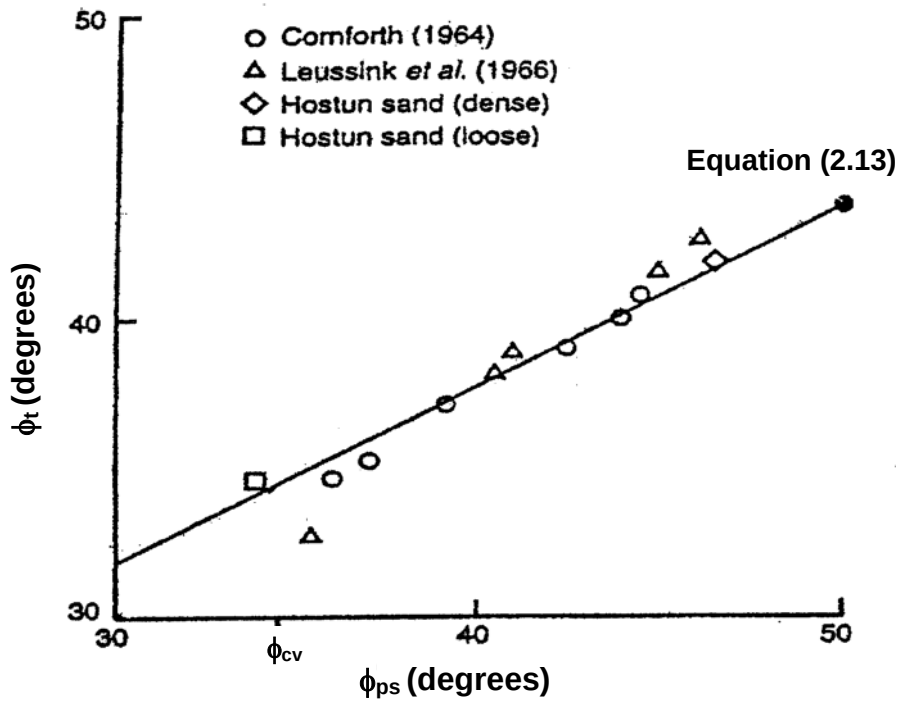

Figure 2.7. Maximum strength under plane strain and triaxial tests (after Schanz & Vermeer, 1996)

18. Mirata & Gökalp (1997) tested the applicability of the cylindrical wedge shear test (cylwest) (Mirata, 1991) to sands. A sand to which 30% crushed stone of up to 10 mm particles was added (sample S1), and the same sand with 30% subangular gravel up to 5 mm particles (sample S2) were tested in cylwests and triaxial tests. They investigated the difference between ϕ_{ps} and ϕ_t by assuming that ϕ_d values measured in cylwests represent ϕ_{ps}; their results are given in Fig. 2.8 against ϕ_t. The circular point represents the results of the tests on sample S1, and the triangular point those on sample S2. The chain-dotted lines representing equation (2.13) for these samples have been plotted by assuming ϕ_{cv} to be equal to the ultimate friction angle measured in cylwests. The full line represents equation (2.13) for the Hostun sand tested by Schanz & Vermeer (1996). The dashed line represents Wroth's (1984) equation (2.8). For a given ϕ_{cv}, the proximity of the results to both

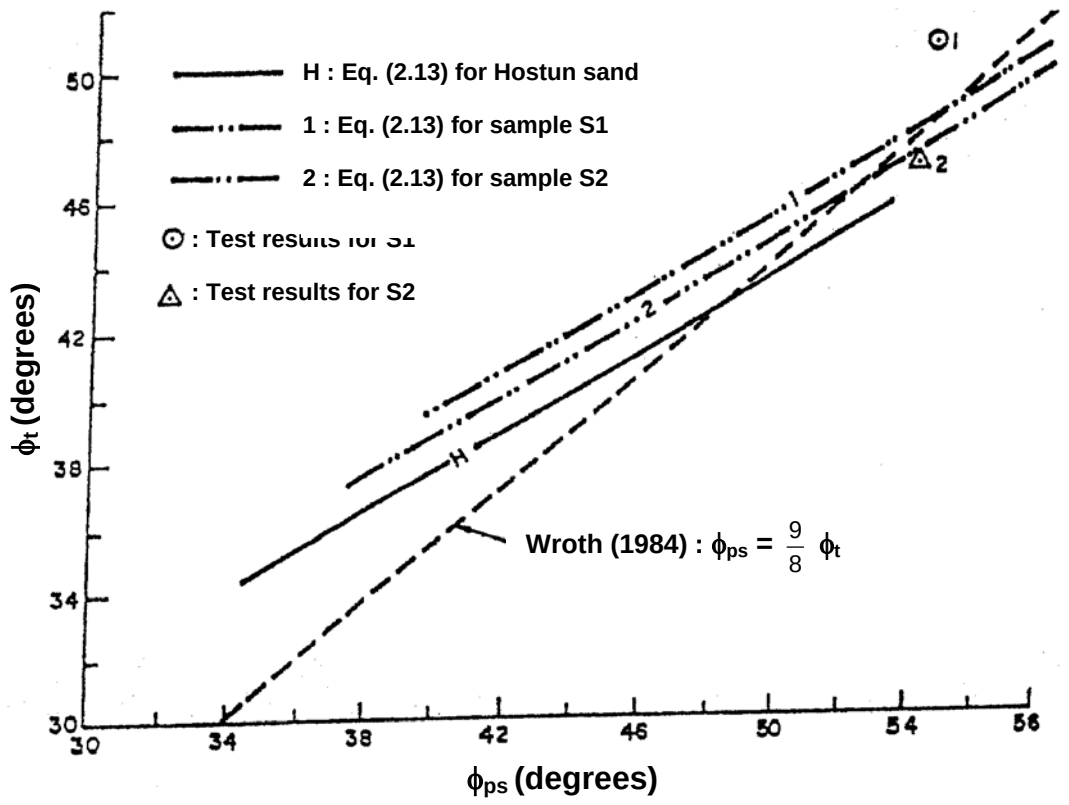

Figure 2.8. Comparison of relationships between peak angles of friction in plane strain and triaxial tests (after Mirata & Gökalp, 1997)

Schanz & Vermeer's (1996) equation (2.13) and to Wroth's (1984) equation (2.8), particularly for sample S2, was found noteworthy by Mirata & Gökalp (1997), who suggested that in the absence of plane strain equipment, the cylwest might be used to investigate the difference between ϕ_{ps} and ϕ_t.

19. Adel (2001) performed triaxial and plane strain tests on samples of three types of silica sand at σ_3 values of 172 kPa and 344 kPa. The physical properties of the sands are summarized in Table 2.2. He obtained results indicating the following.

Table 2.2. Physical properties of the sands (after Adel, 2001)

Sand type	Grading	Particle shape	G_s	e_{max}	e_{min}	C_u	D_{50}
A	Uniform	Rounded	2.65	0.80	0.40	2.40	0.22
B	Uniform	Angular	2.63	0.90	0.50	2.33	0.65
C	Well graded	Angular	2.64	0.95	0.40	2.00	0.65

(a) The values of ϕ_{ps} were about 5% to 12% higher than those of ϕ_t for dense sands, whereas they were slightly higher or equal for the case of loose sands. This is consistent with previous findings (Lee, 1970; Cornforth, 1973; Hussaini, 1973; Marachi et al., 1981; Schanz & Vermeer, 1996) (paragraphs (5), (6), (7), (9), and (17) respectively).

(b) The values of axial strain at failure $(\varepsilon_1)_f$ for triaxial tests were always higher than those for plane strain tests for the same initial porosity. This is in conformity with Fig. 2.5.

(c) The values of volumetric strain (ε_v) were higher for dense sand than for loose sand. The values of ε_v at failure $(\varepsilon_v)_f$ for sand C were higher than those for sands A and B under the same conditions. This was due to the fact that sand C was well graded with angular particles, which resulted in a high degree of interlocking between particles, and so to a larger dilatation during shear.

2.1.5 Effect of Particle Composition

2.1.5.1 Definitions

"The use of relative density correlations based on an average sand to predict soil behaviour without considering the particle composition can result in poor or misleading predictions. So, this question arises: Do granular soils at the same relative density have the same properties? Tests on medium to fine sands with varying particle compositions indicate that granular soils at the same relative density can have drastically different engineering properties. Variations in engineering properties due to particle composition can be as large as variations associated with large differences in relative densities." (Holubec & D'Appolonia, 1973.)

The composition of sand can have an important influence on its friction angle, indirectly by influencing initial void ratio e_o, and directly by influencing the amount of interlocking occurring for a given e_o (Kezdi, 1974).

Composition effect can be explained in terms of the size, shape, gradation, and mineralogy of the particles. The particle size effect on the shear strength can be evaluated by varying the effective size, D_{10}, of the particles. The gradation effect on the shear strength can be evaluated by varying the coefficient of uniformity (C_u) of the soil. The particle shape effect can be evaluated by varying sphericity and angularity. (Koerner, 1970.) The definitions and method of measurement of some of these properties are given in the following paragraphs.

The following paragraph has been summarized from Yudhbir & Rahim (1991); the references are those quoted by the authors.

Sedimentologists generally express particle shape in terms of surface texture, sphericity, and roundness (Blatt et al., 1971). Surface texture is used to describe irregularities of the surface of particles that are too small to affect the overall shape.

Sphericity, as defined by Wadell (1932), is the ratio of the surface area of a sphere having the same volume as the soil particle to the surface area of the particle. A sphericity value of one implies a perfect sphere, and the sphericity value decreases with the irregularity of particles. *Roundness* is related to the sharpness of the corners and edges on grain surfaces. Wadell (1932) defined roundness as the ratio of the average radii of corners of the grain image to the radius of the inscribed circle. Powers (1953) placed particles into classes based on comparisons with photographs of grain types using six grade terms (Table 2.3). The description for each grade term as recommended by Youd (1973) is also presented in Table 2.3. Typical particles assigned to each category as given by Youd (1973) are shown in Fig. 2.9.

Table 2.3. Powers roundness criteria and values (after Youd, 1973)

Roundness class	Description	Roundness interval	Mean roundness
Very angular	Particles with unworn fractured surfaces and multiple sharp corners and edges	0.12 - 0.17	0.14
Angular	Particles with sharp corners and approximately prismodial or tetrahedral shapes	0.17- 0.25	0.21
Subangular	Particles with distinct but blunted or slightly rounded corners and edges	0.25 - 0.35	0.30
Subrounded	Particles with distinct but well-rounded corners and edges	0.35 - 0.49	0.41
Rounded	Irregularly shaped rounded particles with no distinct corners or edges	0.49 - 0.70	0.59
Well rounded	Smooth nearly spherical or ellipsoidal particles	0.70 - 1.00	0.84

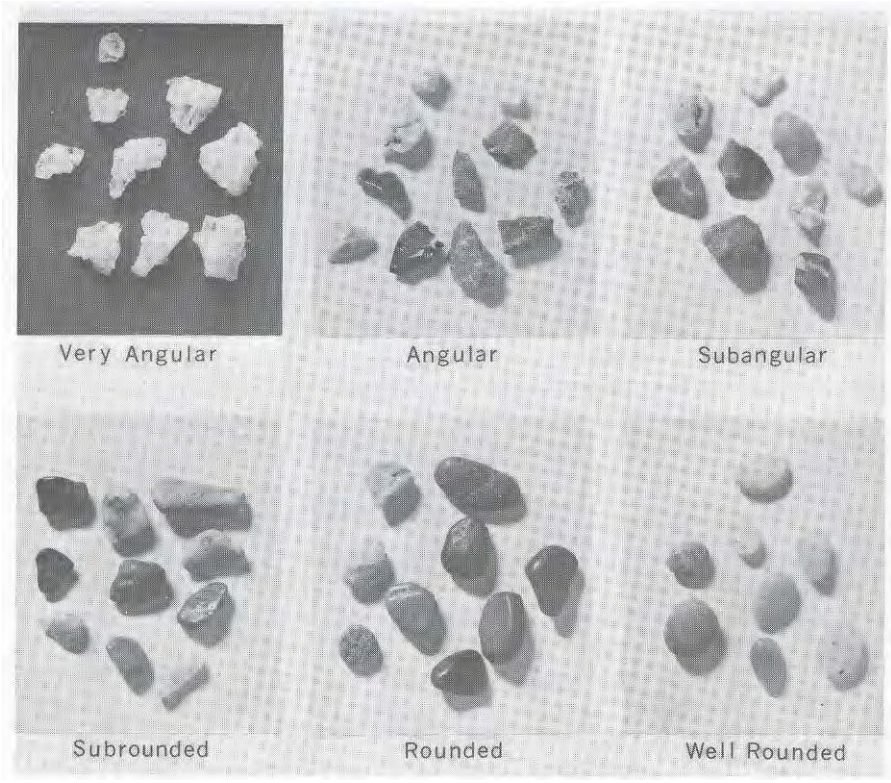

Figure 2.9. Typical particles assigned to each category (after Youd, 1973)

Dobkins & Folk (1970) developed a method for measuring the roundness of the particle. In this method, roundness of a particle (R_F) is calculated by

$$R_F = d_k / d_i \quad \text{.....(2.14)}$$

where d_k is the diameter of curvature of the sharpest corner and d_i is the diameter of the inscribed circle (Fig. 2.10). A very well rounded particle has a maximum R_F of 1.00; an extremely angular particle has a value close to 0.00.

Riley Sphericity S_R developed by Riley (1941) is found by

$$S_R = (d_i/d_c) \quad \text{.....(2.15)}$$

where d_c is the diameter of the circumscribing circle (Fig. 2.10). A perfectly spherical particle has an S_R value of 1.00; smaller values mean departure from a spherical shape, the theoretical extreme being 0.00.

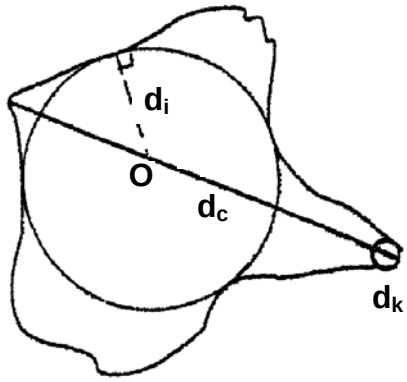

Figure 2.10. Definitions of angularity and sphericity (after Norman, 2000(c))

The calculations of sphericity and roundness are complex; but the values of R_F and S_R can be estimated by using comparison charts (Fig. 2.11) including silhouettes or photographs of grains whose roundness and sphericity values have already been calculated.

2.1.5.2 Effect of Particle Shape and Mineral Composition

The following paragraph has been taken from Shahu & Yudhbir (1998); the references are those quoted by the authors.

The angularity and mineralogical composition of a sand affect its mechanical and engineering properties significantly. Winterkorn & Fang (1986) have stated that the peak angle of friction ϕ_d value for a given initial relative density D_r depends largely upon particle shape and gradation of sand. Rahim (1989) has shown that the mechanical characteristics of a sand such as its compressibility and crushing are strongly influenced by the shape of sand particles (Yudhbir & Wood 1989; Yudhbir & Rahim, 1991).

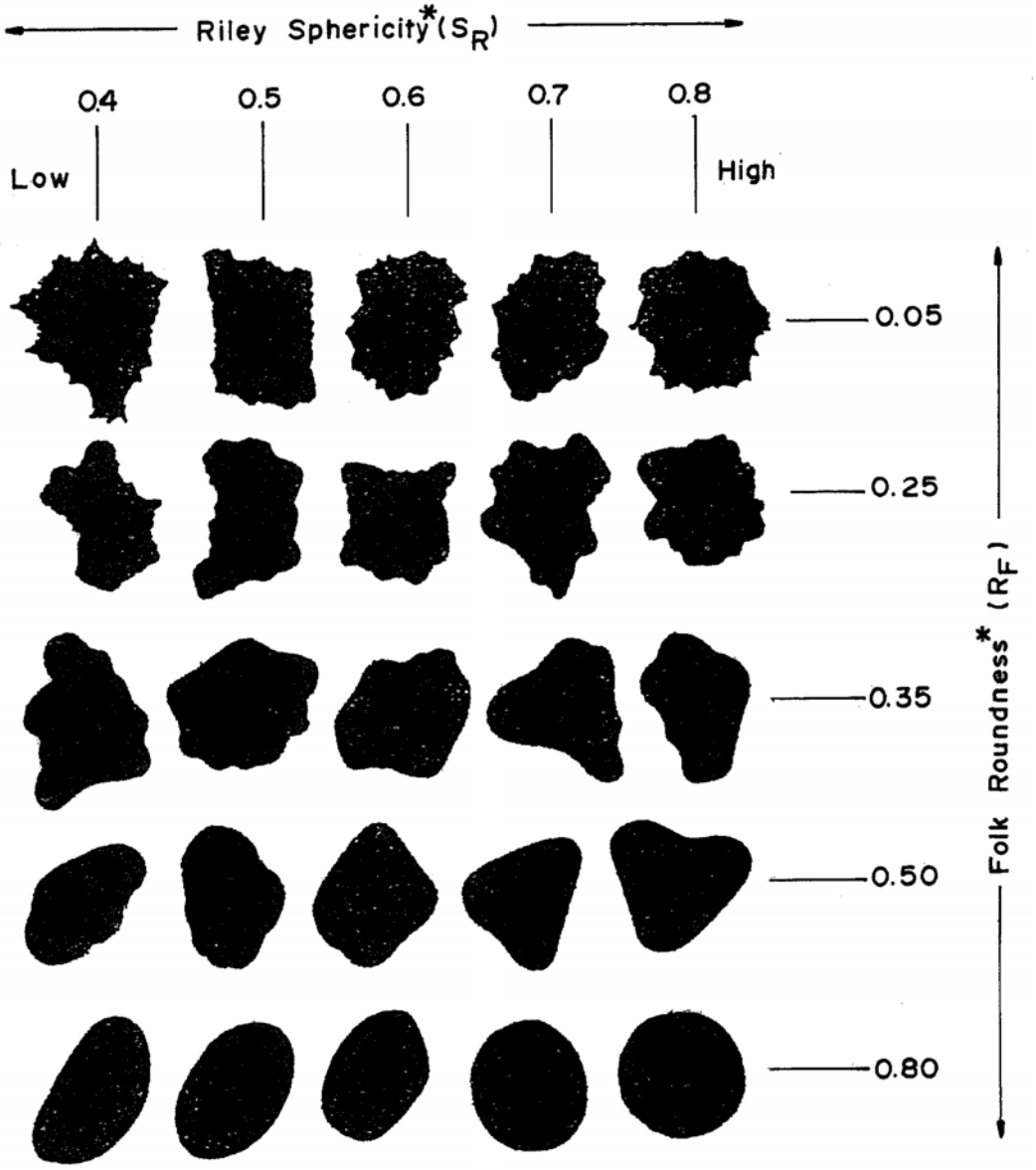

Degrees of roundness according to Russel-Taylor-Pettijohn (after Schneiderhöhn, 1954) (quoted by Norman, 2000(c)). From top to bottom: angular - subangular - subrounded - rounded - well rounded.

* Scales of S_R and R_F added by Norman (2000(c)).

Figure 2.11. A visual comparison chart for roundness and sphericity (after Norman, 2000(c))

The following paragraph has been taken from Ueng & Chen (2000); the references are those quoted by the authors.

"For sands with grains of low strength or with very angular shapes, for example decomposed granite (Miura & O-hara, 1979), calcareous sand (Noorany, 1989), and shaley alluvial sand (Ueng et al., 1988), particle crushing can be quite significant even under the low pressures commonly encountered in a soil deposit. The behaviour of these sands deviated from the relationship developed for sands with hard, less crushable particles."

Koerner (1970) studied the effect of particle shape as measured by its sphericity and angularity on three different saturated quartz samples of the same effective size and gradation. The physical properties of these samples are summarized in Table 2.4. All soils were tested in triaxial tests with σ_3 = 210 kPa and with densities varying from loose to dense. He found that less spherical and more angular soils have significantly higher ϕ_d values. This is an expected result, as these soils would interlock more thoroughly than rounded ones.

Table 2.4. Physical properties of the quartz samples (after Koerner, 1970)

Quartz samples	Sphericity	Particle shape	C_u	D_{10}
A	0.45	Angular	1.25	0.25
B	0.55	Subangular	1.25	0.25
C	0.67	Subrounded	1.25	0.25

The following three paragraphs have been summarized from Holubec & D'Appolonia (1973); the references are those quoted by the authors.

Holubec & D'Appolonia (1973) studied the effect of particle shape on the engineering properties of granular soil. They tested four granular materials with particles in the medium to fine sand range in triaxial tests to obtain stress - strain characteristics of these materials. The materials tested included glass beads, and Ottawa, Southport, and Olivine sands. The particle shape of the sands was measured by an indirect method based on permeability developed by Hoffman (1959). In this measurement, a very well rounded particle has a minimum coefficient of angularity (E) of 1.00 while an extremely angular particle has a value close to 2.00. The index properties of the materials are shown in Table 2.5 in the order of increasing particle angularity.

Table 2.5. Composition properties of glass beads and sands (after Holubec & D'Appolonia, 1973)

Material	E	D_{10}	C_u
Glass beads	1.16	0.40	1.5
Ottawa sand	1.24	0.24	1.9
Southport sand	1.55	0.15	1.8
Olivine sand	1.64	0.38	1.5

The results of triaxial tests for the four materials at various relative densities are shown in Fig. 2.12. This figure shows that each of the four sands has a separate and distinct D_r and ϕ_d relationship. It is seen that the glass beads have the smallest ϕ_d and exhibit the least increase in ϕ_d with increasing D_r. Ottawa sand with subrounded particles has intermediate ϕ_d values and shows the largest increase in ϕ_d with D_r. Finally, Southport and Olivine sands with angular particles have the highest ϕ_d values with an intermediate increase in ϕ_d with increasing D_r.

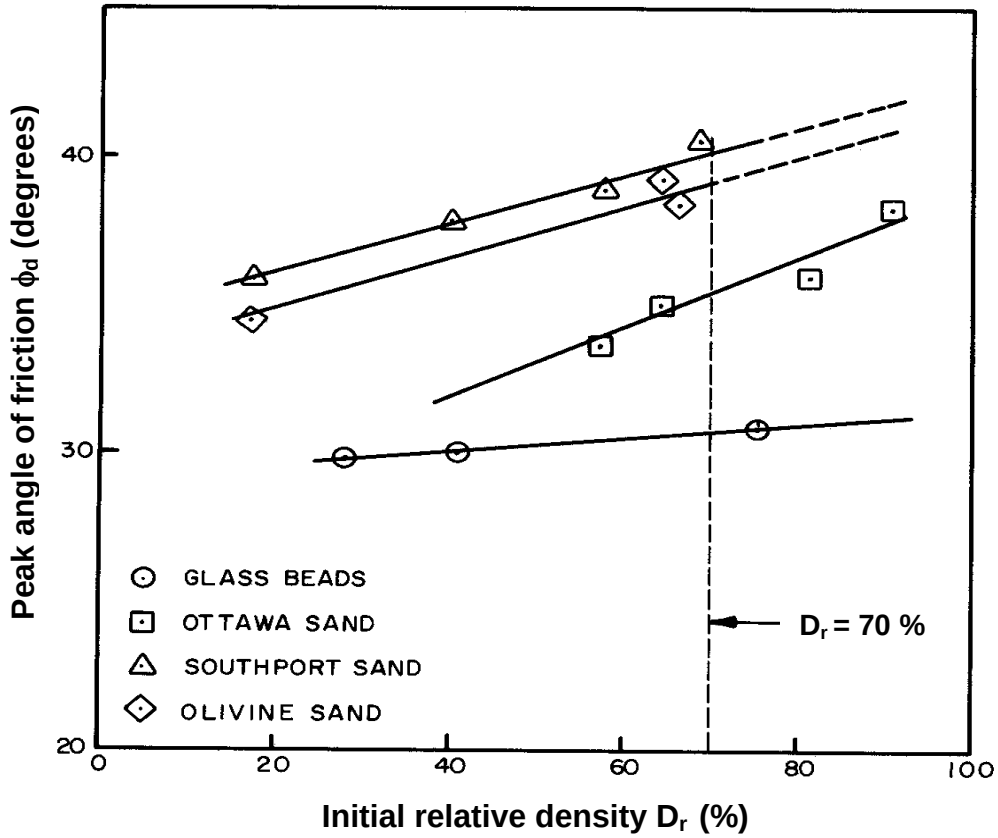

Figure 2.12. Effect of particle shape on the ϕ_d value (after Holubec & D'Appolonia, 1973)

The ϕ_d values obtained at D_r values of 40 %, 70 %, and 90 % have been plotted against the coefficient of angularity in Fig. 2.13 to illustrate the effect of particle shape on the ϕ_d. This figure indicates that the value of ϕ_d is a function of both D_r and particle shape. Furthermore, it is observed that equally large differences in ϕ_d are possible with variations of particle shape as with changes in D_r. The ϕ_d values of Ottawa and Southport sands at D_r = 70 % are 35^o and 40^o, respectively, representing a 5-degree difference. On the other hand, the ϕ_d value of Southport sand increased by 4 degrees with densification from D_r = 40 % to D_r = 90 %.

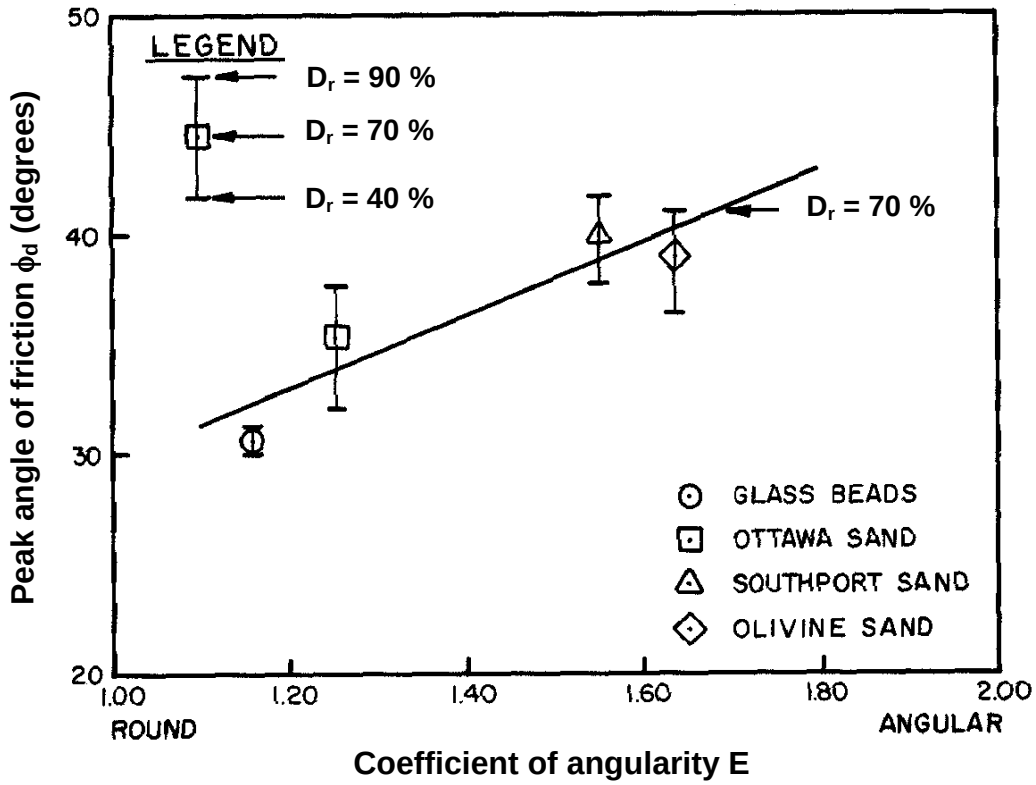

Figure 2.13. Effect of particle shape on the ϕ_d value (after Holubec & D'Appolonia, 1973)

The following paragraph has been summarized from Ueng & Chen (2000); the references are those quoted by the authors.

Ueng & Chen (2000) performed triaxial tests on Fulung sand and Tamsui River sand to investigate the effect of particle crushing on the shear strength of sand. Fulung sand is a fine beach sand composed mainly of subangular quartz grains. Tamsui River sand is a river sand composed of about 40 % - 50% flaky, friable shale and slate particles, 30 % - 40 % angular to subangular quartz particles, and a small amount of other minerals, including limonite and magnetite. They reanalyzed the experimental data obtained by Miura & O-hara (1979) for decomposed granite and used this data for comparison in their study. This decomposed granite is a well graded, very angular sand, and contains both single mineral particles (e.g. feldspar, mica, quartz etc.) and rock particles composed of mixed minerals. Physical

properties of the three different sands are summarized in Table 2.6. Ueng & Chen (2000) obtained data indicating the following points.

Table 2.6. Physical properties of the sands (after Ueng & Chen, 2000)

Sand type	Particle shape	G_s	D_{50} (mm)	C_u	e_{max}	e_{min}	e_{max}- e_{min}
Fulung sand	Subangular	2.66	0.20	1.4	1.010	0.678	0.332
Tamsui River sand	Angular to subangular	2.73	0.29	1.7	1.190	0.818	0.372
Decomposed granite	Angular	2.62	0.82	6.0	0.944	0.505	0.439

(a) Compression of the specimens under consolidation pressures caused some particle crushing; the majority of particle crushing occurred during the shearing process.

(b) The amount of particle crushing increased with σ_3 and D_r.

(c) The effect of particle crushing on the ϕ_d value was the highest for decomposed granite with very angular particles, followed by Tamsui River sand, and was least for Fulung sand with the stronger particles. The decomposed granite, with more angular particles and a higher (e_{max} - e_{min}) value, gave a higher reduction in the values of ϕ_d. This is in agreement with Maeda & Miura's (1999(b)) findings (section 2.1.3, paragraph (9)).

2.1.5.3 Effect of Particle Size

In general, an increase in the particle size increases the load per particle, and hence crushing begins at a smaller confining stress, and causes a reduction in the ϕ_d value (Lambe & Whitman, 1979).

To investigate the influence of grain size on shear strength, Kirkpatrick (1965) performed a series of triaxial tests on Leighton Buzzard sand and glass beads under the confining pressures of 345 kPa and 138 kPa respectively. The results of the tests on six Leighton Buzzard sands of different particle size at three different porosities indicated that an increase in particle size leads to a decrease in the ϕ_d value for the same porosity. A similar trend was observed for three samples of glass beads of different particle size. He stated that this decrease in the ϕ_d values is accompanied by a decrease in the rate of dilatation at failure. The ϕ_d value decreasing with an increase in particle size is in conformity with Lambe & Whitman's (1979) views.

2.1.5.4 Effect of Gradation

A number of researchers investigated the gradation effect on the shear strength by varying the coefficient of uniformity (C_u) of the soil mass. A brief summary follows.

Koerner (1970) performed triaxial tests on saturated samples of three different sands each consisting of only one of these minerals: quartz, feldspar, and calcite. The values of C_u were 1.25, 2, and 5. The results of these tests indicated that there was negligible effect of C_u on ϕ_d in the quartz sands, but for feldspar and calcite, an increasing C_u gave higher ϕ_d values.

Koerner's (1970) findings are a confirmation of Winterkorn & Fang's (1986) views, quoted by Shahu & Yudhbir (1998) (section 2.1.5.2), and Lambe & Whitman's (1979) views (Table 2.7) that a better graded sand has a larger friction angle compared to uniform sand, due to a better interlocking and less particle breakage in the former, the less breakage arising from the fact that in a well graded sand there are more interparticle contacts and the load per contact is thus less than in a uniform sand.

Table 2.7. Effect of particle shape and grading on peak friction angle (quoted from Sowers (1951) by Lambe & Whitman, 1979)

Particle shape and grading	Peak friction angle (degrees)	
	Loose state	Dense state
Rounded, uniform	30	37
Rounded, well graded	34	40
Angular, uniform	35	43
Angular, well graded	39	45

2.2 Effect on Shear Strength of the Inclination of the Shear Plane to the Bedding Plane in Plane Strain Tests

The sand properties depend on the angle between the shear plane and the bedding plane (Arthur & Menzies, 1972; Arthur et al., 1977; Tatsuoka et al., 1986) (quoted by Jewell, 1989). The maximum plane strain friction angle $(\phi_{ps})_{max}$ occurs when the sample is sheared across the bedding planes; the minimum plane strain friction angle $(\phi_{ps})_{min}$ occurs when the sample is sheared along the bedding planes. The difference between $[(\phi_{ps})_{max} - (\phi_{ps})_{min}]$ depends on the soil particle shape and grading, and the method of soil deposition. For laboratory prepared samples of dense sand, the tangent of the plane strain friction angle can vary by as much as 25% due only to the orientation of shearing with respect to the bedding planes (Tasuoka, 1987; Arthur et al., 1988) (quoted by Jewell, 1989). When the inclination of the shear plane to the bedding plane becomes lower, it is possible that lower ϕ_{ps} values and so lower or negative values of the difference $(\phi_{ps} - \phi_t)$, discussed in section 2.1.4, paragraphs (4) to (9), may be obtained, as observed by Oda et al. (1978), and Tatsuoka et al. (1986).

2.3 Wedge Shear Tests

Unless otherwise stated, this section has been summarized from Mirata (1991, 2003(a)).

The in situ wedge shear test (iswest) was developed (Mirata, 1974) as a simpler means than the in situ large shear box test for measuring the shear strength of unsaturated, fissured and/or stony clays. A different version of the iswest is the cylindrical wedge shear test (cylwest) developed for enabling cylindrical samples of clay (up to 10 mm dia.) taken from boreholes to be tested without the risk of entering a test pit in an active landslide to perform an in situ test. The prismatic wedge shear test (priswest) is a larger version of the cylwest, enabling prismatic specimens of gravel, crushed rock or clay containing up to 40 mm particles to be tested, using a portable frame. The test procedures for the last two versions are summarized in sections 5.1.3 and 5.2.3.

2.3.1 Calculation of Stresses and Displacements

2.3.1.1 Introduction

The assumptions and calculations for the different types of analysis, which will be explained below, based mainly on Fig. 2.14, are valid for all versions of the wedge shear test. Basically the problem is one of summing up the normal and shear components of all forces, and dividing these by the corrected area of the shear plane. Differences in analysis arise in deciding which to take as the shear plane and whether to consider the slight rotation β (Fig. 2.15) of the test mould during the test. Distinction is made between three types of analysis explained in the following sub-sections.

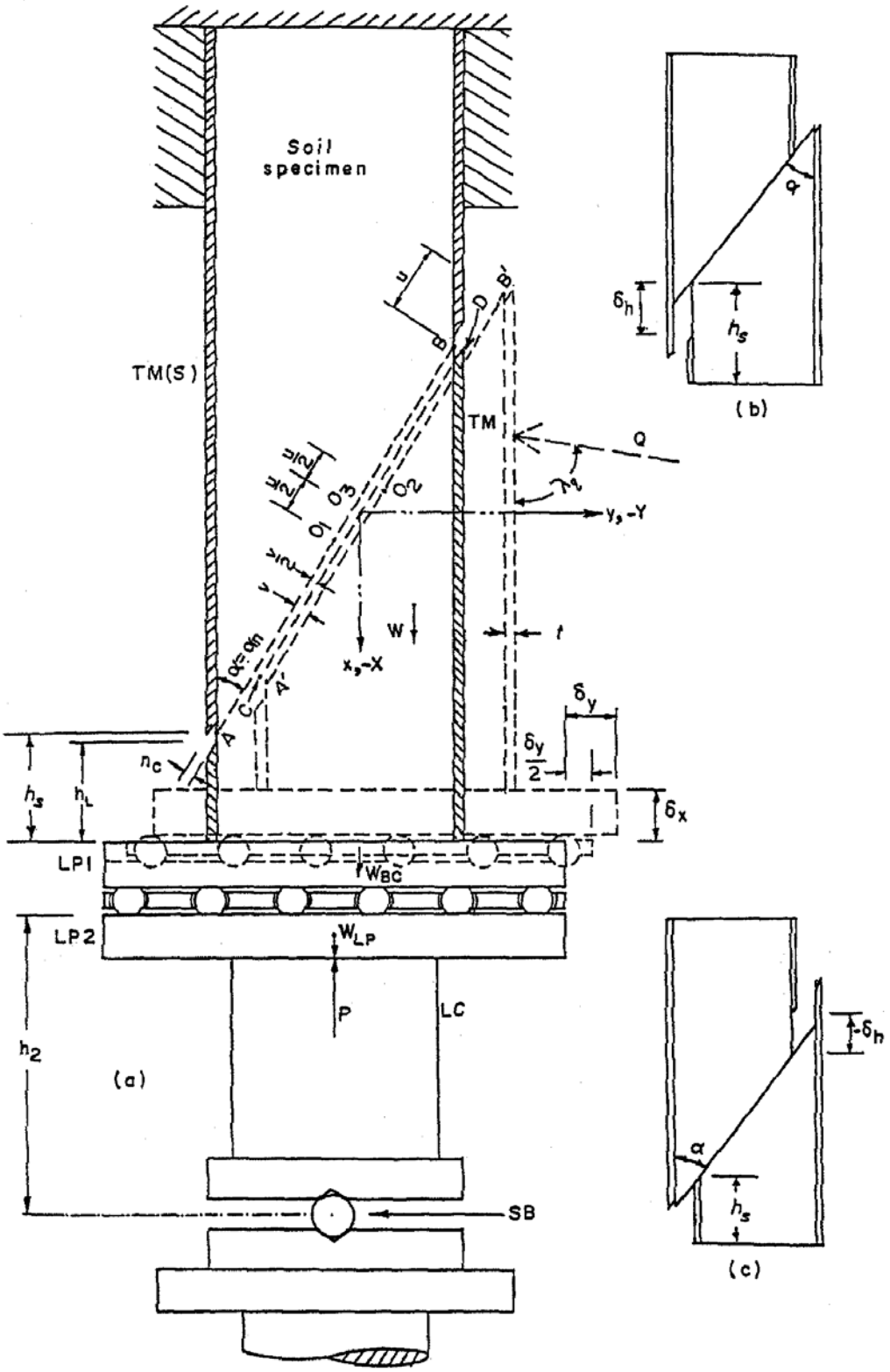

Figure 2.14. Forces, displacements and distances in simplified analysis of cylwest showing (a) usual mode of failure, (b) and (c) alternative modes (after Mirata, 1991; 2003(a))

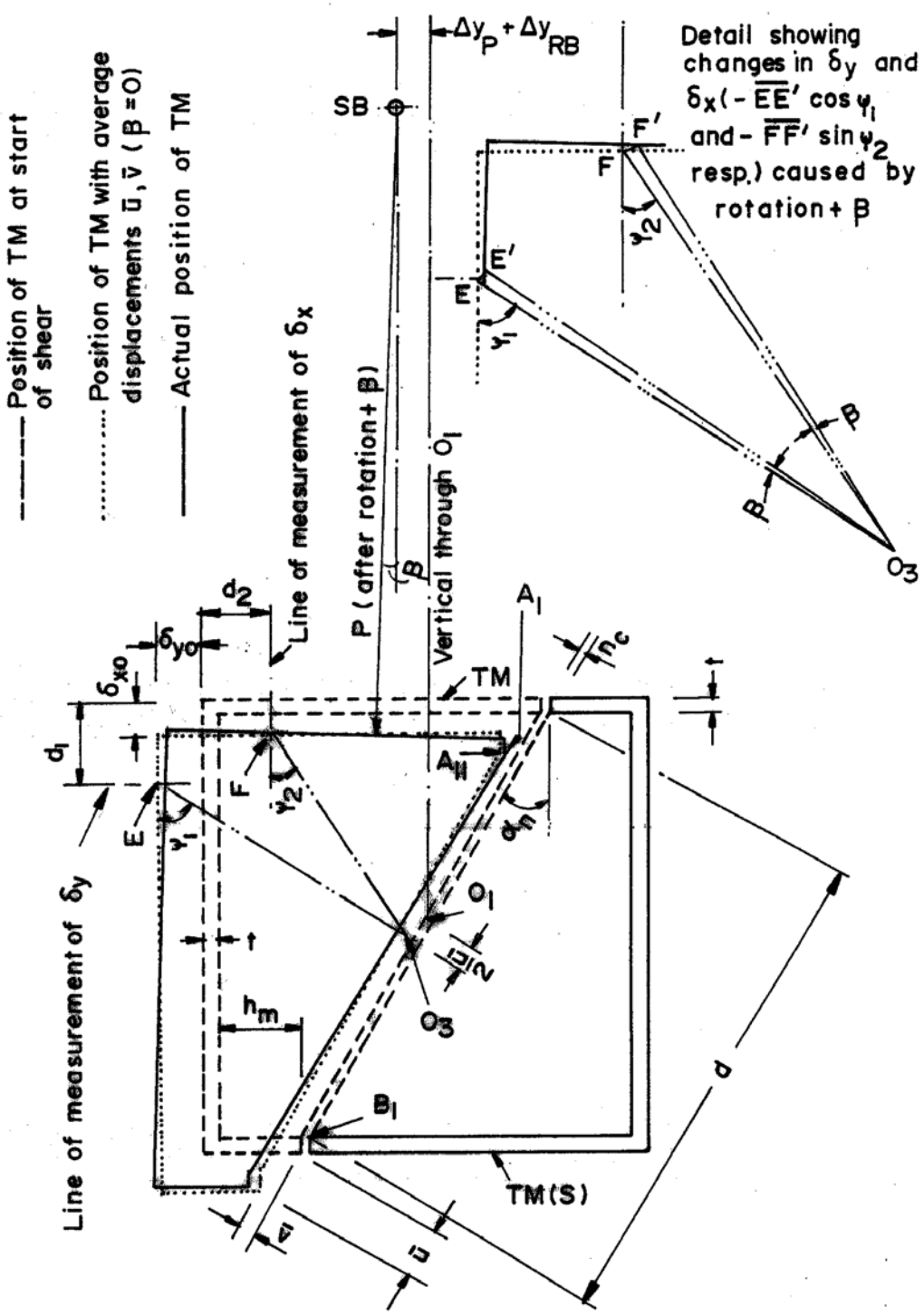

Figure 2.15. Effect of mould rotation on the measured values of δ_x and δ_y in priswests (after Mirata, 1991; 2003(a))

2.3.1.2 Simplified Analysis (Analysis A)

This analysis may be considered adequate for most practical purposes. The soil is assumed to break along the plane AB (Fig. 2.14) midway between the stationary half TM (S) of the test mould and the initial position of the mobile half TM, and to move without rotation so that the lower part of the failure plane lies along A′B′. The average corrected shear plane is taken as CD, midway between AB and A′B′. O_1, O_2, and O_3 denote the midpoints of AB, A′B′, and CD respectively. The components X, Y of all forces parallel and normal to the force P, recorded through the load cell LC, are (Fig. 2.14)

$$X = P - (W + W_{BC} + W_{LP})\sin\theta + \delta X_q \quad \text{.....(2.16)}$$

$$Y = (W + (M_B / D))\cos\theta + \mu P + \delta Y_q \quad \text{…….....…….……(2.17)}$$

where δX_q and δY_q are the additions to X and Y due to the lateral load Q and are given by

$$\delta X_q = Q\cos\lambda_q - SW_{qn}\sin\lambda_q \quad \text{…….....……..……...(2.18)}$$

$$\delta Y_q = Q\sin\lambda_q + SW_{qn}\cos\lambda_q \quad \text{…….....……...(2.19)}$$

and D is the perpendicular distance between the grooves on LP1 and the single ball SB, and is constant in cylwests where a compression machine is used, but increases by δ_x (or δ_{xo} in analyses B and C) during the test in all wedge shear tests where a hydraulic jack is used; the angle θ between P and the horizontal ($\theta = 90^o$ in cylwests; $\theta = -90^o$ in priswests performed as in Fig. 2.15 and $\theta = 0^o$ in priswests performed with P horizontal); M_B is the sum of moments about SB of all components between the grooves of LP1 and SB when $\theta = 0^o$; W is the total weight of the soil wedge, the test mould TM and LP1; W_{BC} and W_{LP} are the weights of the ball cage and the grooved

loading plate LP2 respectively; W_{qn} is the component normal to Q of the simply supported reaction due to the self-weight of the lateral loading device; λ_q is the angle between P and Q; μ is the coefficient of friction against the motion of LP1 relative to LP2 with the steel balls rolling in between; S is a sign term defined by

$$S = (\theta + \delta\theta)/|(\theta + \delta\theta)| \qquad \text{....……(2.20)}$$

where $\delta\theta$ is a small angle like 0.01^o introduced to avoid division by zero when $\theta = 0$.

The average normal and shear stresses (σ, τ) are then calculated from

$$\sigma = (X\ sin\alpha + Y\ cos\alpha)/\ A_c \qquad \text{……...……(2.21)}$$

$$\tau = (X\ cos\alpha - Y\ sin\alpha)/\ A_c \qquad \text{....……(2.22)}$$

where A_c is the corrected area of shear given by the following equations.

For cylwests,

$$A_c = \pi(D_i)^2\ /\ 4\ sin\alpha - D_i u \qquad \text{.....……(2.23)}$$

For iswests and priswests,

$$A_c = b(d - u) \qquad \text{……(2.24)}$$

where D_i is the inside diameter of TM in cylwests; b is the inner width and d is the length of the shearing plane of TM in the iswests and priswests, and u is the shear displacement given by

$$u = \delta_x \cos\alpha + \delta_y \sin\alpha \qquad \text{…….....……(2.25)}$$

where δ_x and δ_y are the displacements measured in the positive directions of X and y (Fig. 2.14), respectively. The normal displacement v is given by

$$v = \delta_y \cos\alpha - \delta_x \sin\alpha \qquad \text{.....(2.26)}$$

where positive values of v indicate dilatation. $\alpha = \alpha_n$, the nominal angle between P and the shearing plane of TM (Fig. 2.15) in priswests and iswests, and in cylwests where the specimen fails as in Fig. 2.14(a). In cylwests on clays, failure can sometimes occur as in Fig. 2.14(b) or (c), in which case α is calculated from the geometry of the failure plane.

2.3.1.3 Average Shear Plane Analysis (Analysis B)

In this analysis, the average shear plane is assumed to be the same as in Analysis A, except that the effect of the slight rotation β of the mould is taken into account. The average shear and normal displacements ($\bar{u}$, $\bar{v}$ respectively), and β are calculated as explained by Mirata (1991). θ in equations (2.16) and (2.17) is then replaced by $\theta_r = \theta + \beta$, and u in equations (2.23) and (2.24) by $\bar{u}$. The value of α is unaltered, implying that both P and the average shear plane rotate by β.

2.3.1.4 True Shear Plane Analysis (Analysis C)

The rotation β is calculated as in analysis B, but shear is assumed to take place initially between the trailing tip A_1 of TM and the point B_1 which represents the opposite tip of TM (S) (Fig. 2.15). The angle α_i between A_1B_1 and the initial direction of P, and the length $\overline{A_1B_1}$ (Fig. 2.16) are calculated as explained by Mirata (1991).

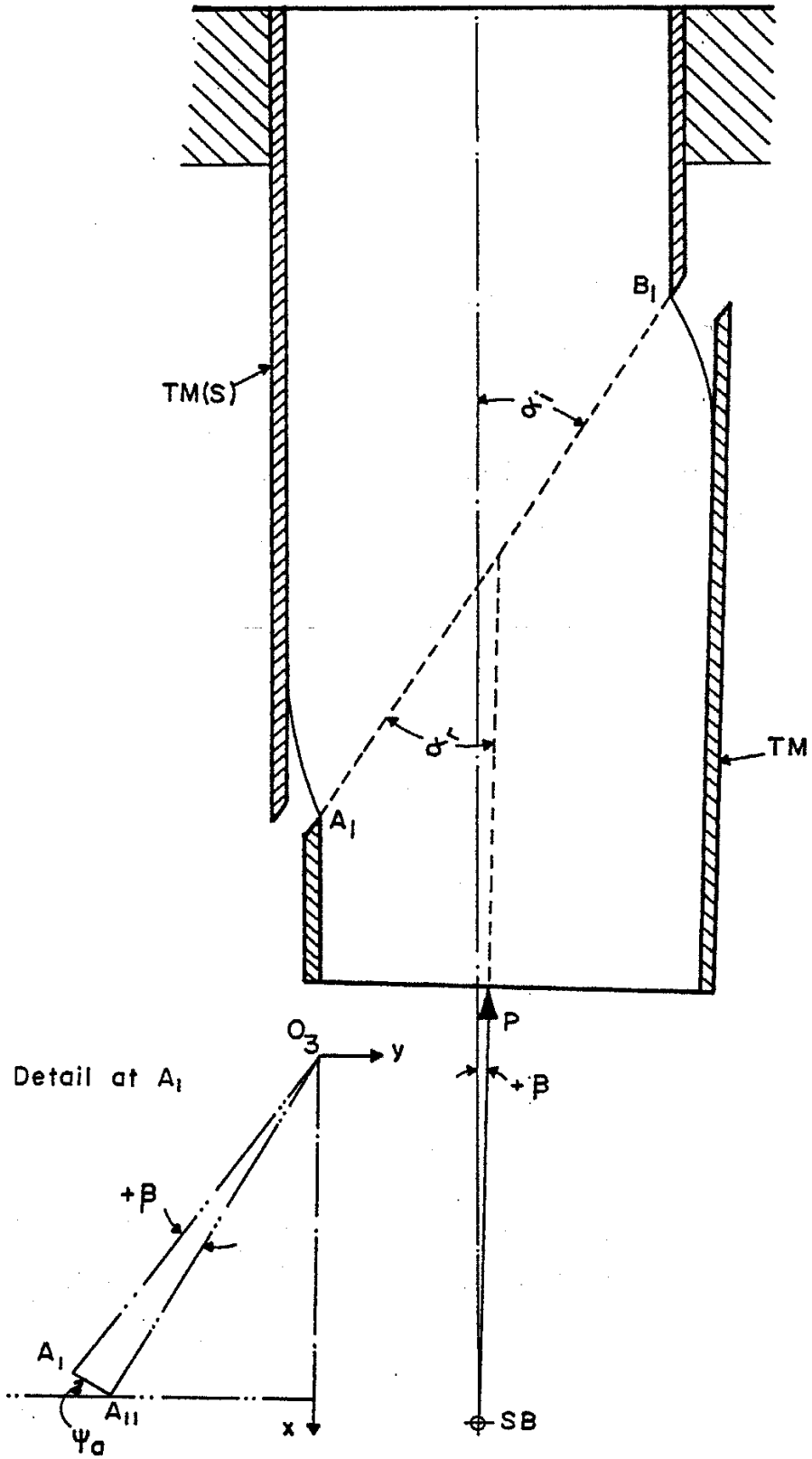

Figure 2.16. Pre-failure deformation of a plastic clay in cylwest (after Mirata, 1991; 2003(a))

The angle α_r between the rotated position of P and A_1B_1 (Fig. 2.16), and the equivalent shear displacement $\bar{u}_1$ are given by

$$\alpha_r = \alpha_i - \beta. \quad \text{.....(2.27)}$$

$$\bar{u}_1 = 2d_{yb} / \sin\alpha_i - \overline{A_1B_1} \quad \text{.....(2.28)}$$

where d_{yb} is defined as $\left(d \sin\alpha_n - n_c / \cos\alpha_n\right)/2$ in priswests and iswests (where n_c is the initial clearance between the shearing planes of the two halves of the priswest box, and is equal to 0 for iswests), and as $(D_i / 2)$ in cylwests. Equations (2.23) and (2.24) are then replaced by equations (2.29) and (2.30), and α in equations (2.21) and (2.22) is replaced by α_r.

For cylwests,

$$A_c = \pi\left(d_{yb}\right)^2 / \sin\alpha - \bar{u}_1 D_i \quad \text{.....(2.29)}$$

For iswests and priswests,

$$A_c = b\left(2d_{yb} / \sin\alpha_i - \bar{u}_1\right) \quad \text{.....(2.30)}$$

After the peak strength is reached, further movement of the soil wedge is assumed to take place in the general direction of the failure plane formed at peak strength, but any further changes in β to be reflected equally to the direction of P and the orientation of the failure plane. So $\bar{u}_1$ in equations (2.29) and (2.30) is replaced by $\bar{u}$ obtained as in analysis B, and α_i and α_r are assumed to remain fixed at the values at peak strength.

2.4 Comparison of the Wedge Shear Test with the Plane Strain Test

For example, the plane strain tests quoted by Bishop (1966) have been performed on prismatic samples 406 mm long, 51 mm wide, and 102 mm high (Fig. 2.17). The sample is encased in a rubber membrane. The sample is loaded through two pistons bearing onto a stiff top plate at the quarter-length points giving an even distribution of stress (Cornforth, 1964). The intermediate principal stress σ_2 is determined from the load on the lubricated platens maintaining zero strain in the σ_2 direction (Bishop, 1966). The cell pressure and axial load are applied in an identical manner to the conventional triaxial test; the sample is sheared by increasing the axial load (Cornforth, 1964). In the plane strain tests, failure always occurs along a single well defined shear plane (Lee, 1970).

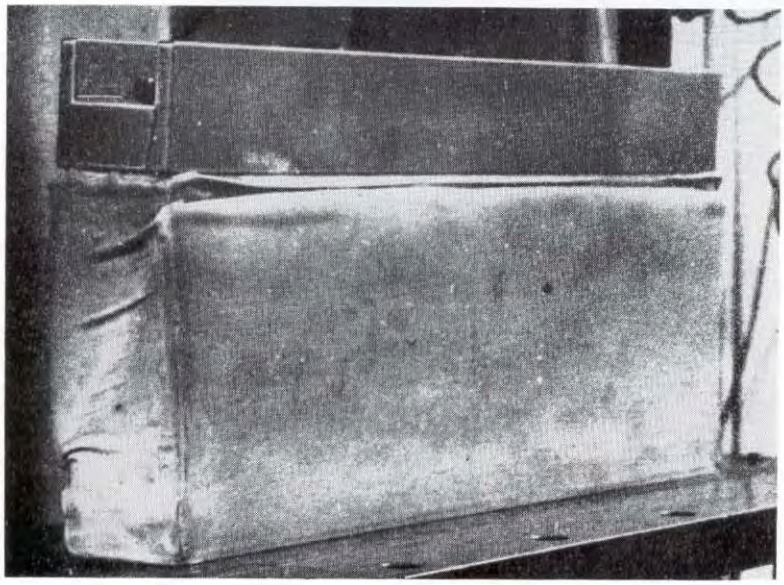

Figure 2.17. Plane strain test sample after failure (after Bishop, 1966)

The following has been taken from Mirata (2003(b)).

In the prismatic wedge shear test (priswest), each half of the sample, such as seen in Fig. 2.15, is enclosed in a 10 - mm thick steel mould; the lateral yield of the sample is thus prevented except along the relatively small gap (Tables 5.9 to 5.14, column 3) between the two halves of the mould. No rubber membrane is used. The sample is sheared by applying a relatively small lateral load (analogous to the cell pressure in Fig. 2.17), and increasing the main load *P* (analogous to the axial load in Fig. 2.17). The angle between the shear plane and the main load is restricted by the test mould used, and the distribution of stress on the faces of the sample, although capable of being controlled to some extent by applying an initial eccentricity to *P*, is not uniform (see Tables 5.9 to 5.14, columns 5, 12, and 19). The initial shear plane area is 300 mm x 300 mm, and the test is evaluated on the basis of average stresses on this plane, as in the conventional shear box test.

In the cylindrical wedge shear test (cylwest), loading is effected in a similar way to the priswest, but the sheared wedge is part of a cylinder, and the shear plane is initially elliptical. On the other hand, the inclination of the shear plane to the layering during sample placement in the cylwest using an $\alpha_n = 30^o$ test mould is closer to that in the plane strain test (Fig. 2.17). In the priswest this inclination is lower, but can be improved by modifying the test mould (Fig. 5.9(b)) so that the side of the mould on which the main load is applied becomes the removable lid.

It is seen that the wedge shear test is similar but not identical with the conventional plane strain test.

CHAPTER 3

MINERALOGICAL AND PARTICLE SHAPE ANALYSES OF THE SAMPLES

3.1 Introduction

In order to investigate the difference in strength measured in the wedge shear test, in the triaxial test, and in the shear box test, Anatolian sands were obtained from different locations in Turkey (Table 3.1).

Table 3.1. Locations of the samples

Sample	Location	Co-ordinates
A	Sand quarry located 5 km south of Kazan, Ankara	32.7^{o} E ; 40.2^{o} N
B	Salt Lake sand located 6 km north-west of Şereflikoçhisar, Ankara	33.5^{o} E ; 38.9^{o} N
C	Sand quarry located 3 km west of Bafra, Samsun	35.8^{o} E ; 41.5^{o} N
D	Beach located 4 km west of Sinop	35.1^{o} E ; 42.1^{o} N
E	Sand hill located 8 km west of Yumurtalık, Adana	35.7^{o} E ; 36.7^{o} N
F	Sand quarry located 4 km west of Ceyhan, Adana	35.7^{o} E ; 37.1^{o} N

A minimum of 350 kg of sand was taken from each location, transported to the Soil Mechanics Laboratory of METU, and prepared for mineralogical and granulometric analyses, and for wedge shear, triaxial shear, and shear box tests. Mineralogical analyses of each sample were carried out by Girgin (2000), and the

results are presented in section 3.4. The results of the particle shape analyses carried out by the author in the Sedimentation Laboratory of the Geological Engineering Department, METU are presented in section 3.5.

3.2 Preparation of the Samples

The samples were in a slightly moist condition. So each sample was first air-dried by spreading in a large tray as a layer of about 5 cm thickness and thoroughly mixing several times during the day. The air - dried sample was sieved through No.6 (3.35 mm) ASTM sieve to enable 6 cm square shear box tests to be carried out; the particles retained on this sieve were discarded. Each sample was then mixed thoroughly and separated into representative sub-samples by passing through the riffle box. In this way were prepared five 40-kg sub-samples for prismatic wedge shear tests (priswests); eight 5-kg sub-samples for triaxial compression tests; five 7-kg sub-samples for cylindrical wedge shear tests (cylwests); one 25-kg sub-sample for the granulometric analyses, specific gravity and compaction tests; one 3-kg sub-sample for shear box tests, and one 2-kg sub-sample for the mineralogical analyses. All shear tests were performed on wet specimens for fear that dry sand might flow out between the two halves of the wedge shear test moulds.

3.3 Mineralogical Analyses Performed

Each of the sub-samples prepared for mineralogical analyses as in section 3.2 were divided into two representative specimens the results of which were eventually averaged. The twelve specimens so prepared were given mixed numbers (Table 3.2), and taken to the General Directorate of Mineral Research and Exploration (MTA) laboratories, where the mineralogical analyses were carried out by Girgin (2000) as follows. Each specimen was first sieved through two sieves chosen by considering the grain size range and divided into three fractions. Then, thin sections were obtained from each fraction and visual grain counting under the microscope was

made on the sections. The mineralogical composition of the samples so obtained is presented in the following sections.

Table 3.2. Specimen numbers for mineralogical analyses

Sample	Mineralogical analysis specimen numbers
A	S5, S11
B	S2, S9
C	S1, S7
D	S4, S10
E	S6, S8
F	S3, S12

3.4 Results of Mineralogical Analyses:

In this section the following notation has been used:

MRF: metamorphic rock fragments;

SRF: sedimentary rock fragments;

EAURF: extensively altered ultrabasic rock fragments;

EIRF: extrusive igneous rock fragments;

IIRF: intrusive igneous rock fragments;

TF: tuffaceous fragments.

The relative contribution to shear strength, based on the assessment by Norman (2000(b)), was indicated as follows: (+): tending to increase shear strength, (-): tending to decrease shear strength and (+-): effect on shear strength unknown.

The mineralogical composition of the samples and relative contribution to strength of the different ingredients, listed in order of abundance in any one category, are given in Tables 3.3 to 3.14.

Table 3.3. Mineralogical composition of sample A

Specimen number:	S5			S11			Average			Weighted average
Size range (mm) :	>2	2 to 1	<1	>2	2 to 1	<1	>2	2 to 1	<1	Whole
Fraction of whole (%) :	24	27	49	22	26	52	23	26.5	50.5	100
Units: / Ingredients	(%)	(%)	(%)	(%)	(%)	(%)	(%)	(%)	(%)	(%)
Minerals	0	2	30	2	2	34	1	2	32	16.9
MRF	26	26	3	0	18	6	13	22	4.5	11.1
SRF	6	22	13	37	18	8	21.5	20	10.5	15.6
EAURF	14	8	13	19	18	18	16.5	13	15.5	15.0
EIRF	54	42	41	42	38	34	48	40	37.5	40.6
TF	0	0	0	0	6	0	0	3	0	0.8

Table 3.4. Details and relative contributions to strength of ingredients in Table 3.3 for sample A

Ingredient	Details and relative contribution to strength
Minerals	Quartz (+), feldspar (plagioclase) (+-), pyroxene (-), calcite (-), biotite (-), and mafic minerals (+-)
MRF	Quartz - muscovite schist (+-), and quartzite (+)
SRF	Siltstone (-), quartz graywacke (clayey sandstone) (+ -), limestone (-), sandy limestone (-), and chert (+)
EAURF	Serpentinite (-)
EIRF	Volcanic rock fragments (andesite (+-), basalt (+), and altered andesite (+-))
TF	Tuffaceous fragments (+-)

Table 3.5. Mineralogical composition of sample B

Specimen number:	S2			S9			Average			Weighted average
Size range (mm):	>2	2 to 1	<1	>2	2 to 1	<1	>2	2 to 1	<1	Whole
Fraction of whole (%):	15	54	31	14	54	32	14.5	54	31.5	100
Units: / Ingredients	(%)	(%)	(%)	(%)	(%)	(%)	(%)	(%)	(%)	(%)
Minerals	33	57	66	26	64	45	29.5	60.5	55.5	54.4
MRF	4	0	0	2	0	0	3	0	0	0.4
SRF	56	28	34	56	34	51	56	31	42.5	38.3
EAURF	0	2	0	2	0	4	1	1	2	1.3
EIRF	0	0	0	5	2	0	2.5	1	0	0.9
IIRF	7	13	0	9	0	0	8	6.5	0	4.7

Table 3.6. Details and relative contributions to strength of ingredients in Table 3.5 for sample B

Ingredient	Details and relative contribution to strength
Minerals	Quartz (+) and feldspar (plagioclase and orthoclase) (+-)
MRF	Quartz - mica schist (+-) and quartzite (+)
SRF	Sandy limestone (-), litharenite sandstone (+-), quartz arenite (+), chert (+), limestone (-), and calcareous sandstone (+-)
EAURF	Serpentinite (-)
IIRF	Felsic to intermediate igneous rocks (granite) (+)
EIRF	Volcanic rocks (andesite)(+-)

Table 3.7. Mineralogical composition of sample C

Specimen number:	S1			S7			Average			Weighted average
Size range (mm):	>2	2 to 1	<1	>2	2 to 1	<1	>2	2 to 1	<1	whole
Fraction of whole (%):	12	14	74	13	15	72	12.5	14.5	73	100
Units: / Ingredients	(%)	(%)	(%)	(%)	(%)	(%)	(%)	(%)	(%)	(%)
Minerals	7	14	32	2	15	33	4.5	14.5	32.5	26.4
MRF	30	32	23	14	35	25	22	33.5	24	25.1
SRF	50	29	19	26	26	12	38	27.5	15.5	20.1
EAURF	8	13	19	30	15	15	19	14	17	16.8
EIRF	0	12	7	25	7	11	12.5	9.5	9	9.5
IIRF	5	0	0	3	2	4	4	1	2	2.1

Table 3.8. Details and relative contributions to strength of ingredients in Table 3.7 for sample C

Ingredient	Details and relative contribution to strength
Minerals	Quartz (+), feldspar (plagioclase) (+-), pyroxene (-), epidote (-), chlorite (-), and calcite (+)
MRF	Quartz schist (-), quartzite (+), calc-silicate schist (-), quartz - mica schist (+-), and quartz - muscovite schist (+-)
SRF	Sandy limestone (-), calcareous sandstone (+-), quartz arenite (+), limestone (-), chert (+), litharenite sandstone (+-), siliceous sandstone (+-), siltstone (-), and dolomite (+-)
EAURF	Serpentinite (-)
IIRF	Volcanic rocks (andesite (+-) and basalt (+))
EIRF	Felsic to intermediate igneous rocks (eg. granite and diorite) (+)

Table 3.9. Mineralogical composition of sample D

Specimen number:	S4		S10			Average		Weighted average
Size range (mm):	>0.5	< 0.5	>0.5	0.5 to 0.25	<.25	>0.5	< 0.5	whole
Fraction of whole (%):	82	18	2	94	4	42	58	100
Units: / Ingredients	(%)	(%)	(%)	(%)	(%)	(%)	(%)	(%)
Minerals	53	42	53	28	51	53	41	46.0
MRF	5	19	18	20	11	11.5	17	14.7
SRF	34	28	27	41	29	30.5	31	30.8
EAURF	4	11	2	11	9	3	11	7.7
EIRF	4	0	0	0	0	2	0	0.8

Table 3.10. Details and relative contributions to strength of ingredients in Table 3.9 for sample D

Ingredient	Details and relative contribution to strength
Minerals	Quartz (+), feldspar (plagioclase and orthoclase) (+-), pyroxene(-), calcite (-), and epidote (-)
MRF	Quartz - mica schist (+-), and quartzite (+)
SRF	Limestone (-), sandy limestone (-), and siltstone (-)
EAURF	Serpentinite (-)
EIRF	Volcanic rock fragments (+-)

Table 3.11. Mineralogical composition of sample E

Specimen number:	S6			S8			Average			Weighted average
Size range (mm):	>.5	.5 to .25	<.25	>.5	.5 to .25	<.25	>.5	.5 to .25	< .25	whole
Fraction of whole (%):	14	64	22	13	66	21	13.5	65	21.5	100
Units: / Ingredients	(%)	(%)	(%)	(%)	(%)	(%)	(%)	(%)	(%)	(%)
Minerals	5	23	27	6	21	31	5.5	22	29	21.3
SRF	90	67	55	87	67	57	88.5	67	56	67.5
EAURF	5	10	18	7	12	8	6	11	13	10.8
EIRF	0	0	0	0	0	4	0	0	2	0.4

Table 3.12. Details and relative contributions to strength of ingredients in Table 3.11 for sample E

Ingredient	Details and relative contribution to strength
Minerals	Quartz (+), feldspar (plagioclase) (+-), epidote (-), and mafic minerals (+-)
SRF	Sandy limestone (-), litharenite sandstone (+-), limestone (-), chert (+), siltstone (-), quartz arenite (+), dolomitic limestone (-), and fossil fragments (-)
EAURF	Serpentinite (-)
EIRF	Volcanic rock fragments (andesite (+-))

Table 3.13. Mineralogical composition of sample F

Specimen number:	S3			S12			Average			Weighted average
Size range (mm):	>2	2 to 1	<1	>2	2 to 1	<1	>2	2 to 1	<1	whole
Fraction of whole (%):	2	4	94	2	4	94	2	4	94	100
Units: / Ingredients	(%)	(%)	(%)	(%)	(%)	(%)	(%)	(%)	(%)	(%)
Minerals	0	7	26	2	14	38	1	10.5	32	30.5
MRF	6	11	2	13	12	6	9.5	11.5	4	4.4
SRF	53	38	45	34	23	32	43.5	30.5	38.5	38.2
EAURF	27	24	19	32	42	17	29.5	33	18	18.8
EIRF	12	16	4	17	7	7	14.5	11.5	5.5	5.9
IIRF	3	4	4	2	2	0	2.5	3	2	2.2

Table 3.14. Details and relative contributions to strength of ingredients in Table 3.13 for sample F

Ingredient	Details and relative contribution to strength
Minerals	Quartz (+), feldspar (+-), calcite (-), pyroxene (-), biotite (-), and epidote (-)
MRF	Quartz - mica schist (+-), quartz - muscovite schist (+-)
SRF	Clayey siltstone (-), quartz arenite (+), chert (+), litharenite sandstone (+-), limestone (-), siltstone (-), and sandy limestone (-)
EAURF	Extensively altered and silicified ultrabasic rock fragments (-)
EIRF	Volcanic rock fragments (andesite (+-) and altered andesite (+-))
IIRF	Felsic to intermediate igneous rocks (granite and granodiorite /diorite) (+)

The mineralogical analyses show that each sample contains both single mineral particles (quartz, feldspar, calcite, epidote, etc) and rock particles (quartz arenite, quartzite, limestone, etc.), which have different contribution to strength. In

any one category, the relative contribution to strength of the different ingredients is listed in order of abundance, but the individual percentages of these ingredients are unknown, yielding unpredictable contribution to strength. To determine the effect on strength of the mineral composition of the sands, more detailed analyses seem to be required, including determination of individual percentages of each ingredient (which was not possible in this study).

3.5 Results of Particle Shape Analyses

Particle shape analyses of each sample were carried out in the Sedimentation Laboratory of the Geological Engineering Department, METU.

Projection was used for determining grain morphology (particle shape) quantified by the roundness R_F and sphericity S_R, defined in section 2.1.5.1. The methods given by Dobkins & Folk (1970) and Riley (1941), given in section 2.1.5.1, were used for R_F and S_R respectively as follows. R_F and S_R were calculated for 60 grains projected for each of the samples by measuring selected grain axes (d_k, d_i, and d_c (Fig. 2.10)); average values of R_F and S_R for each sample were taken. The results of particle shape analyses so obtained are given in Table 3.15.

Table 3.15. The results of particle shape analyses of each sample

Sample	R_F	S_R
A	0.25	0.78
B	0.22	0.80
C	0.21	0.78
D	0.30	0.77
E	0.33	0.80
F	0.34	0.79

According to the classification given in section 2.1.5.1 (Table 2.3), samples A, B, and C consist of angular particles; samples D, E, and F consist of subangular particles. Also, according to the chart given in section 2.1.5.1 (Fig. 2.11), the S_R values indicate grains of high sphericity.

CHAPTER 4

PHYSICAL AND COMPACTION PROPERTIES OF THE SAMPLES

4.1 Introduction

In this chapter, various physical and compaction test results are presented. All of the tests were performed in the Geotechnical Engineering Laboratory of the Civil Engineering Department of METU according to the related Turkish Standards (TS1900, 1987) and British Standards (BS1377/Part 4, 1990).

4.2 Sieve Analyses and Particle Breakage

A minimum of 2 kg of sand was used in all sieve analyses.

4.2.1 Particle Breakage during Shear

Sieve analyses were carried out in order to determine the initial gradation of the samples (full curves in Figs. 4.1 to 4.6). Basic soil parameters determined from the gradation curve for each sample are given in Table 4.1. In this table, D_{10} is the effective size; D_{30} and D_{60} are the largest sizes of the smallest 30% and 60% respectively; C_u is the uniformity coefficient; C_c is the coefficient of curvature; and SP stands for poorly graded sand. Note that sample A, strictly classified as SP, is very close to well graded.

Sieve analyses were also carried out on the samples in order to compare the gradation of the initial samples with those used in the different shear tests. Typical examples of the grain size curves obtained are shown in Figs. 4.1 to 4.6 as dashed lines. These figures show that some crushing has occurred in all shear tests.

Table 4.1. Summary of the gradation and classification of samples A to F

Sample	D_{60} (mm)	D_{30} (mm)	D_{10} (mm)	$C_u = \frac{D_{60}}{D_{10}}$	$C_c = \frac{(D_{30})^2}{(D_{60}).(D_{10})}$	Unified soil classification
A	1.16	0.59	0.20	5.80	1.50	SP
B	1.19	0.84	0.53	2.24	1.12	SP
C	0.80	0.39	0.23	3.48	0.83	SP
D	0.41	0.39	0.33	1.24	1.12	SP
E	0.37	0.29	0.21	1.76	1.08	SP
F	0.46	0.33	0.21	2.19	1.13	SP

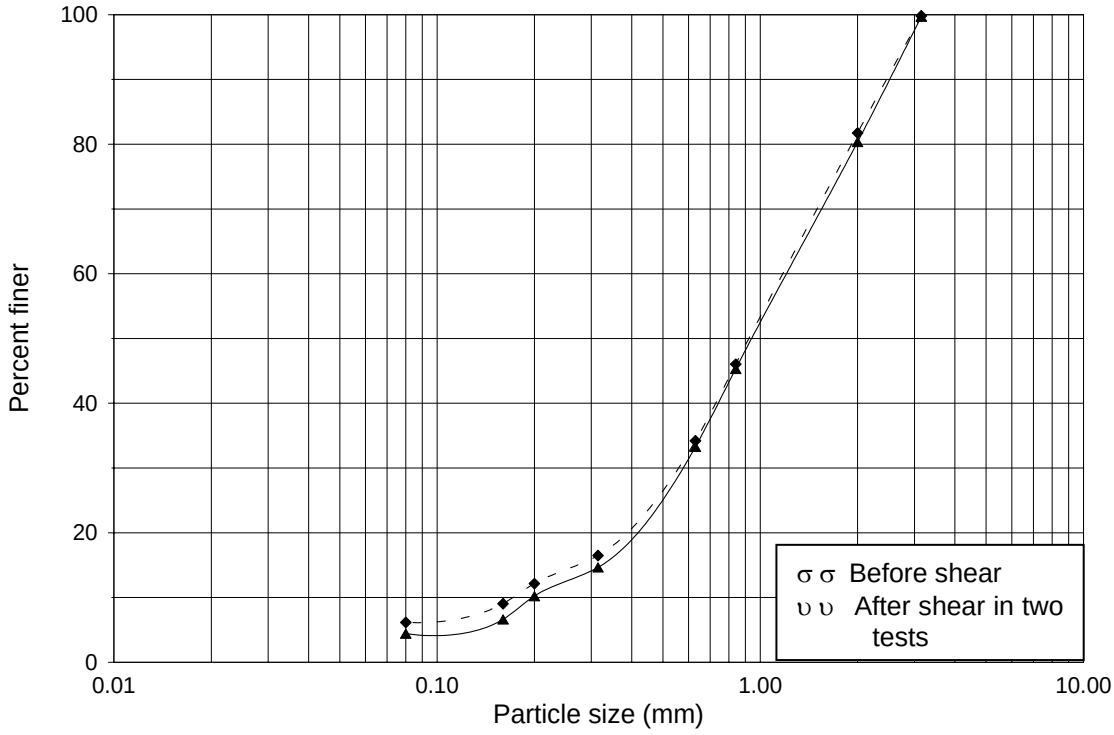

Figure 4.1. Comparison of gradation of sample A at the lower density before testing and after being sheared in cylwests

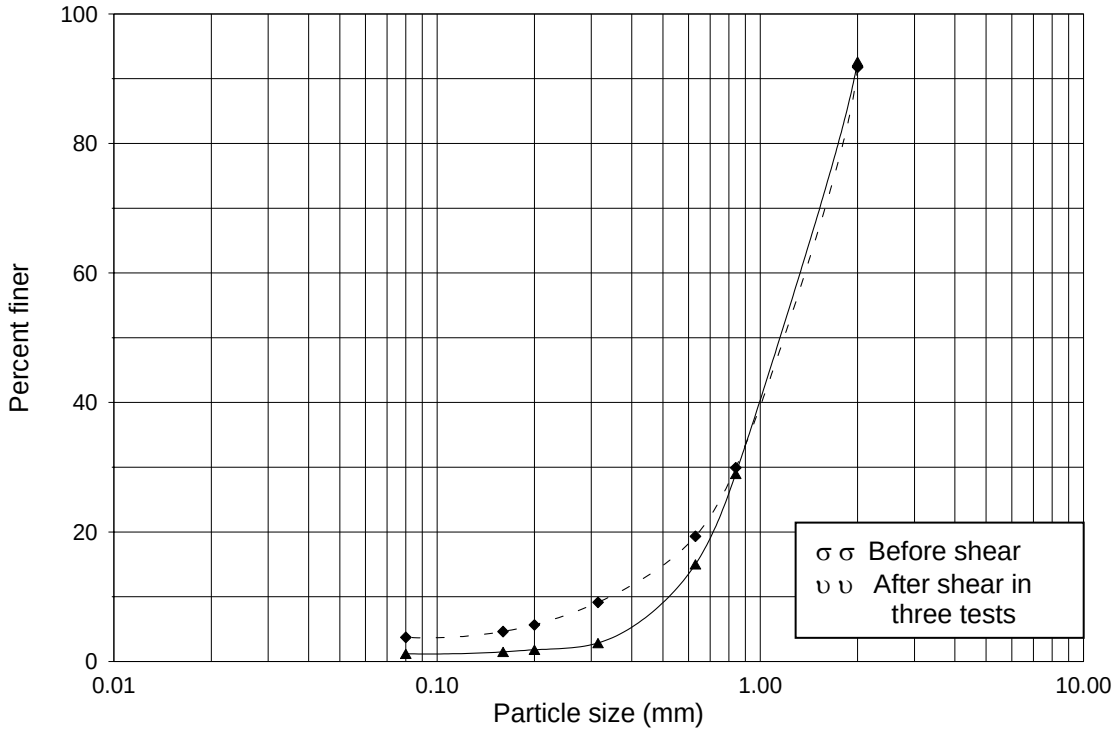

Figure 4.2. Comparison of gradation of sample B at the lower density before testing and after being sheared in priswests using the 30^{o} mould under lower normal stresses

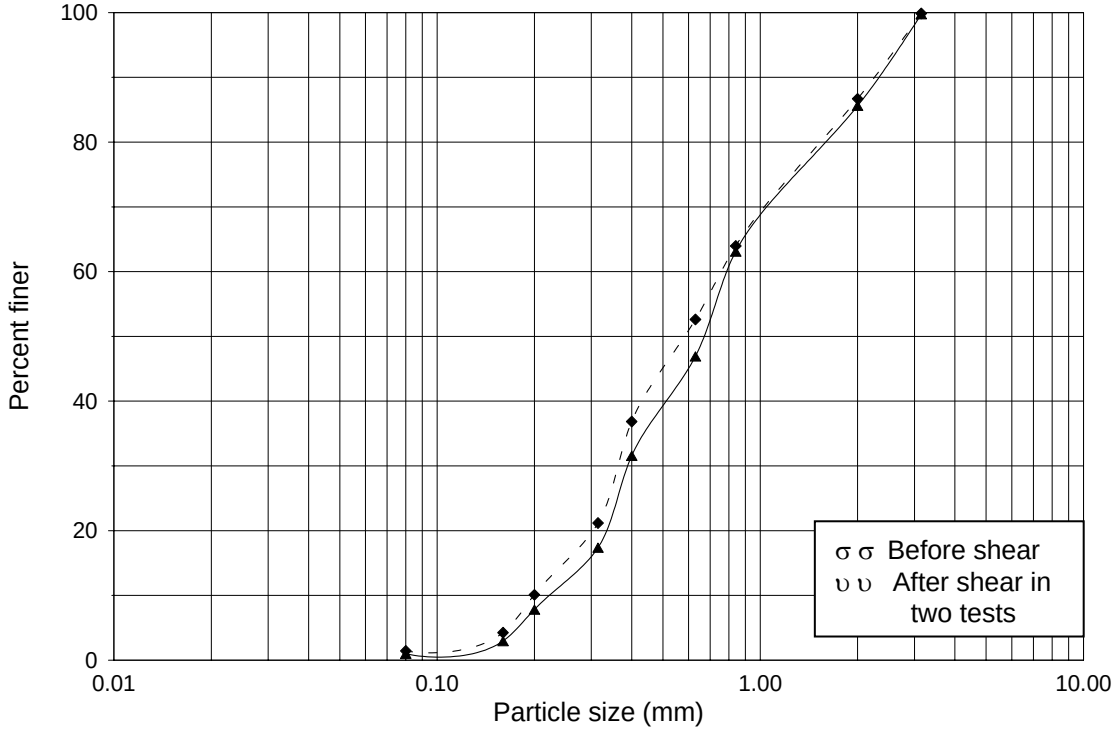

Figure 4.3. Comparison of gradation of sample C at the lower density before testing and after being sheared in triaxial tests

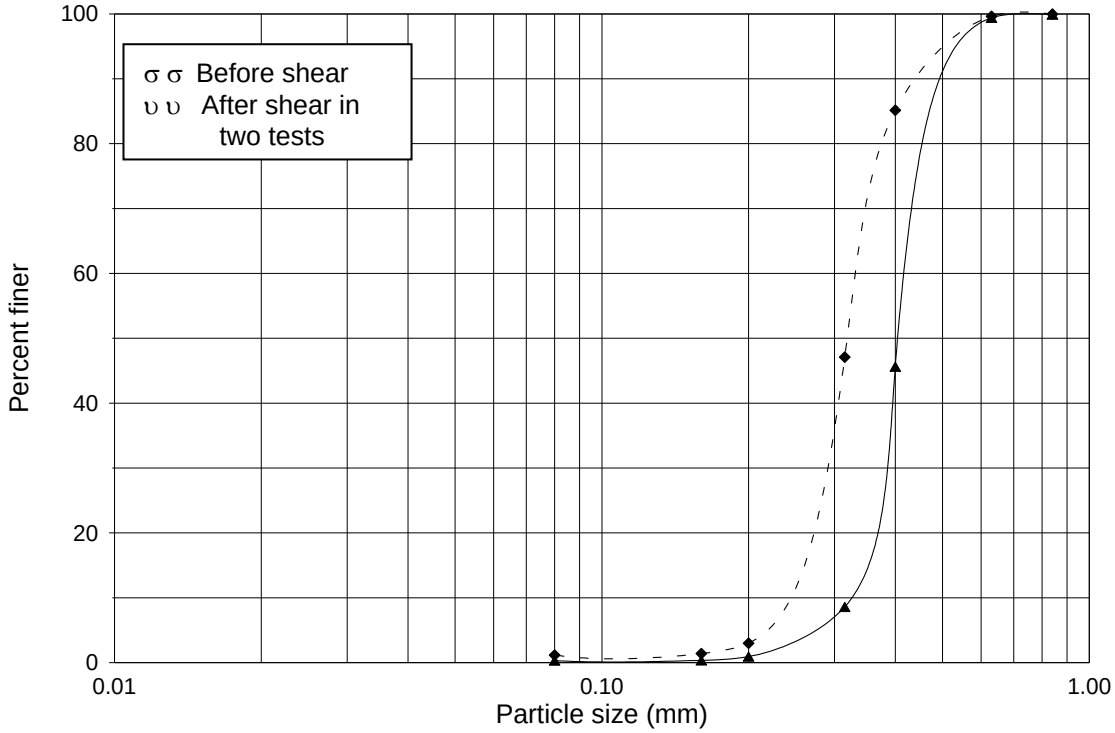

Figure 4.4. Comparison of gradation of sample D at the higher density before testing and after being sheared in cylwests

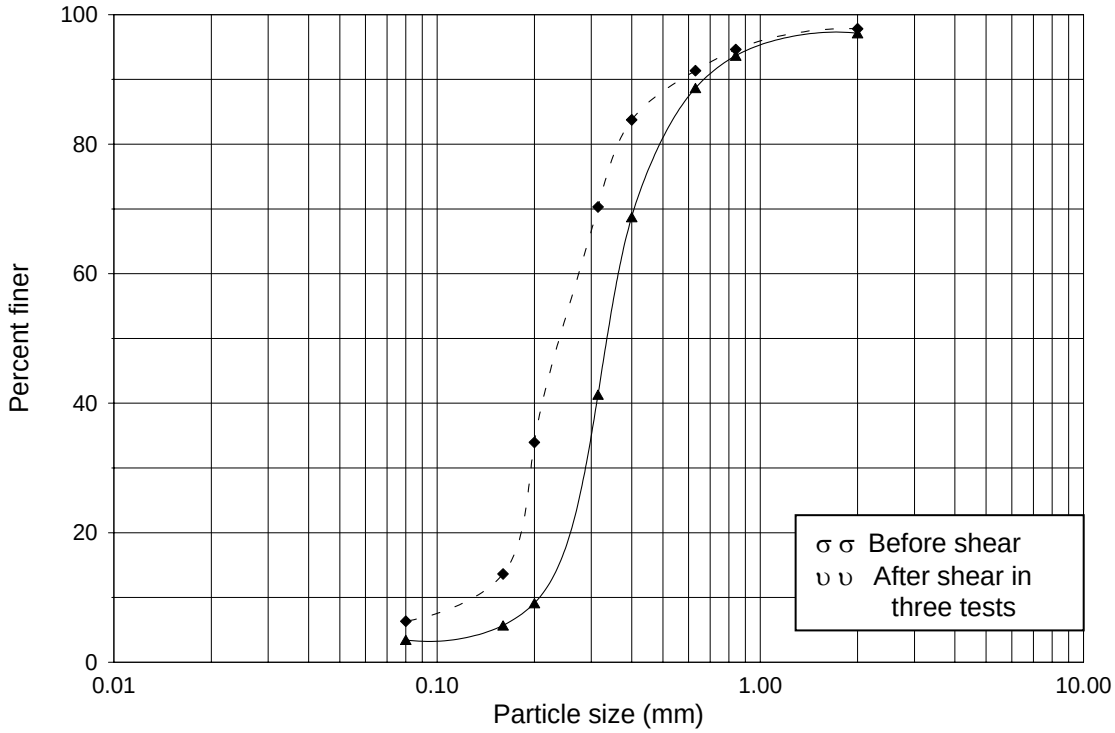

Figure 4.5. Comparison of gradation of sample E at the higher density before testing and after being sheared in priswests using the 40^{o} mould under higher normal stresses

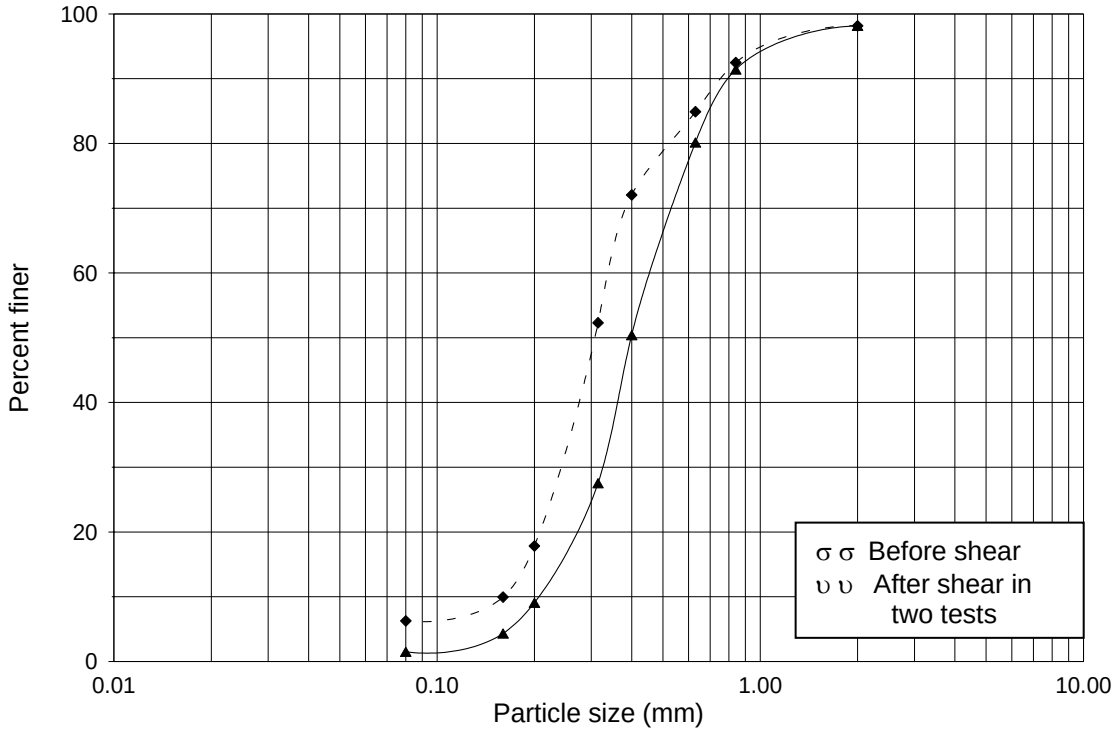

Figure 4.6. Comparison of gradation of sample F at the higher density before testing and after being sheared in triaxial tests

The values of Marsal's (1967) breakage factor B_g (Appendix C) were calculated from the initial and final gradation of samples A to F at the lower and higher densities (Table 4.2). In this table, the test numbers in columns 2 to 9 refer to the test numbers in Tables 5.1, 5.8, and 6.1 for the cylwests, priswests, and triaxial tests respectively.

Comparing the values of B_g of all samples at the lower density (Table 4.2, columns 2 to 5) both under the lower and higher ranges of normal stress σ, the values of B_g for samples A to C are smaller than those for samples D to F. This indicates that samples A to C have particles exhibiting relatively higher resistance to crushing than samples D to F.

Generally, for sands with particles of angular shapes, particle crushing can be quite significant even under low pressure (Ueng & Chen, 2000) (section 2.1.5.2). However, in this study, more particle crushing occurred in samples with subangular particles (samples D to F) compared to the samples with angular particles (samples A

Table 4.2. Breakage factors calculated from the initial and final gradation of samples A to F after different shear test

1	2	3	4	5	6	7	8	9
Sample	Breakage factors of samples A to F at the lower density				Breakage factors of samples D to F at the higher density			
	Cylwests	Priswests		Triaxial tests	Cylwests	Priswests		Triaxial tests
A	After test 4 B_g = 3.1 %	After test 3 B_g = 4.2 %	After test 6 B_g = 4.7 %	After test 7 B_g = 4.5 %	...	…	…	…
B	After test 4 B_g = 6.6 %	After test 3 B_g= 6.2 %	After test 6 B_g = 7.0 %	After test 7 B_g = 6.7 %	…	…	…	…
C	After test 4 B_g = 7.6 %	After test 5 B_g = 5.8 %	After test 6 B_g = 8.3 %	After test 7 B_g = 7.9 %	…	…	…	…
D	After test 4 B_g = 13.7 %	After test 5 B_g = 14.8 %	After test 6 B_g = 19.1 %	After test 7 B_g = 17.7 %	After test 4 B_g = 39.5 %	After test 3 B_g = 44.5 %	After test 6 B_g = 46.4 %	After test 6 B_g = 40.7 %
E	After test 4 B_g = 13.8 %	After test 5 B_g = 20.8 %	After test 6 B_g = 23.7 %	After test 7 B_g = 21.9 %	After test 4 B_g = 25.7 %	After test 3 B_g = 27.2 %	After test 6 B_g = 28.0 %	After test 6 B_g = 26.7 %
F	After test 4 B_g = 10.2 %	After test 5 B_g = 11.3 %	After test 6 B_g = 14.1 %	After test 7 B_g = 14.5 %	After test 4 B_g = 18.5 %	After test 3 B_g = 18.8 %	After test 6 B_g = 22.5 %	After test 6 B_g = 24.8 %

to C) (section 3.5). This shows that particle shape is not the only factor influencing the crushing of particles. Other important factors are the strength of the particles and the gradation (sections 2.1.5.2 and 2.1.5.4). Sample A, which is very nearly a well graded sand, gave the lowest B_g values for the different shear tests.

Comparing Table 4.2 columns 4 and 8 for tests under the higher σ with columns 3 and 7 respectively, it is seen that, the value of B_g increases slightly with increase in σ both at the lower and the higher densities. Comparing Table 4.2 columns 2 to 5 with columns 6 to 9, it is seen that B_g increases significantly with increased density. This is in good agreement with the findings of Ueng & Chen (2000) (section 2.1.5.2) that particle crushing increases with an increase in density and confining pressure.

4.2.2 Particle Breakage during Compaction

The only untested sample left after the shear tests was sample E for which the breakage factor B_g was higher than all other samples in shear tests at the lower density. So sample E was chosen to investigate whether particle crushing occurred during compaction. A 14-kg batch of this sample was mixed thoroughly and separated into two 7-kg sub-samples by passing through the riffle box. One of the sub-samples was compacted in the cylwest mould by using the 2.5 kg rammer to obtain the lower density attained in most of the shear tests. The compacted sample was then removed from the cylwest mould and divided into two equal parts. While sieve analysis was carried out on one part, the other part was again compacted in the cylwest mould to the same density, and the gradation after the second compaction was also determined. This procedure was repeated for the other 7-kg sub-sample by using the Kango vibrating hammer for obtaining the higher density attained in some of the shear tests. The original gradation of sample E and the gradations after the first and second compaction for the lower and higher densities are given in Figs. 4.7 and 4.8 respectively. Comparing the original gradation and the gradations after compaction, some crushing is seen to occur particularly at the higher density, but this crushing was small compared to the crushing which occurred during shear (Fig. 4.5).

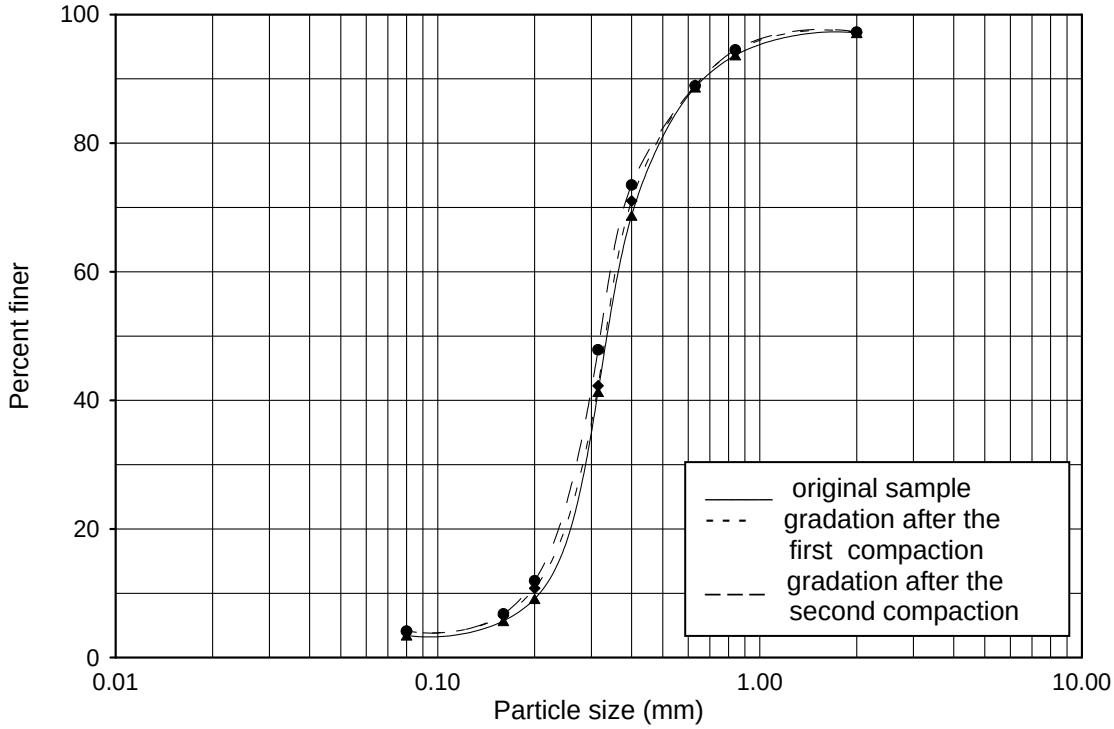

Figure 4.7. Original gradation of sample E and the gradations after first and second compactions at the lower density

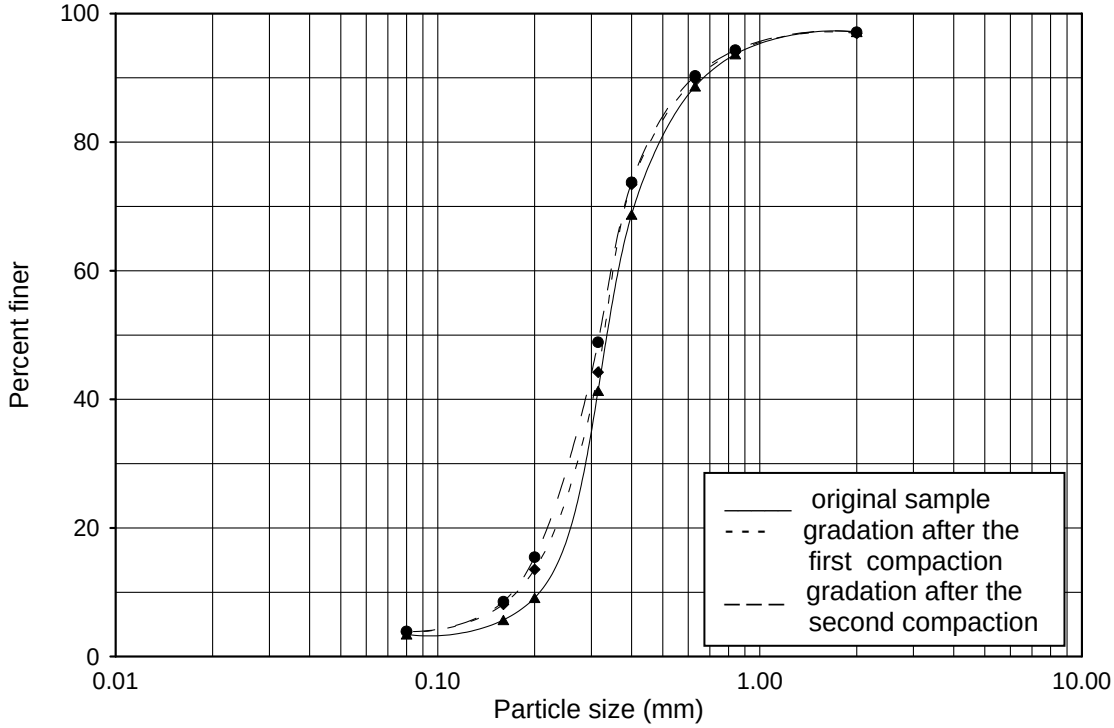

Figure 4.8. Original gradation of sample E and the gradations after first and second compactions at the higher density

4.3 Density Tests

4.3.1 Maximum Density Tests

The maximum density tests were performed on each sample generally following the procedure given in the British Standards (BS 1377, 1990).

This method is suitable for sands containing a small amount of material passing a 63-μm test sieve, and up to 10 % of fine gravel passing a 6.3-mm test sieve. The soil is compacted in a 1-litre mould (105 mm inside diameter, 115.5 mm high) under water using an electric vibrating hammer. In this study, a mould, 152 mm in diameter, 115 mm high was used.

The sample prepared as in section 3.2 was mixed thoroughly on a large metal tray, and divided by riffling into two representative portions of about 5 kg each. Each sample was poured into warm water in a bucket and stirred thoroughly to remove air bubbles. The container was covered, and allowed to stand for several hours, e.g. overnight, to cool.

An extension was attached to the mould and the assembly was placed in a watertight container on the concrete floor. Water was poured to about 50-mm depth in the mould, and to the same level in the surrounding container.

A portion of the soil-water mixture was added to the mould with a scoop, placing it carefully under the water surface without loss of fines and without segregation of coarse particles. The quantity of sample so added was such that the mould was about one-third filled when compacted. Some water was added to the surrounding container up to the same level as in the mould and the soil surface was made approximately level.

A circular tamper was placed on the soil and compacted with a vibrating hammer for at least 2 minutes or until there was no further significant decrease in the sample height. During this period, a steady downward force was applied on the hammer so that the total downward force on the sample (including that from the mass of the hammer) was between 300 N and 400 N.

The procedure was repeated twice more, ensuring that the surface of the sample was always under water. It was aimed that after compaction of the third layer, its surface was at least level with, but not more than 6 mm above the top of the mould body.

The mould containing the soil was removed from the container, any adhering soil from the outside was cleaned off, and the free water was allowed to drain from the sample. The extension was carefully removed and the compacted soil was trimmed off level with the top of the mould, using a straightedge. Cavities were refilled and well pressed in. The compacted soil was then extracted from the mould into a small weighed metal tray, without loss of any particles. The wet sample was weighed for determining the bulk density.

The soil was allowed to dry in the oven at 105^{o}C to 110^{o}C and weighed when it was cool to determine the water content. The whole procedure was repeated for the second batch, and if the dry masses from the two tests differed by more than 50 g, the procedure was repeated using fresh samples. If not, the maximum density of the sample was taken as the larger of the two determinations. The results of the maximum density tests for the different samples are given in Table 4.3.

Table 4.3. Maximum density test results

Sample	Trial no.	Mass of wet sample (g)	Bulk density (Mg/m^3)	Water content (%)	Dry density (maximum highlighted) (Mg/m^3)
A	1	4456	2.135	13.86	1.875
	2	4472	2.143	13.64	**1.886**
B	1	4212	2.019	17.20	1.723
	2	4252	2.038	16.73	**1.746**
C	1	4530	2.171	14.61	1.894
	2	4558	2.184	15.05	**1.899**
D	1	4228	2.026	21.58	**1.667**
	2	4235	2.030	21.83	1.666
E	1	4342	2.081	20.12	**1.732**
	2	4322	2.071	20.00	1.726
F	1	4386	2.102	19.69	**1.756**
	2	4345	2.082	19.77	1.739

4.3.2 Minimum Density Tests

The British Standard (BS 1377, 1990) states that the minimum density test for sands is suitable for samples containing up to 10 % of fine material passing the 63 μm test sieve, and with no material retained on the 2mm test sieve. In this study, all samples except sample D (Fig. 4.4) include some particles retained on the 2-mm test sieve. Minimum density test for gravelly soils in the same standard is suitable for samples passing the 37.5 mm test sieve and containing up to 10 % of fine material passing the 63 μm test sieve. So the minimum density tests were carried out using both these methods, and the results compared.

4.3.2.1 Minimum Density Tests Performed by Following the Procedure for Sands

A representative sample of 1 kg prepared as in section 3.2 was placed in a 1000 cm^3 glass cylinder without a pouring lip, and a piece of rubber membrane was held against the mouth of the cylinder. The cylinder was shaken to loosen the sand and inverted a few times. During the last inversion, the cylinder was turned upside down, and held until all the sample was at rest; then it was quickly turned the right way up. The cylinder was put on a flat surface without jarring it. The volume reading at the mean level of the surface of the sand was recorded to the nearest 10 cm^3. During this operation shaking or jolting the cylinder was avoided. The procedure was repeated to give at least 10 determinations altogether. The minimum dry density $(\rho_d)_{min}$ of the different samples was calculated as set out in Tables 4.4 and 4.5.

Table 4.4. Volume of specimen in the glass cylinder for different trials

Sample	Volume of specimen for ten different trials (maximum highlighted) (cm^3)									
	1	2	3	4	5	6	7	8	9	10
A	610	**620**	610	620	620	620	620	620	610	620
B	**710**	710	700	700	710	710	710	700	710	710
C	580	**600**	590	580	570	580	600	580	580	600
D	670	670	**680**	680	670	670	670	680	680	680
E	660	660	**670**	670	670	660	670	660	660	670
F	**670**	660	670	660	660	670	670	670	670	670

Table 4.5. Calculation of minimum density from the procedure for sands

1	2	3	4	5	6
Sample	Mass of specimen (g)	Maximum volume of specimen (cm^3) (from Table 4.4)	Bulk density ρ_{bulk} (Mg/m^3)	Air-dry water content (%)	$(\rho_d)_{min}$ (Mg/m^3)
A	1000	620	1.613	0.850	1.599
B		710	1.408	0.179	1.406
C		600	1.667	0.336	1.661
D		680	1.471	0.135	1.469
E		670	1.492	0.208	1.489
F		670	1.492	0.472	1.485

4.3.2.2 Minimum Density Tests Performed by Following the Procedure for Gravelly Soils

The sample prepared as in section 3.2 was mixed thoroughly on a large tray, and a representative sample of about 5 kg was obtained by riffling. The sample was placed in a bucket and mixed to ensure an even distribution of particles of all sizes. The CBR mould, 152 mm in diameter and 115 mm high, with base and extension attached, was then placed in a tray and the contents of the bucket was poured into the mould steadily from a height of about 50 cm by using a hand-scoop. The extension was carefully removed and the surface of the soil was leveled to the top of the mould using a straightedge without disturbing the soil in the mould or jarring the mould.

The weight of soil in the mould was determined; this soil was then remixed with the excess soil remaining on the tray. The procedure was repeated to give at least 10 determinations altogether. The minimum density of the different samples was calculated as set out in Tables 4.6 and 4.7.

Table 4.6. Mass of specimen loosely poured in the CBR mould for different trials

Sample	Mass of specimen and mould (g) for ten different trials (minimum highlighted)									
	1	2	3	4	5	6	7	8	9	10
A	8825	8831	8819	8838	**8809**	8812	8816	8821	8820	8835
B	8495	8495	8473	8435	8499	8486	8495	8439	8478	**8431**
C	9002	9008	9000	**8952**	8981	8993	8972	8955	8957	8965
D	8571	8552	**8537**	8558	8560	8574	8544	8554	8563	8547
E	8607	8594	8586	8585	8603	8595	**8583**	8619	8596	8605
F	8618	8619	8613	**8607**	8623	8614	8621	8612	8634	8620

Table 4.7. Calculation of minimum density from the procedure for gravelly soils

1	2	3	4	5	6	7	8
Sample	Mass of mould (g)	Minimum mass of specimen and mould (from Table 4.6) (g)	Minimum mass of specimen (g)	ρ_{bulk} (Mg/m^3)	Air-dry water content (%)	$(\rho_d)_{min}$ (Mg/m^3)	$(\rho_d)_{min}$ from Table 4.5 Column 6 (Mg/m^3)
A	5486	8809	3323	1.592	0.385	1.586	1.599
B	5479	8431	2952	1.415	0.354	1.410	1.406
C	5479	8952	3473	1.664	0.426	1.657	1.661
D	5479	8537	3058	1.465	0.115	1.463	1.469
E	5479	8583	3104	1.488	0.470	1.481	1.489
F	5479	8607	3128	1.499	0.708	1.488	1.485

4.3.2.3 Comparison of Minimum Density Test Results

For ease of comparison the values in Table 4.5 column 6 were entered in column 8 of Table 4.7. Comparing columns 7 and 8 in Table 4.7, it is seen that no significant difference exists between the minimum dry density values obtained in the two types of test. For all samples which contain some particles retained on the 2-mm test sieve, in calculating the values of relative density of the specimens of these samples, minimum dry density values obtained using the procedure for gravelly soils (Table 4.7 column 7) were used; for sample D, the minimum dry density value obtained using the procedure for sands (Table 4.7 column 8) was used.

4.3.3 Determination of Dry Density / Water Content Relation by Standard Proctor Compaction Test

The dry density - water content relationship was determined by using the 2.5 kg rammer method according to the Turkish Standards (TS1900, 1987).

The curves of dry density versus water content for samples A to F are given in Fig. 4.9. The values of maximum dry density (ρ_{dmax}) and optimum water content (w_{opt}) are given in Table 4.8.

Table 4.8. The values of maximum dry density and optimum water content for each sample

Sample	A	B	C	D	E	F
ρ_{dmax} (Mg/m^3)	1.865	1.620	1.721	1.609	1.633	1.650
w_{opt} (%)	13.0	11.2	9.8	12.3	8.2	10.5

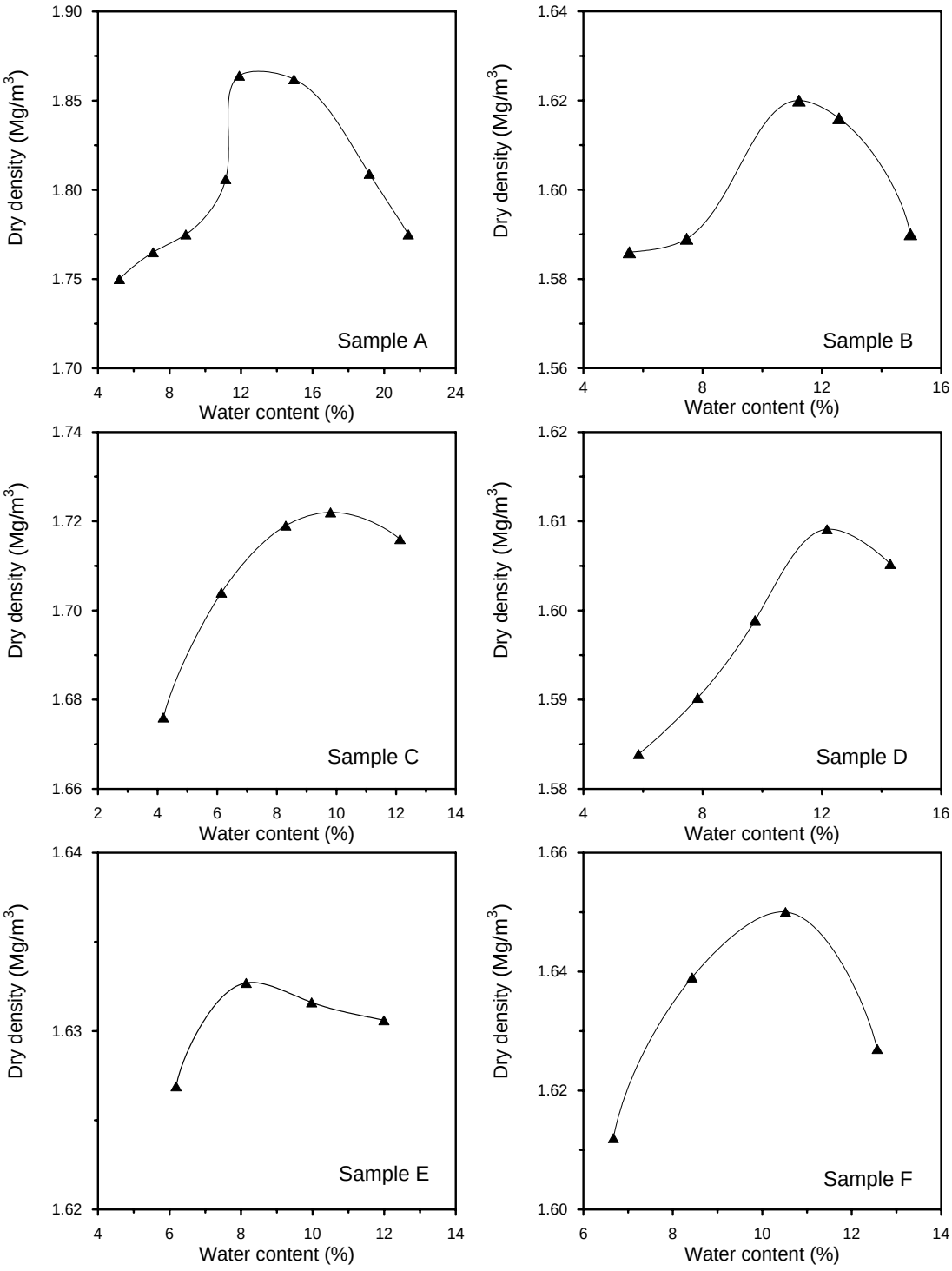

Figure 4.9. The compaction curves for samples A to F

4.4 Specific Gravity Tests

Specific gravity tests were carried out on each sample according to the Turkish Standards (TS1900, 1987) and the results are given in Table 4.9.

Table 4.9. Specific gravity of the samples

Sample	A	B	C	D	E	F
Specific gravity (G_s)	2.64	2.62	2.68	2.64	2.70	2.70

CHAPTER 5

WEDGE SHEAR TESTS PERFORMED

5.1 Cylindrical Wedge Shear Tests Performed

5.1.1 Introduction

Cylindrical wedge shear tests (cylwests) have been carried out using an available compression machine (Fig. 5.1(a)) modified as explained in section 5.1.3, and a double-cut cylwest mould with both cuts inclined at 30^o to the axis (Fig 5.1(b)).

5.1.2 Calculation of Wet Mass of Each Layer

To obtain the same degree of compaction as in the standard Proctor test, the wet mass of each layer and the number of layers in the cylwest mould were calculated to give the same compacted height per layer and the same compactive effort per unit volume as in the standard Proctor test as follows.

In the standard Proctor test, average compacted height per layer is 4 cm and the inside diameter of the mould is 10.16 cm, giving a volume of 324.28 cm^3. When the sand is compacted in the cylwest mould, whose inside diameter is 10.44 cm, using the same height per layer,

$$\text{Compacted volume /layer} = 324.28 \text{ x } \left(\frac{10.44}{10.16}\right)^2 = 342.40 \text{ cm}^3$$

(a)

(b)

Figure 5.1. Apparatus used for cylwests (a) modified compression machine; (b) double-cut mould (after Gürol, 2000)

The wet mass of each layer to be compacted to a height of 40 mm in the cylwest mould = 342.40 x ρ_{bulk}

The bulk density ρ_{bulk} was calculated from

$$\rho_{bulk} = \rho_{dmax} (1+w_{opt})$$

where ρ_{dmax} and w_{opt} for each sample are given in Table 4.8.

To ensure that the top of the sample was well above the upper cut of the mould (Fig. 5.2), the sample was compacted in 9 layers of 40 mm each, giving a total height of 382 mm including the 22 mm high disc at the bottom.

5.1.3 Test Procedure

The following paragraphs have been mostly quoted from Gürol (2000), based on Gün (1997) and Mirata (1991).

1. A tightly fitting wooden disc of 22 mm thickness was inserted in the bottom of the cylwest mould to prevent the cohesionless material from falling out of the mould during handling. The mould was secured on the base plate. For each sample prepared for cylwests as in section 3.2, the calculated amount of sand per layer (section 5.1.2) was weighed, placed in the mould and compacted by using the 2.5 kg rammer to obtain a lower density, and by using the Kango vibrating hammer to obtain a higher density. This procedure was repeated for eight more layers. The specimen compacted in the mould was weighed, the height of the empty portion above the specimen was measured in order to provide the same bulk density in the subsequent shear tests on the same sample, and wooden discs of appropriate height were placed in the empty portion such that they would be flush with the top of the mould.

2. A 5-ton, electrically loaded compression machine was used for loading. To enable the use of this machine for cylwests without impairing its original construction, the cross-beam was replaced by a channel CH as described by Mirata (1991), and the supports for the lateral loading devices mounted on lugs L welded on to the channel CH (Fig. 5.3(a)), and hinged clamps HC; another pair of hinged clamps HC were used to fix the temporary support TS in position on one of the strain rods SR of the compression machine (Fig. 5.3(b)); and a hook HK was welded on to CH for supporting the yoke Y when not in use. Full details of these attachments are given by Mirata (2003(a)). The loading rate was adjusted to 0.15 mm/min and 0.06 mm/min for the samples at the lower and higher densities respectively.

3. The cylwest mould was inserted between the jaws of the clamp C attached to the channel CH, and supported temporarily by the hooked lugs HL (Fig. 5.2(a)) using the rotatable bar TS (Fig. 5.3(b)). The proving ring was set to zero with the grooved plates LP1 and LP2, with the ball cage BC in between, mounted on top. This unit was then placed on the single ball SB resting in a central recess on a steel plate on the loading platen of the compression machine; the test mould was placed on top of LP1, and the loading platen raised until the mould just touched the channel CH (Fig. 5.3(a)). The mould was clamped on to this channel, tightening the vertical screws on the clamp lightly first, then tightening the horizontal screws evenly, and finally tightening the vertical screws. A small load of about 100 N was then applied.

4. The lateral force Q was applied by means of the yoke Y attached to the turnbuckle T and the 900 N capacity spring balance SB (Fig. 5.3(a)). During assembly of the equipment, the yoke rested in the dashed position held by the hook HK. To apply Q, the yoke was swung around to the lower position, and Q was adjusted to the desired value. Q was then kept constant until the peak strength was reached. As relatively large values of Q were to be applied, the rigidity of the stationary part TM (S) of the mould was improved by inserting a cross-bar CB and suitable packing between its lower tip and the strain rods SR (Fig. 5.3(c)).

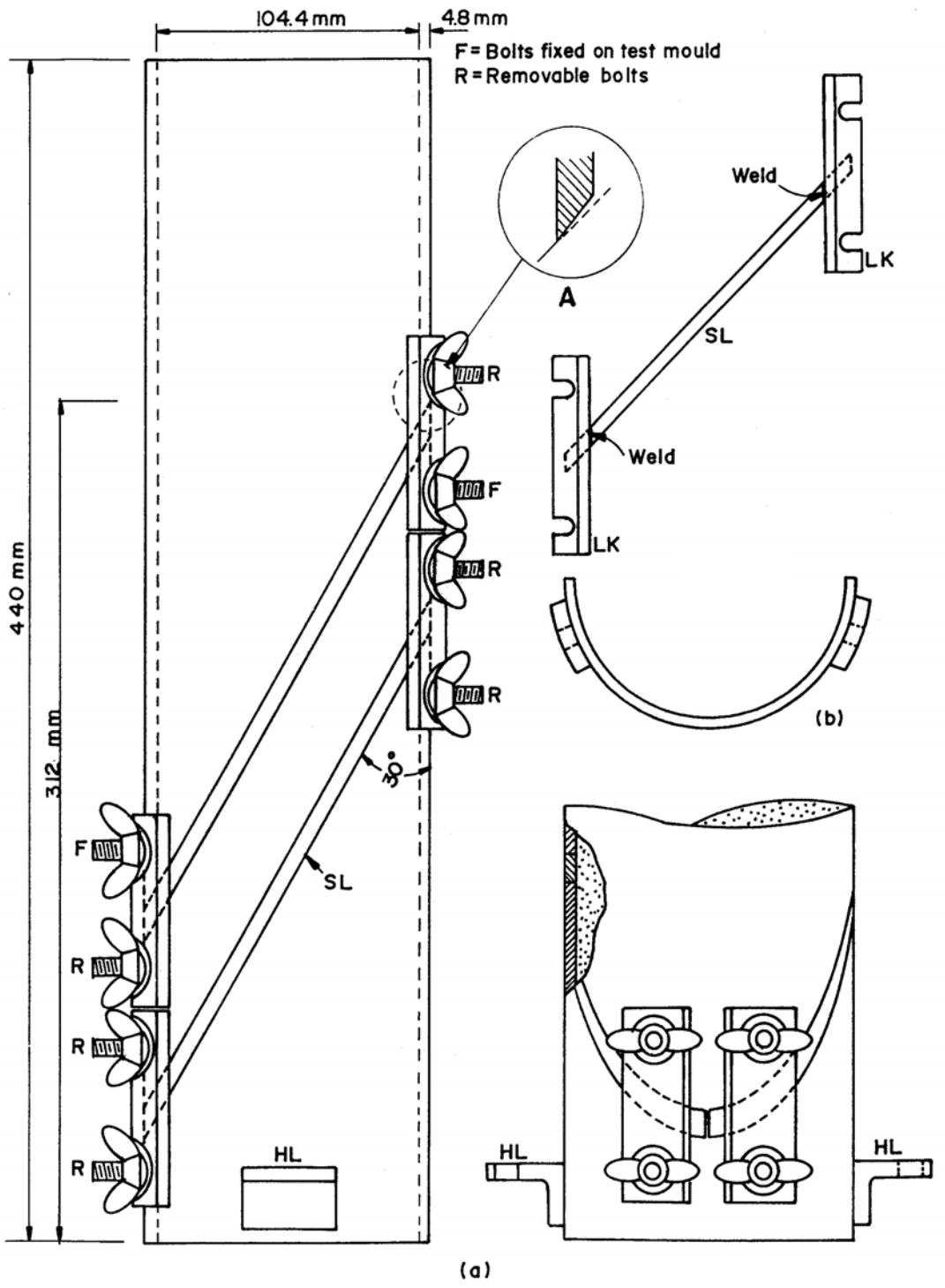

Figure 5.2. The double-cut cylwest mould used (after Gürol (2000), modified from Mirata, 1991; re-modified after Mirata, 2003(a))

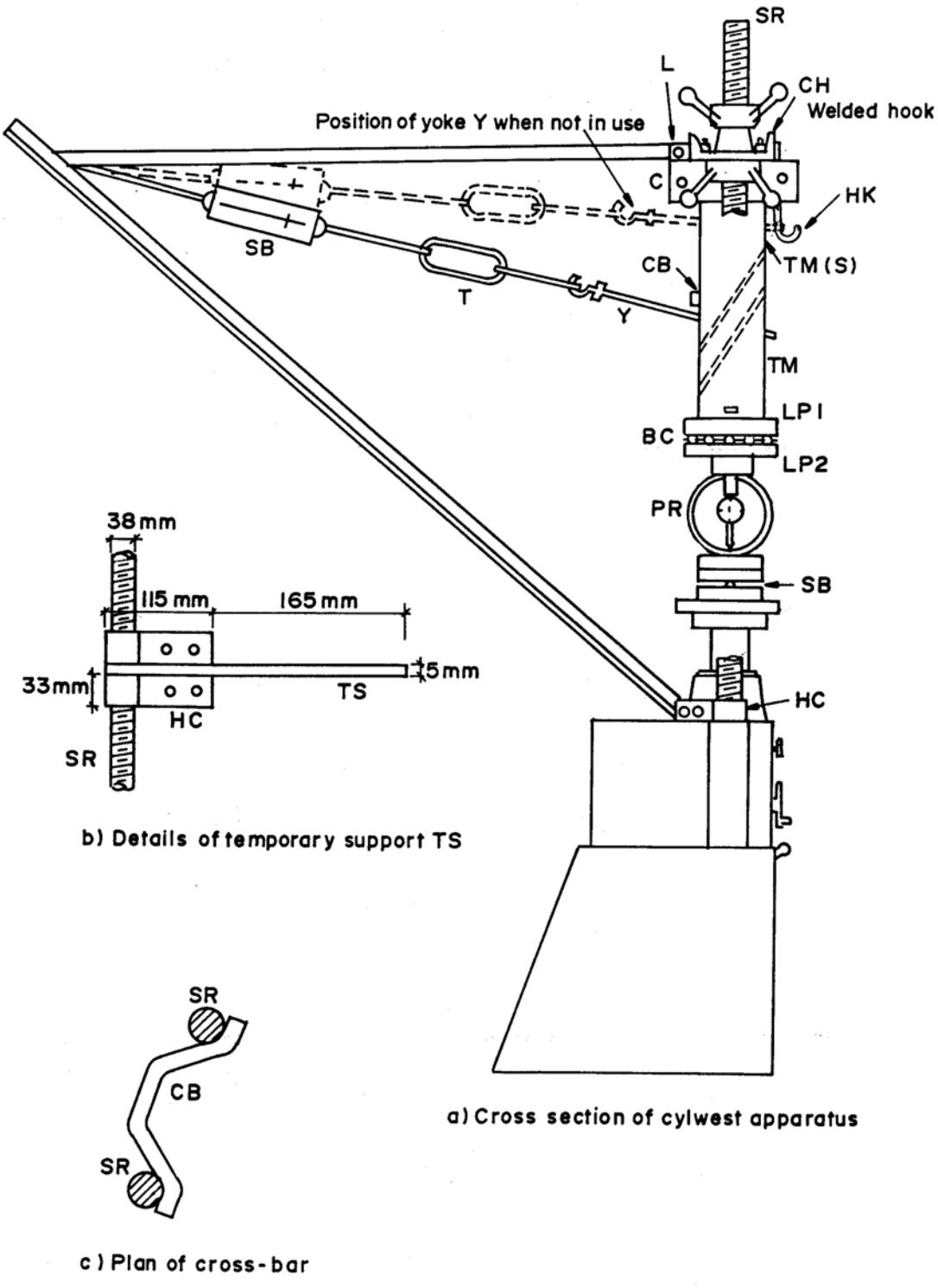

Figure 5.3. Layout for cylwests performed using a 5-ton compression machine (after Gün, 1997)

5. Two dial gauges were mounted in position for measuring the displacements of the mould in the direction of the main load *P* and perpendicular to this direction; for recording the slight rotation β of the mould during the test, another dial gauge was set to register the relative displacement between the grooved plates.

6. As the sand was unable to hold itself in the stationary part of the mould TM (S) after the test, only one test could be performed on the sample after each compaction. So the upper cut of the mould was used in all tests, as this imposed lower moments on the clamp C during application of *Q*. The screws securing the upper pair of mould couplings (Fig. 5.2) were removed and the average clearance n_c between the shearing planes of the two halves of the mould was determined.

7. The catches and brackets on LP1 were turned free of LP2, and the two grooved plates aligned by shifting the single ball. No initial eccentricity was applied. The initial readings of the proving ring dial, and the three displacement dials were recorded.

8. The specimen was sheared by increasing the axial load *P*. After the peak strength was reached, the test was prolonged to measure the ultimate strength. At this stage, calculator programs given by Mirata (2003(a)) were used to adjust *Q* to keep σ at about its value at peak strength. The test was continued until ultimate strength was reached (see Appendix D).

9. The dial gauges were removed. The two grooved plates were fastened together using the swivel catches and brackets. Then *Q* was decreased to about 100 N, and the yoke stretched and hung on to the hook HK (Fig. 5.3(a)). The vertical screws holding one jaw of the clamp were slackened. The horizontal screws of the clamp were slackened evenly. The mould was rotated until it could be supported by means of the rotatable bar TS (Fig. 5.3(b)) through one of the lugs. The loading platen was lowered. The proving ring and the attached grooved plates were

removed, and placed on a plate with a central recess. Holding its two parts together, the mould was removed.

10. The tested specimen was extracted from the test mould and the water content was checked.

11. The same specimen was re-compacted in the cylwest mould as in step 1. Steps 2 to 10 were then repeated using a higher lateral load *Q*.

12. Steps 1 to 11 were repeated on one more specimen of the same sample prepared as in section 3.2.

Each cylwest, including specimen preparation, took about 1.5 hours.

5.1.4 Order of Testing Cylwest Specimens

In accordance with steps (11) and (12) of the test procedure (section 5.1.3), the order of testing of the specimens is summarized below.

In the cylwests at the lower density, the order of testing given in the following paragraph and summarized in Table 5.1, columns 2 to 5 was applied on all samples.

An untested specimen was used for test 1 (column 2). The specimen used in test 1 was recompacted and test 2 (column 3) was performed. Another untested specimen was used for test 3 (column 4). The specimen used in test 3 was recompacted and test 4 (column 5) was performed.

Table 5.1. Specimens used in the cylwests

1	2	3	4	5	6	7	8	9
Sample	Cylwests at the lower density				Cylwests at the higher density			
	Test 1 $Q \approx 93$ N	Test 2 $Q \approx 436$ N	Test 3 $Q \approx 93$ N	Test 4 $Q \approx 436$ N	Test 1 $Q \approx 110$ N	Test 2 $Q \approx 436$ N	Test 3 $Q \approx 110$ N	Test 4 $Q \approx 436$ N
A	S.U. *	R.A.T.** (col. 2)	S.U.	R.A.T. (col. 4)	…	…	…	…
B	S.U.	R.A.T. (col. 2)	S.U.	R.A.T. (col. 4)	…	…	…	…
C	S.U.	R.A.T. (col. 2)	S.U.	R.A.T. (col. 4)	…	…	…	…
D	S.U.	R.A.T. (col. 2)	S.U.	R.A.T. (col. 4)	S.U.	R.A.T. (col. 6)	S.U.	R.A.T. (col. 8)
E	S.U.	R.A.T. (col. 2)	S.U.	R.A.T. (col. 4)	S.U.	R.A.T. (col. 6)	S.U.	R.A.T. (col. 8)
F	S.U.	R.A.T. (col. 2)	S.U.	R.A.T. (col. 4)	S.U.	R.A.T. (col. 6)	S.U.	R.A.T. (col. 8)

* S.U.: separate untested specimen.

* * R.A.T. (col. n): specimen reused after test in column n.

In the cylwests at the higher density, the order of testing given in the following paragraph and summarized in Table 5.1, columns 6 to 9 was applied on samples D to F. Samples A to C were not tested in cylwests at the higher density.

An untested specimen was used for test 1 (column 6). The specimen used in test 1 was recompacted and test 2 (column 7) was performed. Another untested specimen was compacted and test 3 (column 8) was performed. The specimen used in test 3 was recompacted and test 4 (column 9) was performed.

5.1.5 Evaluation of Test Results

The tests were evaluated by using the computer program CYLWEE88 (Mirata, 2003(a)) which performs all three types of analysis explained by Mirata (1991), and summarized in section 2.3.1. The results of cylwests presented are those based on analysis C (section 2.3.1.4).

5.1.6 Test Results

Cylwest series CA to CF of four tests each were performed on samples A to F respectively, at the lower density. The results obtained from the cylwest and triaxial test series on samples A to F at the lower density had shown that the difference in the measured ϕ_d values for samples A to C were higher than those for samples D to F (Table 8.3, column (17)). An increase in density causes the difference in the measured ϕ_d values in plane strain and triaxial tests to increase (section 2.1.4). To see whether the difference in the measured ϕ_d values would increase with density, additional three cylwest series CDH, CEH, and CFH of four tests each were performed on samples D to F respectively, at the higher density.

The principal features of the cylwests are given in Tables 5.2 to 5.4. In these tables, α_n = nominal angle between the shear plane and the axis of test mould; α = true angle between the shear plane and the axis of the test mould at peak

strength; n_c = initial clearance between the stationary and the mobile halves of the test mould; D_r = initial relative density, P = the main load applied; Q = lateral load; $\bar{u}$ = average shear displacement; $\bar{v}$ = average normal displacement; $\delta\sigma/\sigma$ = percentage difference between the normal stress at the trailing end of the soil wedge and the average normal stress; *dv/du* = rate of dilatation (change in $\bar{v}$ (positive values indicating dilatation) divided by the change in $\bar{u}$). Figs. 5.4 and 5.5 show typical curves for series CA and CDH of the variation with $\bar{u}$ of shear stress τ, $\bar{u}$, *dv/du*, and β (Fig. 2.15).

It is observed from the $\bar{u}$ versus $\bar{v}$ curves (Figs. 5.4(b) and 5.5(b)) that at the beginning of the tests, a drop in the $\bar{v}$ values has occurred, especially under the higher values of Q; in the later stages of the tests, dilation has occurred. It is observed from the $\bar{u}$ versus *dv/du* curves (Figs. 5.4(d) and 5.5(d)) that at the end of the tests, the values of *dv/du* are nearly zero, showing that tests have been sufficiently prolonged to yield the ultimate strength.

The results of cylwest series CA to CF and series CDH to CFH are plotted in Figs. 5.6 and 5.7, and summarized in Tables 5.5 to 5.7. In these tables, e is the initial void ratio; D_r is the initial relative density.

Table 5.2. Principal features of cylwest series CA to CC on samples A to C respectively.

1	2	3	4	5	6	7	8	9	10	11	12	13	14	15	16	17	18	19
Test no.	α_n	α	n_c	D_r	Values at peak strength							Values at ultimate strength						
					P	Q	$\bar{u}$	$\bar{v}$	dv/du	β	$\delta\sigma/\sigma$	P	Q	$\bar{u}$	$\bar{v}$	dv/du	β	$\delta\sigma/\sigma$
	(deg)	(deg)	(mm)	(%)	(N)	(N)	(mm)	(mm)	ratio	(deg)	(%)	(N)	(N)	(mm)	(mm)	ratio	(deg)	(%)
CA/1	31.4	29.2	8.2	67.9	1705	100	3.1	0.95	0.55	-0.13	44.9	1326	585	5.9	0.44	-0.25	-0.06	11.9
CA/2	31.4	29.2	8.2	69.4	3201	436	3.9	-0.40	0.33	0.09	11.0	2436	753	6.1	0.06	0.17	0.20	1.0
CA/3	31.4	29.2	8.2	69.8	1662	94	2.3	0.27	0.45	0.10	24.1	1164	437	5.4	0.86	0.11	0.16	8.0
CA/4	31.4	29.2	8.2	67.5	3031	445	3.6	-0.27	0.41	0.09	10.7	2165	760	5.8	0.21	0.03	0.11	0.8
CB/1	31.4	29.2	8.2	61.6	815	89	3.0	1.41	0.46	0.27	28.1	731	336	10.1	1.56	0.02	0.53	-2.1
CB/2	31.4	29.2	8.2	62.7	1874	442	3.1	-0.32	0.28	0.13	5.7	1475	742	8.3	0.59	0.09	0.35	-8.6
CB/3	31.4	29.2	8.2	62.7	693	88	2.1	0.48	0.46	0.14	36.1	629	287	7.7	1.26	-0.06	0.26	11.8
CB/4	31.4	29.2	8.2	63.3	1989	442	3.1	0.01	0.27	0.18	4.1	1610	747	8.5	0.90	0.18	0.47	-11.5
CC/1	31.4	29.2	8.2	29.6	689	94	0.7	0.20	0.48	0.01	42.0	526	186	4.9	1.14	-0.10	0.28	23.3
CC/2	31.4	29.2	8.2	28.2	1763	436	2.5	-0.06	0.27	0.10	7.8	1382	612	9.5	0.53	-0.06	0.23	0.8
CC/3	31.4	29.2	8.2	25.7	650	94	1.0	0.40	0.54	0.06	41.4	488	181	8.3	1.39	0.01	0.44	20.2
CC/4	31.4	29.2	8.2	24.8	1826	436	3.1	-0.95	0.18	-0.15	19.8	1395	677	9.4	-0.31	0.00	0.22	-3.1

Table 5.3. Principal features of cylwest series CD to CF on samples D to F respectively.

1	2	3	4	5	6	7	8	9	10	11	12	13	14	15	16	17	18	19
Test no.	α_n	α	n_c	D_r	Values at peak strength							Values at ultimate strength						
					P	Q	$\bar{u}$	$\bar{v}$	dv/du	β	$\delta\sigma/\sigma$	P	Q	$\bar{u}$	$\bar{v}$	dv/du	β	$\delta\sigma/\sigma$
	(deg)	(deg)	(mm)	(%)	(N)	(N)	(mm)	(mm)	ratio	(deg)	(%)	(N)	(N)	(mm)	(mm)	ratio	(deg)	(%)
CD/1	31.4	29.2	8.2	67.6	567	96	1.2	0.78	0.59	0.11	42.6	472	181	10.3	2.41	0.03	0.45	23.9
CD/2	31.4	29.2	8.2	65.7	1593	441	2.4	0.52	0.41	0.14	6.7	1272	624	7.8	1.27	0.01	0.12	4.2
CD/3	31.4	29.2	8.2	68.1	597	96	1.5	0.04	0.39	0.07	42.2	461	181	7.1	0.86	0.06	0.27	26.3
CD/4	31.4	29.2	8.2	68.1	1674	436	1.7	0.14	0.33	0.05	10.4	1271	667	7.9	0.68	0.03	0.43	-10.8
CE/1	31.4	29.2	8.2	65.5	843	102	2.5	0.56	0.31	0.10	34.3	595	238	8.2	0.15	0.01	0.36	11.0
CE/2	31.4	29.2	8.2	64.0	2226	440	3.0	0.27	0.30	-0.07	20.0	1531	741	10.2	0.19	-0.02	0.29	-5.6
CE/3	31.4	29.2	8.2	65.2	769	102	1.1	0.23	0.38	0.08	33.9	570	243	9.2	0.42	-0.02	0.53	2.7
CE/4	31.4	29.2	8.2	65.2	2309	441	2.5	0.05	0.31	0.11	8.5	1635	740	9.4	0.38	0.02	0.51	-10.3
CF/1	31.4	29.2	8.2	65.3	689	96	1.2	-0.15	0.55	-0.05	45.2	505	199	9.9	2.23	0.21	0.63	9.5
CF/2	31.4	29.2	8.2	65.0	1949	439	2.9	-0.27	0.20	0.11	7.7	1466	659	10.2	0.37	-0.04	0.03	7.3
CF/3	31.4	29.2	8.2	65.0	729	98	1.5	0.04	0.42	0.08	35.8	520	218	10.2	0.69	-0.01	0.57	3.7
CF/4	31.4	29.2	8.2	65.3	2056	441	2.8	0.01	0.20	0.10	9.1	1502	701	12.0	0.74	0.06	0.29	-2.8

Table 5.4. Principal features of cylwest series CDH to CFH on samples D to F respectively.

1	2	3	4	5	6	7	8	9	10	11	12	13	14	15	16	17	18	19
Test no.	α_n	α	n_c	D_r	Values at peak strength							Values at ultimate strength						
						Q	$\bar{u}$	P	dv/du	β	$\delta\sigma/\sigma$	P	Q	$\bar{u}$	$\bar{v}$	dv/du	β	$\delta\sigma/\sigma$
	(deg)	(deg)	(mm)	(%)	(N)	(N)	(mm)	(mm)	ratio	(deg)	(%)	(N)	(N)	(mm)	(mm)	ratio	(deg)	(%)
CDH/1	31.4	29.2	8.2	84.0	805	111	0.6	0.11	.57	0.01	35.4	530	229	7.9	0.97	0.05	0.60	2.7
CDH/2	31.4	29.2	8.2	84.5	2114	438	1.2	-0.03	.24	0.01	12.6	1499	735	7.6	0.45	0.01	0.35	-8.0
CDH/3	31.4	29.2	8.2	85.0	785	111	0.9	-0.15	.71	0.00	36.1	529	210	9.5	1.03	0.01	0.58	6.8
CDH/4	31.4	29.2	8.2	84.5	2043	438	1.2	0.02	.40	0.03	11.4	1407	728	9.2	0.75	0.00	0.37	-8.3
CEH/1	31.4	29.2	8.2	79.9	1851	106	1.9	0.41	0.39	0.06	25.1	1126	460	6.5	0.44	0.15	0.18	5.3
CEH/2	31.4	29.2	8.2	80.3	3069	436	1.5	-0.13	0.38	0.03	12.6	1690	748	8.1	0.27	0.02	0.29	-5.3
CEH/3	31.4	29.2	8.2	79.2	2045	106	1.3	-0.04	0.26	0.00	25.8	1191	506	7.0	0.49	0.00	0.41	-6.1
CEH/4	31.4	29.2	8.2	79.2	3126	436	1.8	-0.39	0.24	-0.05	17.1	1596	746	9.0	-0.12	0.04	0.36	-9.1
CFH/1	31.4	29.2	8.2	84.5	1460	111	1.3	-0.11	0.38	0.01	27.6	962	375	9.6	0.86	0.10	0.56	-7.0
CFH/2	31.4	29.2	8.2	84.1	2937	439	1.9	-0.39	0.23	-0.03	15.7	1556	751	8.7	0.37	0.00	0.14	0.30
CFH/3	31.4	29.2	8.2	84.1	1452	111	1.2	-0.47	0.48	-0.17	39.2	923	413	9.4	0.23	-0.02	0.46	-6.0
CFH/4	31.4	29.2	8.2	84.5	2923	438	1.1	-0.09	0.40	0.02	12.8	1604	752	7.9	0.71	0.02	0.31	-5.8

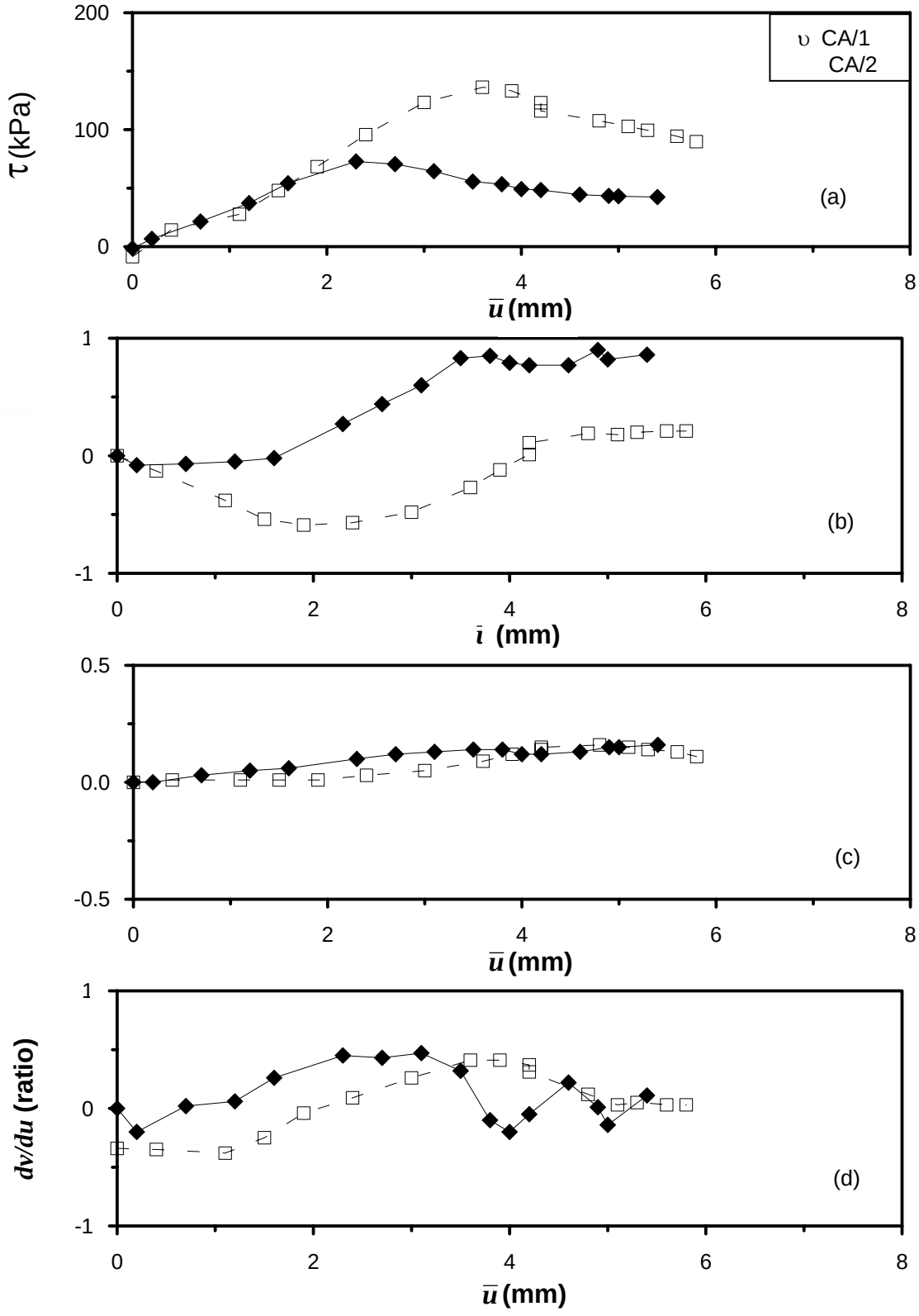

Figure 5.4. Typical curves for series CA of the variation with $\bar{u}$ of (a) τ, (b) $\bar{v}$, (c) β, and (d) dv/du

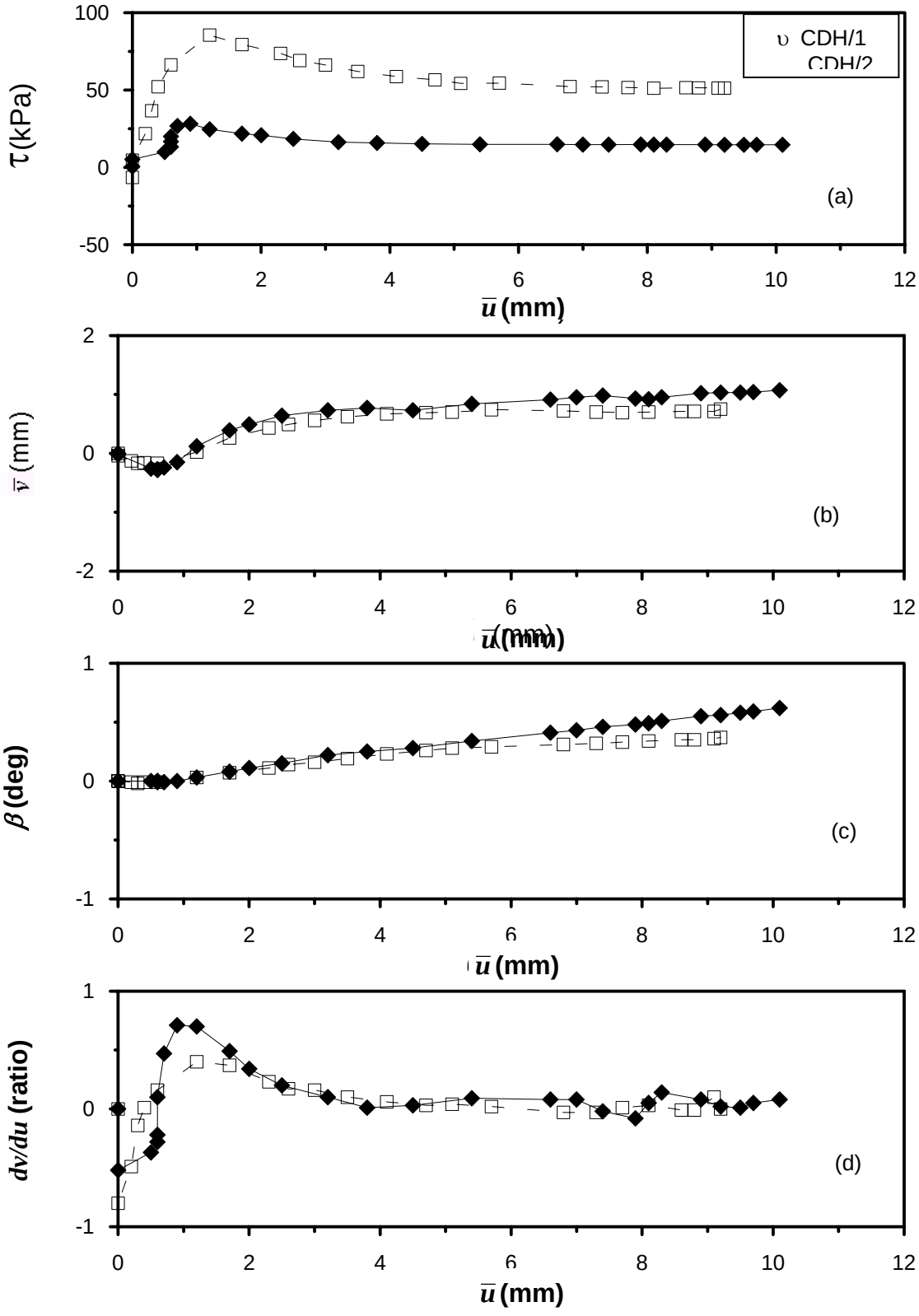

Figure 5.5. Typical curves for series CDH of the variation with $\bar{u}$ of (a) τ, (b) $\bar{v}$, (c) β, and (d) dv/du

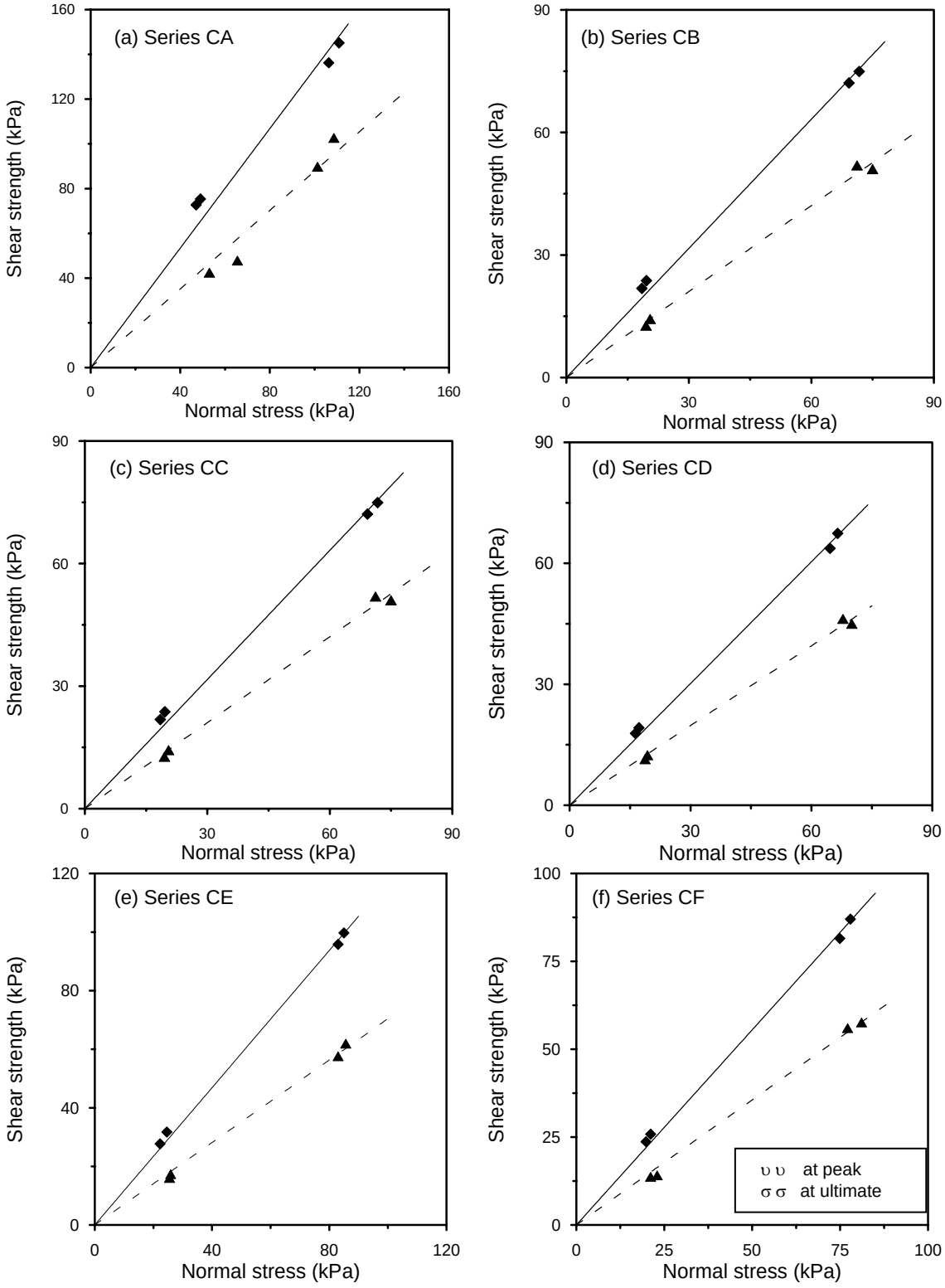

Figure 5.6. The results of cylwests on samples A to F at the lower density

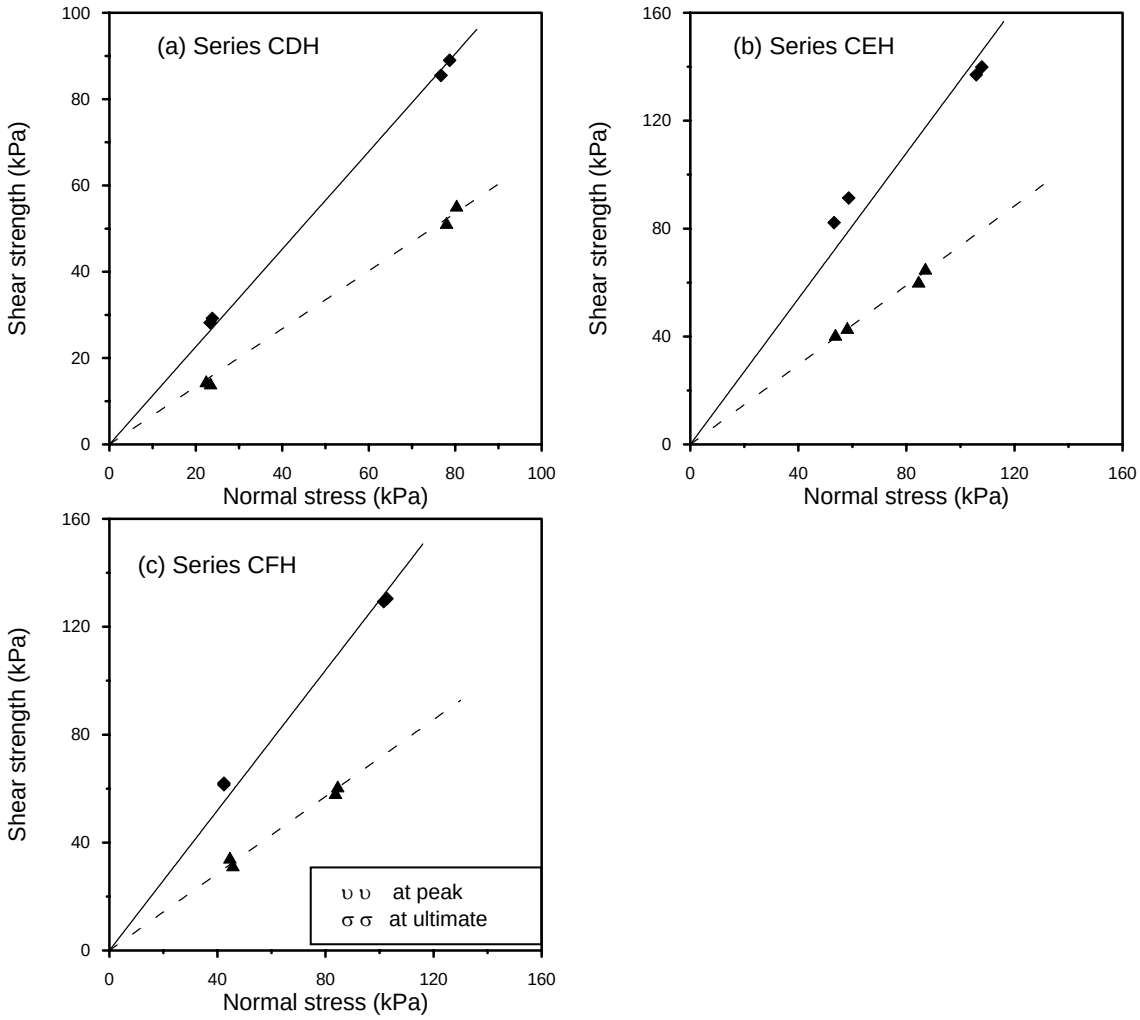

Figure 5.7. The results of cylwests on samples D to F at the higher density

Table 5.5. Results of cylwest series CA to CC

1	2	3	4	5	6	7	8	9	10	11	12	13
Sample	Test no.	e	D_r (%)	Average D_r (%)	Peak strength				Ultimate strength			
					σ (kPa)	τ (kPa)	ϕ (deg)	r	σ (kPa)	τ (kPa)	ϕ (deg)	r
A	CA/1	0.485	67.9	68.7	49.0	75.3	53.2	0.9730	65.5	47.8	41.3	0.9693
	CA2	0.481	69.4		110.9	145.1			108.6	102.6		
	CA/3	0.480	69.8		47.1	72.7			53.0	42.4		
	CA/4	0.486	67.5		106.3	136.2			101.3	89.7		
B	CB/1	0.638	61.6	62.6	23.0	30.8	47.8	0.9923	35.8	23.3	34.6	0.9943
	CB2	0.634	62.7		73.1	78.0			81.4	54.6		
	CB/3	0.634	62.7		19.5	24.4			29.8	18.5		
	CB/4	0.632	63.3		76.2	83.9			85.3	61.6		
C	CC/1	0.556	29.6	27.1	19.6	23.7	46.5	0.9969	20.5	14.3	35.0	0.9975
	CC/2	0.559	28.2		69.2	72.1			71.2	51.9		
	CC/3	0.564	25.7		18.5	21.8			19.5	12.7		
	CC/4	0.566	24.8		71.7	74.9			75.0	51.0		

Table 5.6. Results of cylwest series CD to CF

1	2	3	4	5	6	7	8	9	10	11	12	13
Sample	Test no.	e	D_r (%)	Average D_r (%)	Peak strength				Ultimate strength			
					σ (kPa)	τ (kPa)	ϕ (deg)	r	σ (kPa)	τ (kPa)	ϕ (deg)	r
D	CD/1	0.653	67.6	67.4	16.3	17.8	45.2	0.9984	19.3	12.4	33.4	0.9980
	CD2	0.657	65.7		64.6	63.7			67.8	46.2		
	CD/3	0.652	68.1		17.2	19.2			18.7	11.4		
	CD/4	0.652	68.1		66.5	67.4			70.0	45.0		
E	CE/1	0.650	65.5	65.0	24.6	31.7	49.5	0.9986	25.9	17.3	35.1	0.9978
	CE2	0.654	64.0		83.1	95.8			83.0	57.6		
	CE/3	0.651	65.2		22.4	27.7			25.6	16.0		
	CE/4	0.651	65.2		85.0	99.7			85.6	61.9		
F	CF/1	0.634	65.3	65.2	19.8	23.7	48.0	0.9984	21.1	13.7	35.4	0.9977
	CF/2	0.635	65.0		74.9	81.5			77.1	56.0		
	CF/3	0.635	65.0		21.1	25.8			23.0	14.1		
	CF/4	0.634	65.3		77.9	87.0			81.1	57.6		

Table 5.7. Results of cylwest series CDH to CFH

1	2	3	4	5	6	7	8	9	10	11	12	13
Sample	Test no.	e	D_r (%)	Average D_r (%)	Peak strength				Ultimate strength			
					σ (kPa)	τ (kPa)	ϕ (deg)	r	σ (kPa)	τ (kPa)	ϕ (deg)	r
D	CDH/1	0.618	84.0	85.1	23.8	29.2	48.5	0.9985	23.4	14.1	33.8	0.9981
	CDH/2	0.617	84.5		78.7	89.0			80.3	55.3		
	CDH/3	0.616	85.0		23.3	28.2			22.4	14.6		
	CDH/4	0.617	84.5		76.7	85.5			78.0	51.3		
E	CEH/1	0.612	79.9	79.7	53.2	82.2	53.5	0.9386	53.7	40.6	36.4	0.9929
	CEH/2	0.611	80.3		105.8	137.0			87	65.1		
	CEH/3	0.614	79.2		58.6	91.3			58.1	43.2		
	CEH/4	0.614	79.2		107.9	139.9			84.5	60.3		
F	CFH/1	0.581	84.5	84.3	42.4	62.0	52.4	0.9888	44.6	34.4	35.5	0.9931
	CFH/2	0.582	84.1		102.7	130.4			83.7	58.4		
	CFH/3	0.582	84.1		42.4	61.4			45.7	31.5		
	CFH/4	0.581	84.5		101.5	129.3			84.5	60.8		

5.1.7 Effect on the Cylwest Results of the Order of Testing

In cylwests at the lower and higher densities, both of the untested specimens had been sheared under the lower normal stress σ (Table 5.1). The effect on the cylwest series CA (the plotted peak strength results of which show the largest deviation from the fitted envelope in Fig. 5.6(a)) results of the order of testing can be seen by examining Fig. 5.8. The test numbers are denoted on this figure.

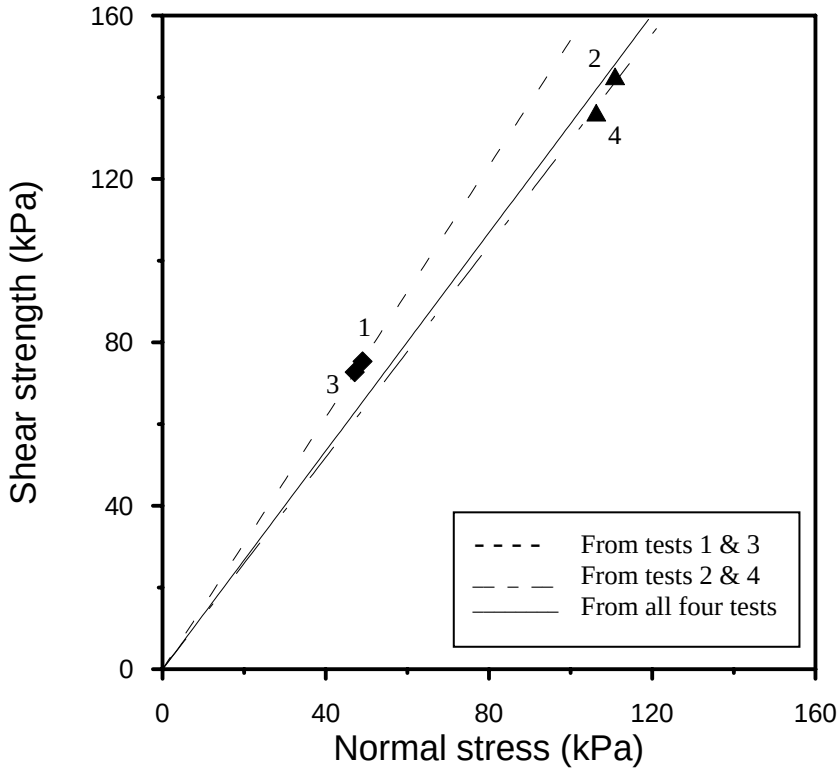

Figure 5.8. The results of cylwest series CA

Fig. 5.8 shows that a higher peak friction angle ϕ_{c2} would be obtained from the two tests 1 and 3 than from tests 2 and 4. According to the sieve analysis before and after cylwests, some particle crushing has occurred (Table 4.2). Crushing of sand particles is considered as the main reason of the reduction in strength; also, an increase in normal stress causes a reduction in strength (section 2.1.3). So, the ϕ_{c2} value defined by tests 2 and 4 in Fig. 5.8 being smaller than that defined by tests 1 and 3 is an expected result. Had test 2, under the higher σ, been performed on an

untested specimen, the corresponding shear strength would be higher than shown in Fig. 5.8; test 3 then would have to be performed on a re-sheared specimen, resulting in a lower shear strength than shown in Fig. 5.8. The net result of this altered order of testing would probably be a relatively small increase in the ϕ value defined by the full line in Fig. 5.8.

5.2 Prismatic Wedge Shear Tests Performed

5.2.1 Introduction

The prismatic wedge shear tests (priswests) have been carried out using a 20-ton loading frame (Mirata, 1992; 2003(a)) and two different test moulds whose shearing planes were inclined at angles α_n = 30^o and 40^o to the main load. In this section, the description of the priswest apparatus, the test procedure, the order of testing priswest specimens, and the results of the tests are presented. Sections 5.2.2 and 5.2.3 have been adapted from Mirata (1991,1992, 2003(a)).

5.2.2 Description of the Priswest Apparatus

The apparatus used in this study is a portable system consisting of loading devices, a test mould and a 20-ton capacity version of the simple, 5-ton frame shown in Fig. 5.9. The modifications to this frame to convert it into a 20-ton one is shown in Fig. 5.10. The priswest mould is made of 10-mm thick mild steel plate, and consists of two identical halves, each with a shear plane measuring 300 mm x 300 mm internally. The mobile half TM has a removable lid; the stationary half TM (S) is bolted on the left - hand beam of the frame (Fig. 5.9(b)). Initially, the two halves of the mould are bolted together through four pairs of links with spacers SR screwed in the middle, and the lid on TM is replaced by a 70 - mm high collar (Fig. 5.9(a)) while the sample is placed in the mould. The grooved loading plates LP1 and LP2, the ball

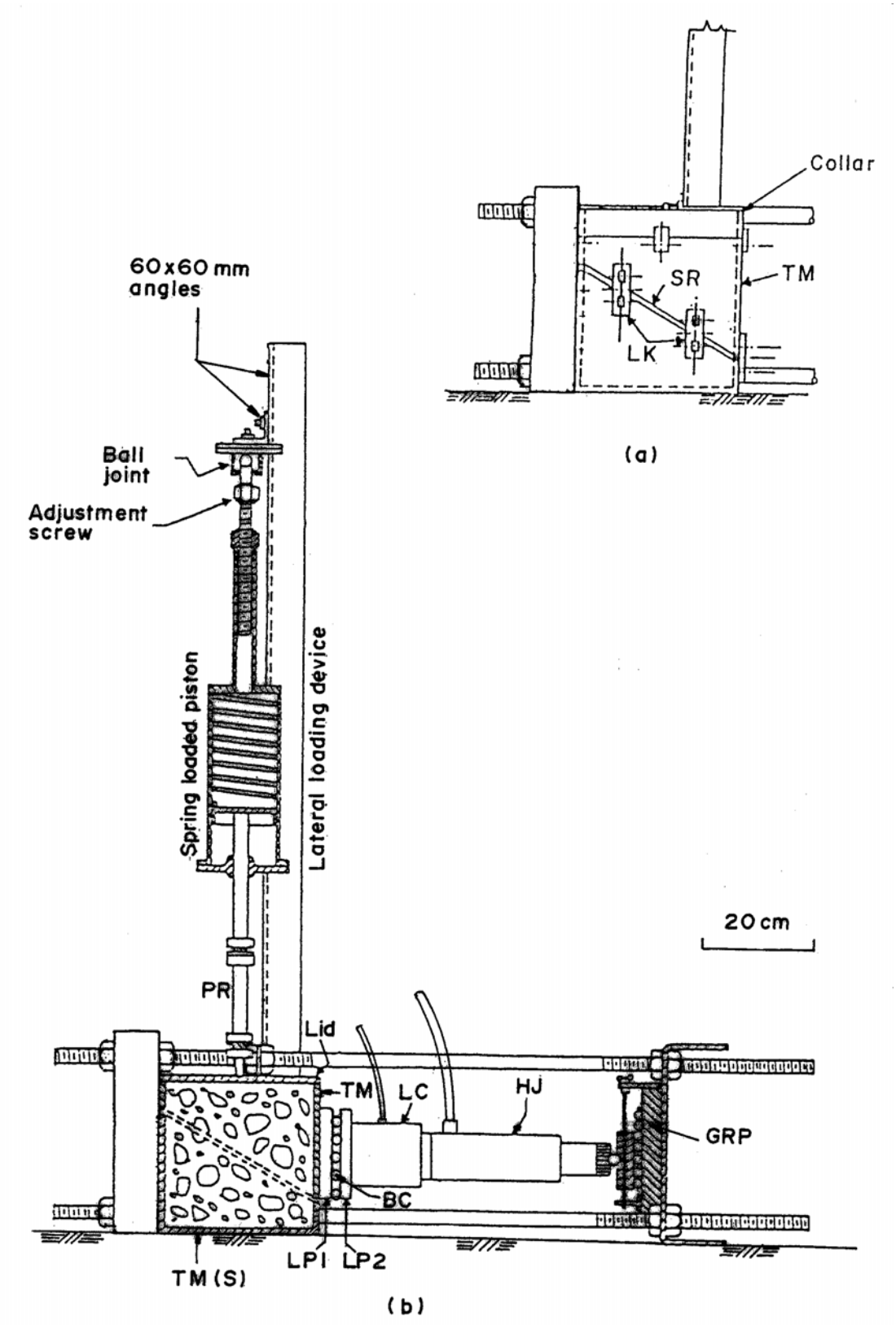

Figure 5.9. Priswest set-up showing (a) box in position for placement of sample and (b) at start of shear (adapted from Mirata, 1991; 2003(a))

cage BC, the load cell LC, and the hydraulic jack HJ are placed between the grooved reaction plate GRP and the test mould TM (Fig. 5.9(b)). The lateral loading device consists of a spring loaded piston, or preferably an air piston as used in this study.

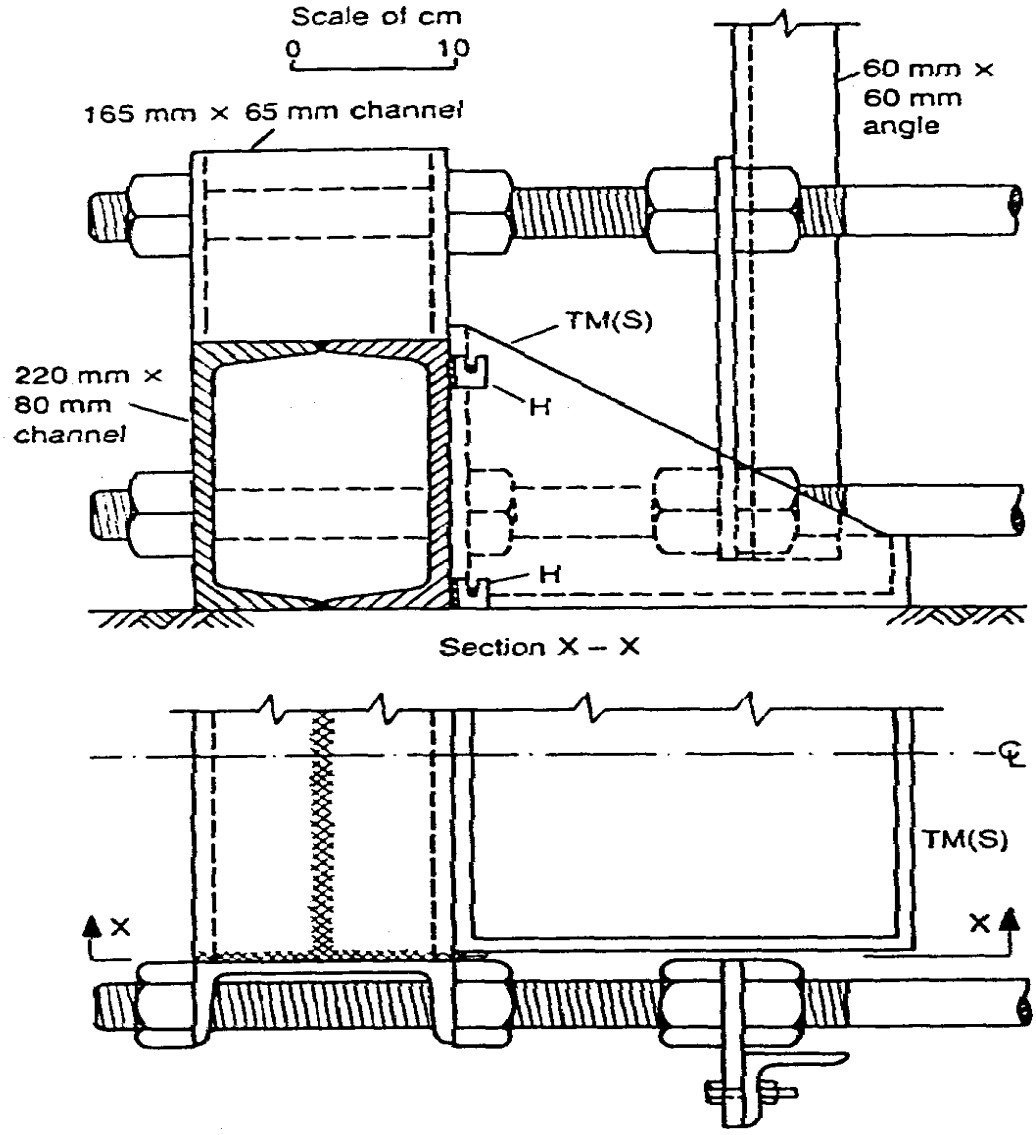

Figure 5.10. Modified cross – beam of 20 ton priswest frame (after Mirata, 1992)

5.2.3 Test Procedure

1. To facilitate the various operations, the lateral loading device (Fig. 5.9(b)) was removed. The lid on TM (Fig. 5.9(b)) was removed, and to prevent grit blocking the tapped holes at the top of the mould, these were temporarily covered with sticky tape. The collar (Fig. 5.9(a)) was screwed on top of the mould through the four lugs.

2. For each sample prepared as in section 3.2, the amount of sand per layer of thickness one-fifth of the total depth of the mould plus 2 mm, required to give the same wet density as that obtained in cylwests was calculated. This amount was compacted to the desired thickness in the priswest mould by applying vibration, using the Kango hammer, directly on the sand for 90 seconds and on a 10-mm thick steel plate placed on top of the sand for another 30 seconds. This procedure was repeated five times, obtaining a compacted sample with the top about 10 mm above the top of the mould.

3. The collar was then removed, the surplus material scraped off, and the surface smoothed. The temporary tapes were removed, and the lid secured in position by fly-bolts. The lateral loading device carrying a proving ring was mounted in position; the proving dial was set to zero before the tip contacted the test mould, and a lateral load of about 150 N was applied.

4. The grooved loading plates LP1 and LP2, the ball cage BC, the load cell LC, and the hydraulic jack HJ were placed between the grooved reaction plate GRP and the test mould TM (Figure 5.9(b)). A main load P of about 200 N was applied.

5. The spacers were removed. Dial gauges were mounted in position for measuring the displacements of the mould in the direction of P and perpendicular to this direction; for recording the slight rotation of the mould during the test, another dial gauge was set to register the relative displacement between the grooved plates.

6. The lateral load Q was raised gradually to the desired value, increasing P by about equal increments. Keeping Q constant, P was gradually increased producing a displacement rate of about 0.5 mm/min in the direction of P. Readings of the displacement dials, and of P and Q were taken. Loading was continued until P started dropping. Then Q was adjusted approximately as explained by Mirata (2003(a)) to keep the normal stress σ at about its value at peak strength; in this approximate method, Q is increased to keep P close to but somewhat below its value at peak strength to account for the reduction in the shear plane area, and the relatively small contribution of Q to σ. At this stage, the rate of loading was increased between readings, restoring this rate to the original value during the readings to minimize rheological effects.

7. At the end of the test, the dial gauges were first removed; Q was then reduced to zero; the lateral loading device was removed. Taking care of the load cell and the grooved plates, P was reduced to zero. The grooved plates, the ball cage, and the load cell were removed. The load cell was stored in a safe place. The grooved plates and ball cage were stored in a dust-proof container. A moisture content specimen was taken from the failure plane; the mould was emptied, cleaned and smeared with machine oil to minimize oxidation.

Each priswest, including specimen preparation, took about 2 hours.

5.2.4 Order of Testing Priswest Specimens

In the priswests on specimens at the lower density, the order of testing given in the following two paragraphs and summarized in Table 5.8, columns 2 to 7 was applied for the different samples.

Table 5.8. Specimens used in the priswests

1		2	3	4	5	6	7	8	9	10	11	12	13
Sample		Priswests at the lower density						Priswests at the higher density					
		Lower σ range			Higher σ range			Lower σ range			Higher σ range		
		Test 1	Test 2	Test 3	Test 4	Test 5	Test 6	Test 1	Test 2	Test 3	Test 4	Test 5	Test 6
A	Specimen used	S.U. *	R.A.T.** (col. 2)	R.A.T. (col. 3)	S.U	R.A.T. (col. 5)	R.A.T. (col. 6)	…	…	…	…	…	…
	Q (N)	1654	3316	4819	1611	3249	4846						
B	Specimen used	S.U.	R.A.T. (col. 2)	R.A.T. (col. 3)	S.U	R.A.T. (col. 5)	R.A.T. (col. 6)	…	…	…	…	…	…
	Q (N)	1665	3316	4954	1649	3167	4900						
C	Specimen used	S.U.	S.U.	S.U.	R.A.T. (col. 4)	R.A.T. (col. 3)	R.A.T. (col. 2)	…	…	…	…	…	…
	Q (N)	1625	3262	4940	1625	3262	4940						
D	Specimen used	S.U.	S.U.	S.U.	R.A.T. (col. 4)	R.A.T. (col. 3)	R.A.T. (col. 2)	S. U.	R.A.T. (col. 8)	R.A.T. (col. 9)	S.U.	R.A.T. (col. 11)	R.A.T. (col. 12)
	Q (N)	610	1151	2105	1665	3316	4940	603	1090	2322	2261	3276	4873
E	Specimen used	S.U.	S.U.	S.U.	R.A.T. (col. 4)	R.A.T. (col. 3)	R.A.T. (col. 2)	S. U.	R.A.T. (col. 8)	R.A.T. (col. 9)	S.U.	R.A.T. (col. 11)	R.A.T. (col. 12)
	Q (N)	610	1131	1990	1652	3276	4900	620	1977	2974	2247	3330	4954
F	Specimen used	S.U.	S.U.	S.U.	R.A.T. (col. 4)	R.A.T. (col. 3)	R.A.T. (col. 2)	S. U.	R.A.T. (col. 8)	R.A.T. (col. 9)	S.U.	R.A.T. (col. 11)	R.A.T. (col. 12)
	Q (N)	589	1246	2410	1652	3289	4893	583	1510	2525	2247	3357	4995

* S.U.: separate untested specimen

* * R.A.T. (col. n): specimen reused after test in column n

For each of the samples A and B, an untested specimen was used for test 1 (column 2). The specimen used in test 1 was recompacted and test 2 (column 3) was performed. The specimen used in test 2 was compacted a third time and test 3 (column 4) was performed. Another untested specimen was used for test 4 (column 5). The specimen used in test 4 was recompacted and test 5 (column 6) was performed. The specimen used in test 5 was compacted a third time and test 6 (column 7) was performed.

For each of the samples C to F, each of the tests under the lower σ (columns 2 to 4) was performed on a separate untested specimen. Each specimen used in tests 3, 2, and 1 was recompacted, and test 4 (column 5), test 5 (column 6), and test 6 (column 7) respectively were performed.

In the priswests on specimens at the higher density, the order of testing given in the following paragraph and summarized in Table 5.8, columns 8 to 13 was applied on samples D to F. Samples A to C were not tested at the higher density.

For each of the samples D to F, an untested specimen was used for test 1 (column 8). The specimen used in test 1 was recompacted and test 2 (column 9) was performed. The specimen used in test 2 was compacted a third time and test 3 (column 10) was performed. Another untested specimen was compacted and test 4 (column 11) was performed. The specimen used in test 4 was recompacted and test 5 (column 12) was performed. The specimen used in test 5 was compacted a third time and test 6 (column 13) was performed.

5.2.5 Evaluation of the Test Results

The tests were evaluated by using the computer program IWPW77 (Mirata, 2003(a)) which performs all three types of analysis explained by Mirata (1991), and summarized in section 2.3.1. The results of priswests presented are those based on analysis C (section 2.3.1.4).

5.2.6 Test Results

Priswests series PA1 to PF1 were carried out on samples A to F under the lower normal stresses σ, using a 30^o test mould. Series PA2 to PF2 were carried out on samples A to F under the higher σ, using a 40^o test mould. For the reason explained in section 5.1.6, additional priswest series PDH1 to PFH1 and PDH2 to PFH2 were performed on samples D to F at a higher density, under the lower and higher σ respectively. Each series consisted of three tests.

The principal features of the priswests are given in Tables 5.9 to 5.14. In these tables, Δy_p = shift in the positive y direction (Fig. 2.15) applied to P prior to testing. The rest of the symbols are defined in section 5.1.6. Typical curves of the variation with $\bar{u}$ of τ, $\bar{v}$, dv/du, and β (Fig. 2.15) are plotted in Figs. 5.11 to 5.14. It is observed from the $\bar{u}$ versus dv/du curves (Figs. 5.11(d) to 5.14(d)) that at the end of the tests, the values of dv/du are nearly zero, showing that all tests have been sufficiently prolonged to yield the ultimate strength.

The results of the priswests are plotted in Figs. 5.15 to 5.19, and summarized in Tables 5.15 to 5.19. The combined results of all priswests performed on each sample are also given in Tables 5.15 to 5.19.

Table 5.9. Principal features of priswest series PA1 to PC1 on samples A to C respectively.

1	2	3	4	5	6	7	8	9	10	11	12	13	14	15	16	17	18	19
Test no.	α_n	n_c	D_r	Δy_p	Values at peak strength							Values at ultimate strength						
					P	Q	$\bar{u}$	$\bar{v}$	dv/du	β	$\delta\sigma/\sigma$	P	Q	$\bar{u}$	$\bar{v}$	dv/du	β	$\delta\sigma/\sigma$
	(deg)	(mm)	(%)	(mm)	(N)	(N)	(mm)	(mm)	ratio	(deg)	(%)	(N)	(N)	(mm)	(mm)	ratio	(deg)	(%)
PA1/1	29.30	8.7	69.8	5.0	10300	1661	5.6	1.14	0.22	0.22	-3.1	7784	3357	45.8	0.04	0.00	-0.34	9.0
PA1/2	29.30	9.2	67.9	5.3	18080	3343	5.8	1.42	0.28	0.02	-0.4	9922	4494	16.2	0.61	-0.17	0.09	-2.1
PA1/3	29.30	6.5	67.2	3.7	25870	4886	7.2	1.01	0.48	0.09	0.7	18780	6740	21.8	1.71	-0.02	0.37	-4.5
PB1/1	29.30	7.3	63.6	4.2	7941	1692	5.0	2.17	0.62	0.38	-2.2	7298	3621	36.4	1.57	-0.06	-0.85	21.1
PB1/2	29.30	6.0	63.0	3.4	11756	3019	9.0	1.12	-0.01	-0.10	10.6	10700	4210	26.3	-0.67	-0.10	-0.63	19.5
PB1/3	29.30	6.0	64.7	3.4	18499	5035	10.9	2.34	0.31	1.06	-25.9	15082	6795	23.3	3.81	0.01	1.08	-19.0
PC1/1	29.30	7.0	29.6	4.0	7379	1611	4.4	-0.41	0.05	0.06	5.0	6811	3012	42.3	-1.54	-0.13	0.84	-19.6
PC1/2	29.30	6.7	26.2	3.8	11287	3289	4.0	-0.56	-0.09	-0.26	10.1	9341	4331	38.3	-3.16	0.20	-0.02	-3.5
PC1/3	29.30	7.0	29.6	4.0	16891	4954	7.4	0.05	0.15	0.31	-7.5	12260	6104	27.1	-0.59	0.06	0.39	-11.1

Table 5.10. Principal features of priswest series PA2 to PC2 on samples A to C respectively.

1	2	3	4	5	6	7	8	9	10	11	12	13	14	15	16	17	18	19
Test no.	α_n	n_c	D_r	Δy_p	Values at peak strength							Values at ultimate strength						
					P	Q	$\bar{u}$	$\bar{v}$	dv/du	β	$\delta\sigma/\sigma$	P	Q	$\bar{u}$	$\bar{v}$	dv/du	β	$\delta\sigma/\sigma$
	(deg)	(mm)	(%)	(mm)	(N)	(N)	(mm)	(mm)	ratio	(deg)	(%)	(N)	(N)	(mm)	(mm)	ratio	(deg)	(%)
PA2/1	39.91	6.8	69.8	3.5	25287	1625	4.5	-1.52	0.11	0.19	-4.6	19364	2937	13.5	-1.38	-0.10	0.28	-0.40
PA2/2	39.91	6.8	69.4	3.5	43982	3262	7.0	-2.81	0.16	0.54	-17.8	25105	6537	31.3	-1.06	-0.08	0.74	-6.60
PA2/3	39.91	6.8	68.3	3.5	50588	4900	9.8	0.90	0.21	1.04	-28.2	25980	6808	38.1	1.33	0.01	0.66	2.00
PB2/1	39.91	5.0	68.1	2.4	19744	1672	4.3	-0.59	0.14	0.29	-2.7	16736	4862	45.3	-1.65	-0.03	0.51	7.80
PB2/2	39.91	4.7	62.5	2.2	24932	3262	4.4	-1.71	0.23	0.34	-6.1	21407	6294	50.4	-1.77	-0.04	0.77	2.60
PB2/3	39.91	4.5	63.3	2.0	31519	4947	4.7	-1.92	0.30	0.25	-4.0	23840	6828	26.5	0.26	0.00	0.74	-3.70
PC2/1	39.91	4.9	24.3	2.3	12747	1665	2.6	-0.40	0.08	0.06	5.3	12066	3316	27.2	-0.51	-0.03	0.12	13.6
PC2/2	39.91	4.7	27.2	2.2	21213	3262	3.4	-2.28	-0.02	-0.01	3.2	19266	5448	41.3	-3.11	-0.05	1.05	-10.0
PC2/3	39.91	4.7	28.2	2.2	34234	4913	3.5	-1.87	0.14	0.29	-6.4	21016	5847	34.6	-1.95	-0.02	0.71	-2.1

Table 5.11. Principal features of priswest series PD1 to PF1 on samples D to F respectively.

1	2	3	4	5	6	7	8	9	10	11	12	13	14	15	16	17	18	19
Test no.	α_n	n_c	D_r	Δy_p	Values at peak strength							Values at ultimate strength						
					P	Q	$\bar{u}$	$\bar{v}$	dv/du	β	$\delta\sigma/\sigma$	P	Q	$\bar{u}$	$\bar{v}$	dv/du	β	$\delta\sigma/\sigma$
	(deg)	(mm)	(%)	(mm)	(N)	(N)	(mm)	(mm)	ratio	(deg)	(%)	(N)	(N)	(mm)	(mm)	ratio	(deg)	(%)
PD1/1	29.30	7.9	70.4	4.5	3471	616	2.0	-6.2	-0.32	-0.74	38.4	2828	1070	42.0	-0.94	-0.04	0.50	3.1
PD1/2	29.30	5.8	68.5	3.4	5136	1162	1.5	0.90	0.88	-0.41	25.5	4189	1811	40.5	-1.6	-0.20	0.52	-5.5
PD1/3	29.30	4.8	69.5	2.8	8334	2132	1.7	-0.28	-0.09	-0.04	9.3	5941	2789	27.0	-1.61	-0.03	-0.26	10.8
PE1/1	29.30	6.3	64.8	3.6	4276	612	5.2	2.02	0.18	0.33	10.0	3217	1110	43.3	0.66	-0.02	0.72	2.2
PE1/2	29.30	6.8	64.8	3.9	6313	1151	2.5	0.01	0.42	-0.28	18.7	4678	1841	21.4	0.07	0.10	-0.27	16.5
PE1/3	29.30	4.8	65.9	2.8	9229	2004	5.7	1.95	0.11	-0.15	17.2	7406	3181	26.0	1.42	-0.04	0.22	4.2
PF1/1	29.30	6.4	67.5	3.7	4072	599	3.7	0.93	0.71	-0.04	20.7	3118	1148	37.5	-1.99	-0.12	-0.75	32.9
PF1/2	29.30	5.7	64.6	3.3	6211	1266	5.4	0.61	-0.08	0.05	11.4	4873	1936	42.9	-0.24	0.19	0.86	-10.6
PF1/3	29.30	6.8	66.1	3.9	9813	2426	5.6	0.78	0.20	-0.06	8.2	7894	3502	48.8	-0.27	-0.10	0.91	-21.3

Table 5.12. Principal features of priswest series PD2 to PF2 on samples D to F respectively.

1	2	3	4	5	6	7	8	9	10	11	12	13	14	15	16	17	18	19
Test no.	α_n	n_c	D_r	Δy_p	Values at peak strength							Values at ultimate strength						
					P	Q	$\bar{u}$	$\bar{v}$	dv/du	β	$\delta\sigma/\sigma$	P	Q	$\bar{u}$	$\bar{v}$	dv/du	β	$\delta\sigma/\sigma$
	(deg)	(mm)	(%)	(mm)	(N)	(N)	(mm)	(mm)	ratio	(deg)	(%)	(N)	(N)	(mm)	(mm)	ratio	(deg)	(%)
PD2/1	39.91	4.9	69.0	2.3	11995	1679	3.6	0.22	0.20	0.17	3.8	11020	3046	28.5	0.19	-0.02	1.20	-11.7
PD2/2	39.91	4.8	71.4	2.2	20941	3337	3.8	0.71	0.15	-0.08	9.0	18236	5116	34.9	0.51	-0.12	1.15	-12.0
PD2/3	39.91	5.2	66.2	2.5	25235	4981	5.4	0.56	0.15	0.27	-1.9	20967	6226	24.2	1.49	0.16	1.05	-11.7
PE2/1	39.91	5.7	64.0	2.8	17915	1683	3.9	-0.17	0.19	0.08	3.1	13555	3369	46.5	-2.55	-0.60	0.71	4.1
PE2/2	39.91	5.0	63.3	2.4	25979	3316	4.8	0.19	0.05	0.14	1.9	18822	4832	51.2	-0.67	-0.03	1.80	-22.5
PE2/3	39.91	5.2	63.3	2.5	33511	4940	7.4	2.11	0.22	0.32	-1.0	21352	5401	44.3	2.53	0.00	0.74	8.2
PF2/1	39.91	4.9	65.3	2.3	15909	1665	3.9	0.20	0.22	-0.08	10.7	12455	2937	30.3	1.37	-0.01	0.76	2.4
PF2/2	39.91	5.2	65.7	2.5	27273	3350	6.0	-0.49	0.12	0.32	-4.2	19072	3939	52.6	-1.53	0.02	1.18	-2.2
PF2/3	39.91	4.7	66.4	2.2	34219	4974	4.3	-1.28	0.07	-0.06	5.4	26078	5590	48.2	-2.09	-0.03	-0.02	30.0

Table 5.13. Principal features of priswest series PDH1 to PFH1 on samples D to F respectively.

1	2	3	4	5	6	7	8	9	10	11	12	13	14	15	16	17	18	19
Test no.	α_n	n_c	D_r	Δy_p	Values at peak strength							Values at ultimate strength						
					P	Q	$\bar{u}$	$\bar{v}$	dv/du	β	$\delta\sigma/\sigma$	P	Q	$\bar{u}$	$\bar{v}$	dv/du	β	$\delta\sigma/\sigma$
	(deg)	(mm)	(%)	(mm)	(N)	(N)	(mm)	(mm)	ratio	(deg)	(%)	(N)	(N)	(mm)	(mm)	ratio	(deg)	(%)
PDH1/1	29.30	6.5	84.5	3.8	4226	610	3.0	0.46	0.32	-0.19	23.9	2536	913	47.8	-0.69	-0.06	1.69	-24.3
PDH1/2	29.30	5.6	85.4	3.2	5224	1097	3.3	0.49	-0.10	-0.09	17.2	3998	1638	47.8	-2.77	-0.19	1.23	-24.3
PDH1/3	29.30	6.2	84.5	3.5	9030	2335	2.9	0.10	0.12	-0.37	17.0	7217	3343	44.4	-1.04	-0.17	1.25	-31.8
PEH1/1	29.30	5.1	80.7	2.9	5470	623	4.5	1.55	0.23	-0.10	31.6	4182	1395	55.7	-1.08	-0.03	1.63	-4.3
PEH1/2	29.30	5.0	79.9	2.8	11020	1981	3.3	0.25	0.21	-0.91	53.6	8874	3303	48.2	-1.68	-0.02	0.05	37.3
PEH1/3	29.30	5.9	79.2	3.4	13458	2971	5.1	0.45	0.21	-0.60	42.7	9460	4169	50.5	-0.68	-0.10	1.25	3.8
PFH1/1	29.30	5.1	84.5	2.9	5816	592	4.2	1.27	0.24	-0.07	20.7	4475	1604	55.6	-2.56	-0.06	0.84	-10.3
PFH1/2	29.30	5.8	84.8	3.3	7704	1530	5.5	0.75	0.33	-0.54	28.4	5364	2366	45.4	-0.56	-0.01	0.69	-10.5
PFH1/3	29.30	5.5	84.1	3.2	10337	2531	4.2	0.20	0.20	-0.50	22.1	7509	3398	48.9	-1.74	-0.04	0.40	-8.9

Table 5.14. Principal features of priswest series PDH2 to PFH2 on samples D to F respectively.

1	2	3	4	5	6	7	8	9	10	11	12	13	14	15	16	17	18	19
Test no.	α_n	n_c	D_r	Δy_p	Values at peak strength							Values at ultimate strength						
					P	Q	$\bar{u}$	$\bar{v}$	dv/du	β	$\delta\sigma/\sigma$	P	Q	$\bar{u}$	$\bar{v}$	dv/du	β	$\delta\sigma/\sigma$
	(deg)	(mm)	(%)	(mm)	(N)	(N)	(mm)	(mm)	ratio	(deg)	(%)	(N)	(N)	(mm)	(mm)	ratio	(deg)	(%)
PDH2/1	39.91	5.8	84.0	2.9	21845	2261	4.0	1.29	0.32	0.18	0.9	15018	4748	60.6	1.52	-0.15	0.64	11.6
PDH2/2	39.91	5.4	85.4	2.6	28964	3330	2.1	-0.22	0.15	-0.02	3.4	22625	7167	56.2	-2.22	0.01	0.63	4.0
PDH2/3	39.91	5.9	85.0	2.9	35107	5013	3.9	-0.65	0.14	0.18	-3.5	22040	6984	56.8	-2.05	-0.01	1.02	-7.8
PEH2/1	39.91	5.6	79.5	2.7	24327	2274	4.9	-0.01	0.18	0.55	-12.0	19894	5279	53.9	-1.28	-0.08	0.77	4.4
PEH2/2	39.91	4.9	80.3	2.3	33352	3370	6.0	-0.01	0.07	0.49	-8.9	27403	7363	58.1	-1.88	-0.03	1.07	-3.7
PEH2/3	39.91	4.9	80.7	2.3	38618	5035	6.7	-0.06	0.12	0.63	-13.2	27988	7471	57.3	-1.84	-0.08	1.37	-13.5
PFH2/1	39.91	5.2	84.8	2.5	22332	2288	6.1	0.13	0.14	0.39	-4.6	16969	4568	49.8	-1.40	0.02	1.18	-9.2
PFH2/2	39.91	5.3	84.1	2.6	29009	3398	5.1	-0.43	0.07	0.23	-2.3	21747	6206	59.5	-2.55	-0.12	0.95	-1.7
PFH2/3	39.91	6.0	83.8	3.0	37680	5051	5.5	-0.58	0.09	0.26	-5.1	26233	7187	50.7	-2.03	0.00	0.64	4.6

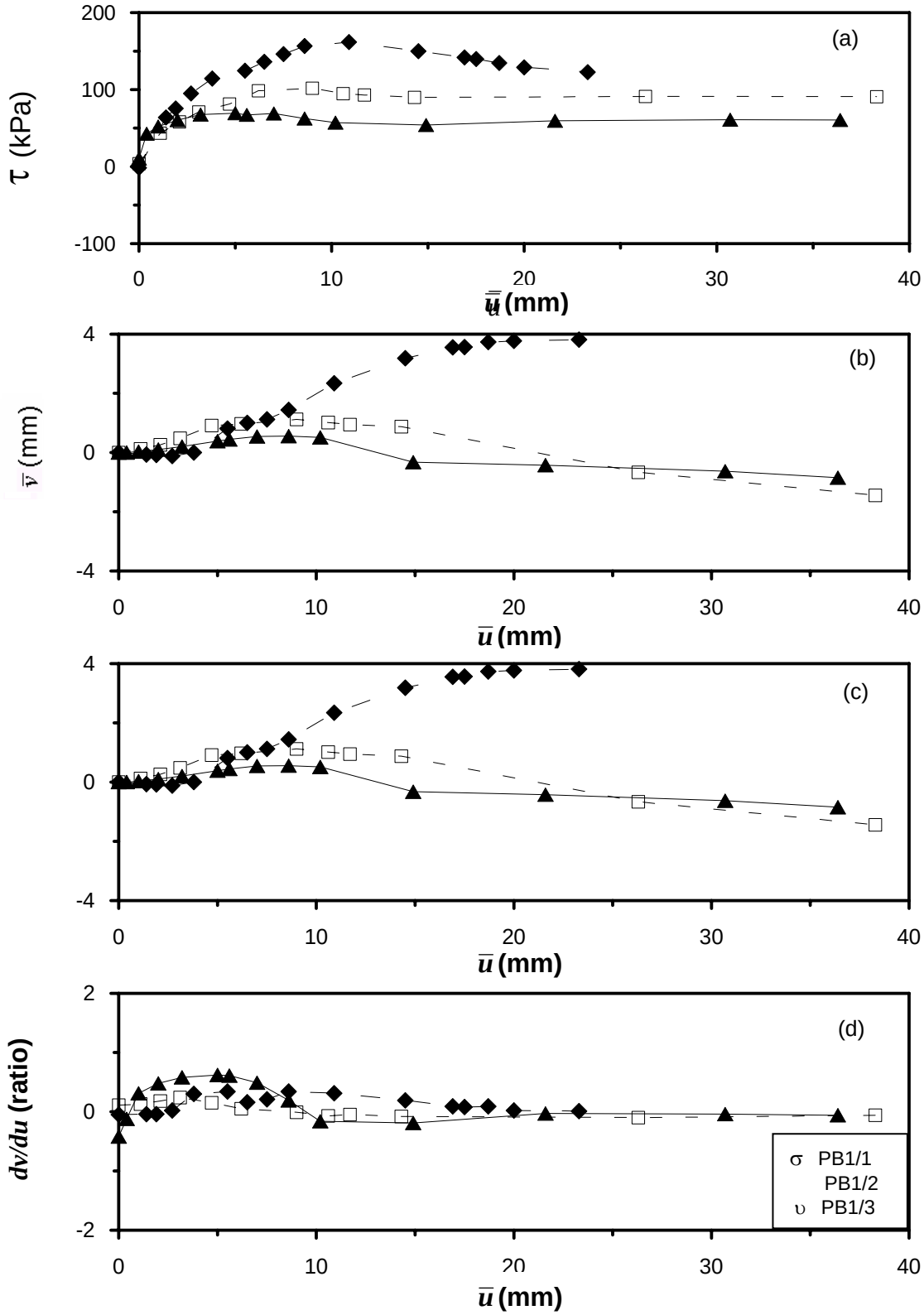

Figure 5.11. Typical curves for series PB1 of the variation with $\bar{u}$ of (a) τ, (b) $\bar{v}$, (c) β, and (d) dv/du

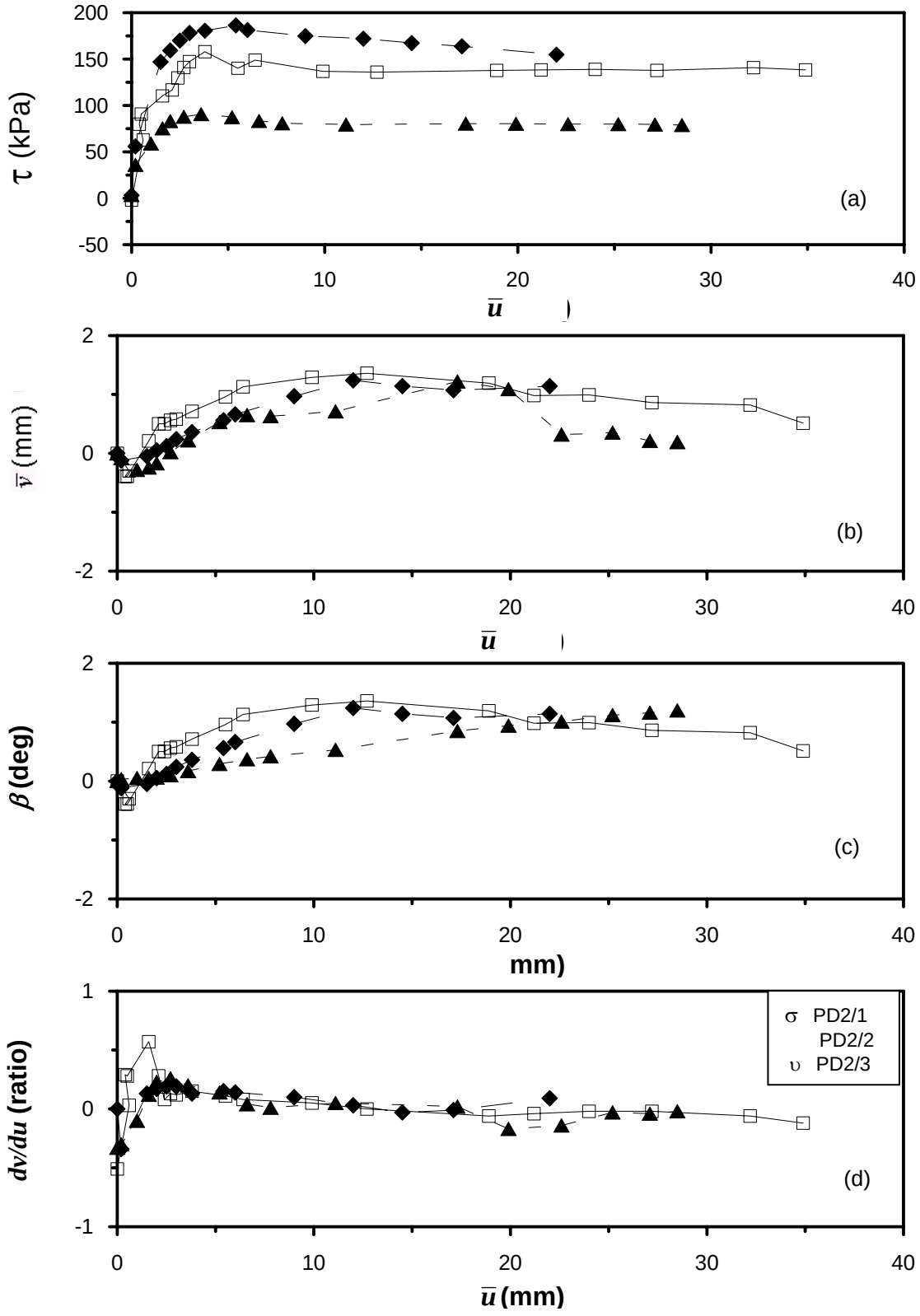

Figure 5.12. Typical curves for series PD2 of the variation with $\bar{u}$ of (a) τ, (b) $\bar{v}$, (c) β, and (d) dv/du

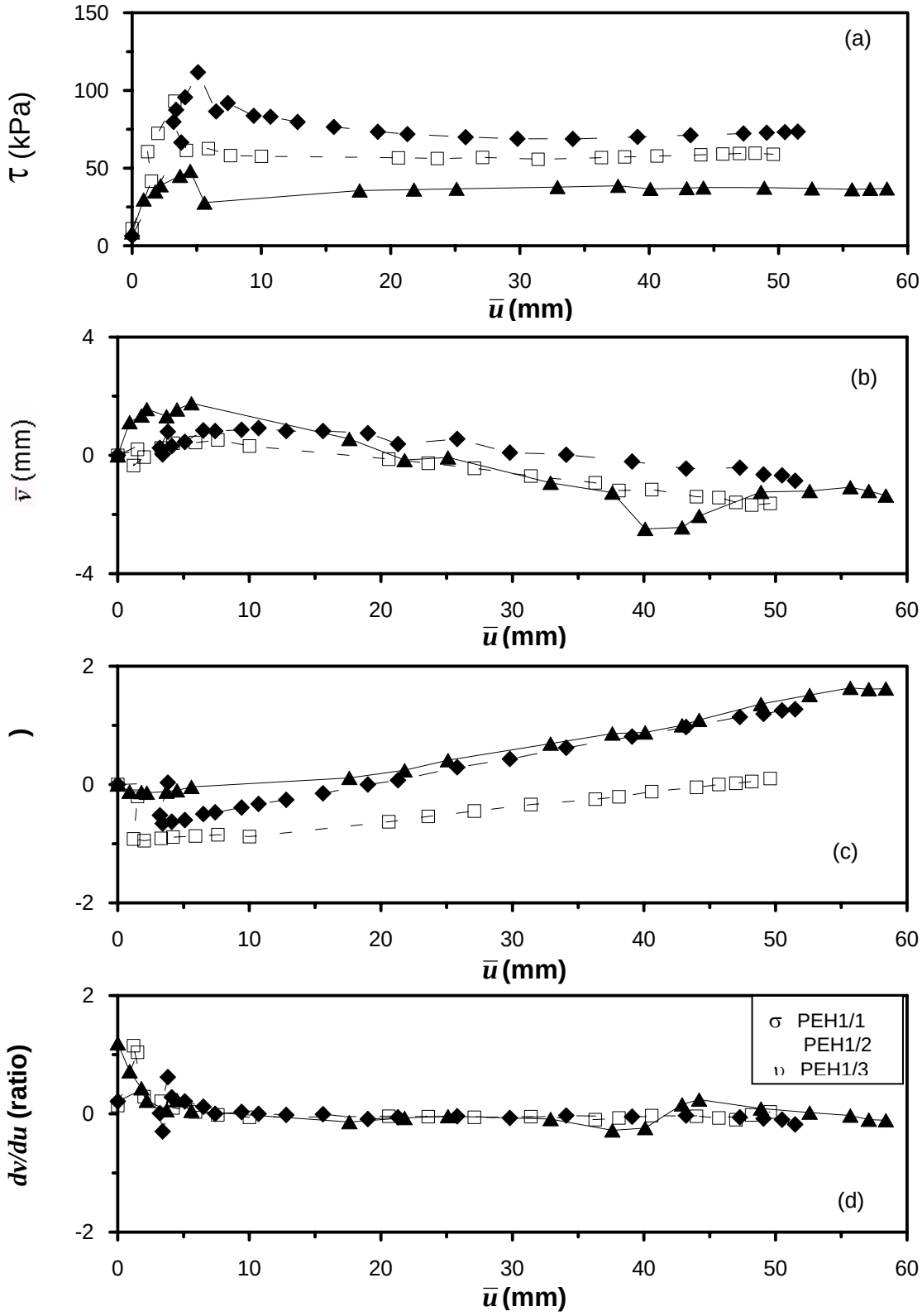

Figure 5.13. Typical curves for series PEH1 of the variation with $\bar{u}$ of (a) τ, (b) $\bar{v}$, (c) β, and (d) dv/du

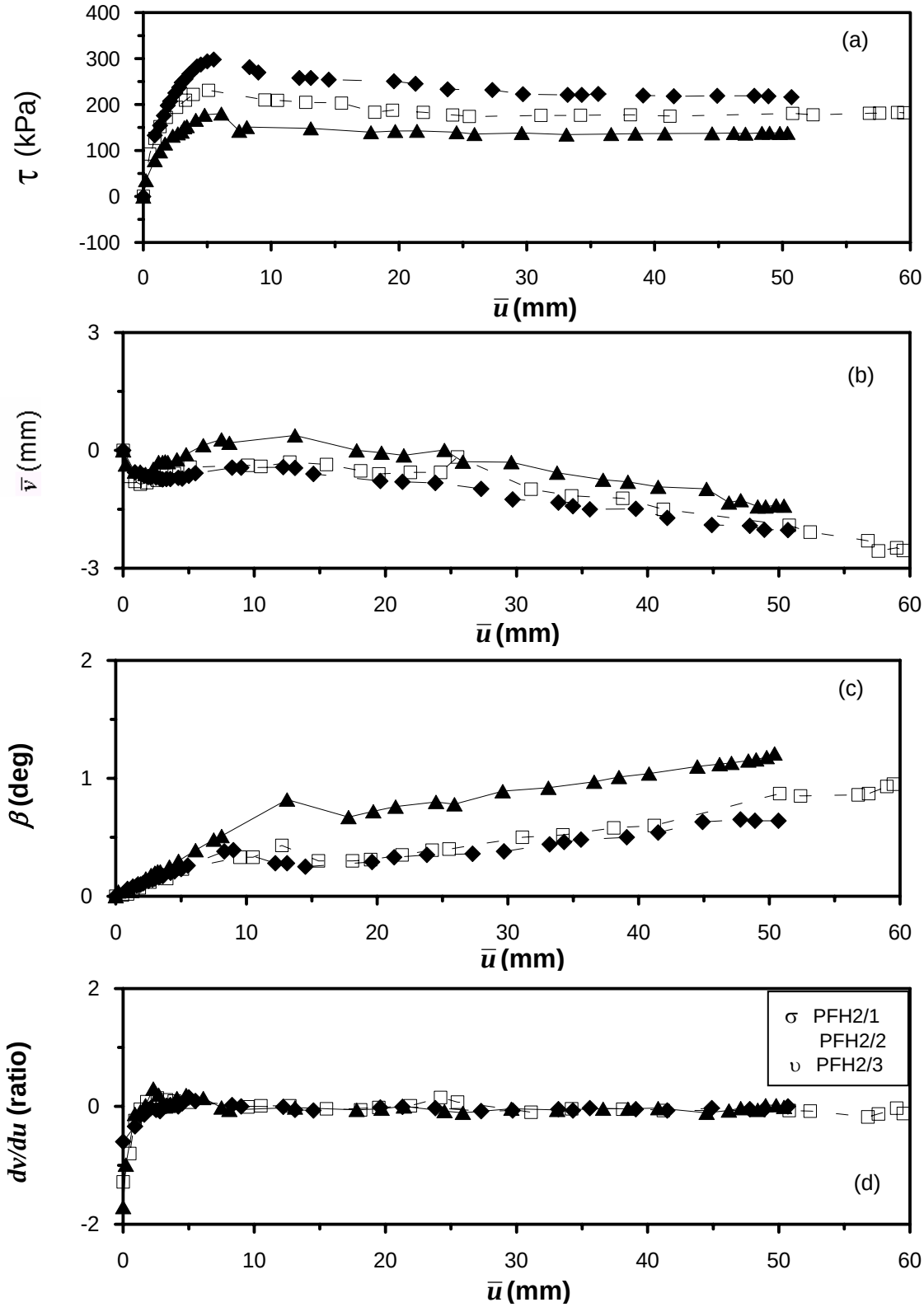

Figure 5.14. Typical curves for series PFH2 of the variation with $\bar{u}$ of (a) τ, (b) $\bar{v}$, (c) β, and (d) dv/du

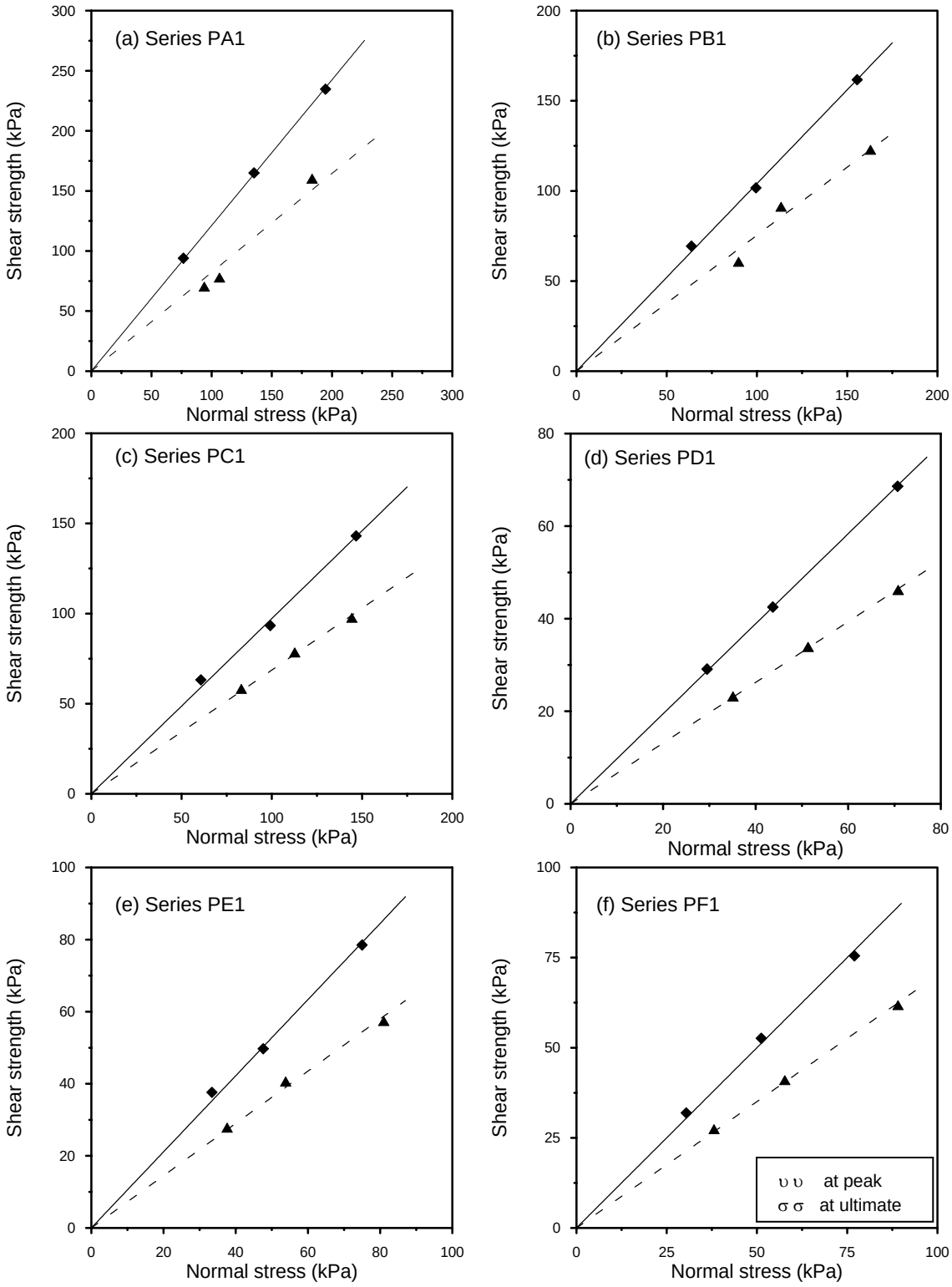

Figure 5.15. The results of priswests on samples A to F at the lower density and lower normal stress range

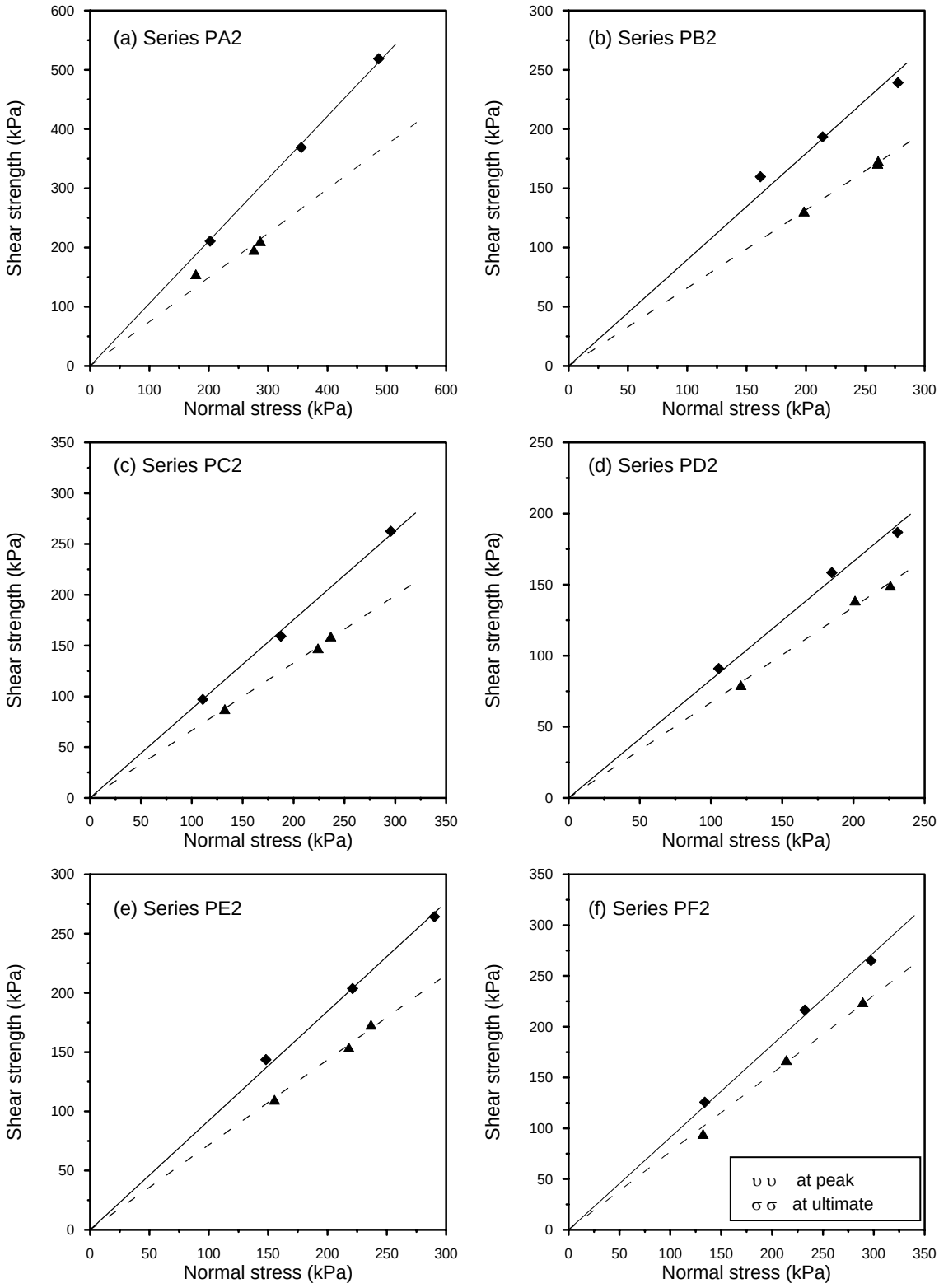

Figure 5.16. The results of priswests on samples A to F at the lower density and higher normal stress range

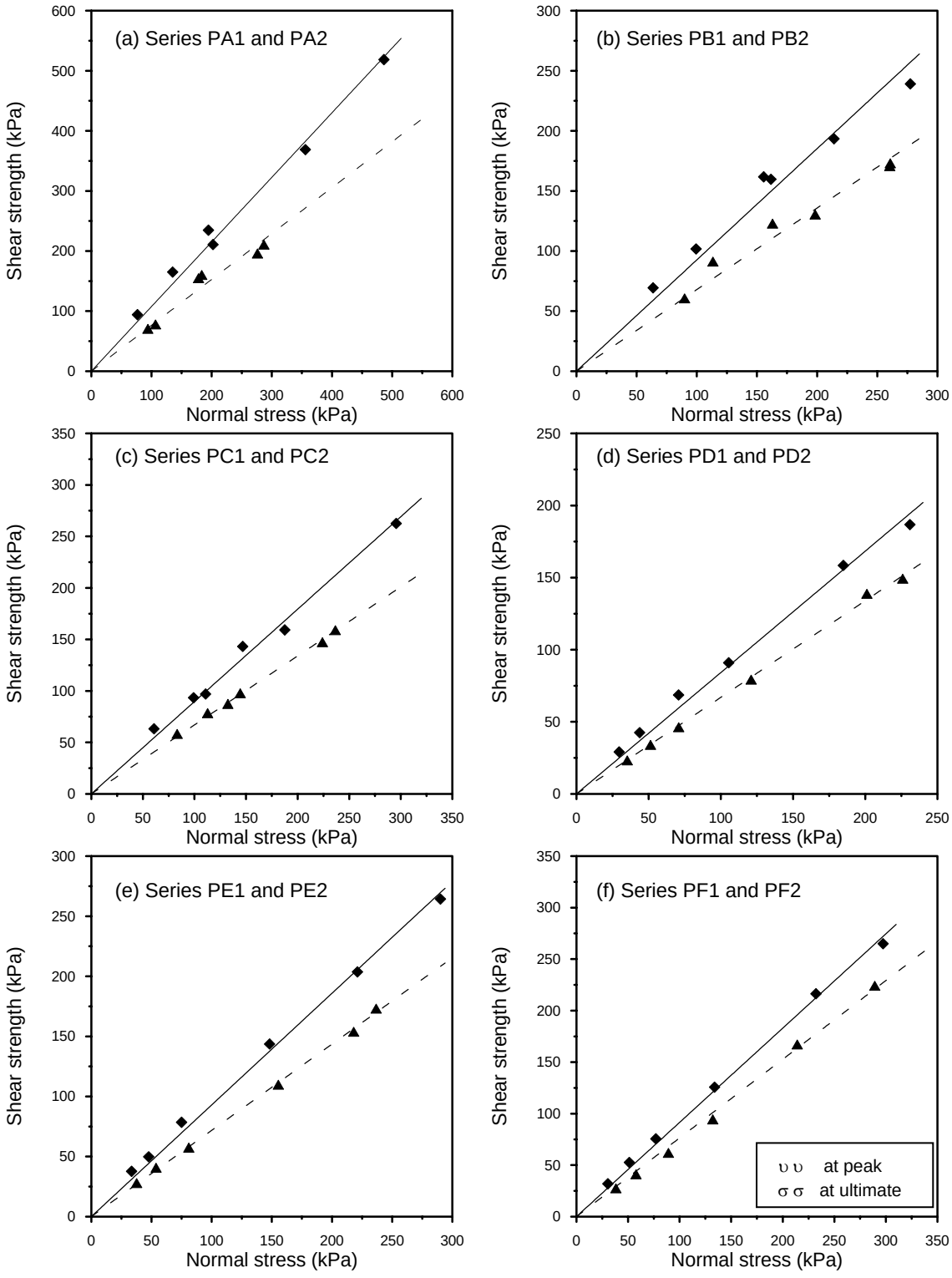

Figure 5.17. The combined results of priswests on each of samples A to F at the lower density

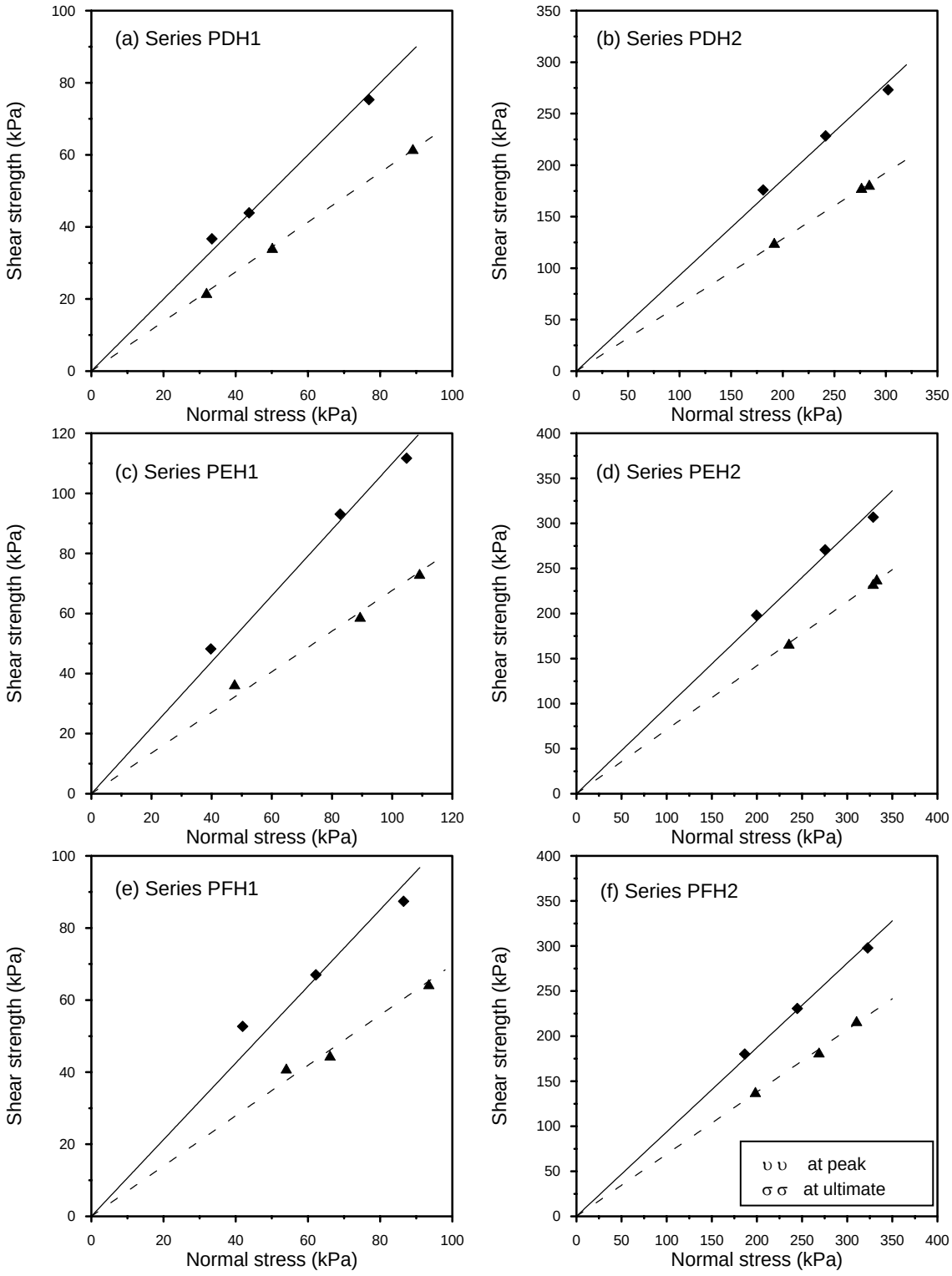

Figure 5.18. The results of priswests series on samples D to F at the higher density: (a), (c), (e): lower normal stress range; (b), (d), (f): higher normal stress range

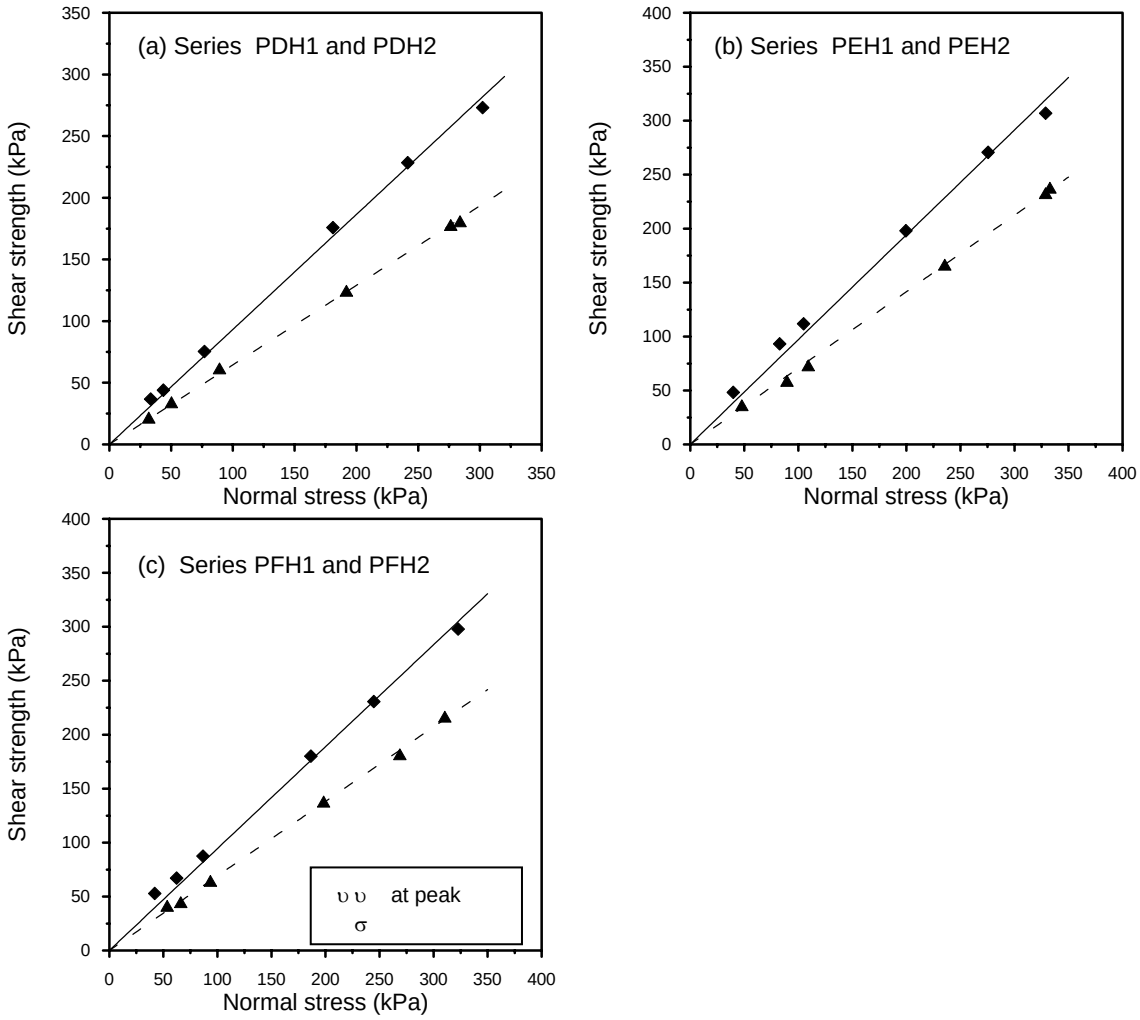

Figure 5.19. The combined results of priswests on each of samples D to F at the higher density

Table 5.15. Results of the priswests performed on samples A and B at the lower density

1	2	3	4	5	6	7	8	9	10	11	12	13	14	15	16	17	18	19
Sample	Test no.	α_n	e	D_r	Average D_r	Overall average D_r	Peak strength				Combined results at peak		Ultimate strength				Combined results at ultimate	
							σ	τ	ϕ	r	ϕ	r	σ	τ	ϕ	r	ϕ	r
		(deg)		(%)	(%)	(%)	(kPa)	(kPa)	(deg)		(deg)		(kPa)	(kPa)	(deg)		(deg)	
A	PA1/1	29.3	0.480	69.8	68.3	68.7	76.5	93.9	50.5	.9998	46.7	.9893	93.8	70.3	39.4	.9769	37.4	.9692
	PA1/2		0.485	67.9			135.1	165.0					106.5	77.8				
	PA1/3		0.487	67.2			194.6	234.7					183.5	160.1				
	PA2/1	39.9	0.480	69.8	69.2		202.1	210.7	45.9	.9998			178.2	154.6	36.7	.8086		
	PA2/2		0.481	69.4			355.7	368.8					276.1	195.8				
	PA2/3		0.484	68.3			415.0	427.3					286.6	210.7				
B	PB1/1	29.3	0.631	63.6	63.8	64.2	63.7	69.3	46.1	.9986	42.8	.9742	89.8	60.6	37.0	.9780	34.2	.9778
	PB1/2		0.633	63.0			99.4	101.7					113.3	91.2				
	PB1/3		0.627	64.7			155.5	161.7					162.9	122.8				
	PB2/1	39.9	0.615	68.1	64.6		161.6	159.7	41.9	.9492			198.3	130.4	33.4	.9991		
	PB2/2		0.635	62.5			214.0	193.4					260.4	170.6				
	PB2/3		0.632	63.3			277.5	239.1					260.9	172.9				

Table 5.16. Results of the priswests performed on samples C and D at the lower density

1	2	3	4	5	6	7	8	9	10	11	12	13	14	15	16	17	18	19
Sample	Test no.	α_n	e	D_r	Average D_r	Overall average D_r	Peak strength				Combined results at peak		Ultimate strength				Combined results at ultimate	
							σ	τ	ϕ	r	ϕ	r	σ	τ	ϕ	r	ϕ	r
		(deg)		(%)	(%)	(%)	(kPa)	(kPa)	(deg)		(deg)		(kPa)	(kPa)	(deg)		(deg)	
C	PC1/1	29.3	0.556	29.6	28.5	27.5	60.7	63.2	44.2	.9958	41.9	.9937	83.1	58.2	34.5	.9972	33.8	.9984
	PC1/2		0.563	26.2			99.1	93.3					112.7	78.4				
	PC1/3		0.556	29.6			146.7	143.1					144.3	97.6				
	PC2/1	39.9	0.567	24.3	26.6		110.7	96.9	41.2	.9986			132.3	87.3	33.6	.9990		
	PC2/2		0.561	27.2			187.5	159.2					224.1	147.3				
	PC2/3		0.559	28.2			295.6	262.6					236.5	158.9				
D	PD1/1	29.3	0.647	70.4	69.4	69.2	29.5	29.1	44.2	.9999	40.1	.9949	35.1	23.2	33.3	.9997	33.8	.9991
	PD1/2		0.651	68.5			43.7	42.5					51.3	33.9				
	PD1/3		0.649	69.5			70.7	68.6					70.8	46.2				
	PD2/1	39.9	0.650	69.0	68.9		105.4	90.9	39.7	.9936			120.9	79.2	33.8	.9958		
	PD2/2		0.645	71.4			184.8	158.4					201.1	138.7				
	PD2/3		0.656	66.2			231.0	186.7					226.0	149.2				

Table 5.17. Results of the priswests performed on samples E and F at the lower density

1	2	3	4	5	6	7	8	9	10	11	12	13	14	15	16	17	18	19
Sample	Test no.	α_n	e	D_r	Average D_r	Overall average D_r	Peak strength				Combined results at peak		Ultimate strength				Combined results at ultimate	
							σ	τ	ϕ	r	ϕ	r	σ	τ	ϕ	r	ϕ	r
		(deg)		(%)	(%)	(%)	(kPa)	(kPa)	(deg)		(deg)		(kPa)	(kPa)	(deg)		(deg)	
E	PE1/1	29.3	0.652	64.8	65.2	64.3	33.5	37.7	47.2	.9982	43.0	.9965	37.6	27.9	35.9	.9995	35.7	.9994
	PE1/2		0.652	64.8			50.0	54.6					51.4	37.1				
	PE1/3		0.649	65.9			74.7	79.9					81.3	58.7				
	PE2/1	39.9	0.654	64.0	63.5		148.4	144.0	42.7	.9957			155.5	110.0	35.7	.9953		
	PE2/2		0.656	63.3			221.5	204.1					218.3	154.3				
	PE2/3		0.656	63.3			290.6	264.6					236.8	178.3				
F	PF1/1	29.3	0.628	67.5	66.1	65.9	32.4	35.3	46.0	.9981	42.6	.9973	37.2	26.2	35.6	.9999	37.4	.9983
	PF1/2		0.636	64.6			51.0	53.4					57.9	41.7				
	PE1/3		0.632	66.1			82.2	84.0					96.8	69.2				
	PF2/1	39.9	0.634	65.3	65.8		134.2	125.9	42.3	.9965			132.3	94.5	37.6	.9964		
	PF2/2		0.633	65.7			232.6	216.9					214.4	167.5				
	PF2/3		0.631	66.4			297.9	265.6					289.8	224.8				

Table 5.18. Results of the priswests performed on samples D and E at the higher density

1	2	3	4	5	6	7	8	9	10	11	12	13	14	15	16	17	18	19
Sample	Test no.	α_n	e	D_r	Average D_r	Overall average D_r	Peak strength				Combined results at peak		Ultimate strength				Combined results at ultimate	
							σ	τ	ϕ	r	ϕ	r	σ	τ	ϕ	r	ϕ	r
		(deg)		(%)	(%)	(%)	(kPa)	(kPa)	(deg)		(deg)		(kPa)	(kPa)	(deg)		(deg)	
D	PDH1/1	29.3	0.617	84.5	84.8	84.8	33.4	36.7	45.0	.9922	43.0	.9981	31.9	21.7	34.5	.9998	32.8	.9995
	PDH1/2		0.615	85.4			43.7	43.9					50.1	34.2				
	PDH1/3		0.617	84.5			76.9	75.3					89.1	61.6				
	PDH2/1	39.9	0.618	84.0	84.8		180.9	175.9	42.9	.9857			191.7	124.5	32.7	.9989		
	PDH2/2		0.615	85.4			241.6	228.4					284.0	180.9				
	PDH2/3		0.616	85.0			302.2	273.2					276.3	177.9				
E	PEH1/1	29.3	0.610	80.7	79.9	80.0	39.7	48.2	47.7	.9910	44.2	.9950	47.6	36.4	35.6	.9730	35.4	.9993
	PEH1/2		0.612	79.9			82.7	93.1					97.6	74.5				
	PEH1/3		0.614	79.2			104.8	111.7					109.1	73.2				
	PEH2/1	39.9	0.613	79.5	80.2		199.5	198.0	43.8	.9871			235.5	166.5	35.4	.9995		
	PEH2/2		0.611	80.3			275.5	270.7					328.8	232.8				
	PEH2/3		0.610	80.7			328.9	306.9					332.9	237.8				

Table 5.19. Results of the priswests performed on sample F at the higher density

1	2	3	4	5	6	7	8	9	10	11	12	13	14	15	16	17	18	19
Sample	Test no.	α_n	e	D_r	Average D_r	Overall average D_r	Peak strength				Combined results at peak		Ultimate strength				Combined results at ultimate	
							σ	τ	ϕ	r	ϕ	r	σ	τ	ϕ	r	ϕ	r
		(deg)		(%)	(%)	(%)	(kPa)	(kPa)	(deg)		(deg)		(kPa)	(kPa)	(deg)		(deg)	
F	PFH1/1	29.3	0.581	84.5	84.5	84.3	41.9	52.7	46.7	.9261	43.4	.9966	54.0	41.0	34.9	.9782	34.6	.9994
	PFH1/2		0.580	84.8			62.2	67.0					66.1	44.6				
	PFH1/3		0.582	84.1			86.5	87.4					93.5	64.4				
	PFH2/1	39.9	0.580	84.8	84.2		186.4	180.1	43.1	.9962			198.2	137.9	34.6	.9966		
	PFH2/2		0.582	84.1			244.6	230.7					268.8	181.8				
	PFH2/3		0.583	83.8			322.6	297.8					310.3	216.6				

CHAPTER 6

TRIAXIAL TESTS PERFORMED

6.1 Introduction

To compare the results of wedge shear tests with those of triaxial tests, triaxial tests were performed on samples A to F. In this chapter, the test procedure, the order of testing the specimens, and the results of the tests are presented.

6.2 Test Procedure

This section has been mostly taken from Mirata (2000), and Gökalp (1994).

1. A 100 ml burette and the attached tubing were filled with deaired, distilled water and connected to the pore pressure valve V_p of the cell (Fig. 6.1(b)); the pore pressure ducts were flushed up to the top of the cell pedestal by opening the valve V_p; then V_p was closed. The sides of the pedestal and the top cap were wiped dry and smeared with castor oil for a better seal between the rubber membrane and these components.

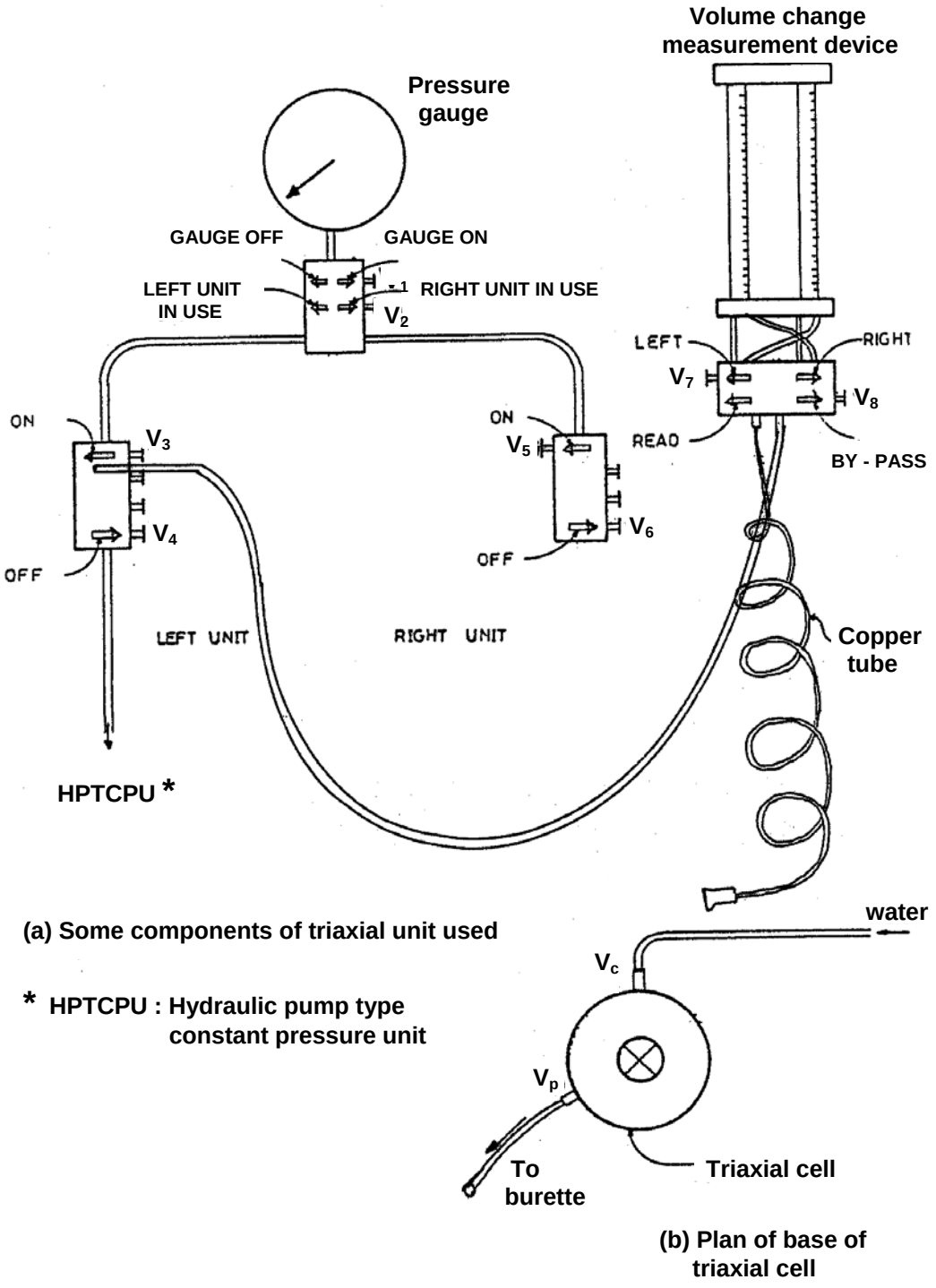

Figure 6.1. Triaxial apparatus used (adapted from Çağnan, 1990)

2. Two 0.3 mm thick rubber membranes were passed through the three-part split mould (Fig. 6.2); the ends turned over the mould and held by two rubber O-rings at each end. The mould was placed on to the base plate, and the fastening screws tightened moderately not to damage the membranes. The split ring SR (Fig. 6.3(b)), carrying three lugs L, displaced at 120^0 with screw S welded on each, was then clamped on to the mould as in Fig. 6.3(a). The collar C carrying three lugs with holes engaging the screws S, was then placed on top of the mould, and the gap between the collar and the top of the mould was adjusted by means of the nuts N so as not to damage the rubber membranes (Fig. 6.4).

Figure 6.2. Rubber membranes on the three-part split mould with special attachment (after Gökalp, 1994)

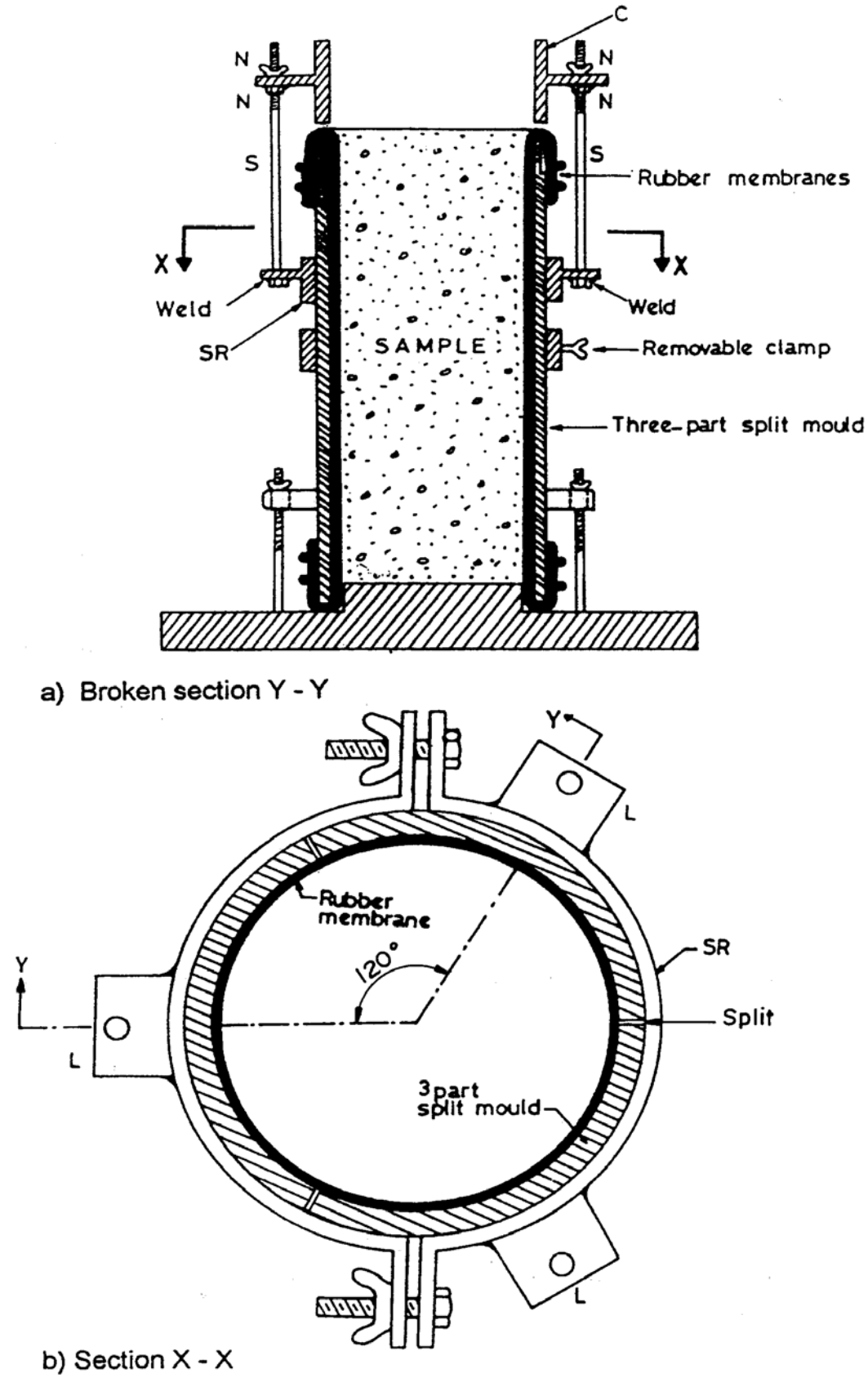

Figure 6.3. Three-part split mould (after Gökalp, 1994)

Figure 6.4. Three-part split mould with collar held gently above the rubber membrane (after Gökalp, 1994)

3. For each sample prepared as in section 3.2, the amount of sand required to give the same wet density as that obtained in cylwests and priswests was calculated. This amount was compacted in the three-part split mould in five layers by the 2.5 kg rammer to yield lower relative densities for samples A to F, and by the Kango vibrating hammer to yield higher relative densities for samples D to F.

4. The collar and the split ring SR were removed and the top of the specimen smoothed level with the top of the rubber membranes passing over the upper rim of the mould. A perspex disc was held on top of the specimen and the whole inverted. The base plate was replaced by a filter paper disc and a coarse porous stone, and the whole re-inverted and placed on the cell pedestal. Another filter paper disc and a coarse porous stone were placed on top of the specimen. The top cap was placed on top; the ends of the rubber membranes were turned over the pedestal and the top cap.

The clamp of the mould was detached and the three segments of the mould removed. During compaction using the Kango vibrating hammer, the membranes could be damaged. So using a membrane placer, the outer membrane was replaced by an intact membrane, and the damaged membrane was used during vibratory compaction in subsequent tests. The rubber membranes were sealed with two rubber O-rings at each end.

5. The cell ram was adjusted to just touch the top cap. To prevent buckling of the loading system under high loads, the anti-friction guide (Fig. 6.5) was passed over the cell ram for specimens at the higher density. The proving ring was mounted in position, and the cell was raised until the ram just touched the proving ring (Fig. 6.6).

6. The cell was filled with deaired distilled water using a separate tube connected to the cell pressure valve V_c of the cell (Fig. 6.1(b)) to speed up the filling; the air vent on top of the cell was closed. This tube was then disconnected and the copper tube leading to the volume change measurement device (VCMD) (Fig. 6.1(a)) was connected to the valve V_c. The water level in the burette was adjusted to the level of the mid-height of the specimen. This adjustment was done throughout the test by lowering the burette when the specimen was compressed, and adding water to the burette when the specimen dilated. If there was a hole in the membrane, after the cell pressure was applied, the water level in the burette would rise continuously; when this occurred, the test was stopped, and a new specimen prepared, using undamaged membranes.

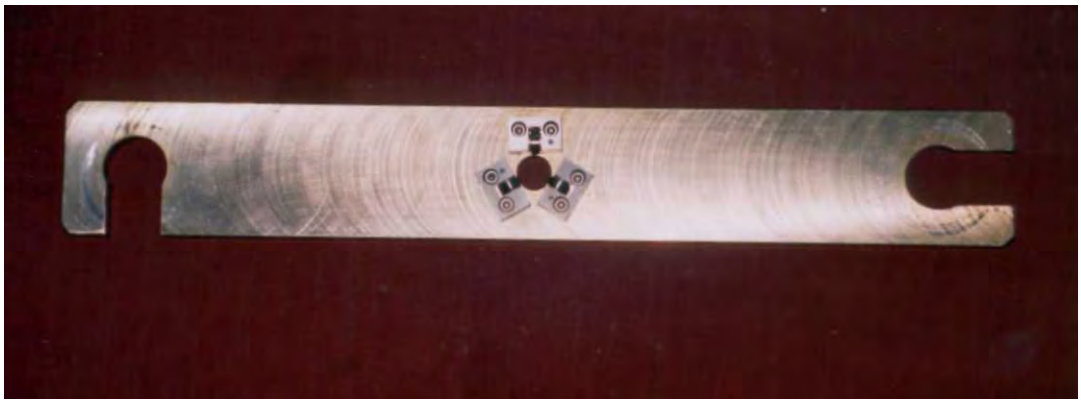

Figure 6.5. Top view of the anti-friction guide

Figure 6.6. Layout of triaxial cell with the anti-friction guide

7. The valve V_c on the cell was shut off. The valve V_8 on the VCMD (Fig. 6.1(a)) was set to the "bypass" position. By using the hydraulic pump type constant pressure unit (HPTCPU), the cell pressure was built up to the desired value to yield about the same average principal stress as that obtained in cylwests and priswests. This cell pressure was calculated and output by the programs CYLWEE88 and IWPW77 (sections 5.1.5 and 5.2.5), assuming the angle between the shear plane and the major principal stress in the wedge shear tests to be equal to $(45^o + \phi/2)$ (Appendix E). Valves V_1, V_3, and V_4 were opened; valve V_2 was set to "left unit in use" position. Valves V_c and V_p on the cell were opened. During this procedure, due to the compression of the specimen, and the penetration of the rubber membrane into the soil pores, air was pressed out of the specimen pushing the water level in the burette up. This level was restored to the level of the mid-height of the specimen by removing some water from the burette if necessary.

8. The cell was left in this condition for about two hours. Then the valve V_8 on the VCMD was shifted to the "read" position. When the volume change readings became steady, the axial strain and proving ring dials were set to zero. The initial burette readings on the VCMD were taken. The strain rate was set to 0.1 mm/min, and axial loading was started. Axial strain, proving ring dial gauge, and the volume change readings were taken at $10x10^{-3}$ inch intervals of axial compression. The test was continued at this rate until the proving ring readings became steady or started to drop. After the peak strength was reached, the strain rate was increased to 0.5 mm/min, but it was reduced to the original value of 0.1 mm/min and time was allowed for the proving ring dial reading to become steady before taking the readings. The test was continued until the proving ring readings become roughly constant.

9. At the end of test, the compression machine was stopped; the valve V_8 on the VCMD was shifted to the "bypass" position. The cell pressure was reduced to zero. The valve V_c on the cell and the valves V_1, V_3, and V_4 were closed. The air vent on top of the cell was opened. The axial load was removed by reversing the

loading mechanism. The cell was emptied, discarding the water. The cell was dismantled, and the specimen removed.

Each triaxial test, including specimen preparation, took about 4 hours.

6.3 Order of Testing Triaxial Test Specimens

For the triaxial tests on specimens at the lower density, the order of testing given in the following three paragraphs and summarized in Table 6.1, columns 2 to 8 was applied on samples A to F. In this table, σ_3 is the cell pressure applied in the tests.

For sample A, an untested specimen was used for test 1 (column 2). The specimen used in test 1 was recompacted and test 2 (column 3) was performed. Another untested specimen was used for test 3 (column 4). The specimen used in test 3 was recompacted and test 4 (column 5) was performed. A third untested specimen was used for test 5 (column 6). The specimen used in test 5 was recompacted and test 6 (column 7) was performed. The specimen used in test 6 was compacted a third time and test 7 (column 8) was performed.

For sample B, an untested specimen was used for test 1 (column 2). The specimen used in test 1 was recompacted and test 2 (column 3) was performed. The specimen used in test 2 was compacted a third time and test 3 (column 4) was performed. Another untested specimen was used for test 5 (column 6). The specimen used in test 5 was recompacted and test 6 (column 7) was performed. The specimen used in test 6 was compacted a third time and test 7 (column 8) was performed.

For each of the samples C to F, each of the tests under the lower σ (columns 2 to 5) were performed on a separate untested specimen. Each specimen used in tests 3, 2, and 1 was recompacted, and test 5 (column 6), test 6 (column 7), and test 7 (column 8) respectively were performed.

Table 6.1. Specimens used in the triaxial tests

1		2	3	4	5	6	7	8	9	10	11	12	13	14
Sample		Triaxial tests at the lower density							Triaxial tests at the higher density					
		Lower σ range				Higher σ range			Lower σ range			Higher σ range		
		Test 1	Test 2	Test 3	Test 4	Test 5	Test 6	Test 7	Test 1	Test 2	Test 3	Test 4	Test 5	Test 6
A	Specimen used	S.U.*	R.A.T.** (col. 2)	S.U.	R.A.T. (col. 4)	S.U.	R.A.T. (col. 6)	R.A.T. (col. 7)	…	…	…	…	…	…
	σ_3 (kPa)	24.8	38.0	58.6	79.6	101.7	138.6	175.7						
B	Specimen used	S.U.	R.A.T. (col. 2)	R.A.T. (col. 3)	…	S.U.	R.A.T. (col. 6)	R.A.T. (col. 7)	…	…	…	…	…	…
	σ_3 (kPa)	14.2	36.9	47.9		77.5	108.5	134						
C	Specimen used	S.U.	S.U.	S.U.	S.U.	R.A.T. (col. 4)	R.A.T. (col. 3)	R.A.T. (col. 2)	…	…	…	…	…	…
	σ_3 (kPa)	11.3	36.2	47.9	58.5	75.4	96.0	153.9						
D	Specimen used	S.U.	S.U.	S.U.	…	R.A.T. (col. 4)	R.A.T. (col. 3)	R.A.T. (col. 2)	S.U.	S.U.	S.U.	R.A.T. (col. 11)	R.A.T. (col. 10)	R.A.T. (col. 9)
	σ_3 (kPa)	17.7	23.1	33.5		55.5	98.9	120.7	16.2	24.5	48.6	95.5	125.8	153.4
E	Specimen used	S.U.	S.U.	S.U.	…	R.A.T. (col. 4)	R.A.T. (col. 3)	R.A.T. (col. 2)	S.U.	S.U.	S.U.	R.A.T. (col. 11)	R.A.T. (col. 10)	R.A.T. (col. 9)
	σ_3 (kPa)	17.6	24.5	41.7		76.2	114.0	148.5	21.7	36.8	51.3	103.6	142.3	167.2
F	Specimen used	S.U.	S.U.	S.U.	…	R.A.T. (col. 4)	R.A.T. (col. 3)	R.A.T. (col. 2)	S.U.	S.U.	S.U.	R.A.T. (col. 11)	R.A.T. (col. 10)	R.A.T. (col. 9)
	σ_3 (kPa)	16.2	25.1	38.2		70.7	120.9	151.3	21.0	31.3	48.6	97.6	126.5	165.2

* S.U.: separate untested specimen

* * R.A.T. (col. n): specimen reused after test in column n

For the triaxial tests on specimens at the higher density, the order of testing given in the following paragraph and summarized in Table 6.1, columns 9 to 14 was applied on samples D to F. Samples A to C were not tested at the higher density.

For each of the samples D to F, each of the tests under the lower σ (columns 9 to 11) were performed on a separate untested specimen. Each specimen used in tests 3, 2, and 1 was recompacted, and test 4 (column 12), test 5 (column 13), and test 6 (column 14) respectively were performed.

6.4 Test Results

Triaxial test series TA to TF were performed on samples A to F respectively, at the lower density. For the reason explained in section 5.1.6, additional three triaxial test series TDH, TEH, and TFH were performed on samples D to F respectively, at the higher density.

The tests were evaluated by using the computer program TRIAX02 (Mirata, 2002(a)), which applies all the area and rubber membrane corrections including the effect of volume change, explained by Mirata (1976).

Typical curves showing the variation of half the deviator stress ($\sigma_1 - \sigma_3$) and volumetric strain ε_v (dilatation positive) with the axial strain ε_a are given in Figs. 6.7 to 6.10. The results of the triaxial test series TA and TDH are plotted in Figs. 6.11 and 6.12. All triaxial test results are given in Tables 6.2 to 6.10. Tests TDH/6 (Table 6.8), TEH/5 and TEH/6 (Table 6.9), TFH/5 and TFH/6 (Table 6.10) could not be prolonged until the ultimate strength was reached due to the interference imposed by the anti-friction guide (Fig. 6.5).

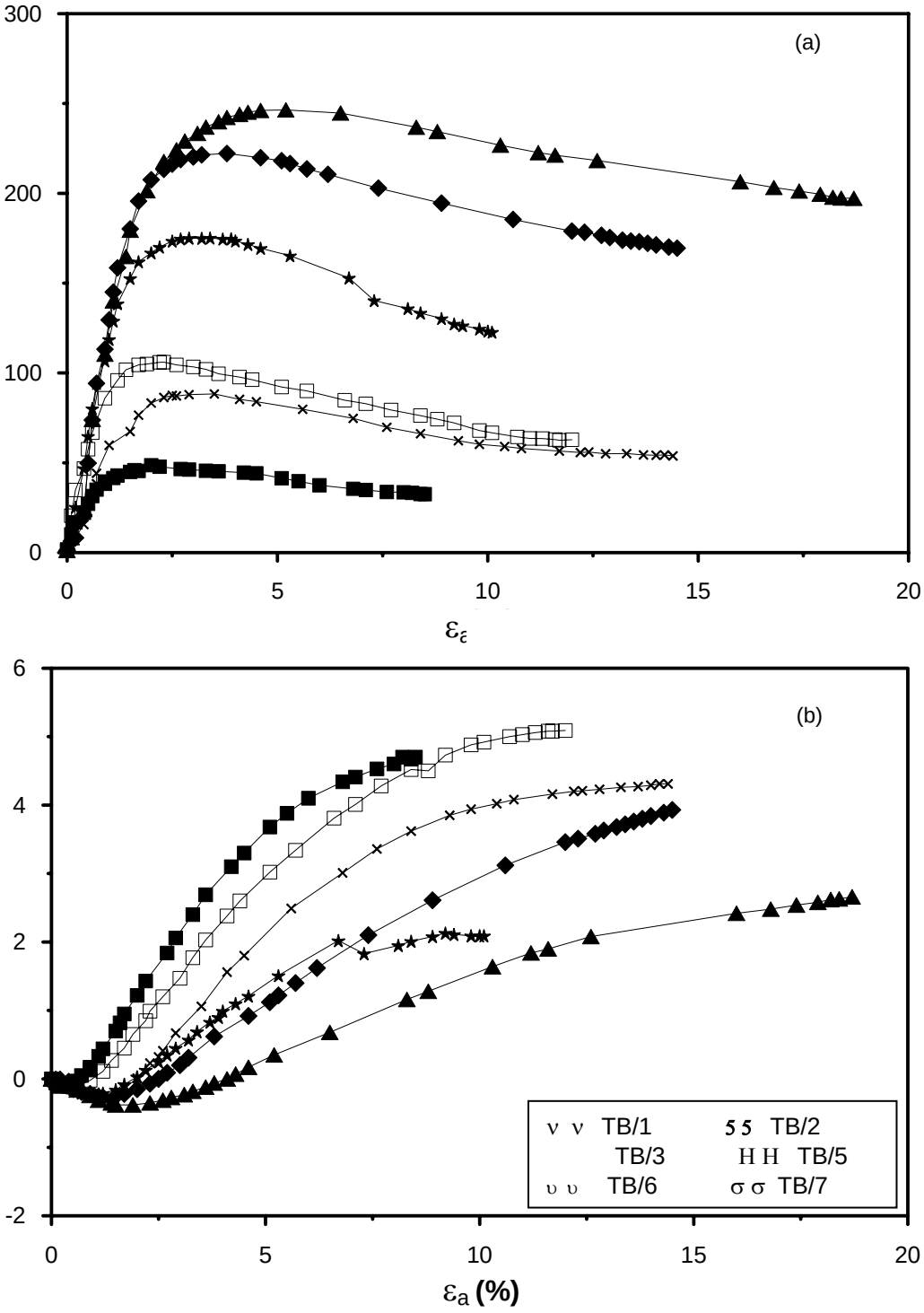

Figure 6.7. Typical curves for series TB of the variation of ε_a of (a) $(\sigma_1 - \sigma_3)/2$ and (b) ε_v

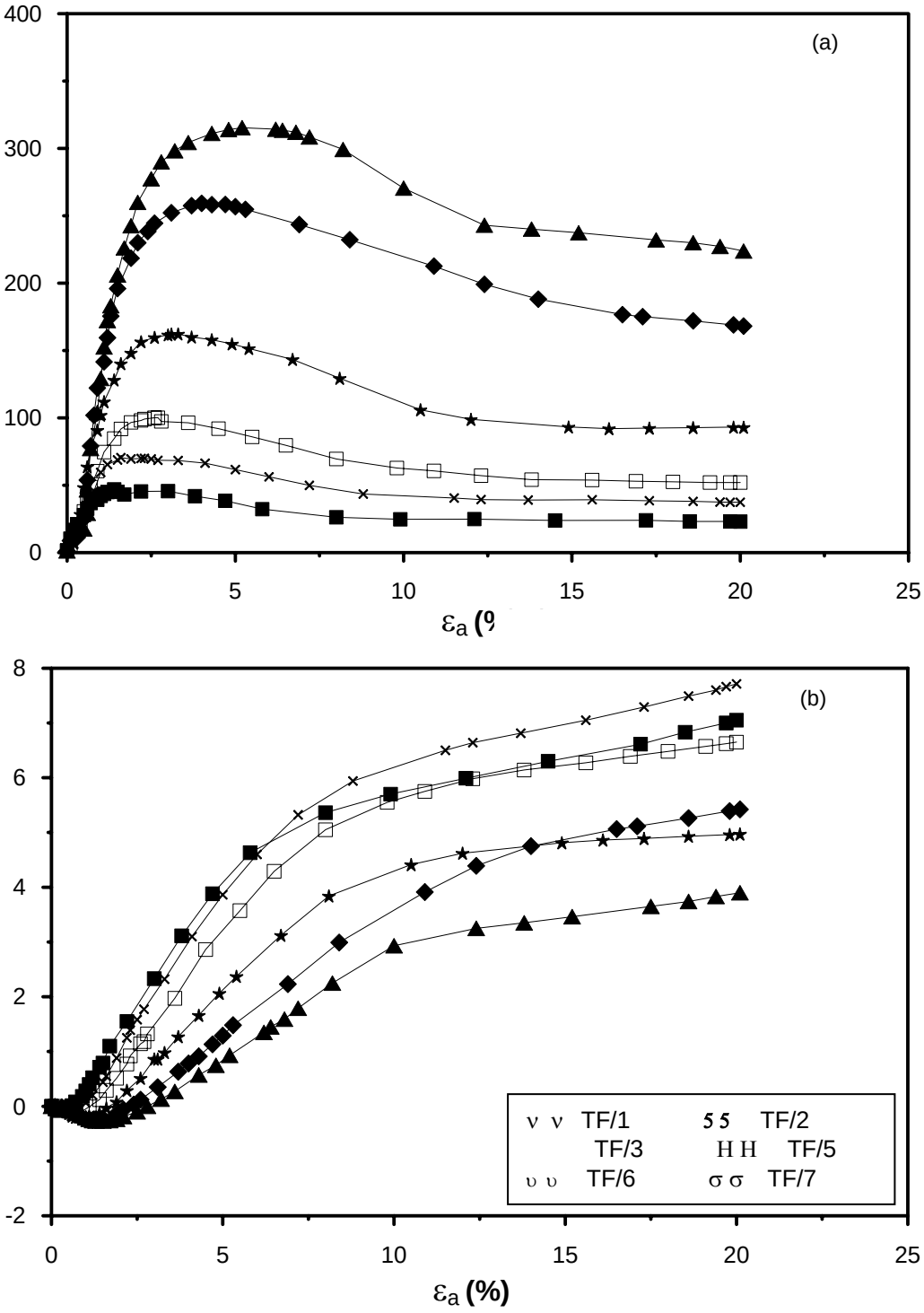

Figure 6.8. Typical curves for series TF of the variation of ε_a of (a) $(\sigma_1 - \sigma_3)/2$ and (b) ε_v

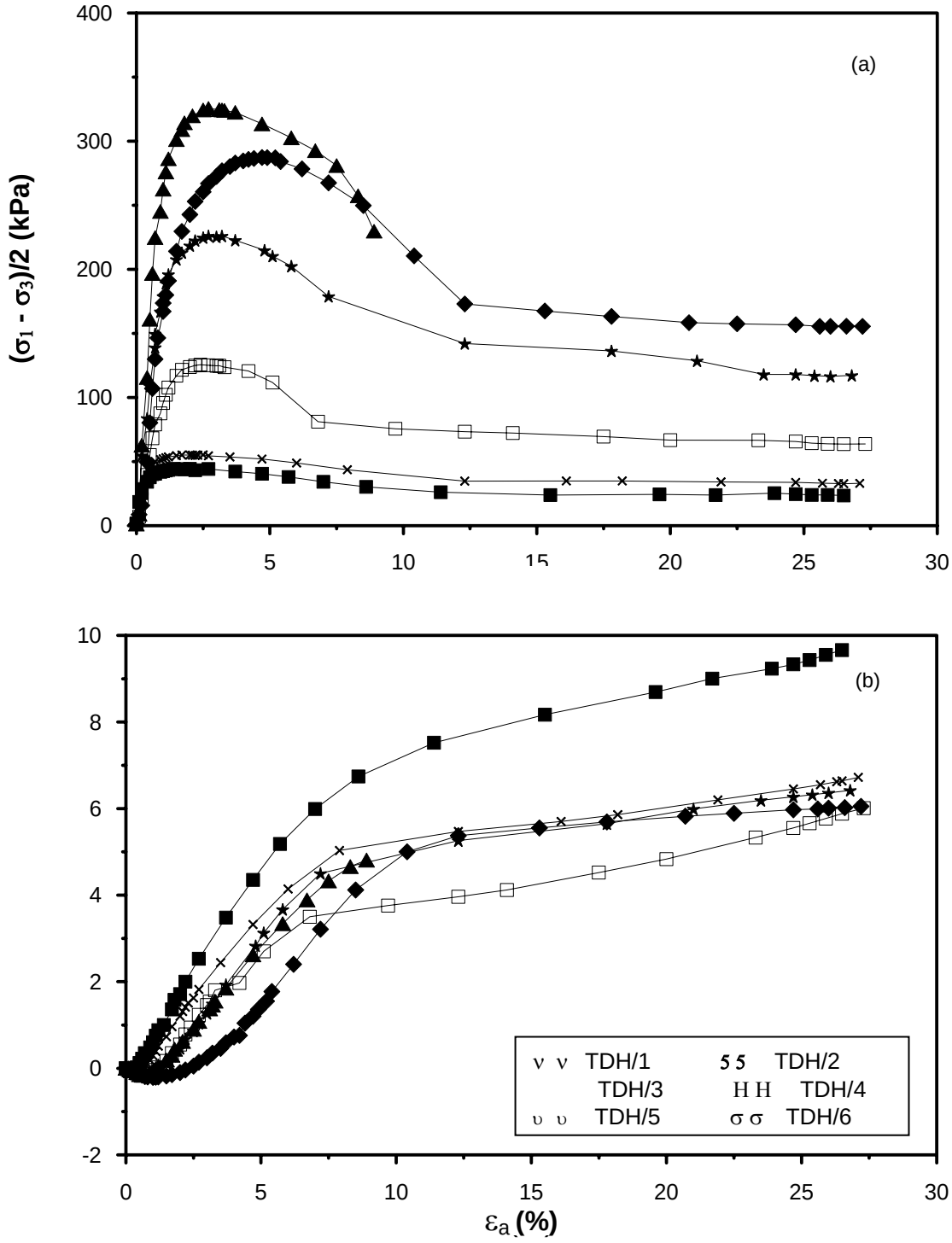

Figure 6.9. Typical curves for series TDH of the variation of ε_a of (a) $(\sigma_1 - \sigma_3)/2$ and (b) ε_v

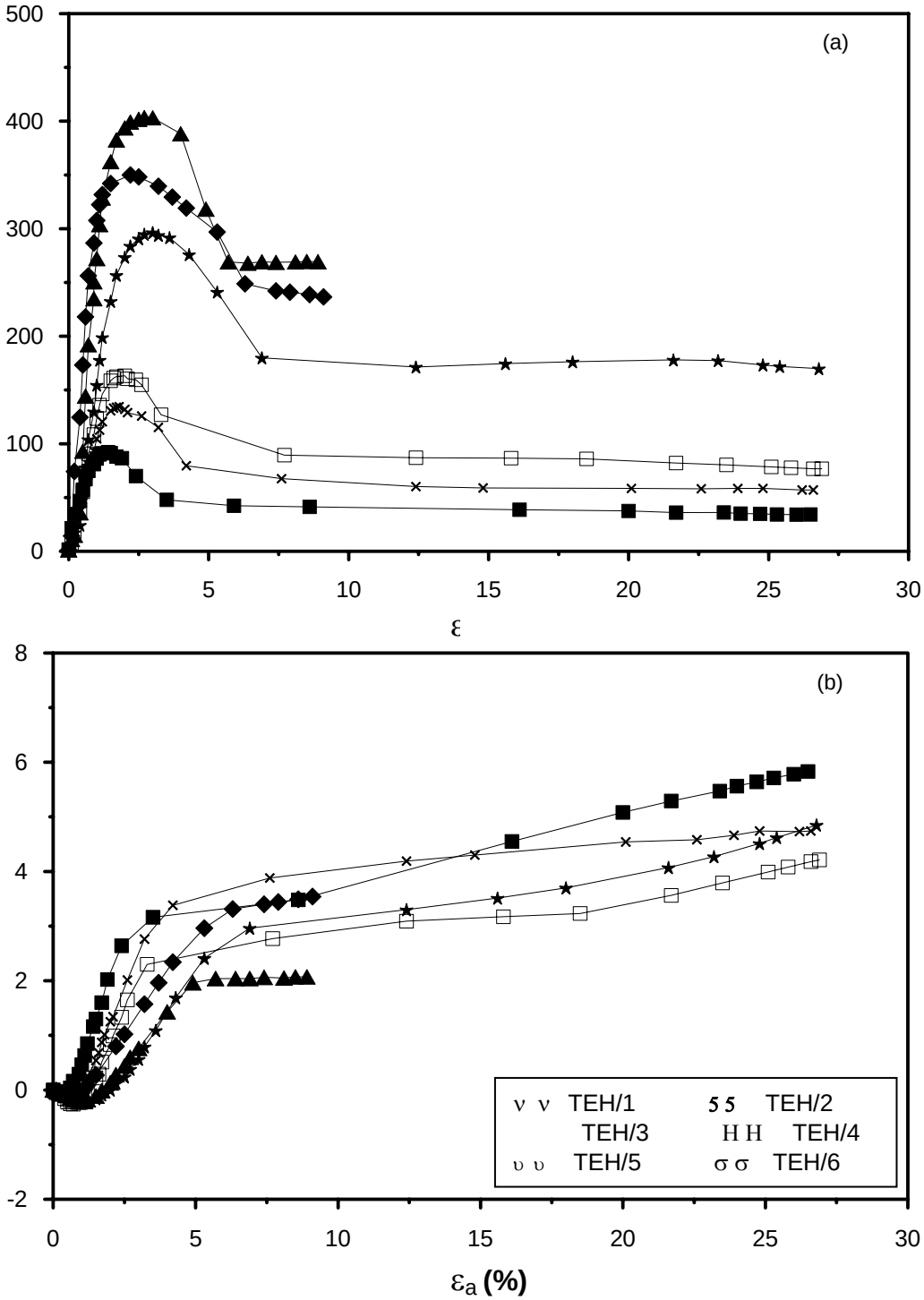

Figure 6.10. Typical curves for series TEH of the variation of ε_a of (a) $(\sigma_1 - \sigma_3)/2$ and (b) ε_v

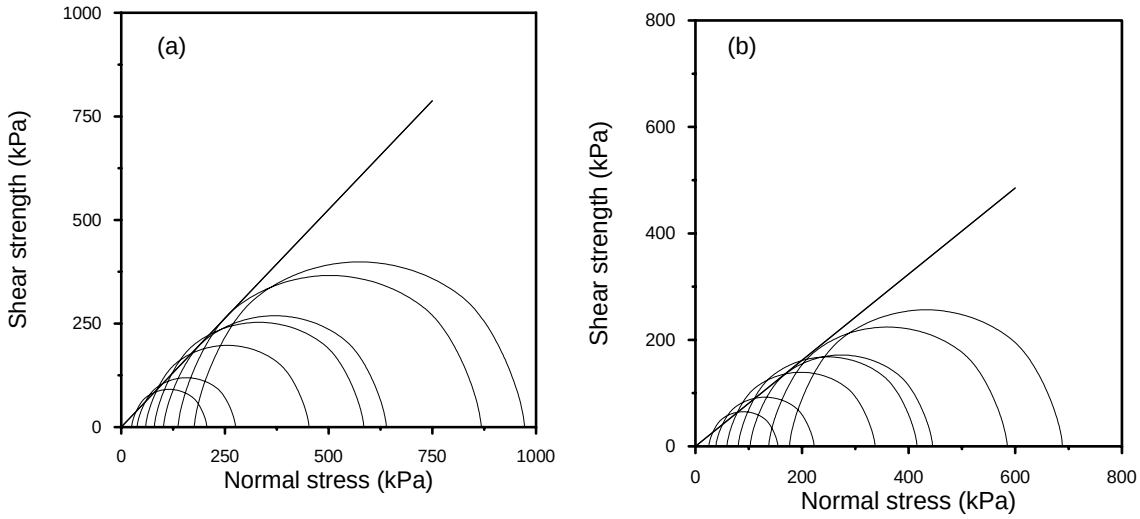

Figure 6.11. The results of the triaxial test series TA on sample A (a) at peak strength, and (b) at ultimate strength

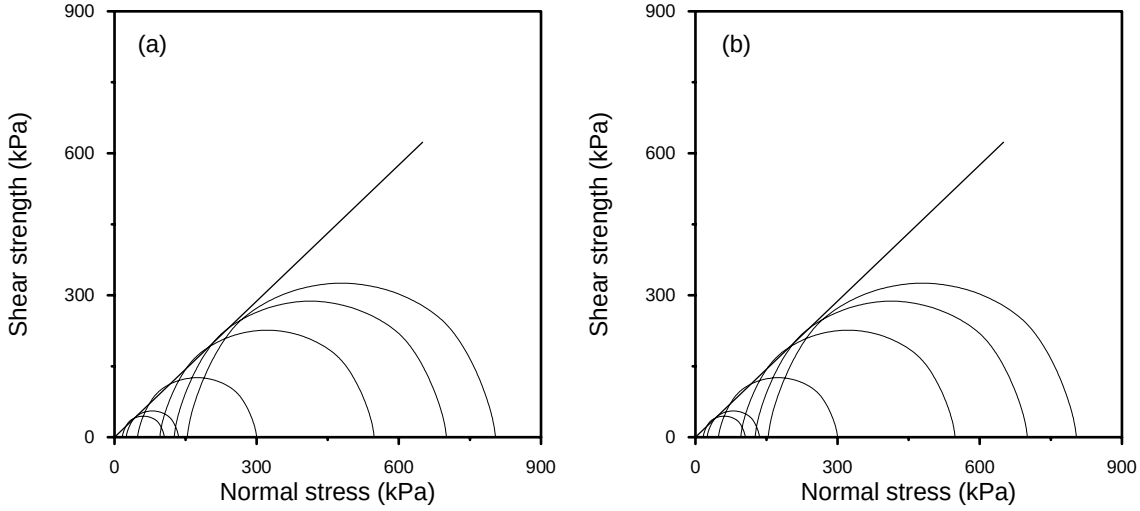

Figure 6.12. The results of the triaxial test series TDH on sample D (a) at peak strength, and (b) at ultimate strength

Table 6.2. Results of triaxial test series TA on sample A

1	2	3	4	5	6	7	8	9	10	11	12	13	14	15	16	17
Test no.	e	D_r (%)	Average D_r (%)	Overall average D_r (%)	At peak strength						At ultimate strength					
					σ_3 (kPa)	$\frac{\sigma_1+\sigma_3}{2}$ (kPa)	$\frac{\sigma_1-\sigma_3}{2}$ (kPa)	ε_a (%)	ε_v (%)	$\frac{d\varepsilon_v}{d\varepsilon_a}$ (%)	σ_3 (kPa)	$\frac{\sigma_1+\sigma_3}{2}$ (kPa)	$\frac{\sigma_1-\sigma_3}{2}$ (kPa)	ε_a (%)	ε_v (%)	$\frac{d\varepsilon_v}{d\varepsilon_a}$ (%)
TA/1	0.488	66.8	68.6	69.6	24.8	115.6	90.8	2.6	1.4	0.93	25.0	90.0	65.0	7.9	4.2	0.26
TA/2	0.487	67.2			38.0	156.8	118.8	3.8	2.4	0.71	38.2	130.4	92.2	13.6	4.8	0.09
TA/3	0.482	69.1			58.6	255.6	197.0	3.6	1.6	0.71	58.8	197.8	139.0	10.1	3.9	.07
TA/4	0.476	71.3			79.6	332.2	252.6	3.8	1.3	0.63	79.8	247.7	167.9	10.2	3.4	.05
TA/5	0.474	72.1	70.6		101.7	370.4	268.7	3.3	0.7	0.54	102.3	273.6	171.3	8.4	.9	0.08
TA/6	0.479	70.2			136.8	502.7	365.9	3.6	0.8	0.61	137.2	361.1	223.9	20.1	3.6	-0.02
TA/7	0.481	69.4			175.7	574.4	398.7	4.9	0.7	0.38	176.2	432.5	256.3	23.8	2.6	0.01
Regression of test results	First 4 tests				$\phi = 49.9^o$ r = .9997						$\phi = 43.8^o$ r = .9978					
	Last 3 tests				$\phi = 45.4^o$ r = .9892						$\phi = 37.5^o$ r = .9881					
	All 7 tests				$\phi = 46.4^o$ r = .9959						$\phi = 38.9^o$ r = .9856					

Table 6.3. Results of triaxial test series TB on sample B

1	2	3	4	5	6	7	8	9	10	11	12	13	14	15	16	17
Test no.	e	D_r (%)	Average D_r (%)	Overall average D_r (%)	At peak strength						At ultimate strength					
					σ_3 (kPa)	$\frac{\sigma_1+\sigma_3}{2}$ (kPa)	$\frac{\sigma_1-\sigma_3}{2}$ (kPa)	ε_a (%)	ε_v (%)	$\frac{d\varepsilon_v}{d\varepsilon_a}$ (%)	σ_3 (kPa)	$\frac{\sigma_1+\sigma_3}{2}$ (kPa)	$\frac{\sigma_1-\sigma_3}{2}$ (kPa)	ε_a (%)	ε_v (%)	$\frac{d\varepsilon_v}{d\varepsilon_a}$ (%)
TB/1	0.628	64.4	63.6	65.0	14.2	62.8	48.6	2.0	1.2	1.00	14.3	46.8	32.5	8.5	4.7	0.19
TB/2	0.635	62.5			36.9	125.2	88.3	3.5	1.1	0.74	37.1	90.9	53.8	14.4	4.3	0.01
TB/3	0.630	63.9			47.9	153.9	106.0	2.3	1.0	0.79	48.2	110.7	62.5	1.7	.1	.06
TB/5	0.624	65.5	66.4		77.5	252.6	175.1	3.4	0.7	0.47	77.6	200.3	122.7	0.1	.1	.05
TB/6	0.616	67.8			108.5	330.6	222.1	3.8	0.6	0.44	108.8	278.3	169.5	14.5	3.9	0.17
TB/7	0.623	65.8			134.0	380.4	246.4	5.2	0.4	0.28	134.4	331.6	197.2	18.7	2.7	0.11
Regression of test results	First 3 tests				$\phi = 44.6^o$ r = .9927						$\phi = 35.9^o$ r = .9968					
	Last 3 tests				$\phi = 41.7^o$ r = .9808						$\phi = 37.1^o$ r = .9975					
	All 6 tests				$\phi = 42.0^o$ r = .9971						$\phi = 37.0^o$ r = .9989					

Table 6.4. Results of triaxial test series TC on sample C

1	2	3	4	5	6	7	8	9	10	11	12	13	14	15	16	17
Test no.	e	D_r (%)	Average D_r (%)	Overall average D_r (%)	At peak strength						At ultimate strength					
					σ_3 (kPa)	$\frac{\sigma_1+\sigma_3}{2}$ (kPa)	$\frac{\sigma_1-\sigma_3}{2}$ (kPa)	ε_a (%)	ε_v (%)	$\frac{d\varepsilon_v}{d\varepsilon_a}$ (%)	σ_3 (kPa)	$\frac{\sigma_1+\sigma_3}{2}$ (kPa)	$\frac{\sigma_1-\sigma_3}{2}$ (kPa)	ε_a (%)	ε_v (%)	$\frac{d\varepsilon_v}{d\varepsilon_a}$ (%)
TC/1	0.552	31.6	28.3	26.0	11.3	41.0	29.7	1.5	0.7	0.94	11.6	32.6	21.0	9.7	5.0	0.22
TC/2	0.554	30.6			36.2	119.7	83.5	2.2	0.8	0.67	36.4	93.5	57.1	10.5	4.2	0.21
TC/3	0.565	25.2			47.9	143.2	95.3	2.7	0.8	0.58	48.1	114.6	66.5	2.0	.2	.07
TC/4	0.564	25.7			58.5	192.9	134.4	2.7	0.7	0.55	58.7	154.5	95.8	.9	.6	.05
TC/5	0.579	18.4	23.6		75.4	226.3	150.9	3.7	0.7	0.45	75.6	184.5	108.9	13.3	3.1	0.09
TC/6	0.570	22.8			96.0	294.6	198.6	3.7	0.8	0.46	96.2	238.3	142.1	10.6	2.5	0.05
TC/7	0.556	29.6			153.9	438.0	284.1	4.5	0.4	0.31	154.2	369	214.8	16.9	2.5	0.07
Regression of test results	First 4 tests				$\phi = 43.5^o$ r = .9985						$\phi = 37.4^o$ r = .9974					
	Last 3 tests				$\phi = 41.1^o$ r = .9976						$\phi = 35.9^o$ r = .9993					
	All 6 tests				$\phi = 41.6^o$ r = .9986						$\phi = 36.2^o$ r = .9992					

Table 6.5. Results of triaxial test series TD on sample D

1	2	3	4	5	6	7	8	9	10	11	12	13	14	15	16	17
Test no.	e	D_r (%)	Average D_r (%)	Overall average D_r (%)	At peak strength						At ultimate strength					
					σ_3 (kPa)	$\frac{\sigma_1+\sigma_3}{2}$ (kPa)	$\frac{\sigma_1-\sigma_3}{2}$ (kPa)	ε_a (%)	ε_v (%)	$\frac{d\varepsilon_v}{d\varepsilon_a}$ (%)	σ_3 (kPa)	$\frac{\sigma_1+\sigma_3}{2}$ (kPa)	$\frac{\sigma_1-\sigma_3}{2}$ (kPa)	ε_a (%)	ε_v (%)	$\frac{d\varepsilon_v}{d\varepsilon_a}$ (%)
TD/1	0.648	70.0	70.6	70.7	17.7	57.9	40.2	3.1	2.0	0.85	18.1	42.3	24.2	20.0	7.4	0.11
TD/2	0.643	72.3			23.1	74.8	51.7	2.7	1.6	0.85	23.5	56.1	32.6	8.2	.3	0.06
TD/3	0.649	69.5			33.5	102.6	69.1	5.1	2.3	0.53	33.9	80.4	46.5	20.0	7.1	.17
TD/5	0.649	69.5	70.8		55.5	167.8	112.3	2.7	1.1	0.66	55.9	132.7	76.8	19.4	5.1	.10
TD/6	0.645	71.4			98.9	291.3	192.4	3.2	1.1	0.65	99.4	222.9	123.5	20.1	6.8	0.04
TD/7	0.645	71.4			120.7	342.7	222.0	5.3	1.7	0.51	121.1	276.3	155.2	20.1	6.4	0.08
Regression of test results	First 3 tests				$\phi = 43.0^o$ r = .9978						$\phi = 35.3^o$ r = .9998					
	Last 3 tests				$\phi = 40.9^o$ r = .9989						$\phi = 34.1^o$ r = .9987					
	All 6 tests				$\phi = 41.1^o$ r = .9995						$\phi = 34.2^o$ r = .9996					

Table 6.6. Results of triaxial test series TE on sample E

1	2	3	4	5	6	7	8	9	10	11	12	13	14	15	16	17
Test no.	e	D_r (%)	Average D_r (%)	Overall average D_r (%)	At peak strength						At ultimate strength					
					σ_3 (kPa)	$\frac{\sigma_1+\sigma_3}{2}$ (kPa)	$\frac{\sigma_1-\sigma_3}{2}$ (kPa)	ε_a (%)	ε_v (%)	$\frac{d\varepsilon_v}{d\varepsilon_a}$ (%)	σ_3 (kPa)	$\frac{\sigma_1+\sigma_3}{2}$ (kPa)	$\frac{\sigma_1-\sigma_3}{2}$ (kPa)	ε_a (%)	ε_v (%)	$\frac{d\varepsilon_v}{d\varepsilon_a}$ (%)
TE/1	0.654	64.0	64.4	64.5	17.6	70.3	52.7	1.9	0.8	1.00	18.1	45.8	27.7	20.0	5.6	0.12
TE/2	0.654	64.0			24.5	95.4	70.9	1.4	0.8	0.46	24.9	63.6	38.7	0.0	4.3	0.09
TE/3	0.651	65.2			41.7	156.9	115.2	2.4	0.9	0.97	42.1	102.4	60.3	0.1	.5	.08
TE/5	0.654	64.0	64.5		76.2	267.0	190.8	2.2	0.7	0.81	76.5	190.8	114.3	0.1	.4	.08
TE/6	0.651	65.2			114.0	362.5	248.5	3.7	0.7	0.48	114.4	288.1	173.7	20.1	3.5	0.14
TE/7	0.653	64.4			148.5	446.6	298.1	4.8	0.5	0.35	148.9	353.3	204.4	19.8	2.9	0.01
Regression of test results	First 3 tests				$\phi = 47.6^o$ r = .9997						$\phi = 36.6^o$ r = .9987					
	Last 3 tests				$\phi = 43.0^o$ r = .9895						$\phi = 36.1^o$ r = .9961					
	All 6 tests				$\phi = 43.4^o$ r = .9976						$\phi = 36.2^o$ r = .9994					

Table 6.7. Results of triaxial test series TF on sample F

1	2	3	4	5	6	7	8	9	10	11	12	13	14	15	16	17
Test no.	e	D_r (%)	Average D_r (%)	Overall average D_r (%)	At peak strength						At ultimate strength					
					σ_3 (kPa)	$\frac{\sigma_1+\sigma_3}{2}$ (kPa)	$\frac{\sigma_1-\sigma_3}{2}$ (kPa)	ε_a (%)	ε_v (%)	$\frac{d\varepsilon_v}{d\varepsilon_a}$ (%)	σ_3 (kPa)	$\frac{\sigma_1+\sigma_3}{2}$ (kPa)	$\frac{\sigma_1-\sigma_3}{2}$ (kPa)	ε_a (%)	ε_v (%)	$\frac{d\varepsilon_v}{d\varepsilon_a}$ (%)
TF/1	0.636	64.6	65.0	65.2	16.2	63.0	46.8	1.4	0.7	1.08	16.7	39.7	23.0	20.0	7.1	0.16
TF/2	0.634	65.3			25.1	95.6	70.5	1.6	0.6	1.03	25.7	63.0	37.3	20.0	.7	0.14
TF/3	0.635	65.0			38.2	138.3	100.1	2.6	1.1	0.68	38.8	90.7	51.9	20.0	6.7	.10
TF/5	0.634	65.3	65.4		70.7	232.9	162.2	3.3	1.0	0.70	71.0	164.0	93.0	20.1	5.0	.02
TF/6	0.635	65.0			120.9	380.1	259.2	4.0	0.8	0.50	121.4	289.5	168.1	20.1	5.4	0.10
TF/7	0.632	66.1			151.3	466.6	315.3	5.2	0.9	0.42	151.7	375.5	223.8	20.1	3.9	0.10
Regression of test results	First 3 tests				$\phi = 46.9^o$ r = .9993						$\phi = 35.4^o$ r = .9988					
	Last 3 tests				$\phi = 42.9^o$ r = .9992						$\phi = 36.0^o$ r = .9985					
	All 6 tests				$\phi = 43.2^o$ r = .9992						$\phi = 36.0^o$ r = .9996					

Table 6.8. Results of triaxial test series TDH on sample D

1	2	3	4	5	6	7	8	9	10	11	12	13	14	15	16	17
Test no.	e	D_r (%)	Average D_r (%)	Overall average D_r (%)	At peak strength						At ultimate strength					
					σ_3 (kPa)	$\frac{\sigma_1+\sigma_3}{2}$ (kPa)	$\frac{\sigma_1-\sigma_3}{2}$ (kPa)	ε_a (%)	ε_v (%)	$\frac{d\varepsilon_v}{d\varepsilon_a}$ (%)	σ_3 (kPa)	$\frac{\sigma_1+\sigma_3}{2}$ (kPa)	$\frac{\sigma_1-\sigma_3}{2}$ (kPa)	ε_a (%)	ε_v (%)	$\frac{d\varepsilon_v}{d\varepsilon_a}$ (%)
TDH/1	0.615	85.4	84.8	84.7	16.2	60.5	44.3	1.4	1.0	1.12	17.0	40.5	23.5	26.5	9.7	0.19
TDH/2	0.618	84.0			24.5	79.7	55.2	2.5	1.6	0.84	25.1	57.8	32.7	6.5	6.6	0.12
TDH/3	0.616	85.0			48.6	174.2	125.6	2.4	0.9	0.90	49.3	112.9	63.6	6.5	.9	.18
TDH/4	0.617	84.5	84.6		95.5	321.6	226.1	2.7	1.0	0.83	96.1	212.6	116.5	26.0	6.4	.08
TDH/5	0.615	85.4			125.8	413.0	287.2	4.7	1.2	0.66	126.5	282.0	155.5	27.2	6.1	0.05
TDH/6	0.618	84.0			153.4	478.8	325.4	2.7	1.1	0.76	153.6	383.3	229.7	8.9	4.8	0.25
Regression of test results	First 3 tests				$\phi = 45.9^o$ r = 0.9993						$\phi = 34.4^o$ r = 0.9998					
	Last 3 tests				$\phi = 43.6^o$ r = 0.9952						$\phi = 35.2^o$ r = 0.9876					
	All 6 tests				$\phi = 43.8^o$ r =0.9994						$\phi =35.2^o$ r =0.9974					

Table 6.9. Results of triaxial test series TEH on sample E

1	2	3	4	5	6	7	8	9	10	11	12	13	14	15	16	17
Test no.	e	D_r (%)	Average D_r (%)	Overall average D_r (%)	At peak strength						At ultimate strength					
					σ_3 (kPa)	$\frac{\sigma_1+\sigma_3}{2}$ (kPa)	$\frac{\sigma_1-\sigma_3}{2}$ (kPa)	ε_a (%)	ε_v (%)	$\frac{d\varepsilon_v}{d\varepsilon_a}$ (%)	σ_3 (kPa)	$\frac{\sigma_1+\sigma_3}{2}$ (kPa)	$\frac{\sigma_1-\sigma_3}{2}$ (kPa)	ε_a (%)	ε_v (%)	$\frac{d\varepsilon_v}{d\varepsilon_a}$ (%)
TEH/1	0.616	78.4	79.0	78.9	21.7	113.8	92.1	1.4	1.2	1.65	22.4	56.4	34.0	26.0	5.8	0.09
TEH/2	0.616	78.4			36.8	171.3	134.5	1.8	1.0	1.53	37.4	94.3	56.9	26.2	.7	0.01
TEH/3	0.611	80.3			51.3	214.5	163.2	2.0	0.8	1.30	51.9	128.5	76.6	26.9	4.2	.09
TEH/4	0.615	78.8	78.8		103.6	399.9	296.3	3.0	0.6	0.83	104.3	274.1	169.8	6.8	.9	.17
TEH/5	0.615	78.8			142.3	492.2	349.9	2.2	0.8	0.76	142.5	379.0	236.5	9.1	3.5	0.08
TEH/6	0.615	78.8			167.2	570.4	403.2	2.7	0.6	0.65	167.2	436.5	269.2	8.9	2.1	0.02
Regression of test results	First 3 tests				$\phi = 50.9^o$ r = 0.9947						$\phi = 36.8^o$ r = 0.9998					
	Last 3 tests				$\phi = 45.7^o$ r = 0.9884						$\phi = 38.3^o$ r = 0.9996					
	All 6 tests				$\phi = 46.2^o$ r = 0.9972						$\phi = 38.2^o$ r = 0.9998					

Table 6.10. Results of triaxial test series TFH on sample F

1	2	3	4	5	6	7	8	9	10	11	12	13	14	15	16	17
Test no.	e	D_r (%)	Average D_r (%)	Overall average D_r (%)	At peak strength						At ultimate strength					
					σ_3 (kPa)	$\frac{\sigma_1+\sigma_3}{2}$ (kPa)	$\frac{\sigma_1-\sigma_3}{2}$ (kPa)	ε_a (%)	ε_v (%)	$\frac{d\varepsilon_v}{d\varepsilon_a}$ (%)	σ_3 (kPa)	$\frac{\sigma_1+\sigma_3}{2}$ (kPa)	$\frac{\sigma_1-\sigma_3}{2}$ (kPa)	ε_a (%)	ε_v (%)	$\frac{d\varepsilon_v}{d\varepsilon_a}$ (%)
TFH/1	0.579	85.2	84.9	84.8	21.0	96.5	75.5	1.1	0.3	1.40	21.8	51.6	29.8	26.5	9.0	0.22
TFH/2	0.580	84.8			31.3	137.3	106.0	2.0	1.0	1.26	32.0	73.6	41.6	6.9	5.9	0.10
TFH/3	0.580	84.8			48.6	207.2	158.6	2.2	0.9	1.17	49.2	116.7	67.5	5.3	.5	0.01
TFH/4	0.580	84.8	84.7		97.6	356.1	258.5	3.7	0.9	0.74	98.1	230.2	132.1	27.2	4.1	.05
TFH/5	0.582	84.1			126.5	428.7	302.2	3.0	0.8	0.66	126.6	336.1	209.5	9.1	3.0	0.06
TFH/6	0.579	85.2			165.2	517.6	352.4	3.9	1.1	0.47	165.2	487.2	322.0	8.5	3.0	0.36
Regression of test results	First 3 tests				$\phi = 50.3^o$ r = 0.9997						$\phi = 35.1^o$ r = 0.9995					
	Last 3 tests				$\phi = 44.3^o$ r = 0.9786						$\phi = 39.7^o$ r = 0.9899					
	All 6 tests				$\phi = 44.9^o$ r = 0.9959						$\phi = 39.5^o$ r = 0.9965					

CHAPTER 7

SHEAR BOX TESTS PERFORMED

7.1 Introduction

To compare the results of wedge shear and triaxial shear tests with those of the shear box tests, shear box tests were performed on previously untested specimens, compacted directly in the shear box, at the lower density under the lower and higher normal stress σ ranges. Shear box tests were also performed on specimens, taken from the shear plane of previously sheared samples compacted in the cylwest and priswest moulds, at the lower density under the lower σ range to study the effect on shear strength of the orientation of the shear plane.

7.2 Description of Shear Box Test Apparatus

The following paragraphs have been mostly taken from Aybak (1988).

The shear box test apparatus (Fig. 7.1) has a shear box (a) split horizontally at the level of the centre of the soil sample, which is held between metal grills and porous stones. The upper and lower parts are held together by two retaining screws; another two knurled screws are provided for raising the upper half relative to the lower after the retaining screws are removed.

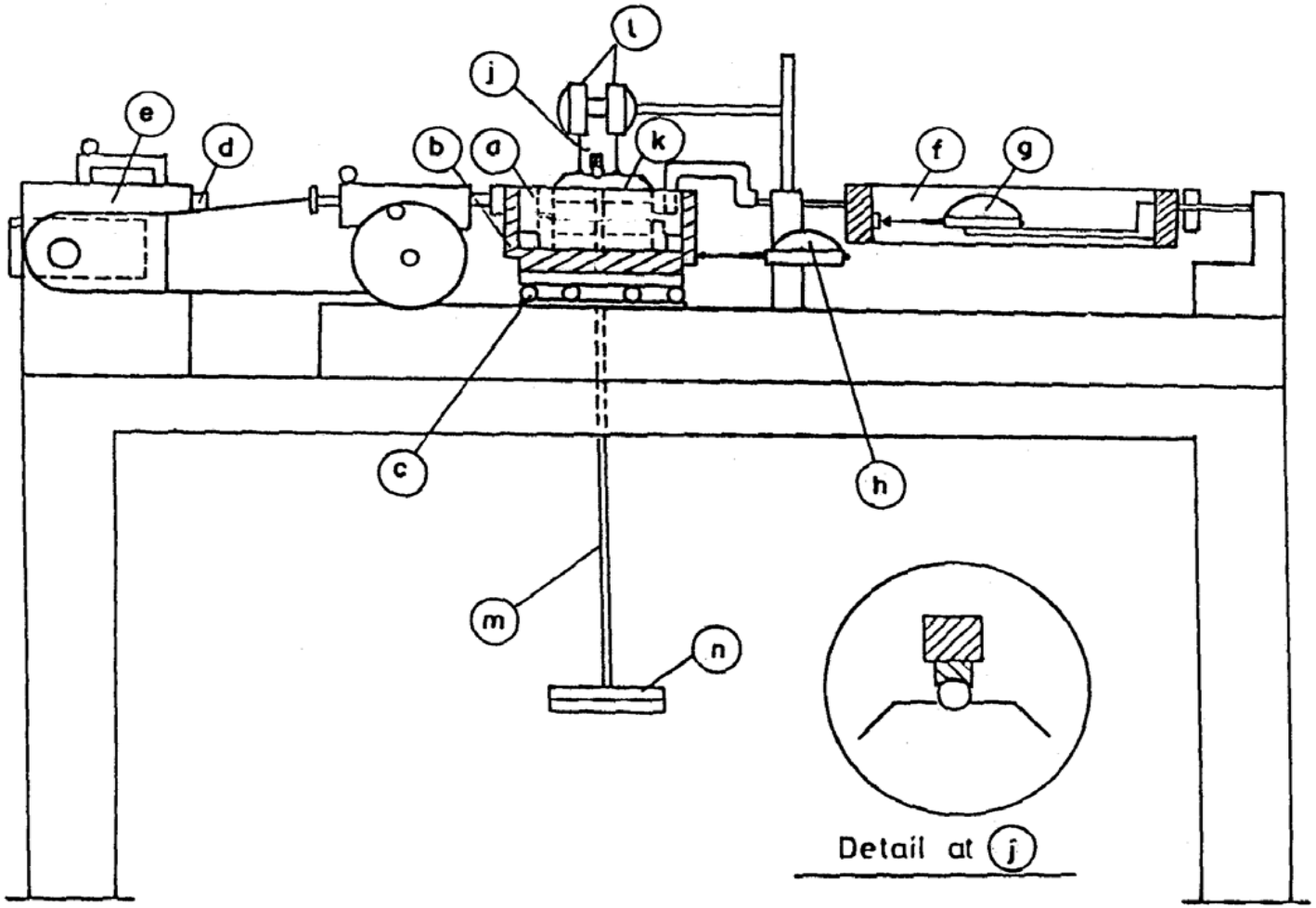

Figure 7.1. Shear box test apparatus (after Aybak, 1988)

A carrier (b), in which the box is placed, restrains the lower half of the box, but allows free movement of the upper half. The carrier rests on a ball track (c) in such a way that it can move only longitudinally. The movement of the carrier is effected at a uniform rate by means of an electric motor (d) and a variable speed gear box (e). The upper half of the box bears against a steel proving ring (f), whose deformation is shown by a dial gauge (g), and can be converted into shearing force. Another dial gauge (h) is attached to the bracket fixed to the main frame to measure the shear displacement.

The vertical load is applied through a yoke (j) bearing on a metal pad (k), which lies on top of the sample, and fits loosely into the shear box. Dead weights (n) can be placed on a hanger (m) suspended from the yoke. A steel ball distributes the load evenly over the sample while transmitting the load from the yoke to the pad. Two dial gauges (l), which bear on the loading pad, are used for measuring vertical displacement during shear, enabling also the slight rotation of the loading pad to be calculated.

7.3 Shear Box Tests Performed on Specimens Compacted directly in the Shear Box

7.3.1 Test Procedure

This section has been mostly taken from Mirata (2001). 60 mm x 60 mm square specimens were used in all shear box tests. The components of the shear box were similar to those shown in Fig. 7.2 for a circular shear box.

1. The shear box (Fig. 7.2) was cleaned, the inner walls were smeared with a thin layer of silicone grease, and the two halves were screwed together. Ensuring that the recesses on the retaining plate engaged the pins at the inner sides of the shear box, this plate and the porous stone were placed in the bottom of the shear box, followed by the serrated, perforated grid plate, making sure that the serrations faced upwards and were at right angles to the direction of shear.

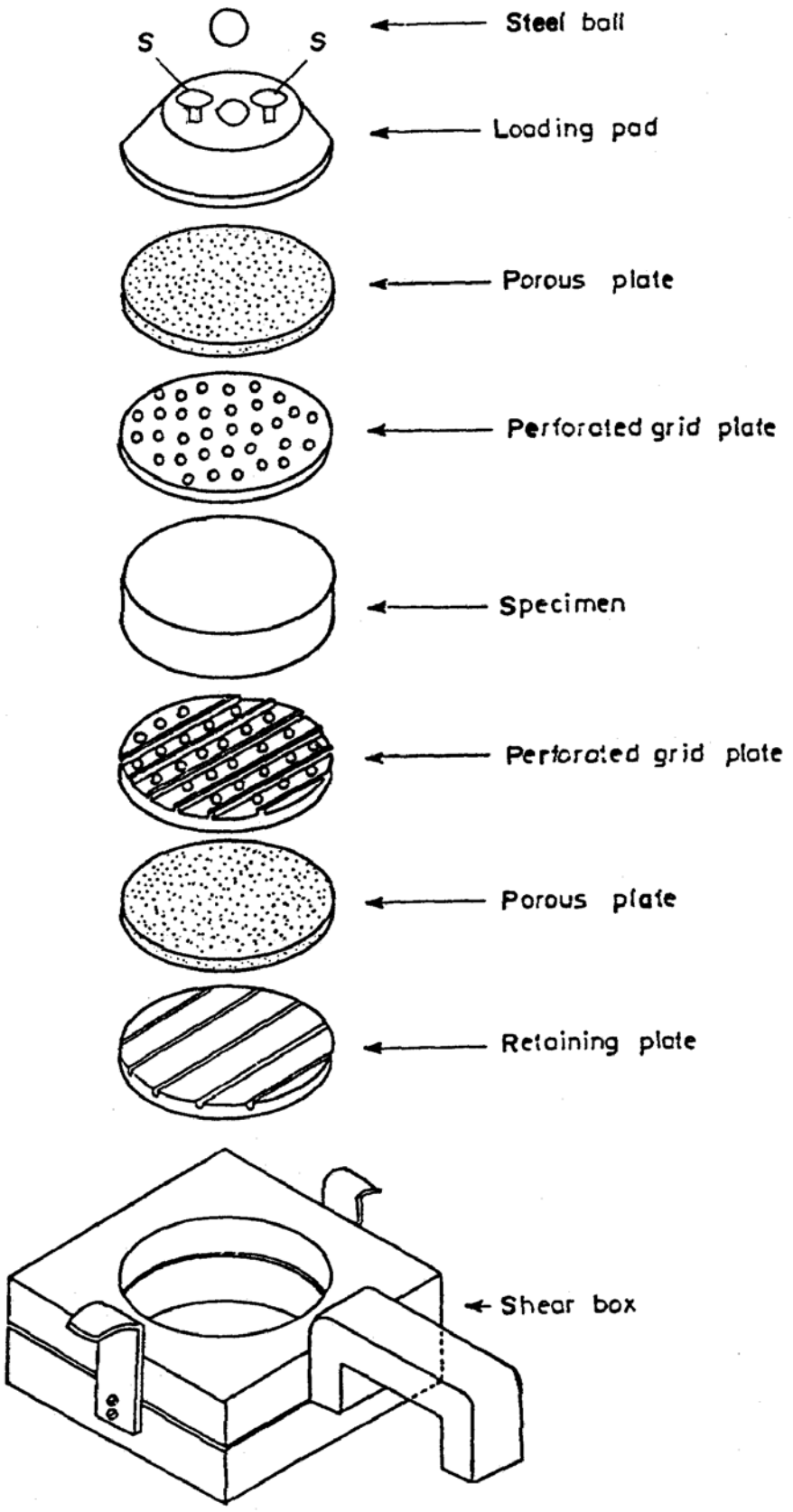

Figure 7.2. Assembly of shear box (modified from Head (1981) by Aybak, 1988)

2. For each sample prepared as in section 3.2, the amount of sand at the desired water content to be placed in the shear box to from a 20 mm thick specimen was calculated to yield the same wet density as that obtained in previous wedge shear and triaxial shear tests. In calculating the volume of the specimen to be placed in the shear box, the total volume of the serrations on the serrated grid plate was deducted, and the total volume of the perforations on this plate was added. So, 0.35 cm^3 was deducted from the calculated volume of the specimen.

3. The height h_1 (mm) from the flat part of the serrated plate to the top of the shear box was measured. The sand, calculated at step 2, was placed in the shear box in three layers. Each layer was tamped at such an intensity that when the whole specimen had been placed in the shear box, the height between the top of the loading pad, temporarily placed on top of the specimen, would be ($h_1 - 20 - t_p$) mm below the top of the shear box, where t_p (mm) was the thickness of the loading pad.

4. The upper serrated grid plate was placed on the specimen, with the serrations facing downwards and at right angles to the direction of shear. The upper porous stone was laid on top of the grid plate, and the loading pad was placed on top, with the two studs S (Fig. 7.2) aligned in the direction of shear.

5. The shear box was placed into the carrier (b in Fig. 7.1), and the hanger was set in position on the loading pad, with a cleaned and lubricated steel ball in between. The two vertical displacement dials (l in Fig. 7.1), were set to bear on the two studs S of the loading pad (k in Fig. 7.1), and adjusted to enable recording displacements of at least 5 mm both ways. The horizontal distance between the tips of these dial gauges was measured.

6. The additional dead weight W_d (lbf) to be placed on the hanger (without the load magnification arm) was calculated from the following equations to give the same normal stress σ (kPa) as that obtained from previous wedge shear tests, and placed on the hanger.

$$W_t = \frac{A\sigma}{44.48} \qquad \text{……..……..(7.1)}$$

$$W_d = W_t - 13.08 \qquad \text{.....……(7.2)}$$

where W_t (lbf) is the total dead weight on the specimen and A (cm^2) is the area of the specimen

7. The two knurled lifting screws were tightened until they just beared on the lower half of the shear box. The two retaining screws were removed and the lifting screws were given sufficient number of turns to make the clearance between the two halves of the box slightly more than the largest size of the particle in the specimen. (One full turn of such screws raised the upper half by 0.9 mm). Then the lifting screws were loosened by more number of turns than they had been tightened.

8. The displacement rate was set to about 0.08 mm/min by choosing the appropriate pair of gear wheels, and the right position of the gear lever. The initial readings of the shear displacement dial, the vertical displacement dials, and the proving ring dial were recorded.

9. The motor feed was engaged by turning the knurled knob at the rear of the hand wheel until the tongue engaged the slot. The motor was switched on and readings were taken at appropriate intervals until the peak strength was reached. Then the displacement rate was increased by 5 times between readings, reducing this rate to the initial value before taking the readings. Readings were continued until the ultimate strength was reached.

10. The motor was stopped. The motor feed was disengaged, and the box was reversed manually until the initial shear displacement was obtained. The pair of the vertical displacement dial gauges were raised and turned to one side without disturbing their horizontal distance from the shear box. The dead weights were lifted off and the shear box was removed.

Each shear box test, including specimen preparation, took about 1 hour.

7.3.2 Test Results

Six shear box test series SA to SF of six tests each were performed on samples A to F respectivelyssss. The tests were evaluated by using the computer program DIST02 (Mirata, 2002(b)). The values output for no area correction and no dilatation correction were taken.

Typical curves of the variation with shear displacement u of shear stress τ, normal displacement v (positive values indicating dilatation), and the slight rotation β of the loading pad (positive values indicating clockwise rotation when viewed as in Fig. 7.1) are given in Figs. 7.3 and 7.4. Test results are plotted in Fig. 7.5, and summarized in Tables 7.1 and 7.2.

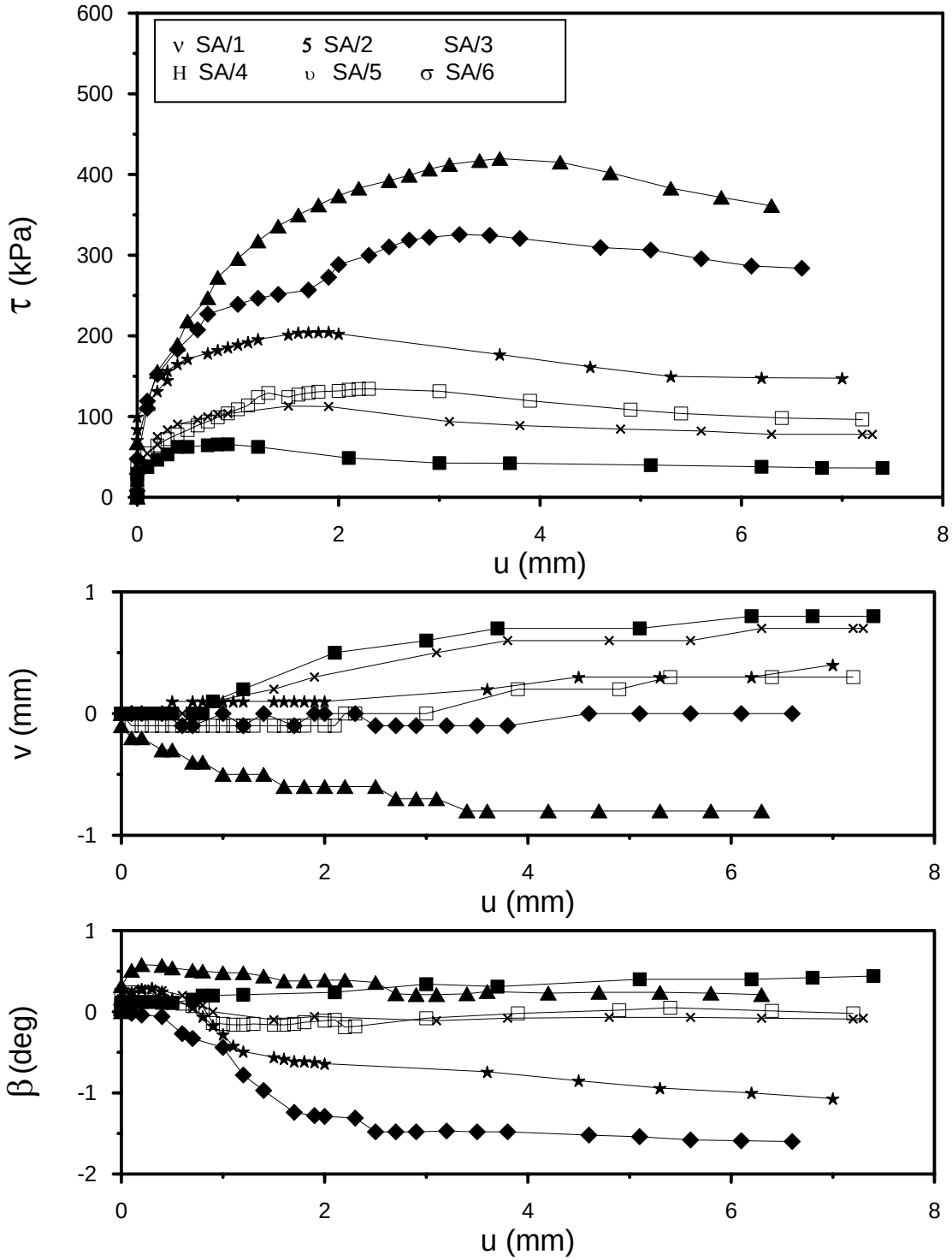

Figure 7.3. Typical curves for series SA of the variation with u of (a) τ, (b) v, and (c) β

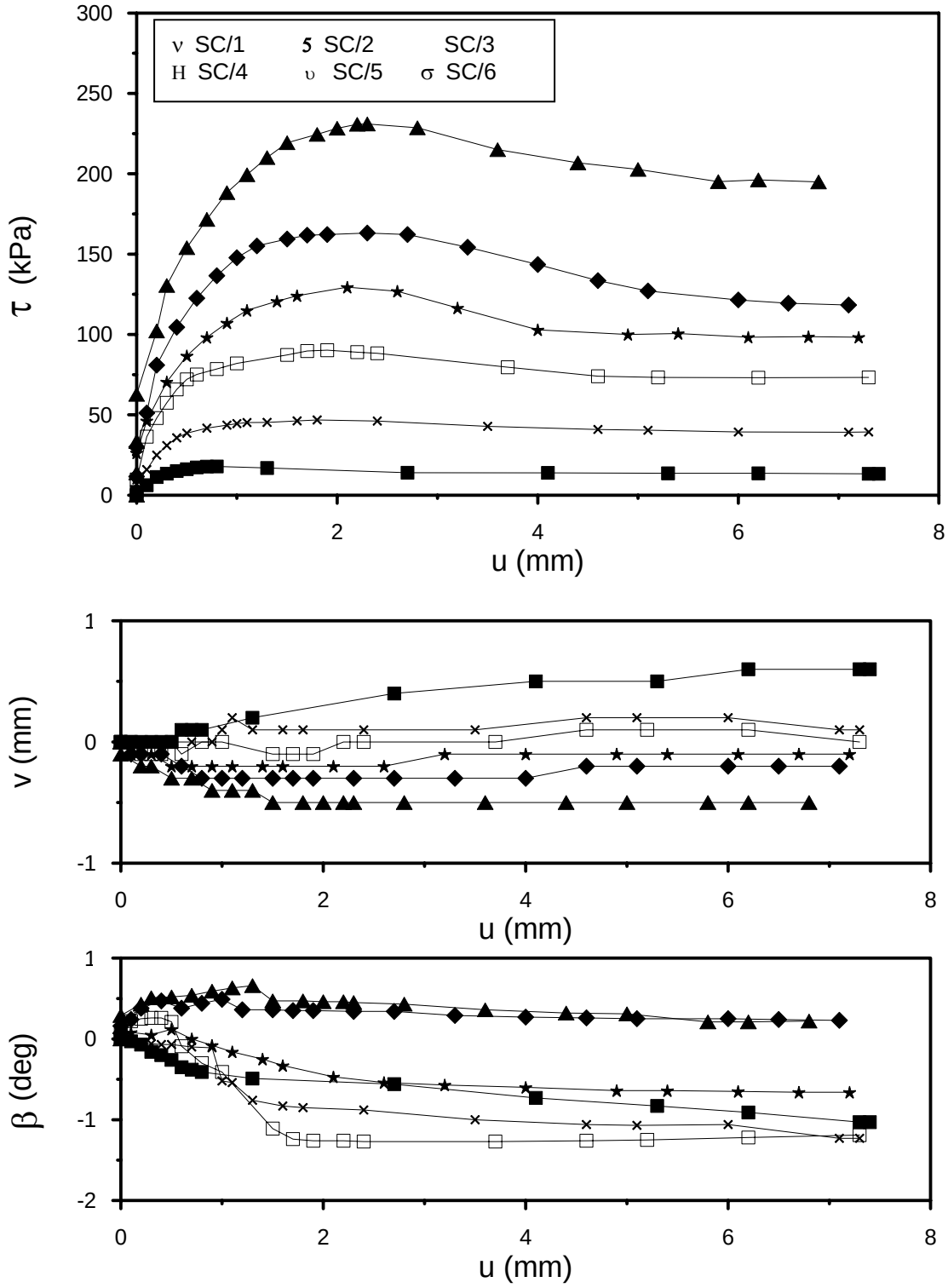

Figure 7.4. Typical curves for series SC of the variation with u of (a) τ, (b) v, and (c) β

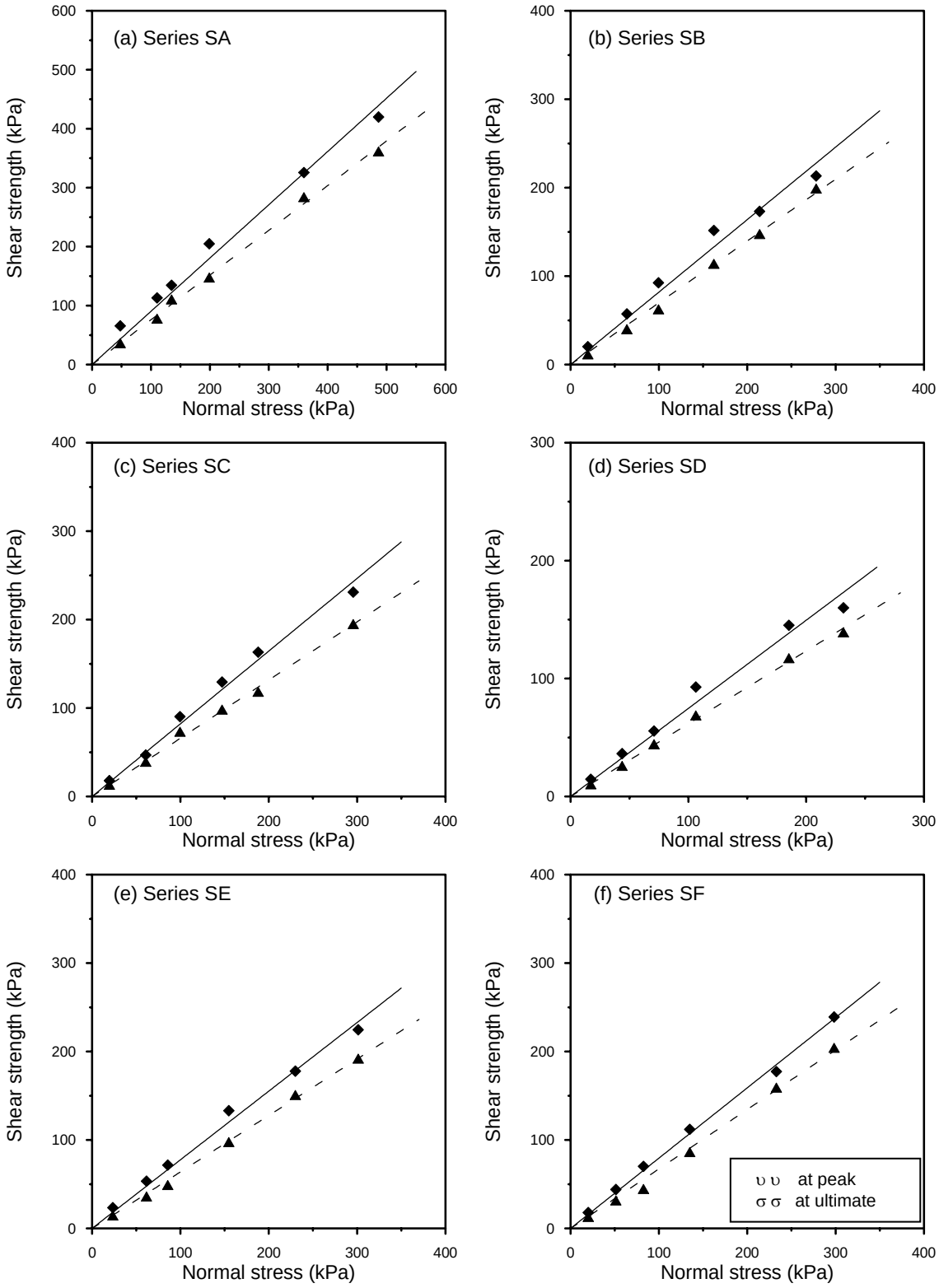

Figure 7.5. The results of shear box tests performed on specimens compacted directly in the shear box

Table 7.1. Results of shear box test series SA to SC

Sample	Test no.	e	D_r (%)	Peak strength				Combined results at peak		Ultimate strength				Combined results at ultimate	
				σ (kPa)	τ (kPa)	ϕ (deg)	r	ϕ (deg)	r	σ (kPa)	τ (kPa)	ϕ (deg)	r	ϕ (deg)	r
A	SA/1	0.481	69.2	47.7	65.5	45.9	.9402	42.1	.9990	47.7	36.2	35.5	.9985	37.0	.9985
	SA/2			110.3	113.0					110.3	77.7				
	SA/3			134.9	134.4					134.9	110.4				
	SA/4			198.9	204.8	41.8	.9788			198.9	147.5	37.2	.9960		
	SA/5			359.6	325.6					359.6	283.8				
	SA/6			486.3	419.7					486.3	361.3				
B	SB/1	0.628	64.3	19.6	20.2	42.7	.9987	40.4	.9939	19.6	11.5	32.1	.9998	34.9	.9980
	SB/2			63.7	57.3					63.7	40.0				
	SB/3			99.4	92.4					99.4	62.5				
	SB/4			162.1	151.6	40.1	.9571			162.1	113.9	35.2	.9974		
	SB/5			213.9	173.1					213.9	147.5				
	SB/6			277.9	231.1					277.9	198.8				
C	SC/1	0.560	27.9	19.6	17.9	41.1	.9904	39.4	.9939	19.6	13.3	35.4	.9939	33.4	.9978
	SC/2			60.7	46.8					60.7	39.2				
	SC/3			99.4	90.2					99.4	73.1				
	SC/4			147.1	129.4	39.3	.9730			147.1	98.3	33.2	.9973		
	SC/5			188.0	163.1					188.0	118.3				
	SC/6			295.6	231.0					295.6	194.9				

Table 7.2. Results of shear box test series SD to SF

Sample	Test no.	e	D_r (%)	Peak strength				Combined results at peak		Ultimate strength				Combined results at ultimate	
				σ (kPa)	τ (kPa)	ϕ (deg)	r	ϕ (deg)	r	σ (kPa)	τ (kPa)	ϕ (deg)	r	ϕ (deg)	r
D	SD/1	0.650	69.0	17.1	14.6	38.6	.9978	36.8	.9880	17.1	10.3	31.6	.9989	31.7	.9987
	SD/2			43.7	36.3					43.7	25.9				
	SD/3			70.8	55.5					70.8	44.2				
	SD/4			106.3	92.8	36.6	.9179			106.3	68.7	31.7	.9937		
	SD/5			185.3	145.1					185.3	117.2				
	SD/6			231.6	160.0					231.6	139.1				
E	SE/1	0.650	65.4	23.5	23.5	40.5	.9935	37.8	.9944	23.5	14.6	30.1	.9987	32.6	.9988
	SE/2			61.5	53.4					61.5	36.1				
	SE/3			85.6	71.6					85.6	49.0				
	SE/4			154.7	133.0	37.6	.9702			154.7	97.6	32.7	.9984		
	SE/5			230.0	177.7					230.0	150.8				
	SE/6			301.1	224.5					301.1	192.0				
F	SF/1	0.634	65.0	19.9	17.9	40.5	.9997	38.5	.9982	19.9	12.9	29.4	.9854	33.9	.9971
	SF/2			51.2	43.9					51.2	31.6				
	SF/3			82.5	70.1					82.5	44.5				
	SF/4			134.9	112.0	38.3	.9947			134.9	86.2	34.2	.9977		
	SF/5			232.9	177.3					232.9	159.1				
	SF/6			298.3	239.0					298.3	204.2				

7.4 Shear Box Tests Performed on Specimens Taken from the Shear Plane of Samples Compacted in the Cylwest and Priswest Moulds

7.4.1 Introduction

The results obtained from the wedge shear tests on samples A to F (section 8.1.1, paragraph (4)) had shown that the values of peak friction angles obtained from cylwests under the lower normal stresses were higher than those obtained from priswests using the 30^o mould. In order to investigate the reason of this difference, samples used in previous shear tests were compacted in the cylwest and priswest moulds, and shear box tests were performed on specimens taken from the shear plane of these samples under the lower σ ranges.

7.4.2 Preparation of the Samples

Sample A was inadvertently discarded after the previous shear tests had been completed. Samples B to F, already used in previous shear tests, were in a slightly moist condition. So each of the samples were first air-dried by spreading them in a large tray as a layer of about 5 cm thickness and thoroughly mixing them several times during the day. Each sample was then mixed thoroughly and separated into representative sub-samples by passing through the riffle box. In this way were prepared one 40-kg sub-sample for compaction in the priswest mould, two 8-kg sub-samples for compaction in the cylwest mould, and one 2-kg sub-sample for the granulometric analyses. The grain size curves of the original samples and the samples taken for shear box tests are shown in Figs. 7.6 to 7.10.

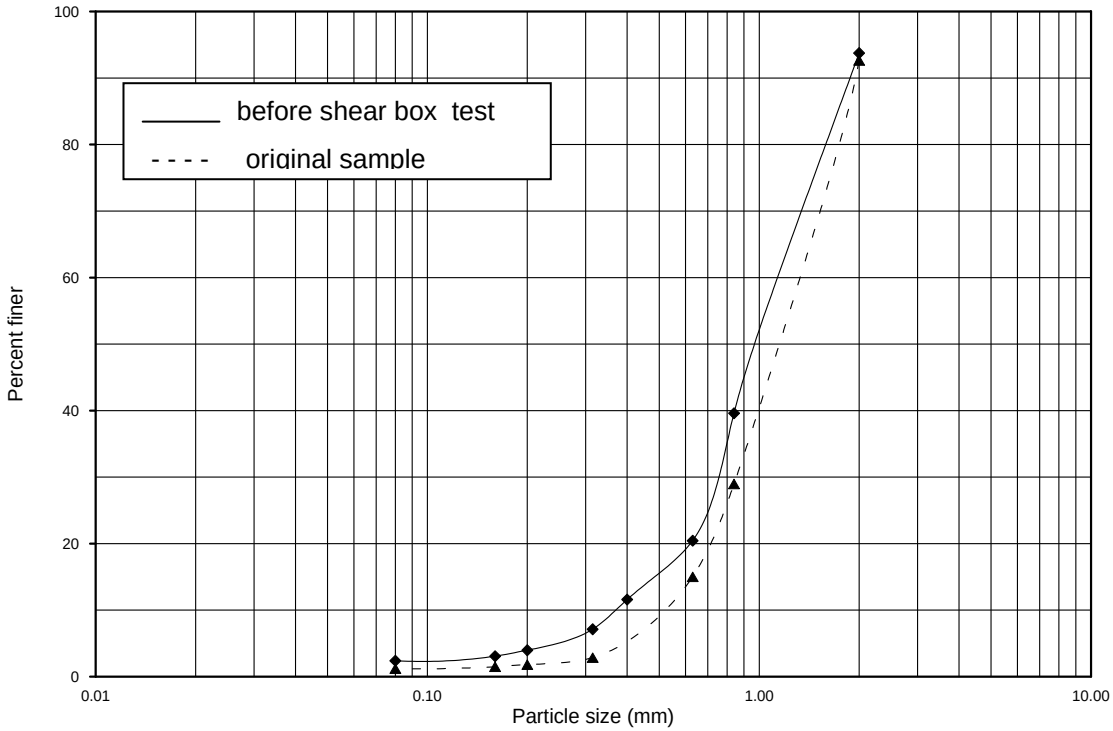

Figure 7.6. Original gradation of sample B and the gradation before shear box tests

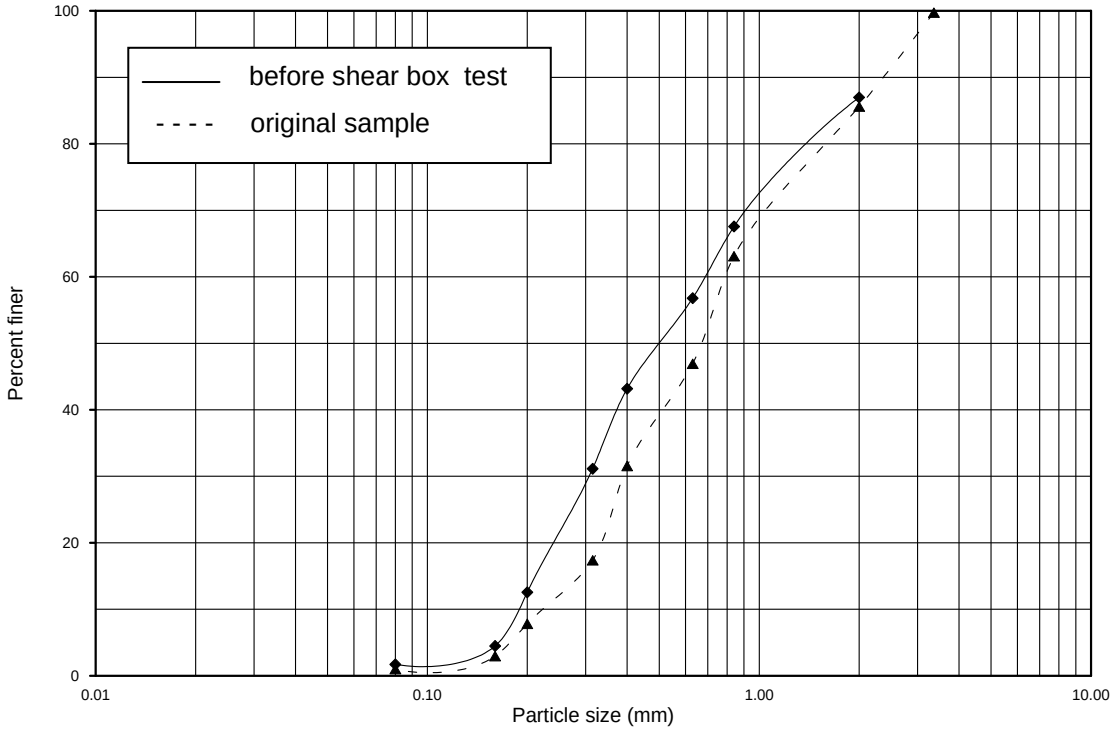

Figure 7.7. Original gradation of sample C and the gradation before shear box tests

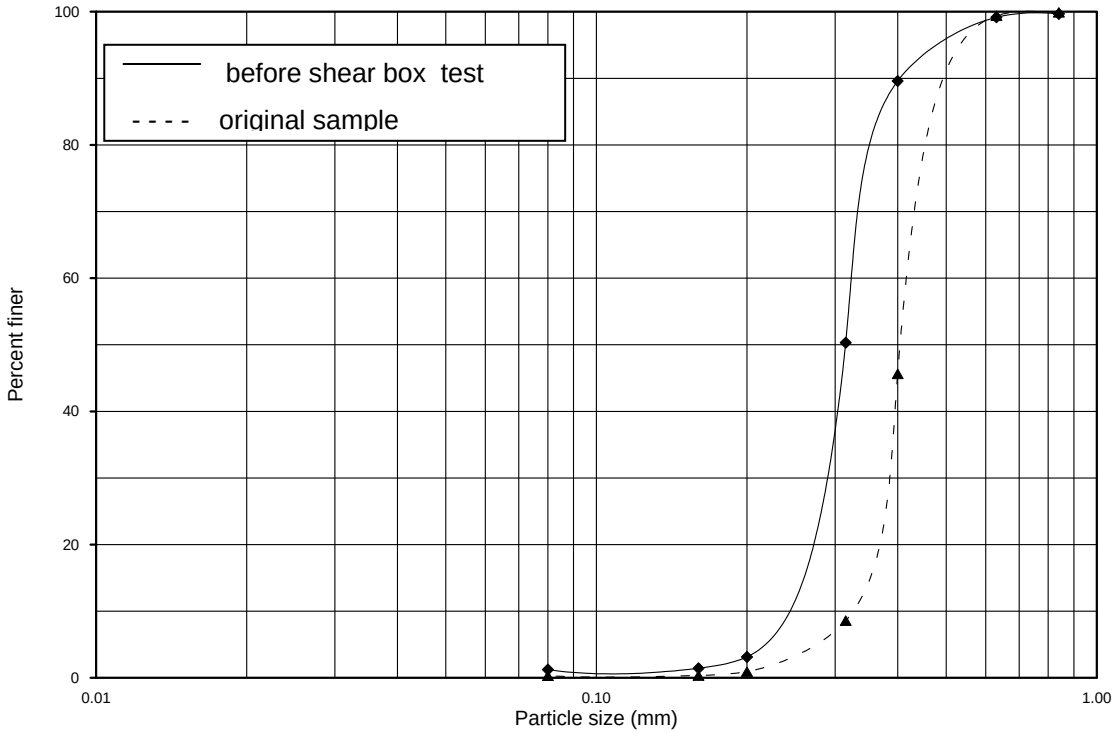

Figure 7.8. Original gradation of sample D and the gradation before shear box tests

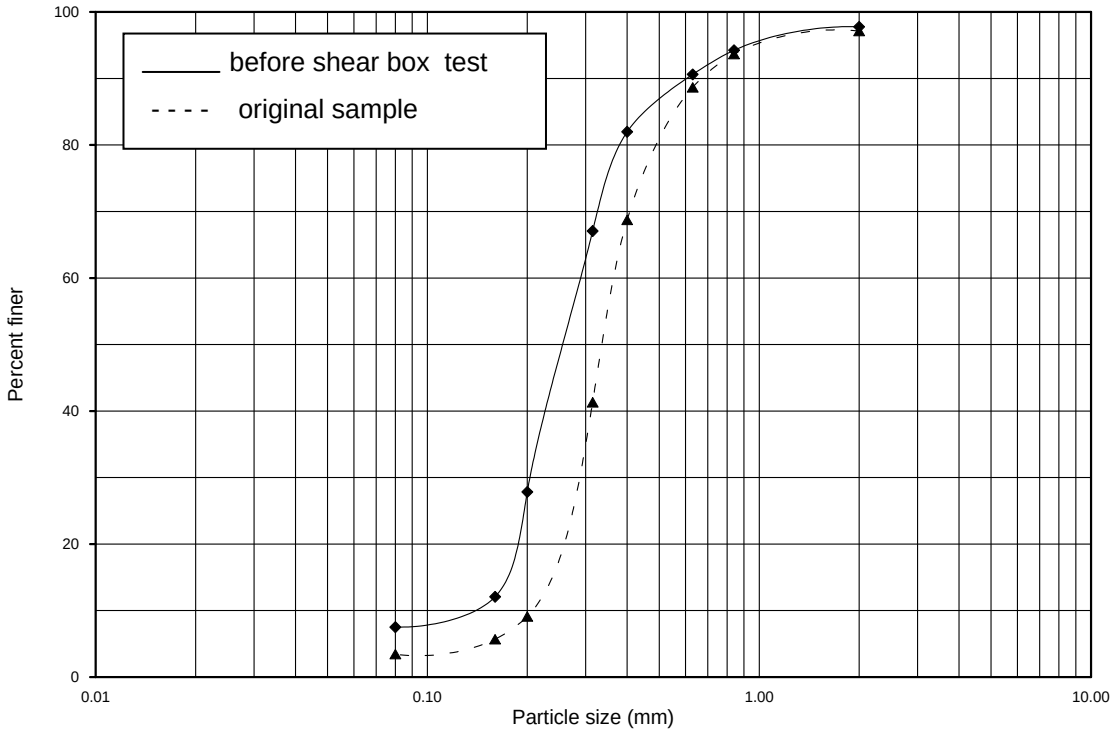

Figure 7.9. Original gradation of sample E and the gradation before shear box tests

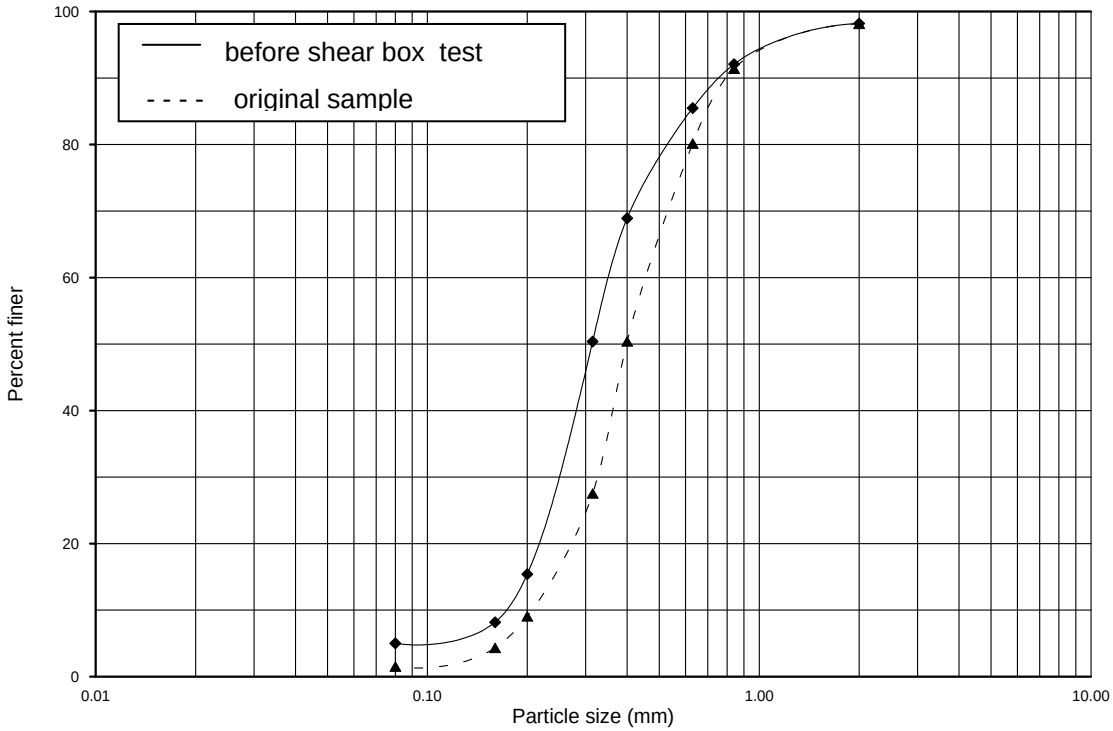

Figure 7.10. Original gradation of sample F and the gradation before shear box tests

7.4.3 Test Procedure for Specimens Taken from the Shear Plane of Samples Compacted in the Cylwest Mould

1. Steps 1 and 2 in section 7.3.1 were applied.

2. For each sub-sample prepared as in section 7.4.2, the amount of sand required to give the desired wet density when compacted to a height of 40 mm in the cylwest mould was calculated, and compacted dynamically in the cylwest mould by the 2.5 kg rammer. This procedure was repeated nine times.

3. The screws securing the upper pair of mould couplings were removed. A stretched steel wire was moved along the shearing plane of the lower part of the mould, cutting the sample along this plane.

4. The lower half of the cylwest mould was placed on a wooden supporting frame holding the shear surface in a horizontal position (Fig. 7.11). The core cutter, of the right size for the shear box and carrying a label which enabled the direction of shear in the shear box to be the same as in the cylwest, was placed on the shear surface. Applying pressure through a wooden disc placed on top, the core cutter was pressed manually into the sample in the cylwest mould until the top of the specimen was flush with the top of the core cutter. The sand around the core cutter was removed by means of a spatula, and the specimen cut at an adequate distance from the cutting edge of the core cutter without disturbing the specimen.

5. The whole was turned up side down, and the upper end of the specimen trimmed flush with the cutting edge of the core cutter. If the mass of the specimen was less than the value calculated at (2), sand was added from the trimmings until the desired mass was obtained. (The maximum amount needed to be added was 1 g to 2 g.)

6. The core cutter containing the specimen was held just above the shear box according to the predefined direction of shear. The retaining plate together with the porous stone and serrated grid plate (Fig. 7.2) were raised by pressing with the fingers from below until the upper surface of the serrated plate touched the bottom of the specimen. Then, the loading plate was placed on top of the specimen in the core cutter and pushed slowly downwards while letting the retaining plate engage the pins at the inner sides of the shear box.

7. After the specimen was placed in the shear box, the height of the specimen was checked. If it was more than 20 mm, (the maximum height recorded at this stage was 23 mm and in no case was this less than 20 mm) additional compaction was applied to bring it down to 20 mm.

8. Steps 4 to 10 in section 7.3.1 were applied.

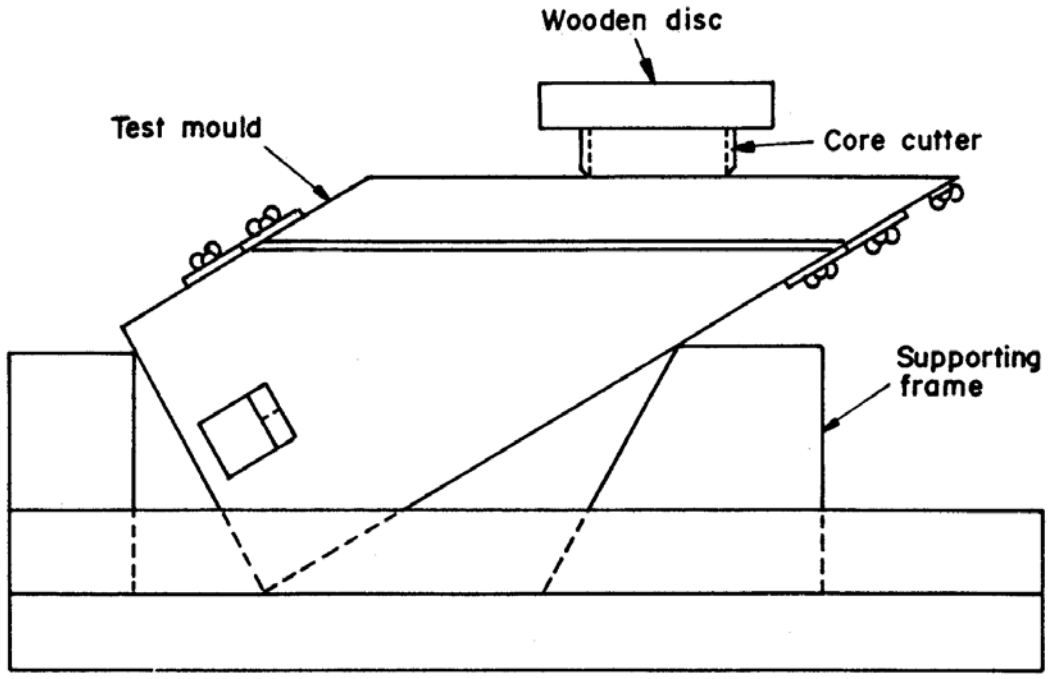

a) Extracting a specimen

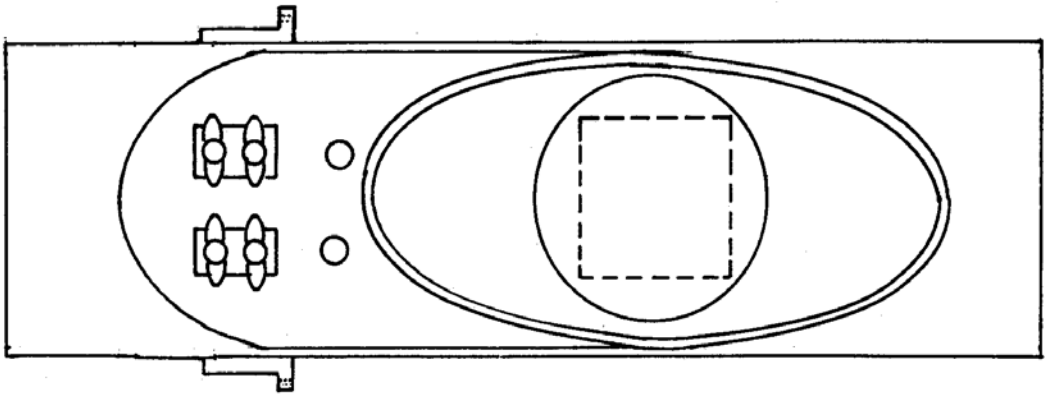

b) Position of specimen taken

Figure 7.11. Setup used for extracting shear box specimens from the cylwest mould

9. For taking the second specimen, an additional wooden disc of height 50 mm was jacked into the bottom of the lower part of the cylwest mould thus pushing the sample upwards by this amount. The protruding part of sample was trimmed flush with the shear plane of the mould. A second shear box specimen was taken as at step 4, and steps 5 to 8 were repeated.

10. Steps 1 to 9 were then repeated on the second sub-sample prepared as in section 7.4.2.

7.4.4 Test Procedure for Specimens Taken from the Shear Plane of Samples Compacted in the Priswest Mould

1. Steps 1 and 2 in section 7.3.1 were applied.

2. For each sub-sample prepared as in section 7.4.2, the mass of sand required to give the desired wet density when compacted to a height of 51 mm in the 30-degree priswest mould was calculated, and compacted in this mould using the Kango vibrating hammer, as in section 5.2.3. This procedure was repeated five times, obtaining a compacted sample with the top about 10 mm above the top of the mould. The collar was then removed, the surplus material scraped off, the surface smoothed, and the lid screwed in position. The link bolts and spacers were removed. The sample was cut by moving a stretched steel wire along the shearing surface of the lower part of the mould.

3. The lower half of the priswest mould was held with the shear surface in a horizontal position by using wooden blocks as in Fig. 7.12. A specimen was extracted from position 1 (Fig. 7.12 (b)), following the same procedure as in section 7.4.3 (4).

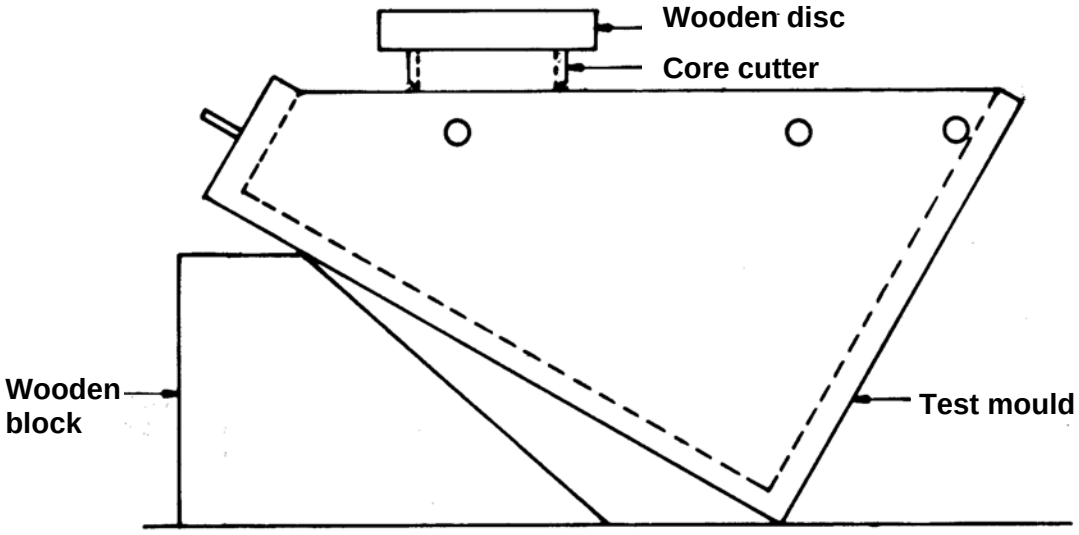

a) Extracting a specimen

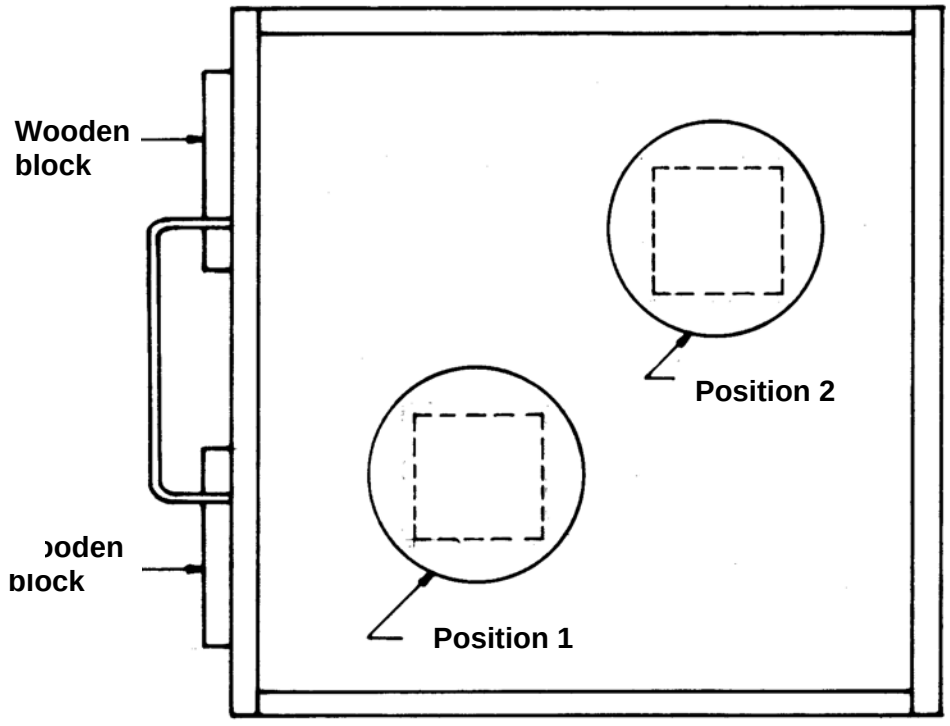

b) Position of specimen taken

Figure 7.12. Setup used for extracting shear box specimens from the priswest mould

4. The steps 5 to 8 in section 7.4.3 were then applied to the specimen.

5. A second shear box specimen was taken as at step 3 from position 2 (Fig. 7.12 (b)), and steps 5 to 8 in section 7.4.3 were repeated

6. Steps 1 to 5 were then repeated on the sub-same sample prepared as in section 7.4.2.

7.4.5 Results of Shear Box Tests on Specimens Taken from the Shear Plane of Samples Compacted in the Cylwest and Priswest Moulds

Ten shear box tests series SBC, SCC, SDC, SEC, SFC; SBP, SCP, SDP, SEP, and SFP of four tests each were performed on the specimens taken from the cylwest and priswest moulds. In this notation, the first letter signifies the shear box test; the second letter denotes the sample tested; the C and P at the end denote the specimens taken from the cylwest and priswest moulds respectively. The tests were evaluated by using the computer program DIST02 (Mirata, 2002(b)). The results are summarized in Tables 7.3 and 7.4 and plotted in Figs. 7.13 and 7.14.

Table 7.3. The results of the shear box test series SBC to SFC

1	2	3	4	5	6	7	8	9	10	11	12
Sample	Test no.	e	D_r	Peak strength				Ultimate strength			
				σ (kPa)	τ (kPa)	ϕ (deg)	r	σ (kPa)	τ (kPa)	ϕ (deg)	r
B	SBC/1	0.635	62.5	18.5	18.0	42.3	.9957	18.5	11.5	33.2	.9985
	SBC/2			45.4	43.7			45.4	27.8		
	SBC/3			71.6	61.2			71.6	46.8		
	SBC/4			99.1	91.9			99.1	65.7		
C	SCC/1	0.575	20.4	18.5	19.9	44.3	.9984	18.5	12.6	34.4	.9998
	SCC/2			45.4	45.2			45.4	31.1		
	SCC/3			71.6	71.6			71.6	49.7		
	SCC/4			99.1	94.9			99.1	67.4		
D	SDC/1	0.682	54.0	17.1	16.7	40.2	.9935	17.1	10.5	31.3	.9728
	SDC/2			35.0	29.6			35.0	16.2		
	SDC/3			43.0	33.7			43.0	29.2		
	SDC/4			71.1	61.2			71.1	43.9		
E	SEC/1	0.638	70.1	22.0	24.7	43.5	.9941	22.0	14.6	32.8	.9994
	SEC/2			43.0	42.6			43.0	28.2		
	SEC/3			64.0	59.4			64.0	40.4		
	SEC/4			85.1	80.0			85.1	54.9		
F	SFC/1	0.647	60.6	20.1	19.6	42.0	.9736	20.1	12.0	33.1	.9776
	SFC/2			40.8	44.5			40.8	27.1		
	SFC/3			62.1	52.3			62.1	45.6		
	SFC/4			83.0	73.3			83.0	50.4		

Table 7.4. The results of the shear box test series SBP to SFP

1	2	3	4	5	6	7	8	9	10	11	12
Sample	Test no.	e	D_r	Peak strength				Ultimate strength			
				σ (kPa)	τ (kPa)	ϕ (deg)	r	σ (kPa)	τ (kPa)	ϕ (deg)	r
B	SBP/1	0.635	62.5	18.5	16.7	40.5	.9880	18.5	11.1	31.4	.9949
	SBP/2			45.4	44.1			45.4	28.8		
	SBP/3			71.6	63.7			71.6	40.6		
	SBP/4			99.1	80.3			99.1	62.3		
C	SCP/1	0.575	20.4	18.5	15.4	41.7	.9941	18.5	9.2	30.6	.9979
	SCP/2			45.4	37.8			45.4	25.5		
	SCP/3			71.6	60.1			71.6	42.3		
	SCP/4			99.1	92.3			99.1	59.6		
D	SDP/1	0.682	54.0	17.1	15.2	39.1	.9953	17.1	9.8	27.4	.9978
	SDP/2			35.0	25.9			35.0	17.3		
	SDP/3			43.0	36.2			43.0	22.7		
	SDP/4			71.1	57.8			71.1	36.7		
E	SEP/1	0.638	70.1	22.0	19.9	40.6	.9926	22.0	12.1	30.7	.9969
	SEP/2			43.0	39.2			43.0	24.2		
	SEP/3			64.0	51.0			64.0	37.1		
	SEP/4			85.1	74.2			85.1	52.0		
F	SFP/1	0.647	60.6	20.1	17.3	39.9	.9975	20.1	12.1	30.5	.9988
	SFP/2			40.8	36.5			40.8	25.1		
	SFP/3			62.1	51.1			62.1	35.8		
	SFP/4			83.0	68.7			83.0	48.8		

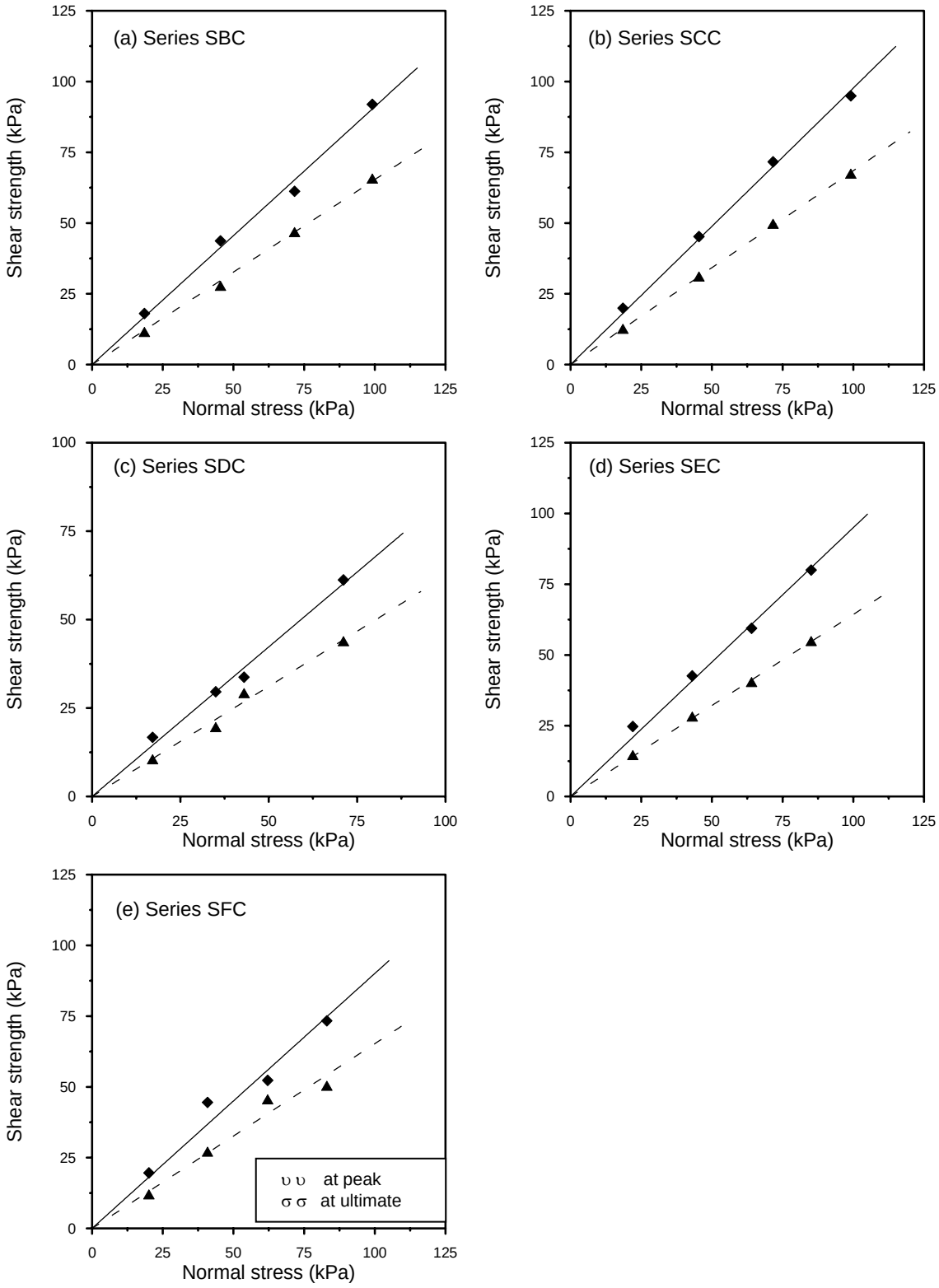

Figure 7.13. The results of shear box tests on specimens taken from the shear plane of cylwest samples

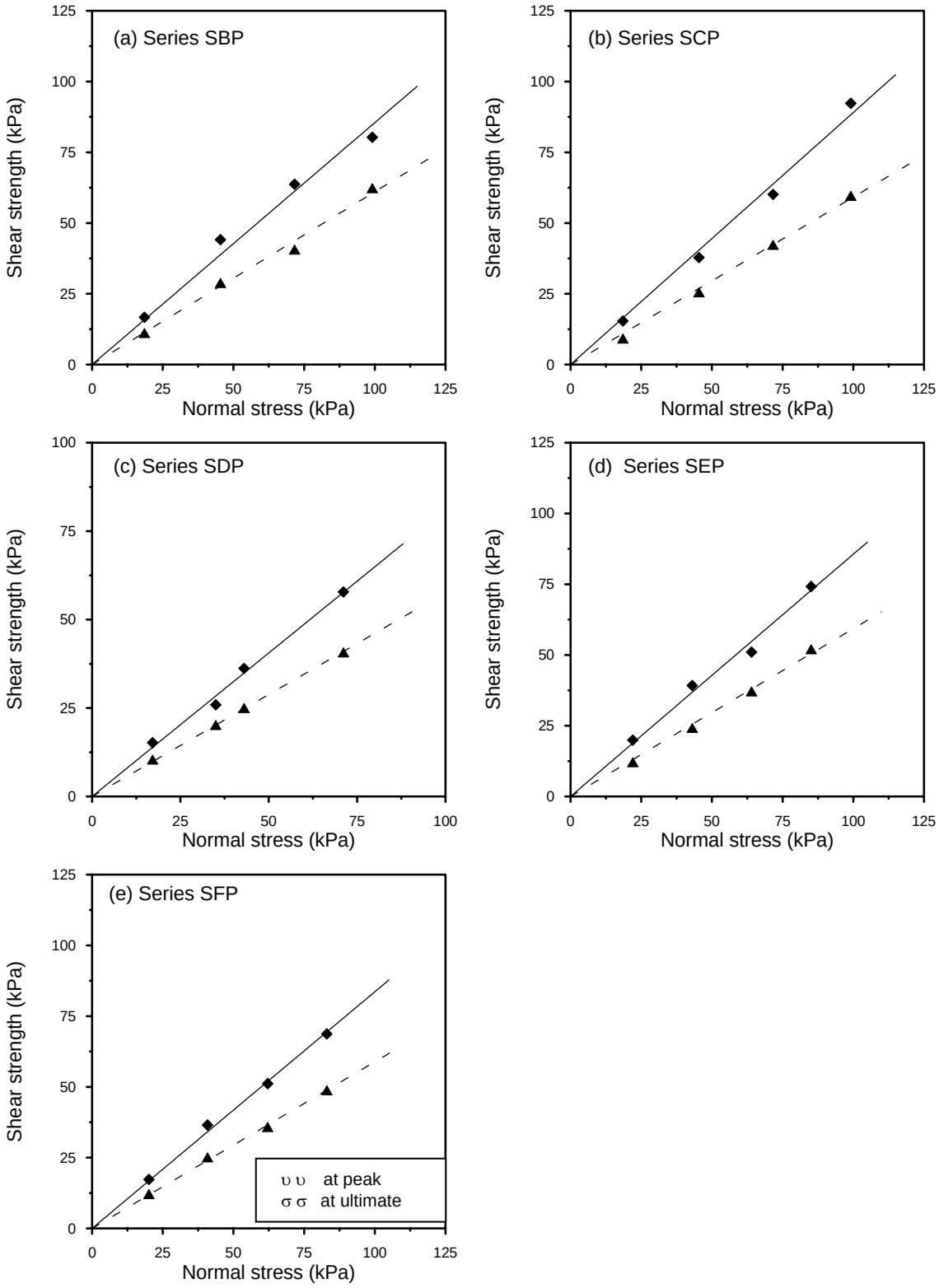

Figure 7.14. The results of shear box tests on specimens taken from the shear plane of priswest samples

CHAPTER 8

DISCUSSIONS

8.1 Discussion of Shear Test Results

The paragraphs in the following sub-sections have been numbered for ease of reference.

8.1.1 Shear Strength Measured in Wedge Shear and Triaxial Tests

1. The summary of cylwests, priswests, and triaxial tests performed on samples A to F at the lower density under the lower and higher ranges of normal stress σ are given in Table 8.1. The corresponding results for samples D to F at the higher density are given in Table 8.2. All peak friction angles measured for each sample are compared in Table 8.3. In this table, for both densities, ϕ_c denotes values obtained from cylwests under the lower ranges of σ; ϕ_{pl} and ϕ_{tl} denote those from the results of priswests and triaxial tests under the lower ranges of σ respectively; ϕ_{ph} and ϕ_{th} denote those from the results of priswests and triaxial tests under the higher ranges of σ respectively; ϕ_{pa} and ϕ_{ta} denote those from the combined results of all priswests and triaxial tests respectively. These results, however, are affected by different degrees of previous particle crushing in specimens used for some of the tests (Tables 5.1, 5.8, and 6.1). To eliminate the effect of particle crushing, bar chart comparisons have been given between the results of tests performed on identical specimens regarding previous use in shear tests. Thus the comparisons in Figs. 8.1 to 8.3 are those of tests on previously untested specimens; the comparisons in Figs. 8.4

Table 8.1. Summary of shear tests for samples A to F at the lower density

1	2	3	4	5	6	7	8	9	10	11	12	13	14
Sample	Type of shear test: / Quantity	Cylwest	Priswest			Triaxial test			Differences between the ϕ values given in different columns (degrees)				
									(3)–(4)	(3)-(7)	(4)-(7)	(5)-(8)	(6)-(9)
A	Normal stress range (kPa)	47-111	76-195	202-415	76-415	46-139	179-291	46-291					
	Peak friction angle (deg)	53.2	50.5	45.9	46.7	49.9	45.4	46.4	2.7	3.3	0.6	0.5	0.3
	Ultimate friction angle (deg)	41.3	39.4	36.7	37.4	43.8	37.5	38.9	1.9	-2.5	-4.4	-0.8	-1.5
B	Normal stress range (kPa)	19-76	63-156	162-277	63-277	29-80	136-217	29-217					
	Peak friction angle (deg)	47.8	46.1	41.9	42.8	44.6	41.7	42.0	1.7	3.2	1.5	0.2	0.8
	Ultimate friction angle (deg)	34.6	37.0	33.4	34.2	35.9	37.1	37.0	-2.4	-1.3	1.1	-3.7	-2.8
C	Normal stress range (kPa)	18-72	61-147	111-296	61-296	21-100	127-251	21-251					
	Peak friction angle (deg)	46.5	44.2	41.2	41.9	43.5	41.1	41.6	2.3	3.0	0.7	0.1	0.3
	Ultimate friction angle (deg)	35.0	34.5	33.6	33.8	37.4	35.9	36.2	0.5	-2.4	-2.9	-2.3	-2.4
D	Normal stress range (kPa)	16-67	29-71	105-231	29-231	30-56	94-197	30-197					
	Peak friction angle (deg)	45.2	44.2	39.7	40.1	43.0	40.9	41.1	1.0	2.2	1.2	-1.2	-1.0
	Ultimate friction angle (deg)	33.4	33.3	33.8	33.8	35.3	34.1	34.2	0.1	-1.9	-2.0	-0.3	-0.4
E	Normal stress range (kPa)	22-85	33-75	148-291	33-291	31-72	137-243	31-243					
	Peak friction angle (deg)	49.5	47.2	42.7	43.0	47.6	43.0	43.4	2.3	1.9	-0.4	-0.3	-0.4
	Ultimate friction angle (deg)	35.1	35.9	35.7	35.7	36.6	36.1	36.2	-0.8	-1.5	-0.7	-0.4	-0.5
F	Normal stress range (kPa)	19-78	32-82	134-298	32-298	29-65	123-252	29-252					
	Peak friction angle (deg)	48.0	46.0	42.3	42.6	46.9	42.9	43.2	2.0	1.1	-0.9	-0.6	-0.6
	Ultimate friction angle (deg)	35.4	35.6	37.6	37.4	35.4	36.0	36.0	-0.2	0.0	0.2	1.6	1.4

Table 8.2. Summary of shear tests for samples D to F at the higher density

1	2		3	4	5	6	7	8	9	10	11	12	13	14
Sample	Type of shear test: / Quantity		Cylwest	Priswest			Triaxial test			Differences between the ϕ values given in different columns (degrees)				
										(3)–(4)	(3)-(7)	(4)-(7)	(5)-(8)	(6)-(9)
D	Normal stress range	(kPa)	23-79	33-77	181-303	33-303	29-84	166-254	29-254					
	Peak friction angle	(deg)	48.5	45.0	42.9	43.0	45.9	43.6	43.8	3.5	2.6	-0.9	-0.7	-0.8
	Ultimate friction angle	(deg)	33.8	34.5	32.7	32.8	34.4	35.2	35.2	-0.7	-0.6	0.1	-2.5	-2.4
E	Normal stress range	(kPa)	53-108	39-105	199-329	39-329	42-88	188-282	42-282					
	Peak friction angle	(deg)	53.5	47.7	43.8	44.2	50.9	45.7	46.2	5.8	2.6	-3.2	-1.9	-2.0
	Ultimate friction angle	(deg)	36.4	35.6	35.4	35.4	36.8	38.3	38.2	0.8	-0.4	-1.2	-2.9	-2.8
F	Normal stress range	(kPa)	42-103	41-87	186-323	41-323	38-85	176-272	38-272					
	Peak friction angle	(deg)	52.4	46.7	43.1	43.4	50.3	44.3	44.9	5.7	2.1	-3.5	-1.2	-1.5
	Ultimate friction angle	(deg)	35.5	34.9	34.6	34.6	35.1	39.7	39.5	0.6	0.4	-0.2	-5.1	-4.9

Table 8.3. Peak friction angles obtained from the cylwests, priswests, and triaxial tests for samples A to F

1	2	3	4	5	6	7	8	9	10	11	12	13	14	15	16	17	18	19	20	21	22	23	24	25
Sample	Peak friction angles at the lower density (degrees)							Peak friction angles at the higher density (degrees)							Differences between the values of peak friction angles given in different columns (degrees)									
	ϕ_c	ϕ_{pl}	ϕ_{ph}	ϕ_{pa}	ϕ_{tl}	ϕ_{th}	ϕ_{ta}	ϕ_c	ϕ_{pl}	ϕ_{ph}	ϕ_{pa}	ϕ_{tl}	ϕ_{th}	ϕ_{ta}	(2) – (3)	(2) – (6)	(3) – (6)	(4) – (7)	(5) – (8)	(9) – (10)	(9) – (13)	(10) – (13)	(11) – (14)	(12) – (15)
A	53.2	50.5	45.9	46.7	49.9	45.4	46.4	…	…	…	…	…	…	…	2.7	3.3	0.6	0.5	0.3	…	…	…	…	…
B	47.8	46.1	41.9	42.8	44.6	41.7	42.0	…	…	…	…	…	…	…	1.7	3.2	1.5	0.2	0.8	…	…	…	…	…
C	46.5	44.2	41.2	41.9	43.5	41.1	41.6	…	…	…	…	…	…	…	2.3	3.0	0.7	0.1	0.3	…	…	…	…	…
D	45.2	44.2	39.7	40.1	43.0	40.9	41.1	48.5	45.0	42.9	43.0	45.9	43.6	43.8	1.0	2.2	1.2	-1.2	-1.0	3.5	2.6	-0.9	-0.7	-0.8
E	49.5	47.2	42.7	43.0	47.6	43.0	43.4	53.5	47.7	43.8	44.2	50.9	45.7	46.2	2.3	1.9	-0.4	-0.3	-0.4	5.8	2.6	-3.2	-1.9	-2.0
F	48.0	46.0	42.3	42.6	46.9	42.9	43.2	52.4	46.7	43.1	43.4	50.3	44.3	44.9	2.0	1.1	-0.9	-0.6	-0.6	5.7	2.1	-3.5	-1.2	-1.5

and 8.5 are those of tests on specimens used once in previous shear tests. The test numbers and normal stresses of single shear tests used for the comparisons in Figs. 8.1 to 8.5 are given in Table 8.4.

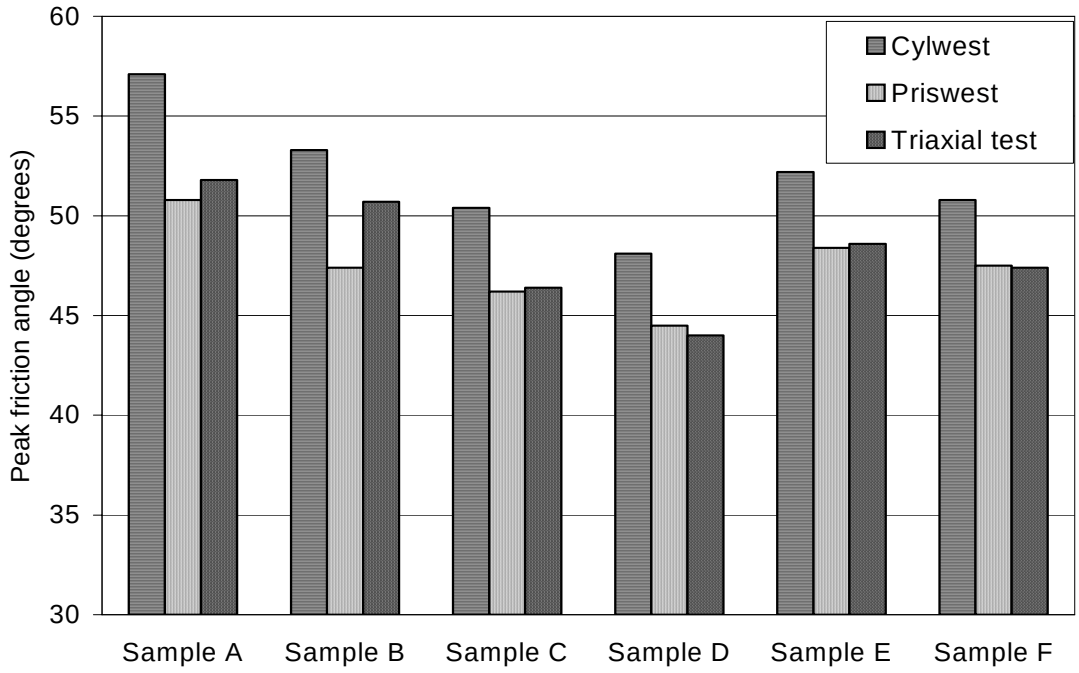

Figure 8.1. Comparison of the peak friction angles measured in single shear tests on previously untested specimens for samples A to F at the lower density under the lower σ range

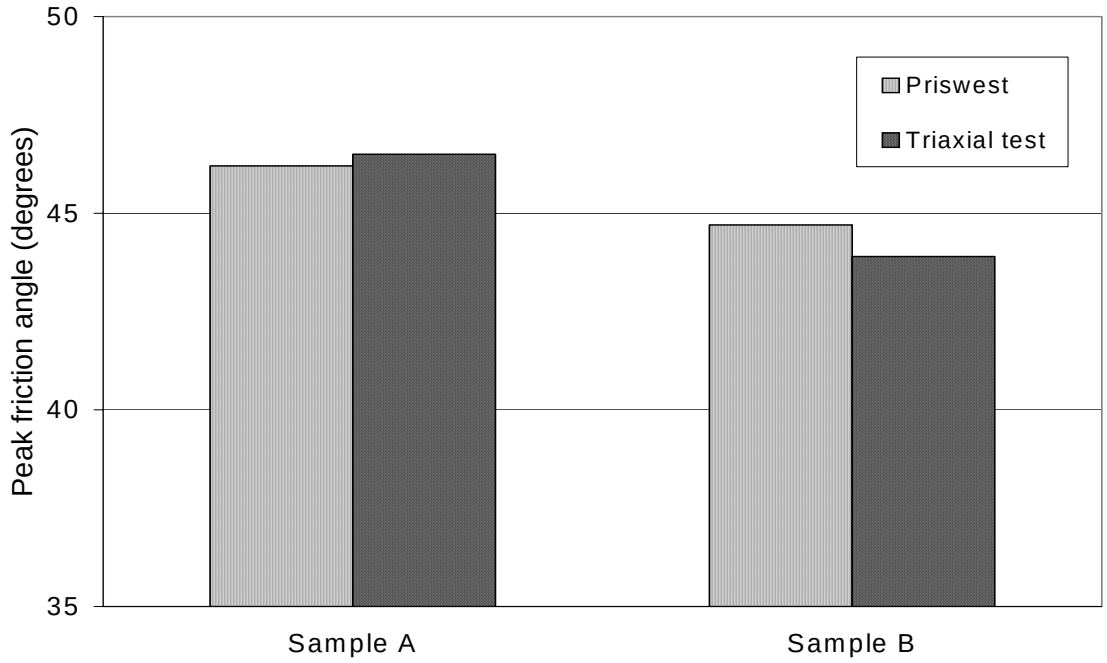

Figure 8.2. Comparison of the peak friction angles measured in single shear tests on previously untested specimens for samples A and B at the lower density under the higher σ range

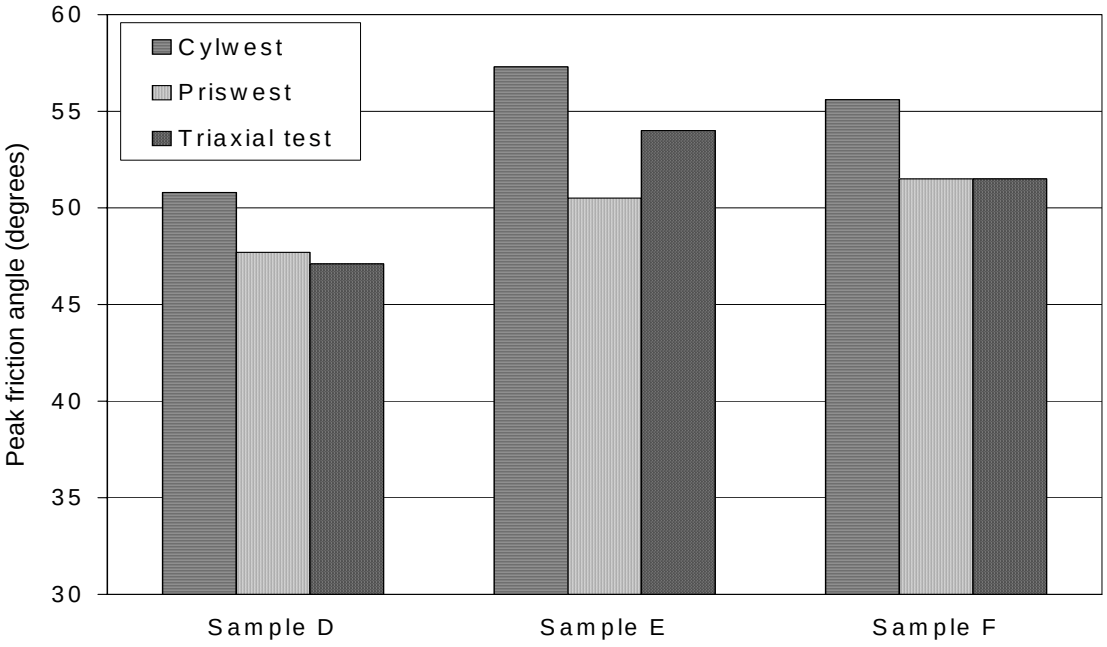

Figure 8.3. Comparison of the peak friction angles measured in single shear tests on previously untested specimens for samples D to F at the higher density under the lower σ range

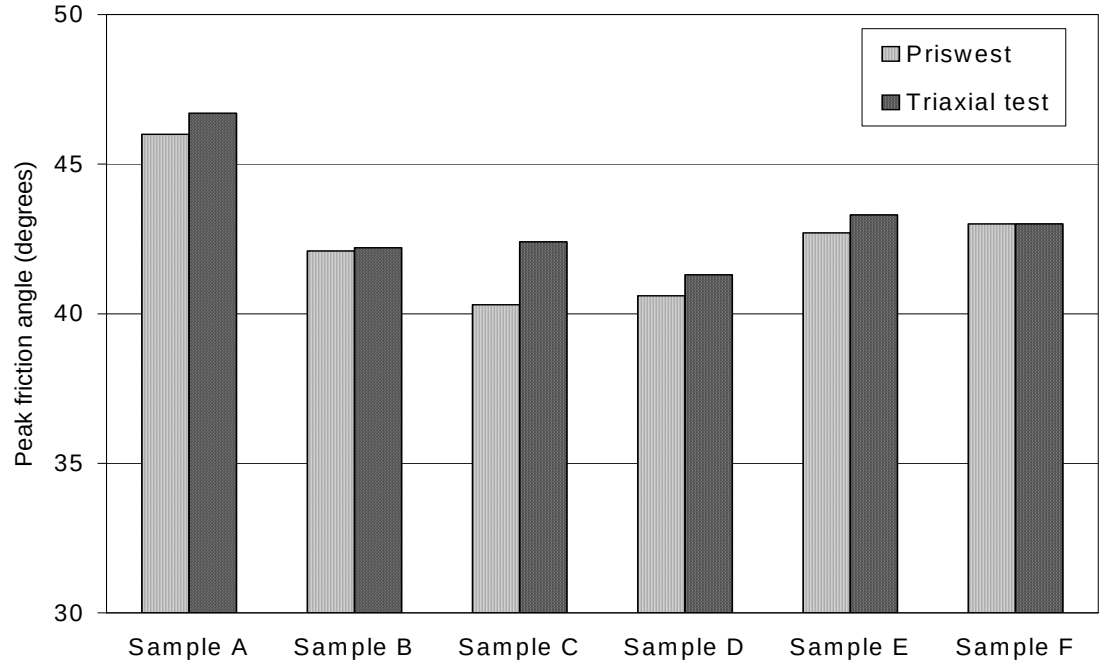

Figure 8.4. Comparison of the peak friction angles measured in single shear tests on specimens previously used once for samples A to F at the lower density under the higher σ range

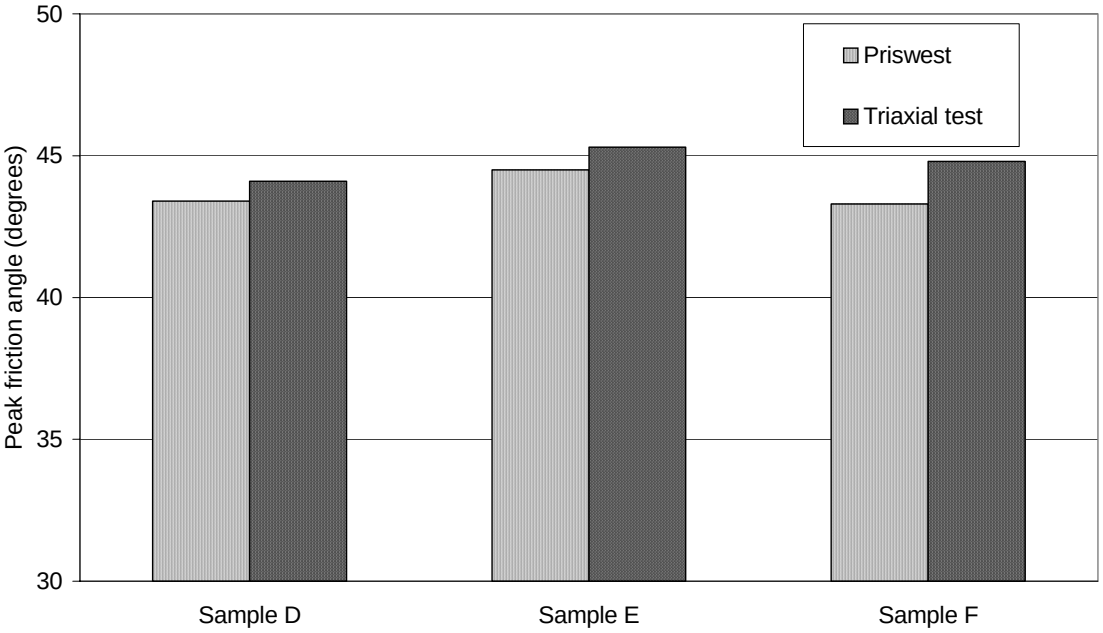

Figure 8.5. Comparison of the peak friction angles measured in single shear tests on specimens previously used once for samples D to F at the higher density under the higher σ range

Table 8.4. Test numbers and normal stresses of single shear tests used for the comparisons in Figs. 8.1 to 8.5

1	2	3	4	5	6	7	8
Figure no.	Sample	Cylwest		Priswest		Triaxial test	
		Test no.*	σ (kPa)	Test no.#	σ (kPa)	Test no.$	σ (kPa)
8.1	A	CA/3	47.1	PA1/1	76.5	TA/1	46.2
	B	CB/1	23.0	PB1/1	63.7	TB/1	28.7
	C	CC/1	19.6	PC1/1	60.7	TC/1	20.6
	D	CD/3	17.2	PD1/1	29.5	TD/1	30.5
	E	CE/1	24.6	PE1/1	33.5	TE/1	31.4
	F	CF/3	21.1	PF1/1	32.4	TF/1	28.8
8.2	A	...	...	PA2/1	202.1	TA/5	179.1
	B	...	...	PB2/1	161.6	TB/5	136.1
8.3	D	CDH/1	23.8	PDH1/1	33.4	TDH/1	28.7
	E	CEH/3	58.6	PEH1/1	39.7	TEH/1	42.3
	F	CFH/1	42.4	PFH1/1	41.9	TFH/1	38.4
8.4	A	...	...	PA2/2	355.7	TA/6	242.2
	B	...	...	PB2/2	214.0	TB/6	182.9
	C	...	...	PC2/2	187.5	TC/6	163.8
	D	...	...	PD2/2	184.8	TD/6	165.3
	E	...	...	PE2/2	221.5	TE/6	193.0
	F	...	...	PF2/2	232.6	TF/6	203.7
8.5	D	...	...	PDH2/2	241.6	TDH/5	214.9
	E	...	...	PEH2/2	275.5	TEH/5	241.8
	F	...	...	PFH2/2	244.6	TFH/5	217.7

* Tables 5.5 to 5.7

Tables 5.15 to 5.19

$ Tables 6.2 to 6.10

2. The bar charts in Fig. 8.1 show that cylwests yield higher values of ϕ_d than triaxial tests by 5.3^o, 2.6^o, 4.0^o, 4.1^o, 3.6^o, and 2.8^o for samples A to F at the lower density under the lower σ range. At the higher density, differences in ϕ_d values are found as 3.7^o, 3.3^o, and 4.1^o for samples D to F respectively (Fig. 8.3). A similar tendency is also observed in the results of test series under the lower σ ranges (Table 8.3, columns 17 and 22). Cylwests giving higher ϕ_d than triaxial tests is explicable by the fact that the cylwest is close to the plane strain test (section 2.4), and the fact that similar differences were observed by Lee (1970), Cornforth (1973), Hussaini (1973), Marachi et al. (1981), Schanz & Vermeer (1996), and Adel (2001) between plane strain and triaxial test results (section 2.1.4, paragraphs (5), (6), (7), (9), (17), and (19)).

3. The ϕ_{cv} values of all samples, except sample A of $\phi_{cv} = 41.3^o$, is around 35^o (Table 8.5, column 2). The results in paragraph (2) showed that the highest difference of 5.3^o was found for sample A; in the remaining samples, this difference is around 3.5^o. This result indicates that the difference in the ϕ_d values measured in cylwests and triaxial tests is linked with ϕ_{cv} values of samples. This is consistent with Bolton's (1986) views, and Schanz & Vermeer's (1996) equation (2.13) (section 2.1.4, paragraph (15) and (16)).

4. The bar charts in Fig. 8.1 show that cylwests yield higher values of ϕ_d than priswests for samples A to F at the lower density under the lower σ range. Differences in the ϕ_d values are found as 6.3^o, 5.9^o, and 4.2^o for samples A to C; and as 3.6^o, 3.8^o, and 3.3^o for samples D to F respectively. Higher differences in the ϕ_d values for samples A to C are probably due to the distinctly higher differences in the normal stresses in the corresponding priswests than in the cylwests (Table 8.4, columns 4 and 6). At the higher density, differences in ϕ_d values are found as 3.1^o, 6.8^o, and 4.1^o for samples D to F respectively (Fig. 8.3). Higher ϕ_d values measured in cylwests than in priswests is also seen from the results of the test series under the lower σ ranges (Table 8.3, columns 16 and 21). Cylwests giving higher ϕ_d than

priswests is most probably due to the differences in the inclination δ of shear plane to the bedding planes, as δ is 60^o in cylwests, while δ is 30^o in priswests using 30^o mould. The decrease of peak friction angle with δ has been reported both by several authors quoted by Jewell (1989), and by Tatsuoka et al. (1986), and Oda et al. (1986) (section 2.2).

5. For the reasons explained in the previous paragraph, the bar charts in Figs. 8.1 to 8.5 show that out of the 20 comparisons, in only four (sample B in Fig. 8.1, sample E in Fig. 8.3, sample C in Fig. 8.4, and sample F in Fig. 8.5) is the ϕ_d value measured in priswests less than that found from triaxial tests by between 1.5^o and 3.5^o; in all the rest, the two values are nearly the same.

6. All ultimate friction angles ϕ_{cv} measured for each sample are compared in Table 8.5. In this table, for both densities, ϕ_{uc} denotes values obtained from cylwests under the lower σ ranges; ϕ_{upl} and ϕ_{utl} denote those from the results of priswests and triaxial tests under the lower σ ranges respectively; ϕ_{uph} and ϕ_{uth} denote those from the results of priswests and triaxial tests under the higher σ ranges respectively; ϕ_{upa} and ϕ_{uta} denote those from the combined results of all priswests and triaxial tests respectively. As for peak strength (paragraph (1)) these results, however, are affected by different degrees of previous particle crushing in specimens used for some of the tests (Tables 5.1, 5.8, and 6.1). To compare the results of tests performed on identical specimens, the bar chart comparisons in Figs. 8.6 to 8.8 are the results of tests on previously untested specimens; the comparisons in Figs. 8.9 and 8.10 are those of tests on specimens used once in previous shear tests. The test numbers and normal stresses of single shear tests used for the comparisons in Figs. 8.6 to 8.10 are given in Table 8.6.

Table 8.5. Ultimate friction angles obtained from the cylwests, priswests, and triaxial tests for samples A to F

1	2	3	4	5	6	7	8	9	10	11	12	13	14	15	16	17	18	19	20	21	22	23	24	25
Sample	Ultimate friction angles at the lower density (degrees)							Ultimate friction angles at the higher density (degrees)							Differences between the values of ultimate friction angles given in different columns (degrees)									
	ϕ_{uc}	ϕ_{upl}	ϕ_{uph}	ϕ_{upa}	ϕ_{utl}	ϕ_{uth}	ϕ_{uta}	ϕ_{uc}	ϕ_{upl}	ϕ_{uph}	ϕ_{upa}	ϕ_{utl}	ϕ_{uth}	ϕ_{uta}	(2) – (3)	(2) – (6)	(3) – (6)	(4) – (7)	(5) – (8)	(9) – (10)	(9) – (13)	(10) – (13)	(11) – (14)	(12) – (15)
A	41.3	39.4	36.7	37.4	43.8	37.5	38.9	…	…	…	…	…	…	…	1.9	-2.5	-4.4	-0.8	-1.5	…	…	…	…	…
B	34.6	37.0	33.4	34.2	35.9	37.1	37.0	…	…	…	…	…	…	…	-2.4	-1.3	1.1	-3.7	-2.8	**…**	**…**	**…**	**…**	**…**
C	35.0	34.5	33.6	33.8	37.4	35.9	36.2	**…**	**…**	**…**	**…**	**…**	**…**	**…**	0.5	-2.4	-2.9	-2.3	-2.4	…	…	…	…	…
D	33.4	33.3	33.8	33.8	35.3	34.1	34.2	33.8	34.5	32.7	32.8	34.4	35.2	35.2	0.1	-1.9	-2.0	-0.3	-0.4	-0.7	-0.6	0.1	-2.5	-2.4
E	35.1	35.9	35.7	35.7	36.6	36.1	36.2	36.4	35.6	35.4	35.4	36.8	38.3	38.2	-0.8	-1.5	-0.7	-0.4	-0.5	0.8	-0.4	-1.2	-2.9	-2.8
F	35.4	35.6	37.6	37.4	35.4	36.0	36.0	35.5	34.9	34.6	34.6	35.1	39.7	39.5	-0.2	0.0	0.2	1.6	1.4	0.6	0.4	-0.2	-5.1	-4.9

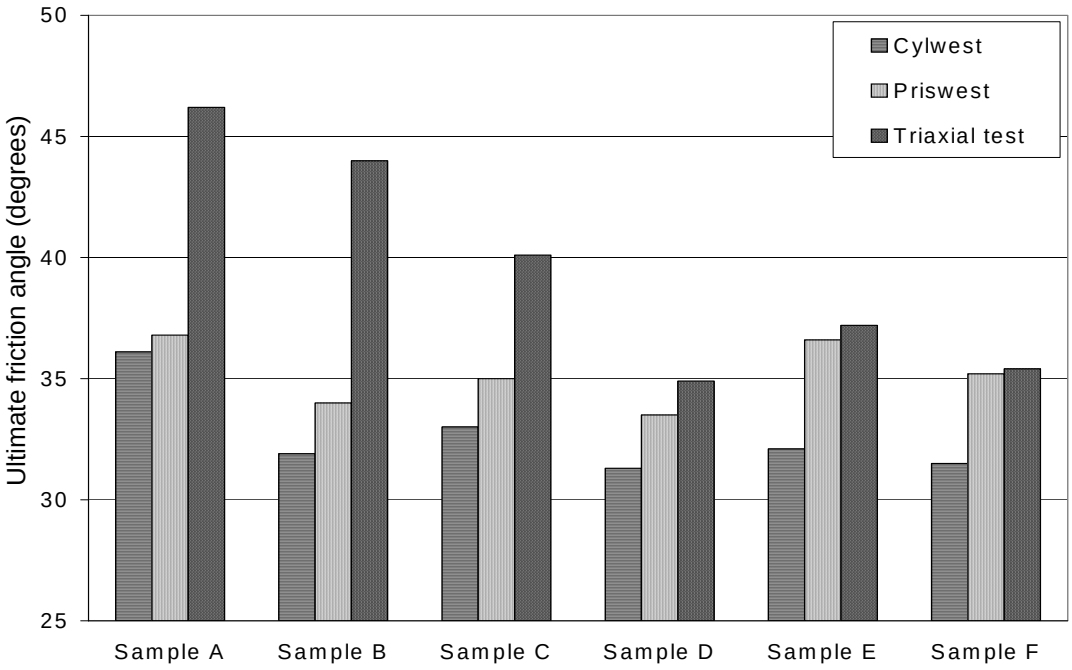

Figure 8.6. Comparison of the ultimate friction angles measured in single shear tests on previously untested specimens for samples A to F at the lower density under the lower σ range

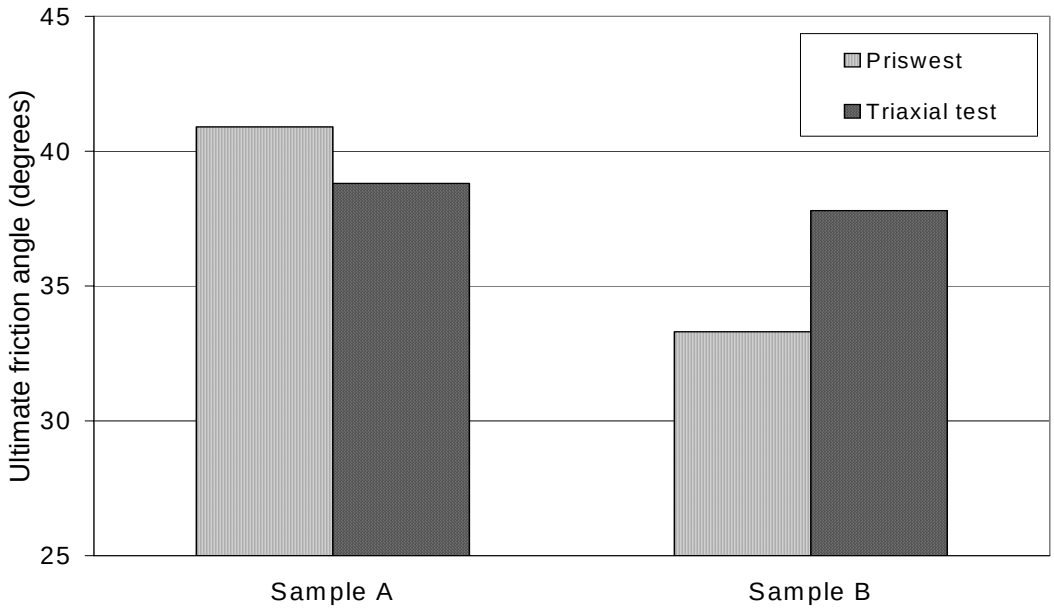

Figure 8.7. Comparison of the ultimate friction angles measured in single shear tests on previously untested specimens for samples A and B at the lower density under the higher σ range

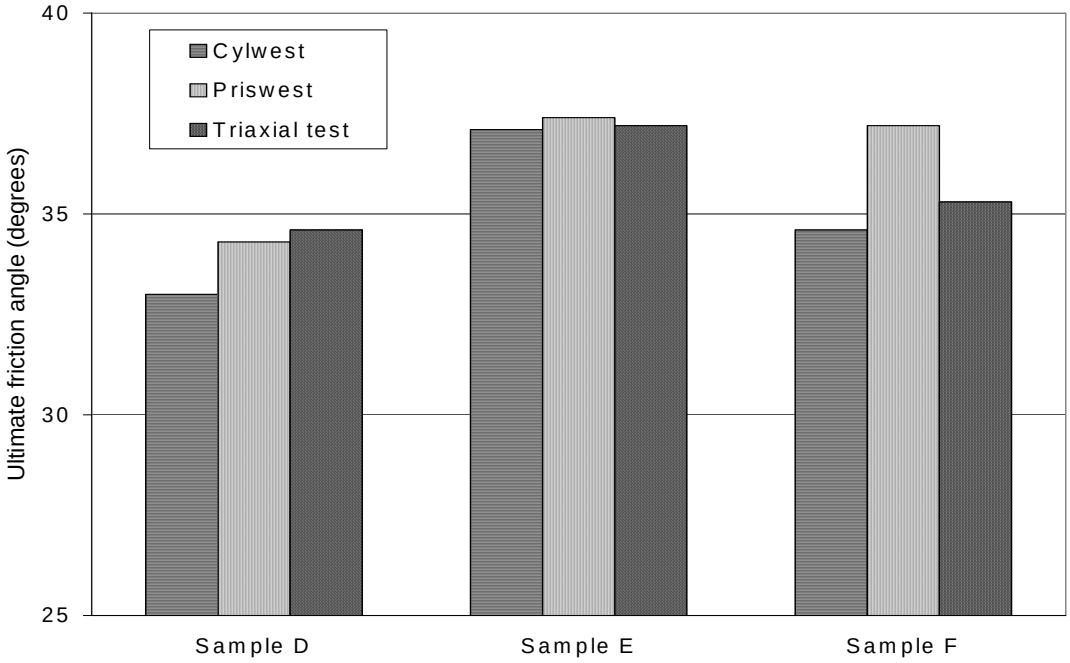

Figure 8.8. Comparison of the ultimate friction angles measured in single shear tests on previously untested specimens for samples D to F at the higher density under the lower σ range

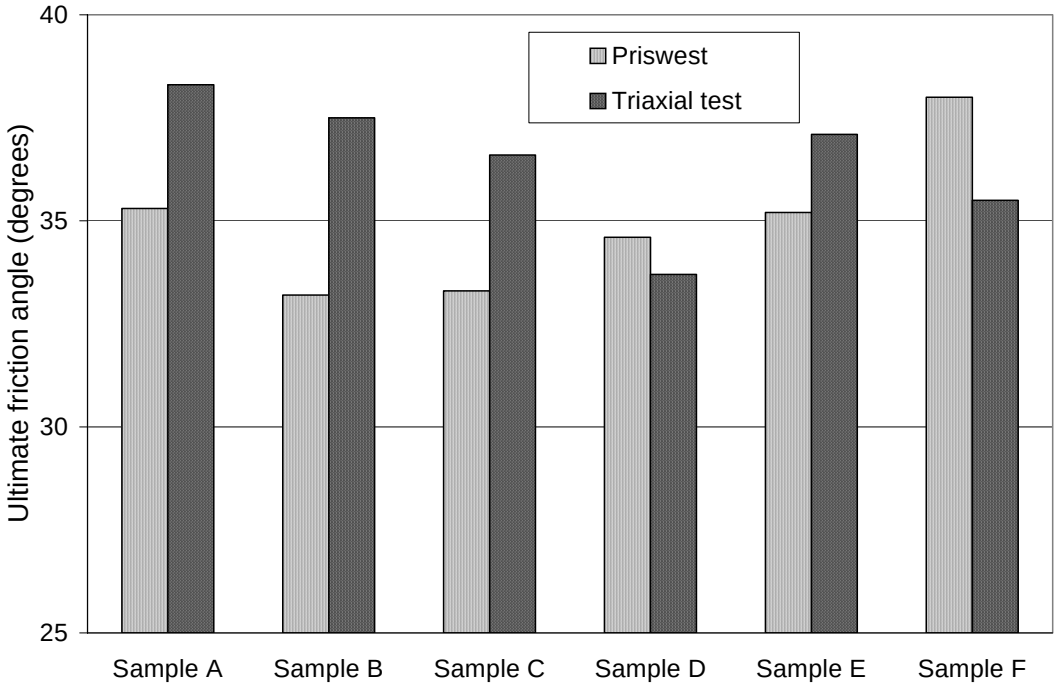

Figure 8.9. Comparison of the ultimate friction angles measured in single shear tests on specimens previously used once for samples A to F at the lower density under the higher σ range

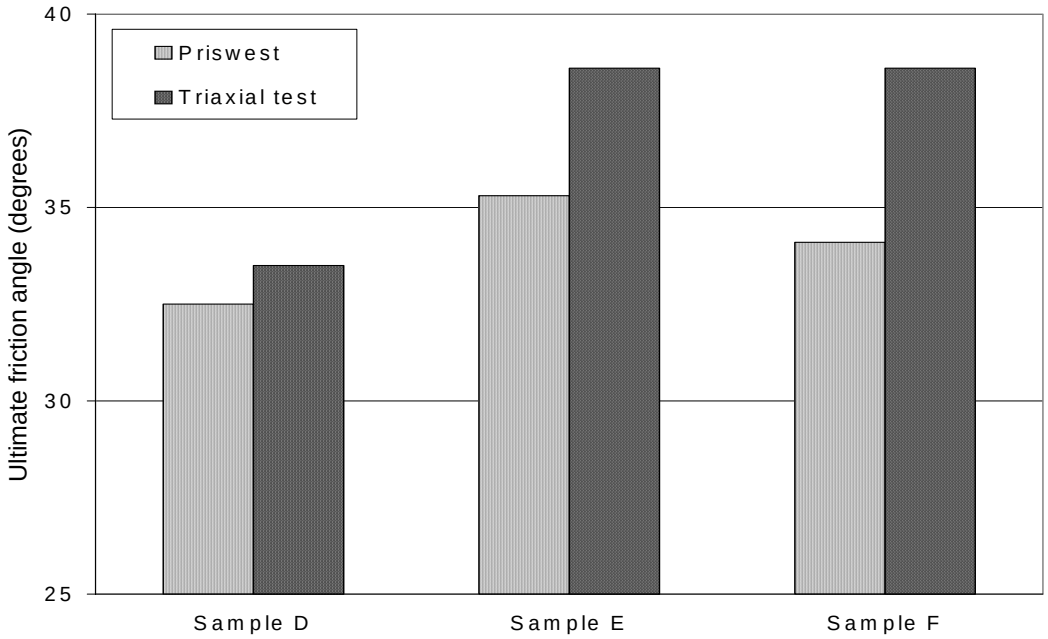

Figure 8.10. Comparison of the ultimate friction angles measured in single shear tests on specimens previously used once for samples D to F at the higher density under the higher σ range

7. The bar charts in Fig. 8.6 show that cylwests yield lower values of ϕ_{cv} (by between 3.6^o and 12.1^o, average difference 7.0^o) than triaxial tests for samples A to F at the lower density under the lower σ range. The higher differences are due to the fact that the relevant triaxial tests have not been sufficiently prolonged to yield the ultimate strength (e.g., Fig. 6.7(a)). At the higher density under the lower σ range (Fig. 8.8), for which the triaxial tests were prolonged sufficiently (e.g., Fig. 6.9(a) and 6.10(a)), the ϕ_{cv} values measured in cylwests and triaxial tests are nearly the same for samples E and F; the ϕ_{cv} value measured in cylwest is less than that obtained from triaxial test by 2.5^o for samples D. These results are in reasonable conformity with Lee (1970), Cornforth (1973), Hussaini (1973), Marachi et al. (1981), and Schanz & Vermeer (1996) (section 2.1.4, paragraphs (5), (6), (7), (9), and (17) respectively), who conclude that the difference between ϕ_{cv} values measured in triaxial and plane strain tests is very small or nil.

Table 8.6. Test numbers and normal stresses of single shear tests used for the comparisons in Figs. 8.6 to 8.10

1	2	3	4	5	6	7	8
Figure no.	Sample	Cylwest		Priswest		Triaxial test	
		Test no.*	σ (kPa)	Test no.#	σ (kPa)	Test no.$	σ (kPa)
8.6	A	CA/1	65.5	PA1/1	93.8	TA/1	45.0
	B	CB/1	29.8	PB1/1	89.8	TB/1	27.7
	C	CC/3	19.5	PC1/1	83.1	TC/1	19.8
	D	CD/3	18.7	PD1/1	35.1	TD/1	28.3
	E	CE/3	25.6	PE1/1	37.6	TE/1	29.3
	F	CF/3	23.0	PF1/1	37.2	TF/1	26.4
8.7	A	...	...	PA2/1	178.2	TA/5	169.4
	B	...	...	PB2/1	198.3	TB/5	126.3
8.8	D	CDH/1	23.4	PDH1/1	31.9	TDH/1	27.2
	E	CEH/3	58.1	PEH1/1	47.6	TEH/1	36.0
	F	CFH/1	44.6	PFH1/1	54.0	TFH/1	34.5
8.9	A	...	...	PA2/2	276.1	TA/6	224.8
	B	...	...	PB2/2	260.4	TB/6	176.1
	C	...	...	PC2/2	224.1	TC/6	155.0
	D	...	...	PD2/2	201.1	TD/6	153.7
	E	...	...	PE2/2	218.3	TE/6	185.5
	F	...	...	PF2/2	214.4	TF/6	190.7
8.10	D	...	...	PDH2/2	284.0	TDH/5	192.4
	E	...	...	PEH2/2	328.8	TEH/5	232.4
	F	...	...	PFH2/2	268.8	TFH/5	202.5

* Tables 5.5 to 5.7

Tables 5.15 to 5.19

$ Tables 6.2 to 6.10

8. The bar charts in Fig. 8.6 show that at the lower density under the lower σ range, cylwests yield lower values of ϕ_{cv} (by between 2.0^o and 4.5^o, average difference 2.9^o) than priswests for samples B to F; the values of ϕ_{cv} measured in the cylwest and priswest are nearly the same for sample A. At the higher density under the lower σ range (Fig. 8.8), the ϕ_{cv} values measured in the priswest and cylwest are nearly the same for sample E; the ϕ_{cv} values measured in cylwests are less than those obtained from priswests by 1.3^o and 2.6^o for samples D and F respectively. Unlike the differences in peak strength (paragraph (4)), these results, as well as those in Table 8.5, columns 16 and 21, indicate that the orientation of the shear plane relative to the bedding plane has no effect on the ϕ_{cv} values.

9. The bar charts in Fig. 8.6 also show that at the lower density under the lower σ range, priswests yield lower values of ϕ_{cv} (by between 1.4^o and 10.0^o, average difference 6.5^o) than triaxial tests for samples A to D; the values of ϕ_{cv} measured in priswests and triaxial tests are nearly the same for samples E and F. The bar charts in Fig. 8.7 show that the priswest yields a higher value of ϕ_{cv} than the triaxial test by 2.1^o for sample A; the value of ϕ_{cv} measured in the priswest is less than that obtained from triaxial test by 4.5^o for sample B. The bar charts in Fig. 8.9 show that at the lower density under the higher σ range, priswests yield lower ϕ_{cv} values (by between 1.9^o and 4.3^o, average difference 3.1^o) than triaxial tests for samples A to C, and E; the values of ϕ_{cv} measured in triaxial tests are less than those obtained from priswests by 0.9^o and 2.5^o for samples D and F respectively. As pointed out in paragraph (7), the higher differences in the ϕ_{cv} values at the lower density are due to the fact that the relavant triaxial tests have not been sufficiently prolonged to yield the ultimate strength. At the higher density under the lower σ range (Fig. 8.8), the value of ϕ_{cv} measured in the priswest is less than that obtained from the triaxial test by 1.2^o for sample D; the priswest yields a higher value of ϕ_{cv} than the triaxial test by 1.9^o for sample F; the ϕ_{cv} values measured in the priswest and triaxial test are nearly the same for sample E. At the higher density under the higher σ range (Fig. 8.10), priswests yield lower ϕ_{cv} values than triaxial tests by 1.0^o, 3.3^o,

and 4.5^o for samples D to F respectively. The larger differences at the higher density under the higher σ range are due to the fact that triaxial tests at the higher density could not be prolonged until the ultimate strength was reached due to the interference imposed by the anti-friction guide (Fig. 6.5).

8.1.2 Comparison of Shear Strength Measured in Shear Box Tests with other Test Results

1. As explained in section 7.1, shear box tests were performed on specimens at the lower density only. The values of ϕ_d obtained from cylwests, priswests, triaxial tests, and shear box tests performed on samples A to F are compared in Table 8.7. In this table, ϕ_{sl} and ϕ_{sh} denote the values obtained from the results of shear box tests with $\delta = 0^o$ performed on previously untested specimens compacted directly in the shear box for the lower and higher σ ranges respectively; ϕ_{sa} denotes those from the combined results of all shear box tests with $\delta = 0^o$; ϕ_{sc} and ϕ_{sp} denote those obtained from the results of shear box tests, at the lower σ range only, with $\delta = 60^o$ and with $\delta = 30^o$ performed on specimens taken from the shear plane of previously sheared samples compacted in the cylwest and priswest moulds respectively. The remaining symbols have been defined in section 8.1.1, paragraph (1), where it was also explained that the cylwest, priswest, and triaxial test results are affected by different degrees of previous particle crushing in specimens used for some of the tests. To compare the results of tests performed on identical specimens, the bar chart comparisons in Figs. 8.11 and 8.12 are the results of tests on previously untested specimens; the comparisons in Fig. 8.13 are those of shear box tests on specimens previously sheared more than once; those in Fig. 8.14 are those of wedge shear tests on specimens used once in previous shear tests. The test numbers and normal stresses of single shear tests used for the comparisons in Figs. 8.11 and 8.12 and in Figs. 8.13 and 8.14 are given in Tables 8.8 and 8.9 respectively.

Table 8.7. Peak friction angles obtained from cylwests, priswests, triaxial tests, and shear box tests for samples A to F at the lower density

1	2	3	4	5	6	7	8	9	10	11	12	13	14	15	16	17	18	19	20	21	22
Sample	Peak friction angles (degrees)												Differences between the values of peak friction angles given in different columns (degrees)								
	ϕ_c	ϕ_{pl}	ϕ_{ph}	ϕ_{pa}	ϕ_{tl}	ϕ_{th}	ϕ_{ta}	ϕ_{sl}	ϕ_{sh}	ϕ_{sa}	ϕ_{sc}	ϕ_{sp}	(2) - (9)	(3) - (9)	(6) – (9)	(4) – (10)	(7) – (10)	(5) – (11)	(8) – (11)	(2) – (3)	(12) – 13)
A	53.2	50.5	45.9	46.7	49.9	45.4	46.4	45.5	41.8	42.1	…	…	7.7	5.0	4.4	4.1	3.6	4.6	4.3	2.7	...
B	47.8	46.1	41.9	42.8	44.6	41.7	42.0	42.7	40.1	40.4	42.3	40.5	5.1	3.4	1.9	1.8	1.6	2.4	1.6	1.7	1.8
C	46.5	44.2	41.2	41.9	43.5	41.1	41.6	41.1	39.2	39.4	44.3	41.7	5.4	3.1	2.4	2.0	1.9	2.5	2.2	2.3	2.6
D	45.2	44.2	39.7	40.1	43.0	40.9	41.1	38.6	36.6	36.8	40.2	39.0	6.6	5.6	4.4	3.1	4.3	3.3	4.3	1.0	1.2
E	49.5	47.2	42.7	43.0	47.6	43.0	43.4	40.5	37.6	37.8	43.5	40.6	9.0	6.7	7.1	5.1	5.4	5.2	5.6	2.3	2.9
F	48.0	46.0	42.3	42.6	46.9	42.9	43.2	40.5	38.3	38.5	42.0	39.9	7.5	5.5	6.4	4.0	4.6	4.1	4.7	2.0	2.1

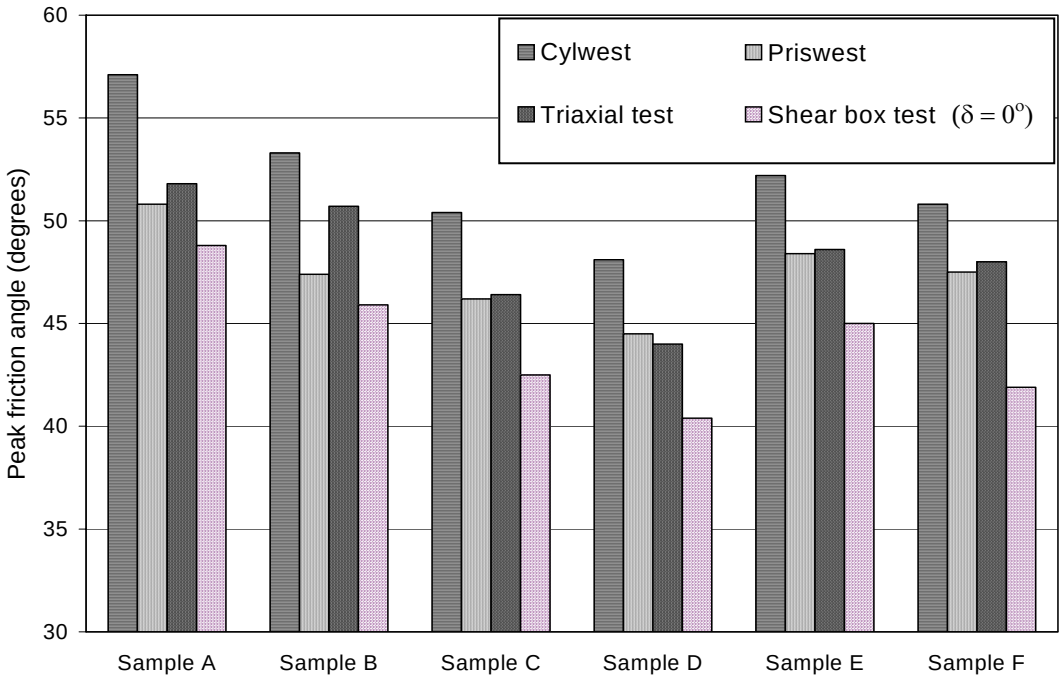

Figure 8.11. Comparison of the peak friction angles measured in single shear tests on previously untested specimens for samples A to F at the lower density under the lower σ range

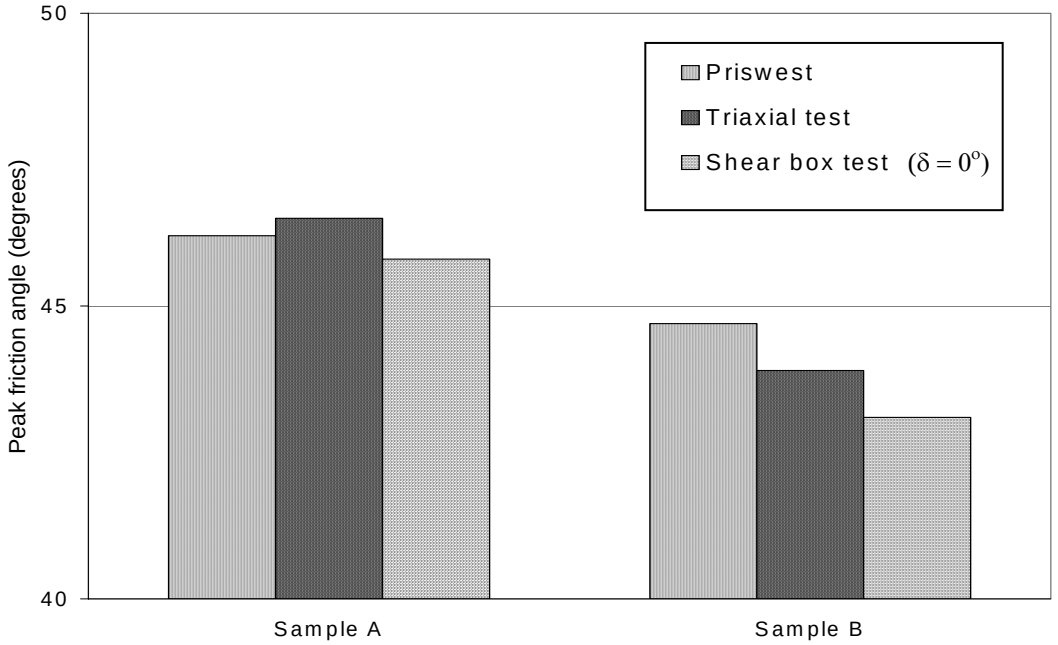

Figure 8.12. Comparison of the peak friction angles measured in single shear tests on previously untested specimens for samples A and B at the lower density under the higher σ range

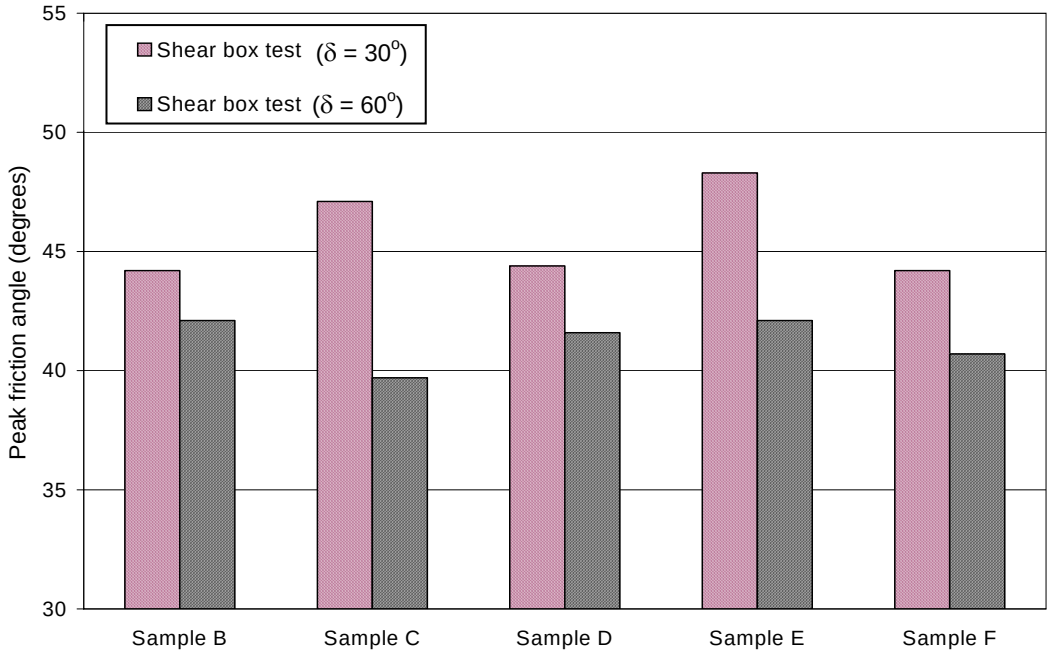

Figure 8.13. Comparison of the peak friction angles measured in single shear tests on specimens previously sheared more than once for samples B to F at the lower density under the lower σ range

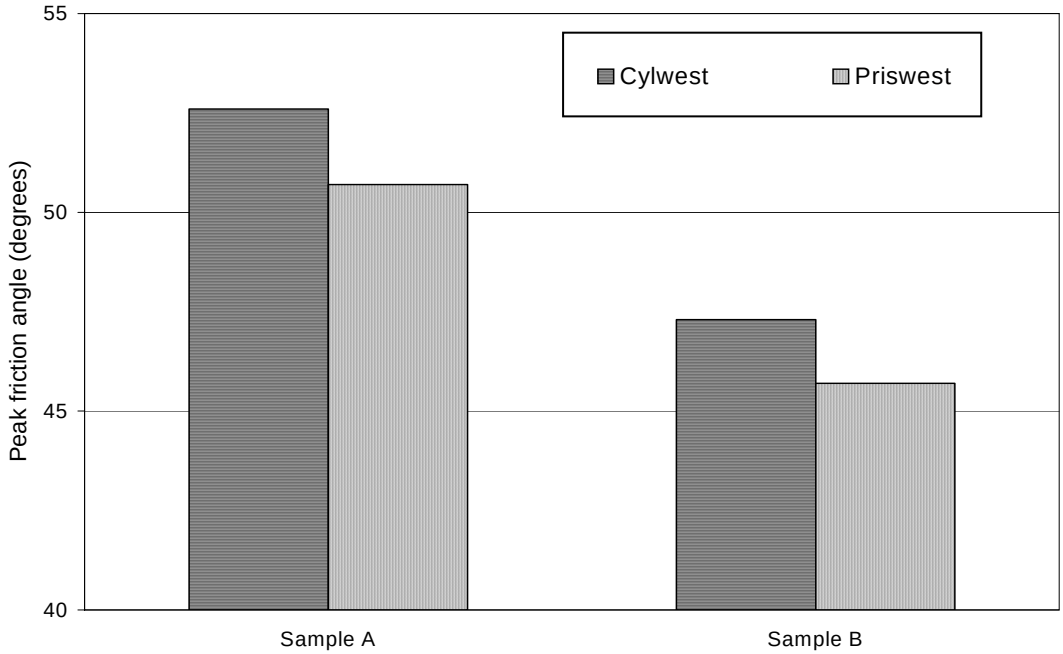

Figure 8.14. Comparison of the peak friction angles measured in single wedge shear tests on specimens used once in previous shear tests for samples A and B at the lower density under the lower σ range

Table 8.8. Test numbers and normal stresses of single shear tests used for the comparisons in Figs. 8.11 and 8.12

1	2	3	4	5	6	7	8	9	10
Figure no.	Sample	Cylwest		Priswest		Triaxial test		Shear box test ($\delta = 0^o$)	
		Test no.*	σ (kPa)	Test no.#	σ (kPa)	Test no.$	σ (kPa)	Test no.≠	σ (kPa)
8.11	A	CA/3	47.1	PA1/1	76.5	TA/1	46.2	SA/1	47.7
	B	CB/1	23.0	PB1/1	63.7	TB/1	28.7	SB/1	19.6
	C	CC/1	19.6	PC1/1	60.7	TC/1	20.6	SC/1	19.6
	D	CD/3	17.2	PD1/1	29.5	TD/1	30.5	SD/1	17.1
	E	CE/1	24.6	PE1/1	33.5	TE/1	31.4	SE/1	23.5
	F	CF/3	21.1	PF1/1	32.4	TF/1	28.8	SF/1	19.9
8.12	A	...	...	PA2/1	202.1	TA/5	179.1	SA/4	198.9
	B	...	...	PB2/1	161.6	TB/5	136.1	SB/4	162.1

* Tables 5.5 and 5.6; # Tables 5.15 to 5.17; $ Tables 6.2 to 6.7; ≠ Tables 7.1 and 7.2

Table 8.9. Test numbers and normal stresses of single shear tests used for the comparisons in Figs. 8.13 and 8.14

1	2	3	4	5	6	7	8	9	10
Figure no.	Sample	Shear box test ($\delta = 60^o$)		Shear box test ($\delta = 30^o$)		Cylwest		Priswest	
		Test no.*	σ (kPa)	Test no.#	σ (kPa)	Test no.$	σ (kPa)	Test no.≠	σ (kPa)
8.13	B	SBC/1	18.5	SBP/1	18.5	...	...	...	...
	C	SCC/1	18.5	SCP/1	18.5	...	...	...	...
	D	SDC/1	17.1	SDP/1	17.1	...	...	...	...
	E	SEC/1	22.0	SEP/1	22.0	...	...	...	...
	F	SFC/1	20.1	SFP/1	20.1	...	...	...	...
8.14	A	...	...	...	...	CA/2	110.9	PA1/2	135.1
	B	...	...	...	...	CB/4	76.2	PB1/2	99.4

* Table 7.3; # Table 7.4; $ Table 5.5; ≠ Table 5.15

2. The bar charts in Fig. 8.11 show that cylwests ($\delta = 60^o$) yield higher values of ϕ_d (by between 7.2^o and 8.9^o, average difference 7.9^o) than shear box tests ($\delta = 0^o$). A similar tendency is also observed in the results of test series under the lower σ ranges (Table 8.7, column 14), and probably results from the higher values of δ in the cylwests.

3. The bar charts in Fig. 8.11 show that priswests ($\delta = 30^o$) yield higher values of ϕ_d than shear box tests ($\delta = 0^o$) for samples A to F at the lower density under the lower σ range. Differences in the ϕ_d values are found as 2.0^o, 1.5^o, and 3.7^o for samples A to C; and as 4.1^o, 3.4^o, and 5.6^o for samples D to F respectively. Lower differences in the ϕ_d values for samples A to C are probably due to the distinctly higher differences in the normal stresses in the corresponding priswests than in the shear box tests with $\delta = 0^o$ (Table 8.8, columns 6 and 10). The bar charts in Fig. 8.12 show that the ϕ_d value measured in priswests are higher than those in shear box tests ($\delta = 0^o$) by 0.4^o and 1.6^o for samples A and B respectively. Higher ϕ_d values measured in priswests than in shear box tests is also seen from the results of the test series under the lower, higher, and combined σ ranges (Table 8.7, columns 15, 17, and 19), and probably results from the higher values of δ in the priswests.

4. The bar charts in Figs. 8.11 show that triaxial tests ($\delta \cong 65^o$) yield higher values of ϕ_d (by between 3.0^o and 6.1^o, average difference 4.2^o) than shear box tests ($\delta = 0^o$) for samples A to F at the lower density under the lower σ range. The bar charts in Fig. 8.12 show that the ϕ_d value measured in triaxial tests are higher than those in shear box tests ($\delta = 0^o$) by 0.7^o and 0.8^o for samples A and B respectively. Higher ϕ_d values measured in triaxial tests than in shear box tests is also seen from the results of the test series under the lower, higher, and combined σ ranges (Table 8.7, columns 16, 18, and 20), and probably results from the higher values of δ in the triaxial tests.

5. The bar charts in Fig. 8.13 show that shear box tests with $\delta = 60^o$ yield higher ϕ_d values (by between 2.1^o and 7.4^o, average difference 4.4^o) than shear box tests with $\delta = 30^o$ for samples B to F under the lower σ range. A similar tendency is observed in the results obtained from shear box test series with $\delta = 60^o$ and $\delta = 30^o$ under the lower σ ranges (Table 8.7, column 22). The difference in the ϕ_d values with change in δ is similar to that observed in cylwests ($\delta = 60^o$) and priswests ($\delta = 30^o$) under the lower σ range (Fig. 8.14): cylwests yield higher ϕ_d values than priswests by 1.9^o and 2.1^o for samples A and B respectively. These results, as well as those in Table 8.7, columns 21 and 22, are verifications of the earlier argument that cylwests yield higher ϕ_d values than priswests due to the larger δ in the cylwests (section 8.1.1, paragraph (4)).

6. The value of the peak friction angle ϕ_d measured in single cylwests on previously untested specimens for samples A and B were 57.1^o and 53.3^o respectively (Fig. 8.11). When these sheared specimen were tested a second time (Fig. 8.14), the ϕ_d values decreased to 52.6^o and 47.8^o, indicating differences of 4.5^o and 5.5^o. Such results raised the question of whether the reason for cylwests yielding higher ϕ_d values than shear box tests ($\delta = 60^o$) (Table 8.7, columns 2 and 12) could be the use of specimens previously sheared more than once in the shear box tests. So an additional cylwest (Table 8.10), at the lower density under the lower σ range, was performed on each of the samples B to F using specimens prepared from the same batch of the samples as those from which the shear box ($\delta = 60^o$) specimens had been prepared. The normal stress σ in these tests (Table 8.10, column 4) were close to those in the second tests of shear box test series SBC to SFC (Table 7.3); so the results of these second tests were used for the bar chart comparisons in Fig. 8.15. Fig. 8.15 shows that the ϕ_d values measured in cylwests and shear box tests are nearly the same for samples C and E; cylwests yield lower ϕ_d values than shear box tests by 1.7^o, 1.1^o and 3.1^o for samples B, D, and F respectively. It is seen that the average difference between the cylwest and shear box test results has decreased from 5^o

(Table 8.7, column 2 and 12) to -1.0^{o} (Fig. 8.15) when the specimens were taken from the same batch of each sample.

Table 8.10. The results of additional five cylwests on specimens previously sheared more than once for samples B to F

1	2	3	4	5	6	7	8	9
Sample	e	D_r	Peak strength			Ultimate strength		
			σ	τ	ϕ	σ	τ	ϕ
		(%)	(kPa)	(kPa)	(deg)	(kPa)	(kPa)	(deg)
B	0.639	61.3	35.2	31.9	42.2	44.4	25.8	30.2
C	0.575	20.4	39.6	39.3	44.8	42.0	26.4	32.2
D	0.679	57.0	31.6	25.8	39.2	37.2	22.6	31.3
E	0.638	70.1	38.9	38.3	44.5	44.5	28.8	32.9
F	0.647	60.6	38.4	37.4	44.3	42.6	27.1	32.4

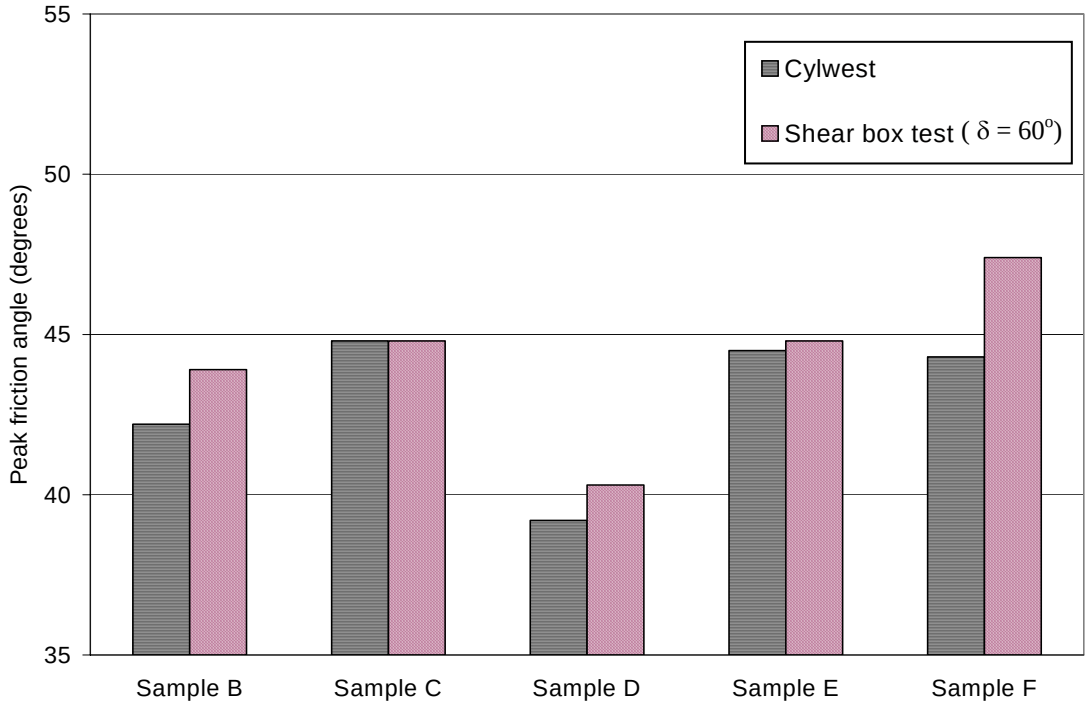

Figure 8.15. Comparison of the peak friction angles measured in single shear tests on specimens previously sheared more than once for samples B to F at the lower density under the lower σ range

8.1.3 Possible Effect of Particle Crushing on Measured Relative Density and Shear Strength

The relative density D_r values given in Tables 5.5 to 5.7 for cylwest; 5.15 to 5.19 for priswests; 6.2 to 6.10 for triaxial tests; 7.1 to 7.4 for shear box test; and 8.10 for the additional cylwests were calculated on the basis of the dry density ρ_d of the specimens, and the e_{max} and e_{min} values determined by using ρ_{max} and ρ_{min} as in section 4.3. When a specimen, which has crushed to some extent in a previous shear test (or tests), is re-tested, a lower compactive effort is sufficient to produce the ρ_d value obtained for previously untested specimens because of the finer particles filling the spaces between the coarser ones. Also the e_{max} and e_{min} values obtained for previously untested specimens are not valid for previously sheared specimens. So the true D_r values of previously sheared specimens are probably lower than given in the tables listed above, and this may be part of the reason for the significant drop in ϕ_d values in tests on such specimens on being re-sheared.

8.2 Comparison of the Results of the Shear Tests with Existing Empirical Relationships

The relationships obtained from equation (2.13), given by Schanz & Vermeer (1996), and equation (2.8), given by Wroth (1984), for samples A to F at the lower density and for samples D to F at the higher density are shown in Figs. 8.16 and 8.17, respectively. Equation (2.13) is represented as full lines, starting with the corresponding ϕ_{cv}, taken as the average of the ultimate friction angles measured in the wedge shear tests (Table 8.5, columns 2 and 5); equation (2.8) is represented by dashed lines. The peak friction angles measured in wedge shear tests (assumed to be plane strain tests) have been plotted in Figs. 8.16 and 8.17 against the corresponding values measured in triaxial tests. To eliminate the effect of crushing in previous shear tests, peak friction angles ϕ_{cu}, ϕ_{pu}, and ϕ_{tu} measured in single cylwest, priswest, and triaxial tests respectively in which previously untested specimens had been used are also compared in these figures.

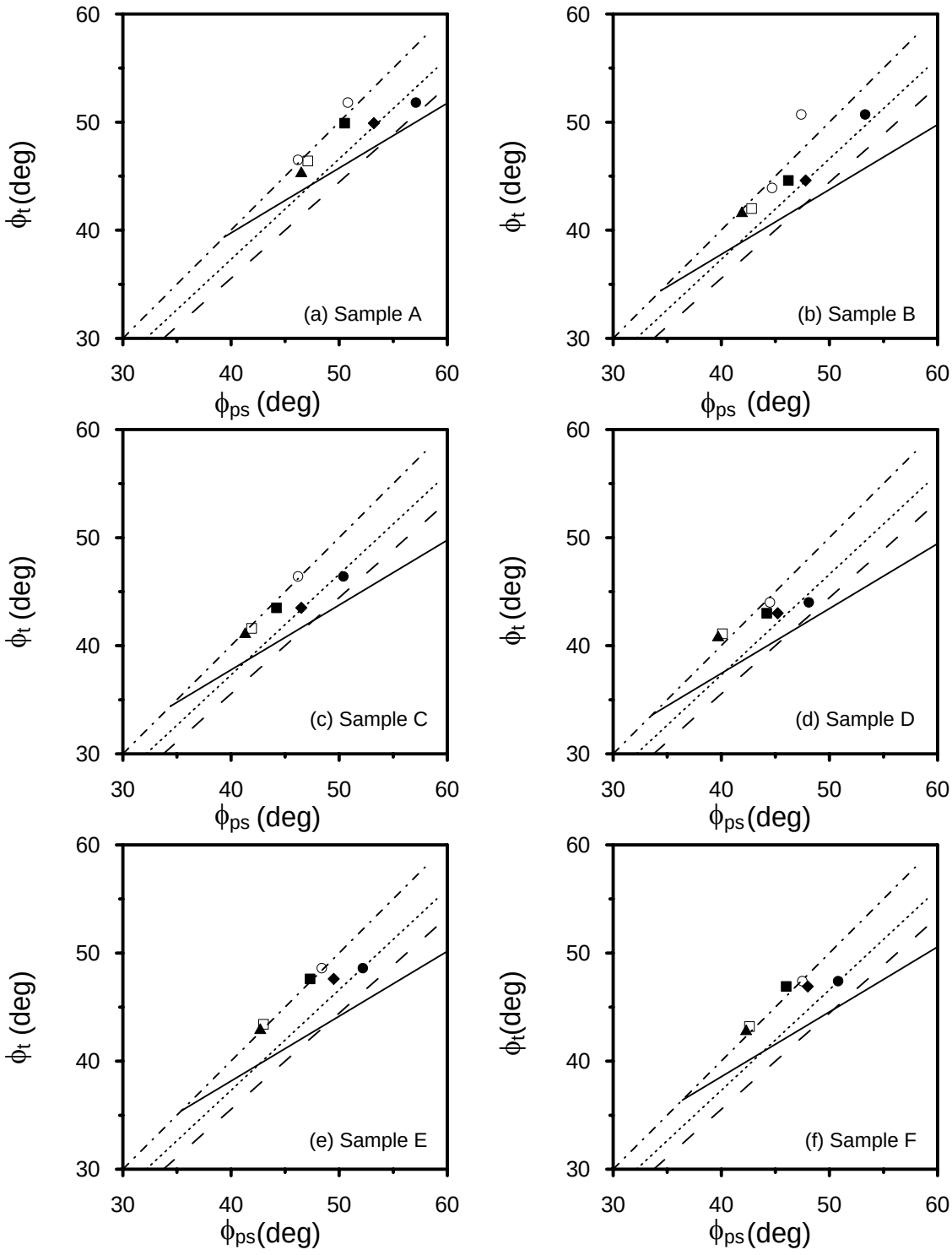

See Fig. 8.17 for legend

Figure 8.16. Comparison of relationships between peak friction angles in wedge shear and triaxial shear tests for samples A to F at the lower density

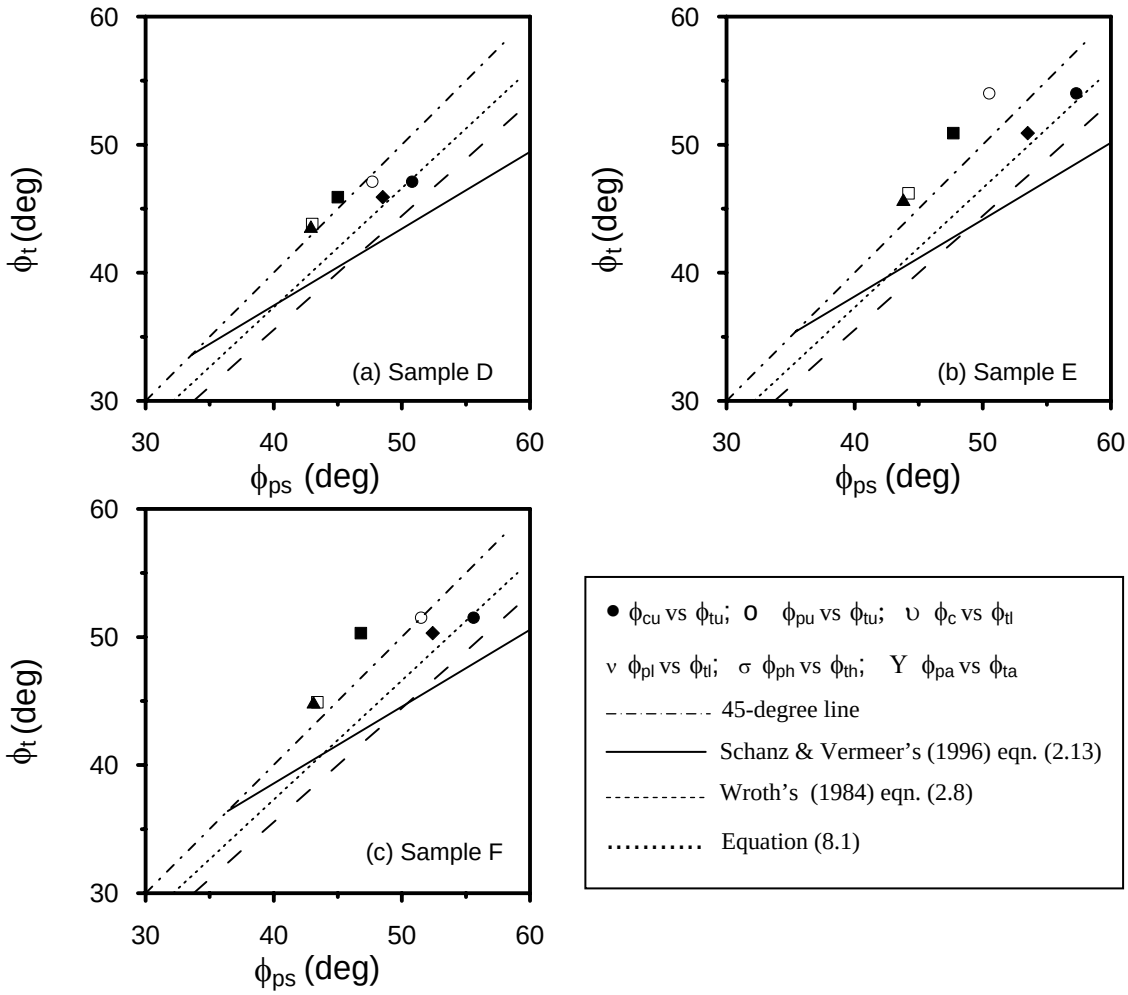

Figure 8.17. Comparison of relationships between peak friction angles in wedge shear and triaxial shear tests for samples D to F at the higher density

From Figs. 8.16 and 8.17, it can be seen that the plotted points representing cylwest versus triaxial test results, especially on untested specimens, (except for sample B at the lower density (Fig. 8.16(b)) and sample E at the higher density (Fig. 8.17(b)), all lie above but are quite close to both of the representations of equations (2.8) and (2.13). This tendency is in good agreement with Mirata and Gökalp's (1997) findings (section 2.1.4, paragraph (18)), and is a verification of the earlier argument that the wedge shear test is similar although not identical with the conventional plane strain test (section 2.4), when the orientation of the shear plane to the bedding plane is about the same.

To correlate the cylwest results with those of the triaxial test, linear regression forced through the origin was carried out between the values ϕ_{cu} and ϕ_{tu} for samples A to F at the lower density and for samples D to F at the higher density. This gave the following result with a coefficient of correlation r of 0.9999.

$$\phi_{cu} = 1.08\ \phi_{tu} \quad \text{..... (8.1)}$$

Equation (8.1) is represented by the dotted lines in Figs. 8.16 and 8.17. It is interesting to note that the plotted points of ϕ_c versus ϕ_{tl} obtained from the test series also fall fairly close to the correlation given by equation (8.1). The coefficient 1.08 in equation (8.1) may be compared with the corresponding value of 1.13 in Wroth's (1984) equation (2.8), indicating less difference between cylwests and triaxial tests than between actual plane strain tests and triaxial tests.

The plotted points representing priswest versus triaxial test results are close to the 45-degree line, indicating that the results of the two types of test are in close agreement. As mentioned in section 8.1.1, paragraph (5), this is probably due to the lower δ in priswests than in triaxial tests. A similar tendency has been observed in the results of the tests performed on gravel and rockfill by Tosun et al. (1999).

8.3 Comparison of the Results of the Shear Tests with the Strength Limits Calculated by Using Stress - Dilatancy Equation

8.3.1 Wedge Shear and Triaxial Tests

According to the values of ϕ_{cv} measured in wedge shear tests (Table 8.5, columns 2 and 5), samples A to F were separated into three groups. Each group with its ϕ_{cv} and ϕ_{μ} value, obtained by using the relation between ϕ_{μ} and ϕ_{cv} (Fig. 2.1) given by Rowe (1969), is given below:

(a) Group 1 (Sample A) ($\phi_{cv} = 39.4^o$; $\phi_{\mu} = 33^o$)

(b) Group 2 (Samples B, C, E, and F) ($\phi_{cv} = 35.2^o$; $\phi_{\mu} = 28^o$)

(c) Group 3 (Sample D) ($\phi_{cv} = 33.6^o$; $\phi_{\mu} = 26^o$)

Following Rowe (1969) (section 2.1.1), it was assumed that *D* (equation (2.2)) varies approximately between 1 and 2 as the material passes from the loosest to the densest state in both triaxial tests and wedge shear tests (assumed to be plane strain tests). By substituting these *D* values in equation (2.1) together with the limiting values of ϕ_f (given in section 2.1.1), the limiting values of peak friction angle ϕ_d were calculated from the corresponding values of *R* (defined in section 2.1.1, and explained in Appendix A) for each group, both for the plane strain and the triaxial tests. The limiting values for the plane strain tests were connected by a full line, and those for the triaxial tests were connected by a dashed line, as shown in Figs. 8.18 to 8.22. The peak friction angle of each sample in each group measured in wedge shear and tiaxial test series under the lower, higher, and combined σ ranges was also plotted against the average initial relative density D_r in Figs. 8.18 to 8.20. The symbols in the legends used in Figs. 8.18 to 8.20 have been defined in section 8.1.1, paragraph (1), where it was also explained that the cylwest, priswest, and triaxial test results are affected by different degrees of previous particle crushing in specimens used for some of the tests. To compare the results of tests performed on identical specimens, peak friction angles measured in single shear tests on previously untested specimens were plotted against D_r values in Figs. 8.21 and 8.22. The symbols in the legends used in Figs. 8.21 and 8.22 have been defined in section 8.2.

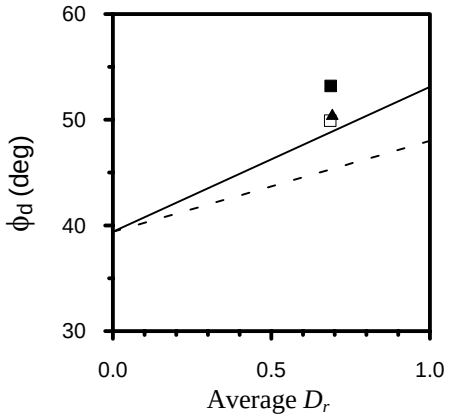

(a) Group 1

(ϕ_{cv} = 39.4°; ϕ_{μ} = 33°)

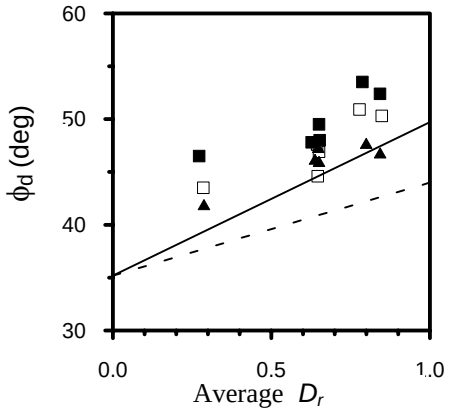

(b) Group 2

(ϕ_{cv} = 35.2°; ϕ_{μ} = 28°)

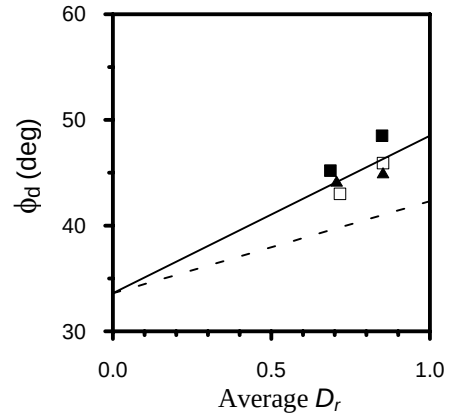

(c) Group 3

(ϕ_{cv} = 33.6°; ϕ_{μ} = 26°)

ν ϕ_c versus average D_r

σ ϕ_{pl} versus average D_r

Y ϕ_{tl} versus average D_r

plane strain

triaxial

Figure 8.18. Comparison of the ϕ_d values measured in wedge shear and triaxial test series under the lower σ ranges with the limiting ϕ_d values calculated for different sample groups

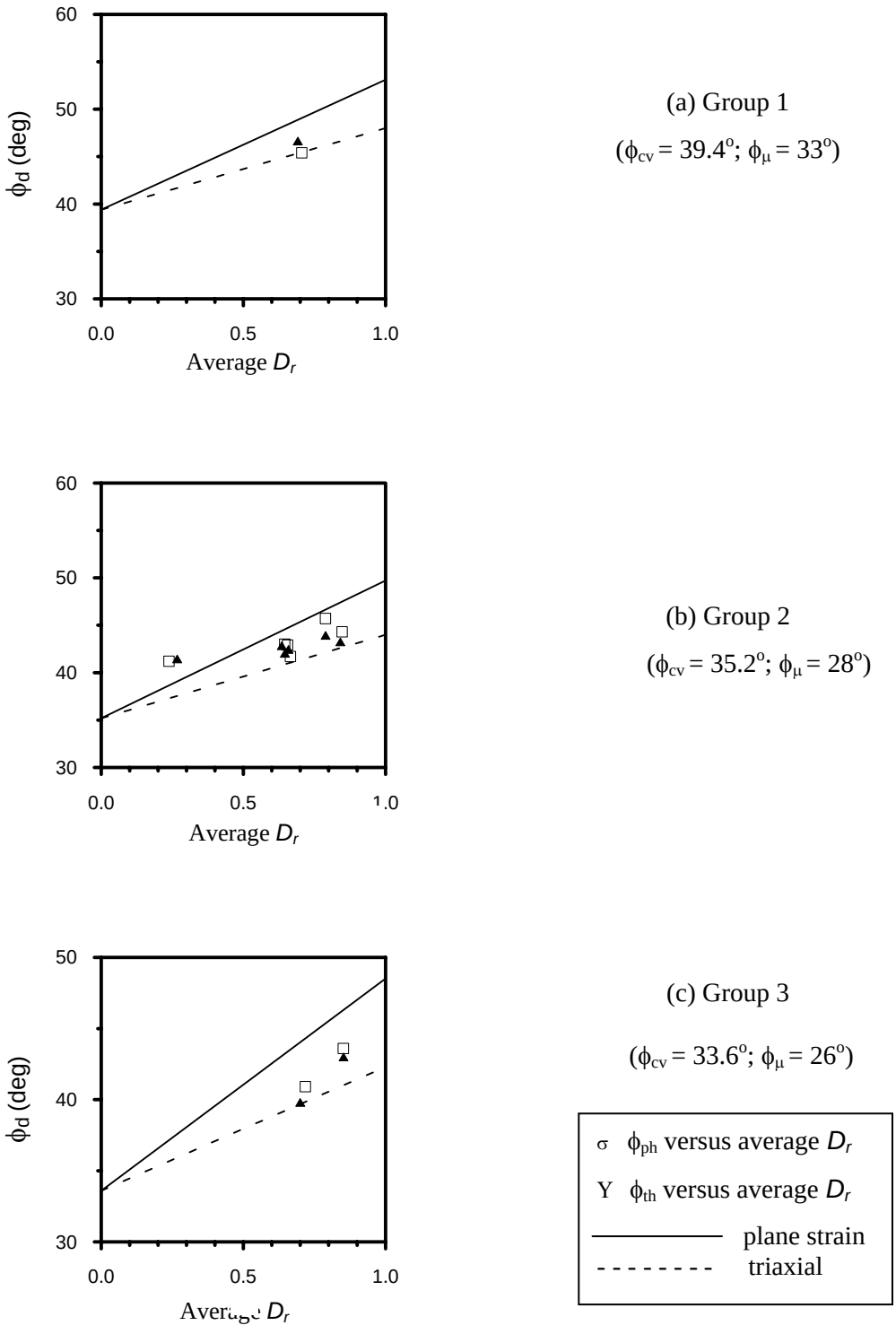

Figure 8.19. Comparison of the ϕ_d values measured in priswest and triaxial test series under the higher σ ranges with the limiting ϕ_d values calculated for different sample groups

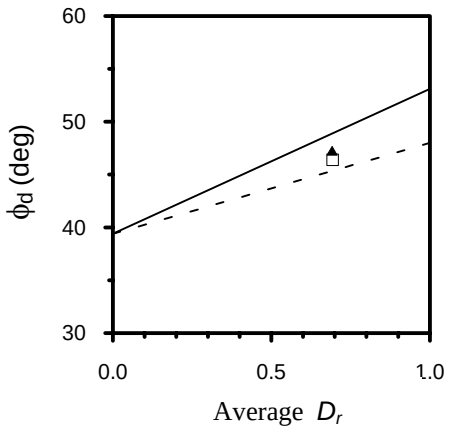

(a) Group 1

(ϕ_{cv} = 39.4°; ϕ_{μ} = 33°)

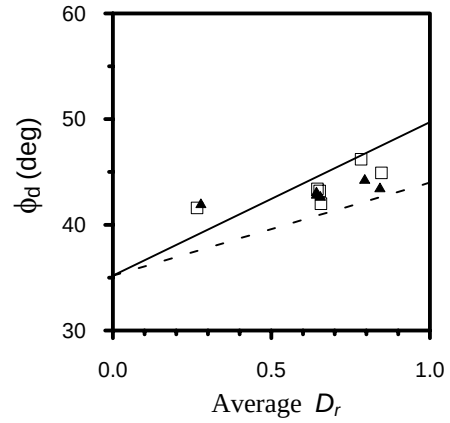

(b) Group 2

(ϕ_{cv} = 35.2°; ϕ_{μ} = 28°)

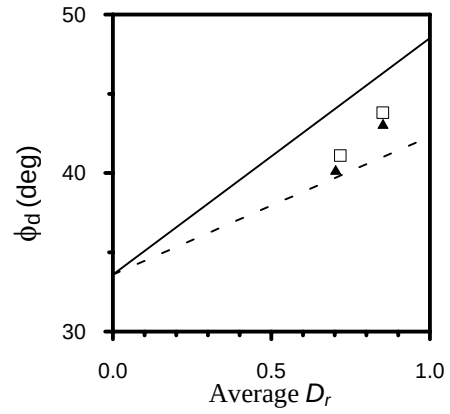

(c) Group 3

(ϕ_{cv} = 33.6°; ϕ_{μ} = 26°)

σ ϕ_{pa} versus average D_r

Y ϕ_{ta} versus average D_r

——— plane strain

- - - - - - - - triaxial

Figure 8.20. Comparison of the ϕ_d values measured in priswest and triaxial test series under the combined σ ranges with the limiting ϕ_d values calculated for different sample groups

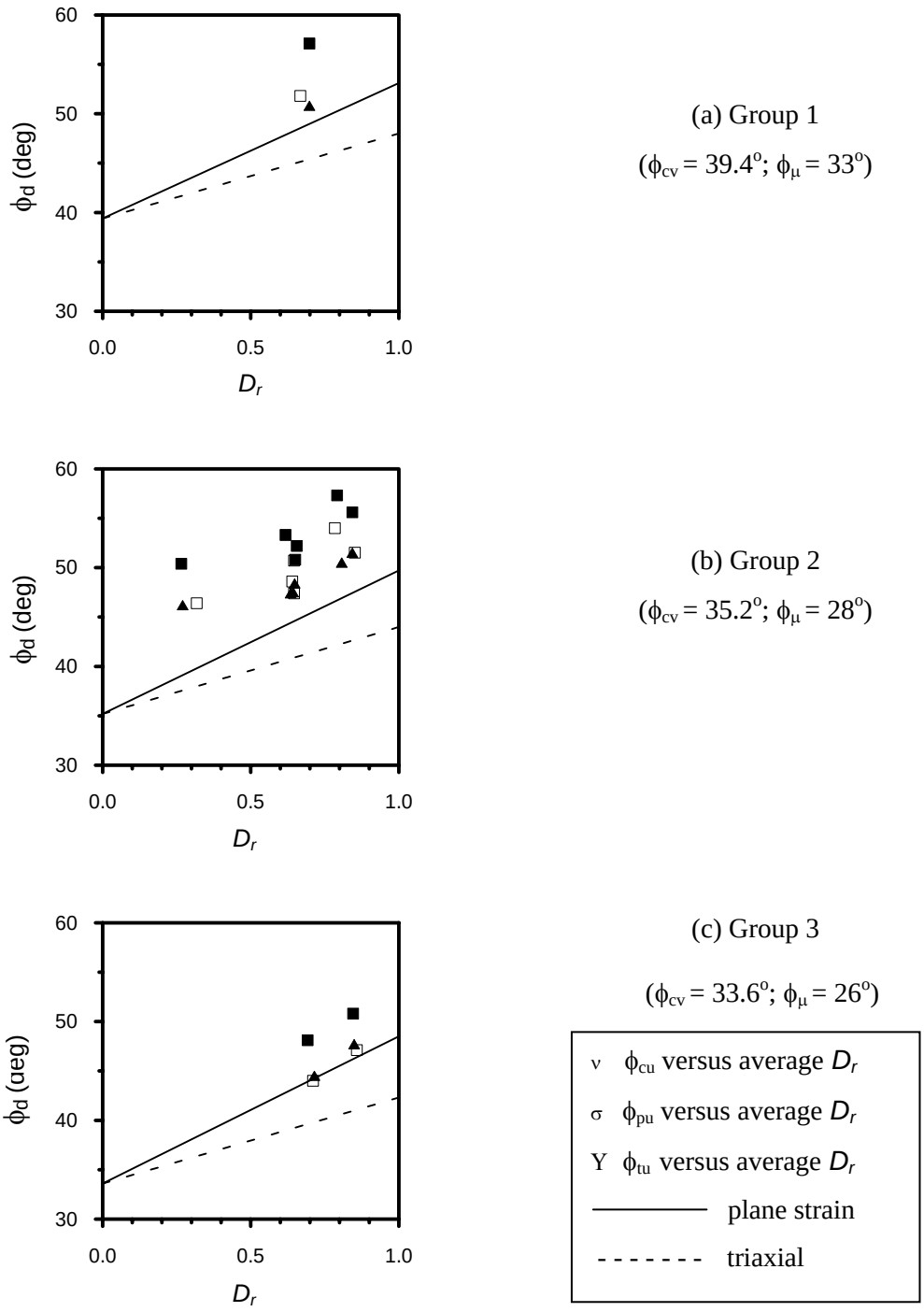

Figure 8.21. Comparison of the ϕ_d values measured in single shear tests on previously untested specimens under the lower σ range with the limiting ϕ_d values calculated for different sample groups

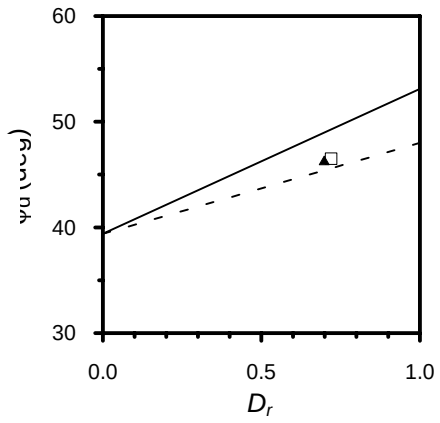

(a) Group 1

($\phi_{cv} = 39.4^o$; $\phi_{\mu} = 33^o$)

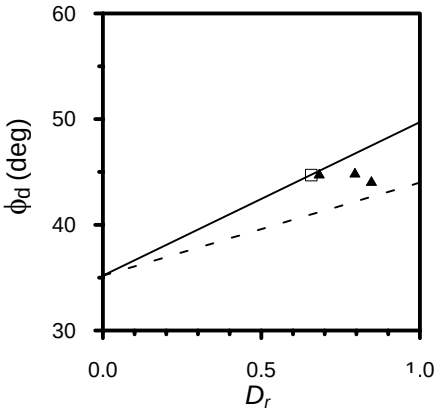

(b) Group 2

($\phi_{cv} = 35.2^o$; $\phi_{\mu} = 28^o$)

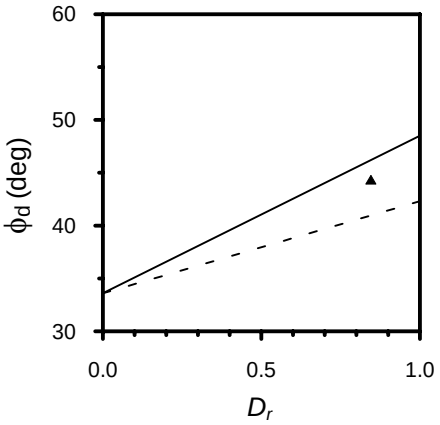

(c) Group 3

($\phi_{cv} = 33.6^o$; $\phi_{\mu} = 26^o$)

σ ϕ_{pu} versus average D_r

Y ϕ_{tu} versus average D_r

plane strain

triaxial

Figure 8.22. Comparison of the ϕ_d values measured in single shear tests on previously untested specimens under the higher σ range with the limiting ϕ_d values calculated for different sample groups

For the cylwests, Fig. 8.21 shows that the plotted points representing ϕ_{cu} versus D_r for each group are located well above the full line for the plane strain test. A similar tendency is also observed in the plotted points representing ϕ_c versus average D_r in cylwest series (Fig. 8.18), except those for group 3 in Fig. 8.18(c). These results show that cylwests generally yield higher values of ϕ_d than those calculated by using stress - dilatancy equation.

For the triaxial tests, Fig. 8.21 also shows that under the lower σ range, the plotted points representing ϕ_{tu} versus D_r for each group are well above the dashed line for the triaxial test. A similar tendency is also observed in the plotted points representing ϕ_{tl} versus average D_r in triaxial test series under the lower σ range (Fig. 8.18). Fig. 8.22 shows that the plotted point representing ϕ_{tu} versus D_r for group 1 is close to the dashed line for the triaxial test; that for group 2 is located well above this line. In triaxial test series under the higher σ ranges (Fig. 8.19), three of the ϕ_{th} values are located well above the dashed line for the triaxial test; the remaining six ϕ_{th} values are close to this line. A similar tendency is observed in triaxial test series under the combined σ ranges (Fig. 8.20).

For the priswests, Fig. 8.21 shows that under the lower σ range, the plotted points representing ϕ_{pu} versus D_r for groups 1 and 3 are close to the full line for the plane strain test; those for group 2 are located well above this line. Under the higher σ range (Fig. 8.22), two of the ϕ_{pu} values are located below the line for the plane strain test; in the remaining three, the ϕ_{pu} value is close to this line. In priswest series under the lower σ ranges (Fig. 8.18), the plotted points representing ϕ_{pl} versus average D_r for each group are close to the full line for the plane strain test. In priswest series under the higher σ ranges (Fig. 8.19), three of the ϕ_{ph} values are located well below the full line for the plane strain test; the remaining six ϕ_{ph} values are close to this line. A similar tendency is observed in priswest series under the combined σ ranges (Fig. 8.20).

8.3.2 Shear Box Tests

Following Rowe (1969) (section 2.1.1), the limiting values of ϕ_d in plane strain tests, calculated in section 8.3.1 for each group, together with the ϕ_{cv} values of each group, were substituted in equation (2.5), correlating ϕ_d values obtained from plane strain and shear box test results, and the limiting values of ϕ_d in shear box tests were calculated for each group. These limiting values were connected by straight lines, as shown in Fig. 8.23. On this figure, peak friction angle of each sample in each group measured in shear box test series performed on previously untested specimens, compacted directly in the shear box, under the lower, higher, and combined σ ranges is also plotted against average D_r. The symbols in the legends used in Fig. 8.23 have been defined in section 8.1.2, paragraph (1).

Figure 8.23 shows that out of the 18 plotted points, in only five is the ϕ_d value measured in shear box tests located well above the straight line connecting the limiting values of ϕ_d; in all the rest, the ϕ_d value measured in shear box tests are close to this line.

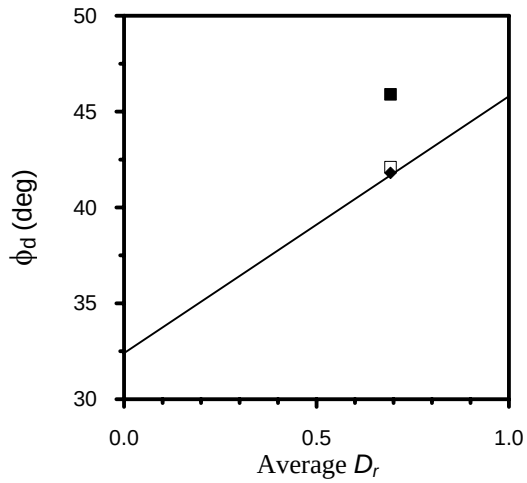

(a) Group 1

(ϕ_{cv} = 39.4°; ϕ_μ = 33°)

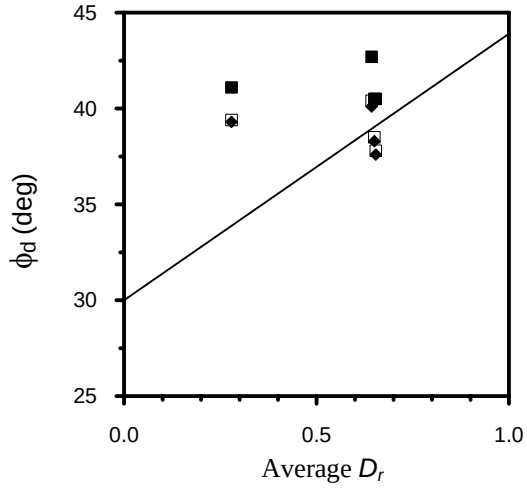

(b) Group 2

(ϕ_{cv} = 35.2°; ϕ_μ = 28°)

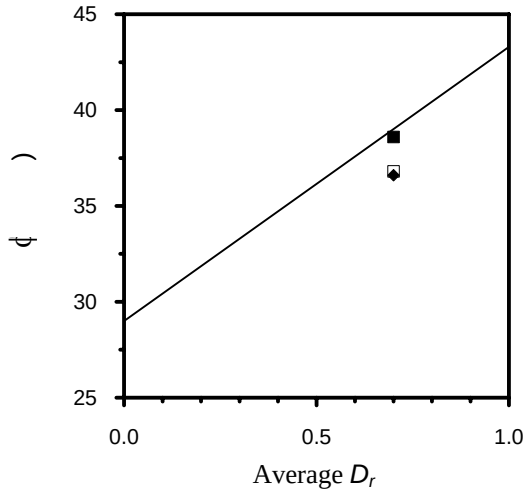

(c) Group 3

(ϕ_{cv} = 33.6°; ϕ_μ = 26°)

ν ϕ_{sl} versus average D_r

υ ϕ_{sh} versus average D_r

Y ϕ_{sh} versus average D_r

Figure 8.23. Comparison of the ϕ_d values measured in shear box tests with the limiting ϕ_d values calculated for different sample groups

CHAPTER 9

CONCLUSIONS AND RECOMMENDATIONS

Particle crushing has occurred in all shear tests even under low normal stresses. In the samples tested, it was verified that particle shape was not the only factor influencing the crushing of particles; other important factors were the strength of the particles, and the gradation.

Cylwests yielded higher shear strength than priswests under the lower normal stress σ range (between 17 kPa and 59 kPa). This is probably due to the difference in the inclination δ of the shear plane to the bedding planes: δ is 60^o in cylwests, while in priswests using the 30^o mould δ is 30^o.

Cylwests yielded higher shear strength than triaxial tests under the lower σ range, and there was some indication that this difference in strength was linked with the ϕ_{cv} values of the samples, as observed by past researchers. The results of the cylwests and triaxial tests, especially on untested specimens, were quite close to the existing correlations between ϕ_{ps} obtained from actual plane strain tests and ϕ_t from triaxial tests. This indicated that the wedge shear test is similar although not identical with the conventional plane strain test, when the orientation of the shear plane to the bedding planes is about the same. Correlating the results on previously untested specimens, the ϕ_{cu} from cylwests were found to be 1.08 times the ϕ_{tu} from triaxial tests; the corresponding ratio between actual plane strain test and triaxial test results given by Wroth's (1994) equation (2.8) is 1.13.

The results of priswests and triaxial tests under the same σ ranges are in close agreement; this is probably due to the lower δ in priswests than in triaxial tests. This may also explain the close agreement between priswests and triaxial tests on < 40 mm gravel and crushed rock reported by Tosun et al. (1999).

Shear box tests ($\delta = 0^o$) performed on specimens compacted directly in the shear box yielded lower shear strength than both wedge shear and triaxial shear tests under the same σ ranges. It was shown that the shear strength measured in shear box showed an increase when δ was increased from 30^o to 60^o; this increase was of the order of the difference between priswest ($\delta = 30^o$) and cylwest ($\delta = 60^o$) results mentioned earlier. Shear box specimens with $\delta = 60^o$, prepared from the same batch of any sample as the corresponding cylwests, yielded nearly the same strength as that obtained in cylwests ($\delta = 60^o$).

When the triaxial shear tests could be sufficiently prolonged to yield the ultimate strength, the ϕ_{cv} values measured in the wedge shear test and the triaxial test were nearly the same.

Following Rowe (1969), the results of the wedge shear, triaxial, and shear box tests were compared with the strength limits calculated by using the stress – dilatancy equation for plane strain, triaxial, and shear box tests. Compared to the calculated values, under the lower σ ranges, cylwests generally yielded higher shear strength; under the lower σ ranges, priswests generally yielded nearly the same shear strength, triaxial tests yielded higher shear strength; under the higher and combined σ ranges, priswests yielded lower shear strength, triaxial tests yielded nearly the same shear strength. The shear strength measured in shear box tests was generally close to the calculated values.

As an overall conclusion, it can be said that for the analysis of a plane strain type of problem like the stability of slopes in sand, the cylwest or the priswest may be used depending on in which test the inclination of the shear plane to the bedding planes is closer to the average inclination in the actual stability problem. If the size of the particles permit, the shear box test may be used, provided specimens are prepared with the correct inclination of the shear plane to the bedding planes. Triaxial tests would give a conservative factor of safety, and conventional shear box tests with horizontal bedding planes even more conservative values for such problems.

For future studies, the following recommendations can be made.

(a) Each shear test should be performed on an untested specimen to eliminate the effect of particle crushing.

(b) To determine the effect on shear strength of mineral composition, more detailed mineralogical analyses should be carried out, including the determination of individual percentages of each ingredient.

(c) The effect of δ on the peak friction angle measured in priswests may be investigated by modifying the test mould (Fig. 5.9(b)) so that the side of the mould on which the main load is applied becomes the removable lid.

(d) Slope failures in sand may be studied and back analyses performed to estimate the ϕ_d mobilized in the slips and compare these with the laboratory test results.

REFERENCES

Adel, H. (2001). Determination of Plane Strain Shear Strength of Sand from the Results of Triaxial Tests. Canadian Geotechnical Journal **38**, pp. 1231-1240.

Aybak, T. (1988). Improved Measurement of Shear Strength in the In Situ Wedge Shear Test. MS thesis, Middle East Technical University, Ankara.

Barden, L. & Khayatt, A.J. (1966). Incremental Strain Rate Ratios and Strength of sand in the Triaxial Test . Géotechnique **16**, No. 4, pp. 338 – 357.

Bardet, J. P. (1997). Experimental Soil Mechanics. Prentice Hall, New Jersey.

Bishop, A.W. (1966). The Strength and Soils as Engineering Materials. Géotechnique **16**, No. 2, pp. 91 – 130.

Bolton, M.D. (1986). The Strength and Dilatancy of Sands. Géotechnique **36**, No. 1, pp. 65 – 78.

Cornforth, D.K. (1964). Some Experiments on the Influence of Strain Conditions on the Strength of Sand. Géotechnique **14**, No. 2, pp. 143 – 167.

Cornforth, D.K. (1973). Prediction of Drained Strength of Sands from Relative Density Measurements. ASTM Special Technical Publication 523, pp. 281 – 303.

Çağnan, Ş. (1990). Measurement of Shear Strength of Coarse Gravels by the Wedge Shear Test. MS thesis, Middle East Technical University, Ankara.

Dobkins & Folk. (1970). Shape Development on Tahiti – Nui. Journal of Sedimentary Petrology **40**, pp. 1167 – 1203.

Girgin, İ. (2000). Results of Mineralogical Analyses. Unpublished work. Mineral Research and Exploration Directorate Laboratories, Ankara.

Gökalp, A. (1994). Investigation of Certain Problems related with the Wedge Shear Test. MS thesis, Middle East Technical University, Ankara.

Gün, F. (1997). Comparison of the Shear Strength of Statically and Dynamically Compacted Clays. MS thesis, Middle East Technical University, Ankara.

Gürol, A. (2000). Effect of Curing on the Undrained Shear Strength of Compacted Clays. MS thesis, Middle East Technical University, Ankara.

Hardin, B.O. (1985). Crushing of Soil Particles. Getechnical Testing Journal **14**, No. 3, pp. 296 – 308.

Holubec, I. & D'Appolonia, E. (1973). Effect of Particle Shape on the Engineering Properties of Granular Soils. ASTM Special Technical Publication 523, pp. 304 – 318.

Hussaini, M.M. (1973). Influence of Relative Density and Deformation of Sand under Plane Strain Conditions. ASTM Special Technical Publication 523, pp. 332 – 347.

Jewell, R. A. (1989). Direct Shear Tests on Sand. Géotechnique **39**, No.2, pp. 309 – 322.

Kezdi, A. (1974). Handbookof Soil Mechanics. Elsevier Scientific Publishing Company, New York.

Kirkpatrick, W.M. (1965). Effects of Grain Size and Grading on the Shear Behaviour of Granular Materials. Proceedings of 6th International Conference on Soil Mechanics and Foundation Engineering, Montreal **1**, pp. 273 –277.

Koerner, M.R. (1970). Effect of Particle Characteristics on Soil Strength. Journal of Soil Mechanics and Foundation Division, ASCE **96**, SM4, pp. 1221 –1234.

Lambe, W.T. & Whitman, R.V. (1979). Soil Mechanics. John Wiley, USA.

Lee, K.L. (1970). Comparison of Plane Strain and Triaxial Tests on Sand. Journal of Soil Mechanics and Foundation Division, ASCE **96**, SM3, pp. 901 –923.

Leussink, H. & Wittke, W. (1963). Difference in Triaxial and Plane Strain Shear Strength. ASTM Special Technical Publication. No.361, pp. 281 – 303.

Maeda, K. & Miura, K. (1999(a)). Relative Density Dependency of Mechanical Properties of Sands. Soils and Foundations **39**, No. 1, pp. 69 - 79.

Maeda, K. & Miura, K. (1999(b)). Confining Stress Dependency of Mechanical Properties of Sands. Soils and Foundations **39**, No. 1, pp. 53 - 67.

Marachi, N.D., Duncan, J.M., Chan, C.K., & Seed, H.B. (1981). Plane Strain Testing of Sand . ASTM Special Technical Publication. No. 740, pp. 294 -302

Marsal, R.J. (1967). Large Scale Testing of Rockfill Materials. Journal of Soil Mechanics and Foundation Division, ASCE **93**, SM2, pp. 27 –43.

Mirata, T. (1974). The In Situ Wedge Shear Test -- A New Technique in Soil Testing. Géotechnique **24**, No.3, pp. 311–332. Corrigenda: Géotechnique **24**, No.4, p. 698; **25**, No.1, pp. 157-158; **36**, No.1, p. 144; **37**, No.3, p. 420; **38**, No.1, p. 163.

Mirata, T. (1976). Short-term Stability of Slopes in Ankara Clay. PhD Thesis, University of London.

Mirata, T. (1991). Developments in Wedge Shear Testing of Unsaturated Clays and Gravels. Géotechnique **41**, No.1, pp. 79 – 100. Corrigenda: Géotechnique **41**, No.2, p. 296 and **41**, No.4, pp. 639.

Mirata, T. (1992). Author's Reply to Discussion on Developments in Wedge Shear Testing of Unsaturated Clays and Gravels. Géotechnique **42**, No.4, pp. 645-648.

Mirata, T. (2000). Test Procedure for the Triaxial Shear Test on Sand. Unpublished Work. Middle East Technical University, Ankara.

Mirata, T. (2001). Test Procedure for the Shear Box Test on Sand. Unpublished Work. Middle East Technical University, Ankara.

Mirata, T. (2002(a)). TRIAX02. A Computer Program for the Evaluation of Triaxial Tests. Middle East Technical University, Ankara.

Mirata, T. (2002(b)). DIST02. A Computer Program for the Evaluation of Shear Box Tests. Middle East Technical University, Ankara.

Mirata, T. (2002(c)). Examination of the Effect on Cylwest Results of the Use of the Double-cut Cylwest Mould with no Trimming. Unpublished Work. Middle East Technical University, Ankara.

Mirata, T. (2003(a)). Manual for Wedge Shear Testing of Soils. Department of Civil Engineering, Middle East Technical University, Ankara. (obtainable from ULAKBİM Library)

Mirata, T. (2003(b)). Comparison of the Wedge Shear Test with the Plane Strain Test. Unpublished Work. Middle East Technical University, Ankara.

Mirata, T. & Gökalp, A. (1997). Discussion. Géotechnique **47**, No.4, pp. 887 – 889.

Mitchell, J.K. (1976). Fundamentals of Soil Behaviour. Wiley & Sons. USA

Norman, T. (2000(a)). Personal Communication. Middle East Technical University, Ankara.

Norman, T. (2000(b)). Personal Communication. Middle East Technical University, Ankara.

Norman, T. (2000(c)). Sedimentary Petrography Class Notes. Unpublished Work. Middle East Technical University, Ankara.

Oda, M., Koishikawa, I., & Higuchi, T. (1978). Experimental Study of Anisotropic Shear Strength of Sand by Plane Strain Test. Soils and Foundations **18**, No. 1, pp. 25–37.

Riley, N.A. (1941) Projection Sphericity. Journal of Sedimentary Petrology **1**, pp. 94 – 97.

Rowe, P. W. (1962). The Stress- Dilatancy Relation for Static Equilibrium of an Assembly of Particles in Contact. Proc. R. Soc. A 269, pp. 500- 527.

Rowe, P. W. (1969). The Relation between the Shear Strength of Sands in Triaxial Compression, Plane Strain, and Direct Shear. Géotechnique **19**, No. 1, pp. 75 – 86.

Şakar, M. (1997). Wedge Shear Testing of Clayey Gravels under Higher Normal Stresses. MS thesis, Middle East Technical University, Ankara.

Schanz, T. & Vermeer, P.A. (1996). Angles of Friction and Dilatancy of Sand. Géotechnique **46**, No. 1, pp. 145 – 151.

Seed, H.B. & Lee, K.L. (1967). Drained Strength Characteristics of Sand. Journal of Soil Mechanics and Foundation Division, ASCE **93**, SM6, pp. 117 –141.

Shahu, J. T., & Yudhbir (1998). Model Tests on Sands with Different Angularity and Mineralogy. Soils and Foundations **38**, No. 4, pp. 151 –158.

Tatsuoka, F., Sakamato, M., Kawamura, T., & Fukushima, S. (1986). Strength and Deformation Characteristics of Sand in Plane Strain Compression at Extremely Low Pressures. Soils and Foundations **26**, No. 1, pp. 65 –84.

Timeshenko, S. & Goodier, J.N. (1970). Theory of Elasticity, McGraw Hill, New York

Tosun, H., Mirata, T., Mollamahmutoğlu, M., & Çolakoğlu, N.S. (1999). Shear Strength of Gravel and Rockfill Measured in Triaxial and Plane Strain Tests. Electronic Journal of Geotechnical Engineering: http://www.ejge.com/

Ueng, T. & Chen, T. (2000). Energy Aspects of Particle Breakage in Drained Shear of Sands. Géotechnique **50**, No. 1, pp. 65– 72.

Vesic, A.S. & Clough, G.W. (1968). Behavior of Granular Materials under High Stresses. Journal of Soil Mechanics and Foundation Division, ASCE **94**, SM3, pp. 661–687.

Wroth, C.P. (1984). The Interpretation of In Situ Soil Tests. Géotechnique **34**, No. 4, pp. 449 – 489.

Youd, T.L. (1973). Factors Controlling Maximum and Minimum Densities of Sands. ASTM Special Technical Publication 523, pp. 98 – 112.

Yudhbir & Rahim, A. (1991). Quantification of Particle Shape and Angularity Using the Image Analyzer. Getechnical Testing Journal **14**, No. 3, pp. 296 – 308.

_____ (1987). İnşaat Mühendisliği için Zemin Deneyleri, TS 1900 Türk Standardları Enstitüsü, Ankara.

_____ (1990). Soils for Civil Engineering Purposes; part 4, Compaction-related Tests. BS 1377 British Standards Institution.

APPENDIX A

CALCULATION OF PEAK FRICTION ANGLE ϕ_d FROM THE VALUES OF *R*

From Fig. A.1, $\sin\phi_d$ is

$$\sin\phi_d = \frac{\left(\frac{\sigma_1-\sigma_3}{2}\right)}{\left(\frac{\sigma_1+\sigma_3}{2}\right)} = \left(\frac{\sigma_1-\sigma_3}{\sigma_1+\sigma_3}\right) = \frac{\sigma_3\left(\frac{\sigma_1}{\sigma_3}-1\right)}{\sigma_3\left(\frac{\sigma_1}{\sigma_3}+1\right)} = \frac{\left(\frac{\sigma_1}{\sigma_3}-1\right)}{\left(\frac{\sigma_1}{\sigma_3}+1\right)} \quad \text{..... (A.1)}$$

By replacing $\frac{\sigma_1}{\sigma_3}$ by R, the ϕ_d value is obtained as

$$\phi_d = \sin^{-1}\left(\frac{R-1}{R+1}\right) \quad \text{.....(A.2)}$$

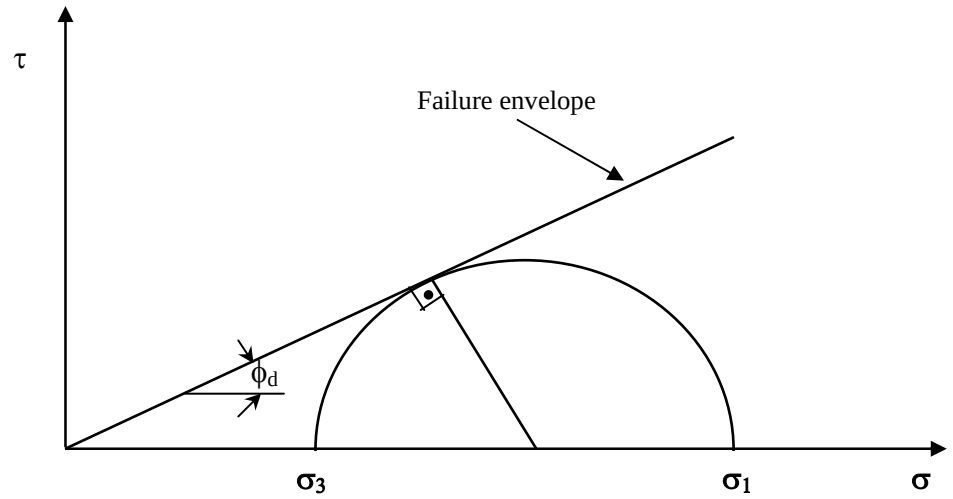

Figure A.1. Sketch showing the state of stress for sands

APPENDIX B

THE RELATION BETWEEN RELATIVE POROSITY AND RELATIVE DENSITY

The relative porosity n_r is defined (Adel, 2001) as

$$n_r = \frac{n_{max} - n}{n_{max} - n_{min}} \quad \text{.....(B.1)}$$

where n_{max}, n_{min}, and n are the maximum, minimum, and current porosities of the sand respectively.

Denoting the maximum, minimum, and current void ratios of the sand by e_{max}, e_{min}, and e, respectively, the relations between the porosity and the void ratio are given below.

$$n = \frac{e}{1+e} \quad \text{.....(B.2)}$$

$$n_{min} = \frac{e_{min}}{1+e_{min}} \text{ . .....(B.3)}$$

$$n_{max} = \frac{e_{max}}{1+e_{max}} \quad \text{.....(B.4)}$$

By substituting equations (B.2) to (B.4) into equation (B.1), the relation between n_r and D_r is obtained as follows:

$$n_r = \frac{\left(\frac{e_{max}}{1+e_{max}}\right)-\left(\frac{e}{1+e}\right)}{\left(\frac{e_{max}}{1+e_{max}}\right)-\left(\frac{e_{min}}{1+e_{min}}\right)} = \frac{\frac{e_{max}(1+e)-e(1+e_{max})}{(1+e_{max})(1+e)}}{\frac{e_{max}(1+e_{min})-e_{min}(1+e_{max})}{(1+e_{max})(1+e_{min})}} \quad \text{.....(B.5)}$$

$$n_r = \frac{\frac{e_{max}+e_{max}.e-e-e.e_{max}}{(1+e_{max})(1+e)}}{\frac{e_{max}+e_{max}.e_{min}-e_{min}-e_{min}.e_{max}}{(1+e_{max})(1+e_{min})}} \quad \text{.....(B.6)}$$

$$n_r = \frac{(e_{max}-e)}{(e_{max}-e_{min})}\frac{(1+e_{min})}{(1+e)} \quad \text{.....(B.7)}$$

$$n_r = D_r \frac{(1+e_{min})}{(1+e)} \quad \text{.....(B.8)}$$

where D_r is the relative density and given by

$$D_r = \frac{(e_{max}-e)}{(e_{max}-e_{min})} \quad \text{.....(B.9)}$$

When $e = e_{min}$;

$$Dr = n_r = 1$$

When $e_{min} < e < e_{max}$;

$$0 < D_r < 1 \qquad 0 < n_r < 1 \qquad n_r < D_r$$

When $e = e_{max}$;

$$Dr = n_r = 0$$

APPENDIX C

CALCULATION OF MARSAL'S (1967) PARTICLE BREAKAGE FACTOR

Several different particle breakage factors have been proposed to quantify the amount of particle breakage. These breakage factors are empirical in nature, and are based on changes in particle size as the key measurement. The most widely used particle breakage factor is the one developed by Marsal (1967). He suggests that the breakage factor, B_g, defined as the sum of the positive differences between the percentages of particles in different size ranges before and after testing, provides some indication of the overall fragmentation process. An example of the calculation of B_g is given in Table C.1, using the gradation curves in Fig. 4.1 in section 4.2.1.

Table C.1. Sample calculation for Marsal's breakage factor

1	2	3	Difference
Size range (mm)	Initial percentage in this range (%)	Final percentage in this range (%)	(2) – (3) (%)
3.15 – 2.00	19.4	18.1	1.3
2.00 – 0.84	35.1	35.7	-0.6
0.84 – 0.63	12.0	11.8	0.2
0.63 – 0.32	18.6	17.7	0.9
0.32 – 0.20	4.5	4.3	0.2
0.20 – 0.16	3.6	3.1	0.5
0.16 – 0.08	2.2	2.9	-0.7
0.08 – 0.00	4.4	6.2	-1.8

B_g = 3.1 %

APPENDIX D

EXAMINATION OF THE EFFECT ON CYLWEST RESULTS OF THE USE OF THE DOUBLE-CUT CYLWEST MOULD WITH NO TRIMMING

According to the original design by Mirata (1991), the upper part of the shear plane of TM (S) and the lower part of the shear plane of mobile part of the mould TM (Fig. 5.3) should be chamfered slightly (see detail A in Fig. 5.2) to prevent the soil in the opposite half from bearing on the test mould wall during shear. The test mould used in the present study had no such chamfer. To examine the effect of this defect on the test results, the shear plane was observed closely in a special cylwest on sample E compacted at the lower density. It was seen that the part of the sand sample moving past TM(S), being unrestrained in any way, did not bear on TM(S); there was a distinct gap between this part of the sample and TM(S) as seen in Fig. D.1. Apart from this observation, Mirata (2002(c)) repeated calculations for cylwest series CA to CD (Tables 5.2 and 5.3), without applying an area correction, and it was seen that the ϕ values both at peak and ultimate strength were not affected by more than $\pm 0.01^{o}$. So even if the separation shown in Fig. D.1 did not occur, and the tests were evaluated without applying an area correction, the results would not significantly differ from those presented in this thesis.

Figure D.1. The sand specimen does not bear on the test mould during shear

APPENDIX E

ESTIMATION OF CELL PRESSURES TO BE APPLIED IN THE TRIAXIAL TEST

Based on the results of the wedge shear test, and on the assumption that the angle ψ between the failure plane and the plane on which the major principal stress acts (Fig. E.1) is $(45+\phi/2)$, the cell pressure σ_3 to be used in triaxial tests to give about the same average principal stresses at failure are calculated as follows (Mirata (1996), quoted by Şakar, 1997).

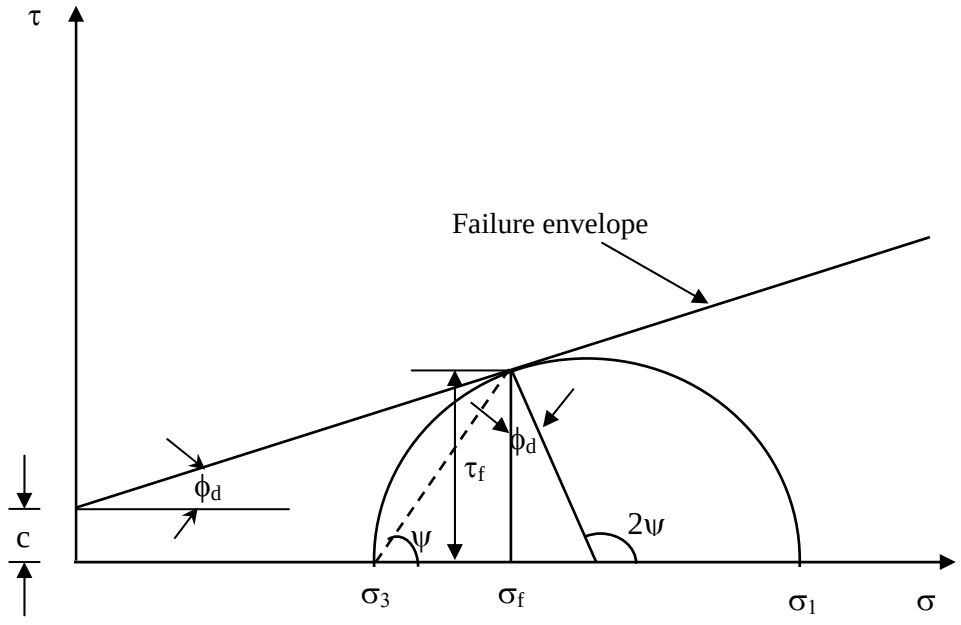

Figure E.1. Sketch showing the state of stress

From Fig. E.1,

$$\frac{\sigma_1 + \sigma_3}{2} = \sigma_f + \tau_f \tan\phi_d \quad \text{.....(E.1)}$$

For the same ϕ_d value, in the triaxial state of stress,

$$\frac{\sigma_1 - \sigma_3}{2} = \left(\frac{\sigma_1 + \sigma_3}{2} + c \frac{\cos\phi_d}{\sin\phi_d} \right) \sin\phi_d \quad \text{.....(E.2)}$$

For sands, c = 0. Then,

$$\frac{\sigma_1 - \sigma_3}{2} = \left(\frac{\sigma_1 + \sigma_3}{2} \right) \sin\phi_d \quad \text{..... (E.3)}$$

Also,

$$\sigma_3 = \left(\frac{\sigma_1 + \sigma_3}{2} \right) - \left(\frac{\sigma_1 - \sigma_3}{2} \right) \quad \text{.....(E.4)}$$

Substituting equation (E.3) in equation (E.4),

$$\sigma_3 = \left(\frac{\sigma_1 + \sigma_3}{2} \right) (1 - \sin\phi_d) \quad \text{.....(E.5)}$$

Assuming plane strain conditions in the wedge shear test, the intermediate principal stress σ_2 is given by (e.g. Timeshenko & Goodier, 1970)

$$\sigma_2 = \nu(\sigma_1 + \sigma_3) \quad \text{.....(E.6)}$$

where ν= poisson's ratio.

The average principal stress σ_p is

$$\sigma_p = \left(\frac{\sigma_1 + \sigma_2 + \sigma_3}{3} \right) \quad \text{.....(E.7)}$$

Substituting equation (E.6) in equation (E.7)

$$\sigma_p = \left(\frac{1+\nu}{3} \right) (\sigma_1 + \sigma_3) \quad \text{.....(E.8)}$$

If $\nu = 0.3$ is assumed (based on ν determinations on 5 mm – 10 mm gravel and on unsaturated Ankara clay),

$$\sigma_p = \frac{2.6}{3} \left(\frac{\sigma_1 + \sigma_3}{2} \right) \quad \text{.....(E.9)}$$

where $\left(\frac{\sigma_1 + \sigma_3}{2} \right)$ is estimated from equation (E.1)

After calculating σ_p for the wedge shear test in this way, one can equate this to $\left(\frac{\sigma_1 + \sigma_3}{2} \right)$ in the triaxial test, and evaluate σ_3 from equation (E.5) as

$$\sigma_3 = \sigma_p (1 - \sin\phi_d) \quad \text{.....(E.10)}$$

An example of the calculation of σ_3 values is given in Table E.1, using the ϕ_d value of 39.7^o obtained from the results of priswest series PD2 (Table 5.16).

Table E.1. Sample calculation for the cell pressures to be applied in the triaxial test

Test no.	σ_f (kPa)	τ_f (kPa)	$(\sigma_1 + \sigma_3)/2$ from equation (E.1) (kPa)	σ_p from equation (E.9) (kPa)	σ_3 from equation (E.10) (kPa)
PD2/1	105.4	90.9	180.9	156.7	56.6
PD2/2	184.8	158.4	316.3	274.1	99.0
PD2/3	231.0	186.7	386.0	334.5	120.8

CURRICULUM VITAE

Yusuf Erzin was born in Adana on 5 January 1970. After graduating from the Yumurtalık High School, he studied civil engineering at Selçuk University. He received the degree of Bachelor of Science in January 1992. He worked as a site engineer at Temelsu A. Ş. on an irrigation project at Çatalca, İstanbul. In April 1993, he became a research assistant in the Geotechnics Division, Department of Civil Engineering, Cumhuriyet University. As from September 1993, he carried out postgraduate study on “Swell pressure – soil suction relationship” at the Middle East Technical University (METU), obtaining his M. S. degree in September 1997. He started his Ph. D. studies in January 1998. During his M. S. and Ph. D. studies at METU, he was a research assistant in Soil Mechanics.